

Microwave Electronics

**DESIGN AND DEVELOPMENT OF COMPACT
PLANAR FILTERS FOR ULTRA WIDE BAND
APPLICATIONS**

A thesis submitted by

Bindu C J

in partial fulfilment of the requirements for the degree of

DOCTOR OF PHILOSOPHY

Under the guidance of

Dr. S Mridula



Division of Electronics Engineering, School of Engineering

COCHIN UNIVERSITY OF SCIENCE AND TECHNOLOGY

Kochi-682022, India

December 2015

Design and Development of Compact Planar Filters for Ultra Wide Band Applications

Ph.D Thesis under the Faculty of Engineering

Author

Bindu C J

Research Scholar

Division of Electronics Engineering

School of Engineering

Cochin University of Science and Technology

Email: bindudevan@gmail.com

Supervising Guide

Dr. S Mridula

Associate Professor

Division of Electronics Engineering

School of Engineering

Cochin University of Science and Technology

Email:mridula@cusat.ac.in

School of Engineering

Cochin University of Science and Technology

Cochin - 682 022, Kerala, India.

www.cusat.ac.in

December 2015

To The Almighty...



DIVISION OF ELECTRONICS ENGG., SCHOOL OF ENGINEERING
COCHIN UNIVERSITY OF SCIENCE AND TECHNOLOGY
COCHIN-682 022

Dr. S Mridula
Associate Professor

Certificate

*This is to certify that this thesis entitled ‘**Design and Development of Compact Planar Filters for Ultra Wide Band Applications**’ is a bonafide record of the research work carried out by **Smt. Bindu C J** under my supervision in the Division of Electronics Engineering, School of Engineering, Cochin University of Science and Technology. The results presented in this thesis or parts of it have not been presented for the award of any other degree.*

*I further certify that the corrections and modifications suggested by the audience during the pre-synopsis seminar and recommended by the Doctoral committee of **Smt. Bindu C J** are incorporated in the thesis.*

Kochi - 22
14/12/2015

Dr. S Mridula
(Supervising Guide)

Phone : +91 9567883856

Email: mridula@cusat.ac.in

Declaration

I, Bindu C J, hereby declare that this thesis titled, ‘Design and Development of Compact Planar Filters for Ultra Wide Band Applications’ is based on the original research work carried out by me under the supervision of Dr. S Mridula in the Division of Electronics Engineering, School of Engineering, Cochin University of Science and Technology. The results presented in this thesis or parts of it have not been presented for the award of any other degree.

Kochi - 22

Bindu C J

14/12/2015

Acknowledgments

It is truly a privilege and blessing to have Dr. S. Mridula as the supervisor of my research work and I am afraid no words can fully express my gratitude towards her and God almighty for the same. Her patient guidance and enthusiastic encouragement helped me to reach this goal. Her high research standards, keen observation and technical precision will always remain my professional goals.

It is my radiant sentiment to place on record, my deepest sense of gratitude to Dr.P Mohanan, Professor of Department of Electronics, CUSAT. I have benefited from his insightful comments and valuable suggestions throughout my research. A dedicated teacher, who always readily and generously gives his precious time and energy out of his busy schedule for clarifying my doubts, he has given full freedom to use the lab facilities at Centre for Research in Electromagnetics and Antennas(CREMA). I am deeply indebted to him.

I am grateful to Dr. K. Vasudevan, Retd. Professor of the Department of Electronics, CUSAT, for his encouragement and support for my research. I thank Dr. Binu Paul, HOD, Division of Electronics Engineering, School of Engineering, CUSAT, for the suggestions and support I received from her during my research and also for her valuable suggestions in my thesis. I express my deepest thanks to Mrs. Anju Pradeep, Associate Professor, Division of Electronics Engineering, School of Engineering, CUSAT for her sincere efforts to take part in technical discussions. I choose this moment to acknowledge her contribution gratefully.

I thank all my great teachers over the years, from the first grade of elementary school to the university who carved me to this level.

I gratefully acknowledge members of CREMA, especially Mr. Deepak, Mr. Nijas, Mr. Dinesh and Mrs. Roshna for their technical assistance and valuable discussions. Special thanks to Mr. Lindo Ouseph, Research Scholar, RCS lab, Department of Electronics, CUSAT who kept aside his work to help me. I also appreciate the friendly help of Mr. R Rajesh Mohan, Mr. Basil J Paul, Mr. Anjith T A and Mrs. Jaya Mohan, Research scholars, SOE, CUSAT. Technical support offered by Mr. Jathin K P, Application Engineer at Entuple Technologies, Mr. Anil Kumar, Maintenance Engineer, Department of Electronics and Mr. Narayanan, CTech are also gratefully remembered. Creative suggestions and continuous support offered by Dr. Deepu V Nair, Technical Lead, Cambium Networks, helped a lot in boosting my confidence.

I appreciate the support from my friends Archana R, Dr. Laila.D, Mrs. Sumitha Mathew and Mrs. Sarah Joseph. The hectic pressure during the research period was eased by my friends Sumi M, Saira Joseph and Ramya T K. Working with them was a pleasant experience.

I wish to acknowledge The Director, Institute of Human resources and Development (IHRD), Thiruvananthapuram and Principal, Model Engineering College, Ernakulam for the support and help rendered to me. I also appreciate the friendly support from my colleagues at Model Engineering College.

I value the support offered by my caring parents, family members and relatives. Words are not enough to thank my mother and my husband Devan whose love and understanding have been my solid ground to stand on. I could not have accomplished

this without their boundless love, sacrifice and encouragement.

*... and finally I thank my Lord, the Supreme Consciousness who personified himself
in all the above forms to help me through...*

Bindu C J

Preface

Ultra Wide Band (UWB) technology permits short-range, high-bandwidth communication at very low energy levels by utilizing a large portion of the radio spectrum. The deregulation of the 7.5 GHz band from 3.1 GHz to 10.6 GHz by U.S. Federal Communications Commission in 2002 triggered the use of UWB in most of the commercial communication systems. UWB communication stimulates both opportunities and challenges in the design and implementation of fully integrated RF front-ends. UWB or broad band microwave filters are essential components for applications such as UWB wireless and radar systems. The introduction of filter optimizes the front-end characteristics of the UWB antenna.

In this work, different planar filters in the UWB range are designed, developed and analyzed. These filters are developed from interdigital coupled lines. The structures are made compact without compromising on the filter performance. The different UWB filter structures investigated are:

- ★ Filter using Stepped Impedance Stub Resonators
- ★ Filter using Folded Stepped Impedance Resonators and Complementary Split Ring Resonators
- ★ Filter using Chip Inductors and Complementary Split Ring Resonators
- ★ Filter using Cascaded Resonators
- ★ Filter using Series Capacitor and Defected Ground Structures

A filter with a WLAN notch and a coplanar waveguide filter using stub resonators are included in the appendix. The performances of these filters are studied using ANSYS® HFSS™ and experimentally verified using Vector Network Analyzers (HP8510C and Agilent PNA E8362B).

Conventional filter design methods cannot be directly employed in compact UWB filter design. The main design challenge is achieving the ultra wide band response with compact dimensions fit for fabrication. Lumped element equivalent circuit model is developed for each of the planar filters designed, which helps in identifying the circuit behavior in a better detail. Generalized design equations are made in all cases to help designing similar filters with different materials. Analysis of the designed filter in time and frequency domain ensures their usefulness in communication applications. The designs are compact, planar and single layered thus facilitating easy integration into any PCB.

Contents

1	Introduction	1
1.1	Ultra Wide Band Technology	2
1.2	Role of Filters in UWB Communication	5
1.3	Overview of Filters	7
1.3.1	Different Types of Filters	7
1.3.2	Various Technologies in Use for Microwave Filters	7
1.3.3	Design Considerations for UWB Filters	10
1.4	Important Filter Parameters	13
1.4.1	Frequency Domain Parameters	13
1.4.2	Time Domain Parameters	19
1.5	Related Work	21
1.6	Motivation	26
1.7	Thesis Organization	28
2	Tools and Techniques	45
2.1	Simulation and Optimization	46
2.2	Multivariable Regression	48
2.3	Fabrication and Testing	49
2.3.1	Substrate Material	49

2.3.2	Testing	50
2.4	Summary	52
3	RF Planar Components	55
3.1	Planar Transmission Lines	56
3.1.1	Microstrip Line	57
3.1.2	Coplanar Waveguide	62
3.1.3	Coupled Lines	65
3.1.4	Interdigital Coupled Lines	69
3.2	Resonators	71
3.2.1	Stub Resonators	72
3.2.2	Open Ring Resonators	82
3.2.3	Complementary Split Ring Resonators	87
3.2.4	Defected Ground Structures	90
3.3	Lumped/Semi Lumped Elements	93
3.3.1	Inductors	93
3.3.2	Chip Inductors	95
3.3.3	Capacitors	96
3.4	Summary	97
4	Stepped Impedance Stub Resonator Filter	103
4.1	Geometry	104
4.2	Simulation Studies	108
4.3	Analysis and Design	108

4.4	Lumped Element Model	113
4.5	Dispersion Studies	116
4.6	Time Domain Analysis	118
4.7	Measurement Results	119
4.8	Summary	121
5	Compact UWB Filters	125
5.1	Filter Using Folded SIR and CSRR's	126
5.1.1	Geometry	127
5.1.2	Simulation Studies	131
5.1.3	Analysis and Design	132
5.1.4	Lumped Element Model	135
5.1.5	Dispersion Studies	137
5.1.6	Time Domain Analysis	137
5.1.7	Measurement Results	138
5.2	Filter Using Chip Inductors and CSRR's	142
5.2.1	Geometry	143
5.2.2	Simulation Studies	146
5.2.3	Analysis and Design	149
5.2.4	Lumped Element Model	152
5.2.5	Dispersion Studies	154
5.2.6	Time Domain Analysis	154
5.2.7	Measurement Results	155
5.3	Summary	156

6	UWB Filters with Improved Performance	161
6.1	Filter using Cascaded Resonators	162
6.1.1	Geometry	163
6.1.2	Simulation Studies	166
6.1.3	Analysis and Design	168
6.1.4	Lumped Element Model	172
6.1.5	Dispersion Studies	173
6.1.6	Time Domain Analysis	174
6.1.7	Measurement Results	175
6.2	Filter Using Series Capacitors and Defected Ground Structures	179
6.2.1	Geometry	180
6.2.2	Simulation Studies	183
6.2.3	Analysis and Design	184
6.2.4	Lumped Element Model	188
6.2.5	Dispersion Studies	190
6.2.6	Time Domain Analysis	191
6.2.7	Measurement Results	191
6.3	Summary	193
7	Conclusion	199
7.1	Thesis Highlights	200
7.2	Comparison of Salient Features of Various Filters Developed	203
7.3	Suggestions for Future Work	205

Appendix	206
A UWB Filter with WLAN Notch	209
A.1 Geometry	210
A.2 Simulation Studies	213
A.3 Measurement Results	216
A.4 Summary	218
B Coplanar Waveguide UWB Filter	223
B.1 Geometry	224
B.2 Simulation Studies	231
B.3 Measurement Results	231
B.4 Summary	234
Publications by the Author	237
Author Biodata	240
Index	243

1 Introduction

Contents

- ★ *Ultra Wide Band Technology*
- ★ *Role of Filters in UWB Communication*
- ★ *Overview of Filters*
- ★ *Important Filter Parameters*
- ★ *Related Work*
- ★ *Motivation*
- ★ *Thesis Organization*

This chapter discusses modern wireless communication with emphasis on Ultra Wide Band technology. The chapter highlights the role of filters in communication systems. It also includes different classification of filters and filter technologies. The design considerations of UWB filters along with important filter parameters are pointed out. A brief literature review, motivation of the thesis and scheme of work and measurement set up used are also given. Finally the chapter presents the organization of the thesis.

Wireless communication is the fastest growing segment in communication industry. From satellite transmission, radio and television broadcasting to the now ubiquitous mobile telephone, wireless communication has revolutionized the way societies function [1]. However, the increasing demand for higher data rates and better quality of service necessitate the development of new communication systems.

1.1 Ultra Wide Band Technology

U.S. Federal Communications Commission (FCC) defines a UWB device as any device operating with the fractional bandwidth greater than 20% or that occupies 500MHz or more of spectrum [2]. The formula proposed by FCC for calculating fractional bandwidth is $2(f_H - f_L)/(f_H + f_L)$ where f_H is the upper frequency of the 3 dB point and f_L is the lower frequency of the 3 dB point. The center frequency of the transmission is defined as the average of the upper and lower 3 dB points, i.e., $(f_H + f_L)/2$.

The usage of UWB technology and consideration for commercial applications such as home networking picked up after the FCC ruling in 2002. On February 14, 2002, FCC Report and Order authorized the unlicensed use of UWB in the frequency range from 3.1 to 10.6 GHz. This triggered the use of UWB in most of the commercial communication systems. Thus UWB system has become one of the most expected technologies in Wireless Personal Area Networking (WPAN), home entertainment, multimedia interfaces, high precision location RFID etc. Credit should also be given to the potential advantages of UWB transmissions such as low power consumption, high

data rate, immunity to multipath propagation and less complex transceiver hardware. The main attraction of the large bandwidth for UWB pulses is the improved channel capacity. Channel capacity, or data rate, is the maximum amount of data that can be transmitted per second over a communication channel. The channel capacity C is directly proportional to bandwidth B and logarithmically proportional to signal to noise ratio (SNR) as evident from Hartley Shannon's formula, $C = B \ln(1 + SNR)$. Thus UWB communications systems can offer large channel capacity even when operating in communication channels with low SNR values.

Two technologies are used for UWB systems: Single band (Impulse Radio) and Multi band (OFDM). Impulse Radio UWB(IR-UWB) technology transmits binary data, using low energy and extremely short duration impulses or bursts (in the order of picoseconds) over the entire spectrum. It delivers data over 15 to 100 meters and does not require a dedicated radio frequency, so is also known as carrier-free, impulse or base-band radio. Each pulse in a pulse-based UWB system occupies the entire UWB bandwidth, thus reaping the benefits of relative immunity to multipath fading. In multiband system, the 3.1-10.6GHz band is divided into 14 sub bands each occupying a bandwidth of 528MHz. This utilizes the spectrum efficiently, but require complex (de)modulation schemes and sophisticated signal processing units. The immunity to multipath fading is also affected.

Technical standards and operational restrictions given by FCC are intended to enable the co-existence of UWB with existing radio technologies such as IEEE 802.11 (Wi-Fi), HomeRF, and HiperLAN. The allowed power spectral densities for various regions of the spectrum will be different to avoid interference with existing communication systems.

FCC has assigned certain Effective Isotropic Radiated Power (EIRP) for each frequency band [3]-[5]. The level of -41.3dBm/MHz [75nW/MHz] in the frequency range $3.1\text{--}10.6\text{GHz}$ is set to limit interference and to protect existing radio services. As can be seen from Fig. 1.1, the spectral mask for outdoor radiation limit is 10dB lower than the indoor mask. The amplitude of the UWB pulses are normalized to comply with the above spectral mask limits. The allowable indoor and outdoor EIRP levels for different bands are shown in Table 1.1.

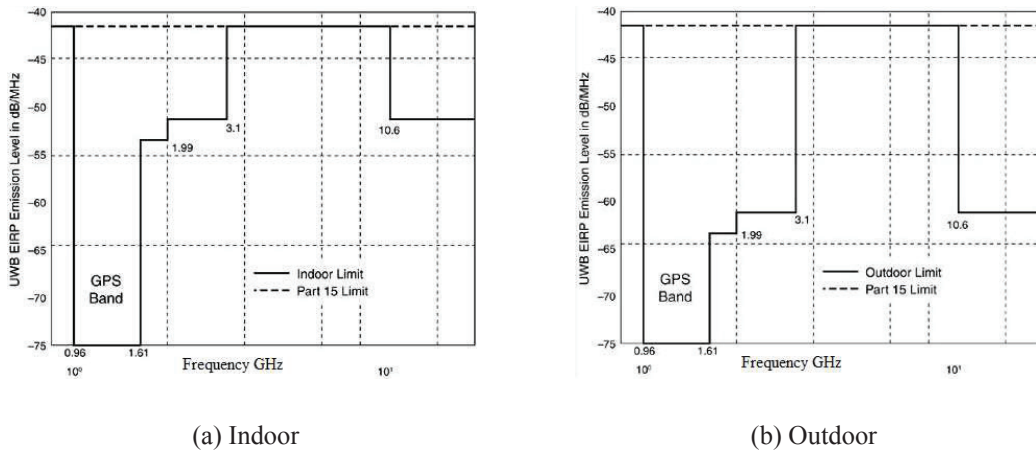


Figure 1.1: FCC Spectral Mask

Gaussian pulses which can be easily generated by pulse generators are used for UWB systems. Impulses are not transmitted and received effectively through practical antennas because of their large portion of DC or low frequency spectral contents, which cannot be transmitted (or transmitted with low efficiency) by practical antennas [6] -[7]. Hence higher derivatives (4^{th} derivative and above) which sufficiently suppress the DC contents of Gaussian pulses, are generally used.

Table 1.1: Allowable Indoor and Outdoor EIRP Levels for Different Bands

Frequency (MHz)	EIRP dBm/MHz(Indoor)	EIRP dBm/MHz(Outdoor)
960-1610	-75.3	-75.3
1610-1990	-53.3	-63.3
1990-3100	-51.3	-61.3
3100-10600	-41.3	-41.3
Above 10600	-51.3	-61.3

1.2 Role of Filters in UWB Communication

The electromagnetic spectrum is limited and hence has to be shared for different applications. Filters are used to select or confine signals within assigned spectral limits. UWB communication stimulates both opportunities and challenges in the design and implementation of fully integrated RF front-ends. UWB systems are usually designed with filters being incorporated to obtain the precise system frequency response. Both in transmitter and receiver architectures, the first and second components of the system chain are identified as an antenna and a UWB front-end preselected filter [8]. A typical UWB receiver and transmitter system is shown in Fig. 1.2. Because filters are the narrowest bandwidth components in the system, it is usually the filters that limit such system parameters as gain and group delay flatness over frequency.

UWB or broad band microwave filters are essential components for applications such as UWB wireless and radar systems. There are communication subsystems, wherein a UWB filter will be integrated with UWB antenna and placed in the microstrip feed line of the antenna. The purpose is twofold. Firstly, it acts as a wide

band match circuit to enhance the performance of the antenna in the passband. Secondly, it improves the out-of-band performance [9]. Thus introduction of filter allows optimizing the front-end characteristics of the UWB antenna. Also, for Impulse Radio-UWB, filters used in transmitters can regulate the emission power of short duration pulses to comply with the FCC spectral mask and eliminate the use of additional pulse shaping circuits.

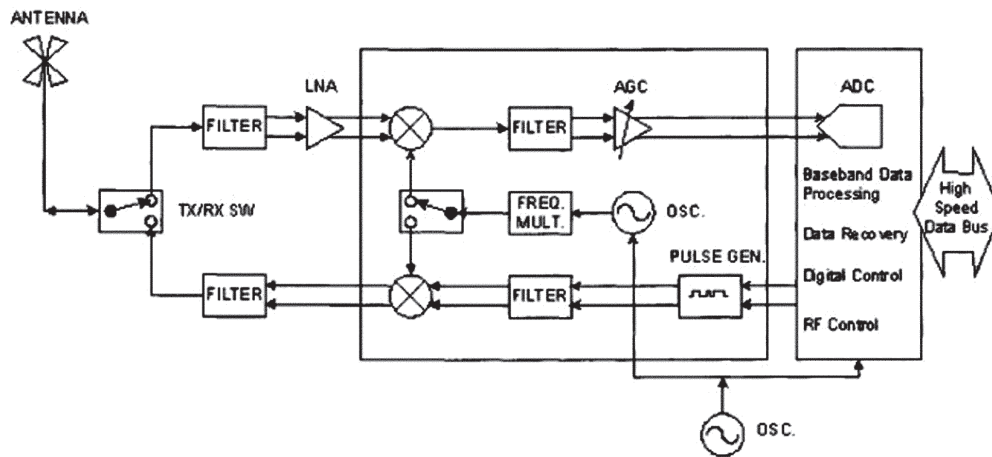


Figure 1.2: UWB Receiver and Transmitter System

Frequency selectivity on the lower side of the UWB band is benefited by so many wireless communication systems operating in the GSM and mobile services. Towards the upper side, The European Conference of Postal and Telecommunications Administrations (CEPT) recommend that the 10.7 - 11.7 GHz band radio frequency channel arrangement may be considered for digital point-to-point fixed wireless systems [10].

Thus to satisfy the UWB system requirements, a bandpass filter with a broad pass band width, high selectivity, low insertion loss and high stopband suppression are

needed; justifying this work.

1.3 Overview of Filters

The filter functionality can be implemented in a variety of different forms like passive lumped element filters, active filters, switched capacitor filters, digital filters, microwave filters etc. The choice of filter type depends on many factors and tradeoffs and is critically dependent on the type of application, but the key factor is the frequency range of operation.

1.3.1 Different Types of Filters

Software Digital filters, implemented in any high level language on PC or any DSP chip, are best suited for frequencies less than 20KHz. Extending to higher frequencies, hardware digital filters designed using interconnected VLSI chips are preferred as they are much faster compared to their software counterpart. But their operating frequencies are limited by the available VLSI technology. Between 20KHz and 0.1GHz, the choice is between discrete active RC filters, switched capacitive filters or passive RLC filters. Above 0.1GHz, microwave filters become the apt choice [11].

1.3.2 Various Technologies in Use for Microwave Filters

From the practical point of view, miniaturization is an important issue for all portable equipments. The reduction of size and weight becomes critical for wearable equipments such as mobile phones and Personal Digital Assistants(PDA). Miniaturization of RF

circuits is made possible through the introduction of microwave integrated circuits (MIC) and Monolithic Microwave Integrated Circuits (MMIC).

Choosing suitable technology such as Bulk Acoustic Wave (BAW)/ Surface Acoustic Wave (SAW), helical, dielectric resonators, coaxial, waveguide and microstrip/stripline is a key issue in the realization of multiplexers and filters (Fig. 1.3). The selection depends mainly on frequency range of operation. Other aspects such as physical size, unloaded quality factor Q , power handling capability, temperature drift and production cost are also to be considered.

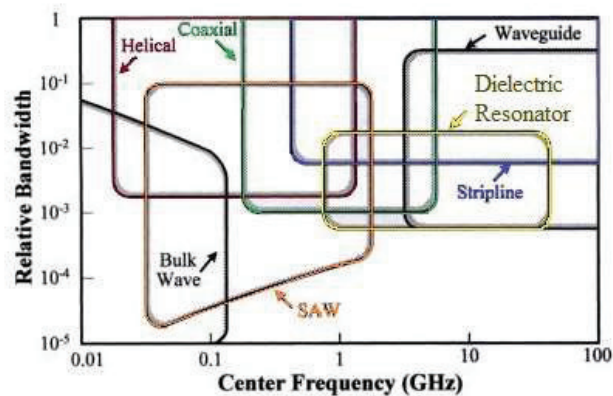


Figure 1.3: Various Filter Technologies

For frequencies below 1GHz, BAW, SAW or helical resonators and filters are used on demand of miniaturization and low loss. These are used in 2G receiver front ends, duplexers and filters. Helical resonators are employed for high level of power handling. For RF to microwave range dielectric, coaxial, waveguide, microstrip/stripline resonators are used. Dielectric resonator filters achieve higher unloaded Q (more than 40000 can be obtained) and very good temperature stability. These filters have low loss

and small size but have the disadvantages of close out-of-band spurious response and relatively low power handling capability along with high cost. Coaxial line filters operating in the TEM mode can also be considered in the waveguide category. They are common in wireless base stations and TV broadcasting. Microwave filters implemented in air filled rectangular waveguides, ridge waveguides and circular waveguides operate in their fundamental TE mode. For silver-plated resonators, unloaded Q factors of 10000 to 20000 can be achieved. Their insertion loss is low and they can handle higher power. However, they are usually bulky and their mass and temperature stability must be carefully considered in satellite applications. Aluminium can be used to reduce the weight. Temperature stability can be improved by an adequate design methodology, using special materials (e.g. invar) and smart mechanical structures [12]. Coaxial resonators provide excellent shielding to the structure and have low loss characteristics and small size. But minute physical dimensions at high frequencies make fabrication difficult.

Low Temperature Cofired Ceramic (LTCC) technology is also commonly used now a days for designing compact filters. It is possible to integrate on the same substrate baseband/digital components together with RF miniaturized filters, active and passive devices. However this option is not considered in this work as manufacturing facility is not currently available with our laboratories.

Considering the above factors, planar structures like microstrip lines, striplines, coplanar lines and suspended striplines are the common choice for most of the MIC's and MMIC's. Their supporting features include small size, easy processing by photolithography, easy integration with other circuit elements and wide frequency

range. Striplines support a pure Transverse Electromagnetic (TEM) mode which allows better noise immunity than microstrip. However, microstrips are preferred because they are lighter, more compact and easier to fabricate. Microstrip supports a quasi-TEM mode or a hybrid mode that is due to the inhomogeneous medium surrounding the transmission line. The power handling capability and Q factors are usually low (in order of 100's), unless special materials are used [13]. Thus in this work, microstrip filters are designed and developed.

1.3.3 Design Considerations for UWB Filters

The development of a high-performance UWB filter is an involved task that poses many challenges. A UWB bandpass requires 110% fractional bandwidth. More over UWB filters for communications applications should have good selectivity and flat group delay performance over the entire passband to ensure distortion- free propagation.

Traditional filter design approaches fail to meet these specifications due to requirements of tight coupling and uncontrolled nonlinear frequency dispersion over the wide bandwidth of interest. This demands a high-order configuration which implies excessive passband insertion loss and a physically large size.

It is possible to meet the bandwidth requirements of UWB systems by means of coupled lines using apertures on the ground plane and interdigital coupled lines with multi-mode resonators for effective coupling over a wide bandwidth. These structures require tight fabrication tolerances and may be sensitive to the proximity effect of the metal enclosures and the fields generated by other components, for example, when packaged with RF integrated circuits (IC's). Electromagnetic (EM) bandgap structures

and defected ground structures (DGS) approaches have also been applied to the design of UWB filters. These approaches require accurate fabrication procedures as the dimensions of these structures may be in sub wavelength order. All these are to be carefully looked into while designing UWB filters. For the design of a planar filter, the electrical performance in terms of out of band rejection and in-band transmission losses must be weighed along with the cost, reliability and physical size.

Fig. 1.4 shows the design flow chart followed. There is a vast variety of planar components exhibiting identical behaviour with differing performance trade offs. Accuracy and compactness of the design depend on the choice of suitable geometry.

The design procedures are vastly enabled by the availability of high speed computers, development of efficient electromagnetic simulation tools, numerical optimization techniques and innovative structures in various transmission media that enable realization of the optimal performance.

The design starts with the required filter specifications. Planar transmission line suitable for the bandpass filter is identified. The basic requirements of the UWB bandwidth (3.1-10.6 GHz) is then attained by choosing suitable planar resonators. Electromagnetic simulation with parametric optimization is then applied to make the response of the realized microwave structures close to the idealized circuit response. Performance optimization is done by introducing additional resonators and fine tuning the dimensions.

Once a final acceptable simulated response is achieved, the filters can be directly fabricated either by photolithography or by using PCB milling machine for more accurate fabrication. The performance of the fabricated prototype can be

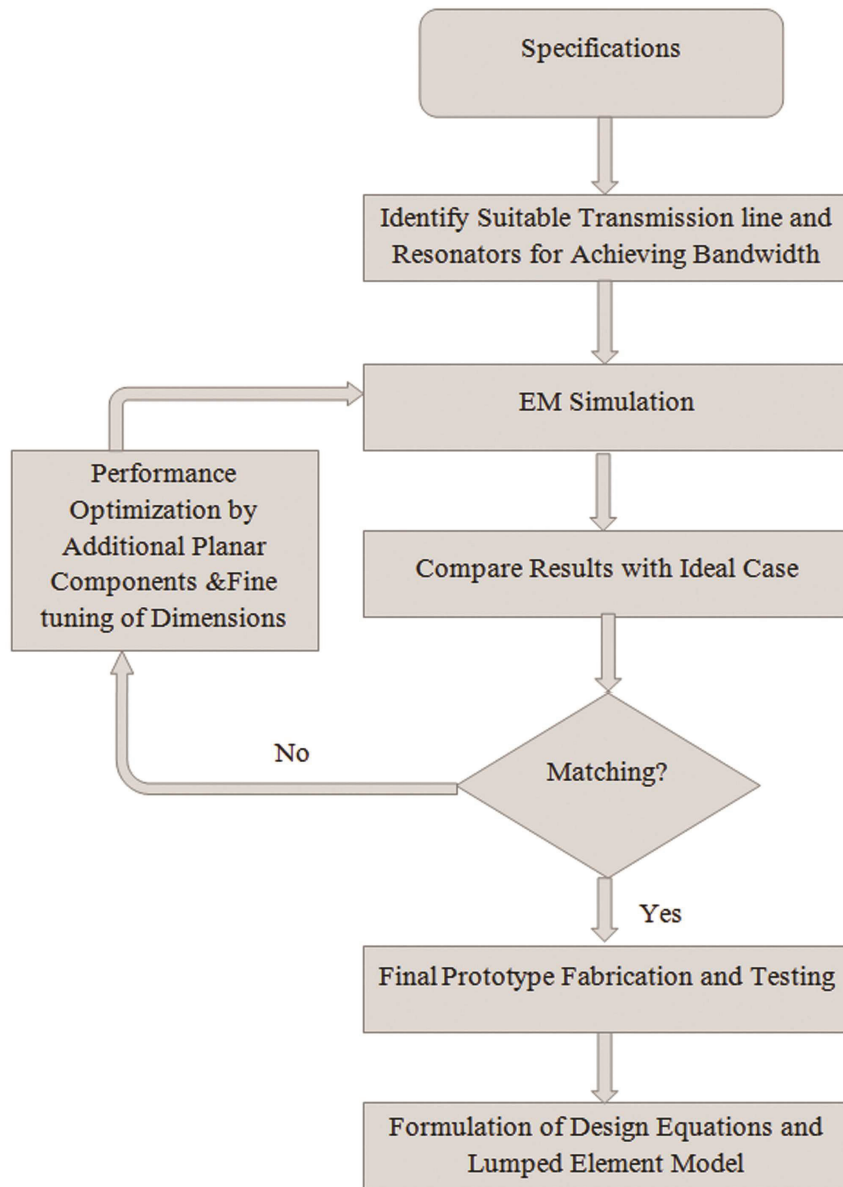


Figure 1.4: The Design Flowchart

experimentally verified by using Vector Network Analyzers (VNA). Lumped element models are then obtained to validate the designs. Design equations are formulated using multivariable regression analysis on the data set obtained from various parametric iterations.

1.4 Important Filter Parameters

The functional requirements of a filter are specified in terms of filter parameters. Fig. 1.5 shows the important filter parameters in both time as well as frequency domain, considered in the design of various filters. The performance of the designed filters are assessed from these parameters.

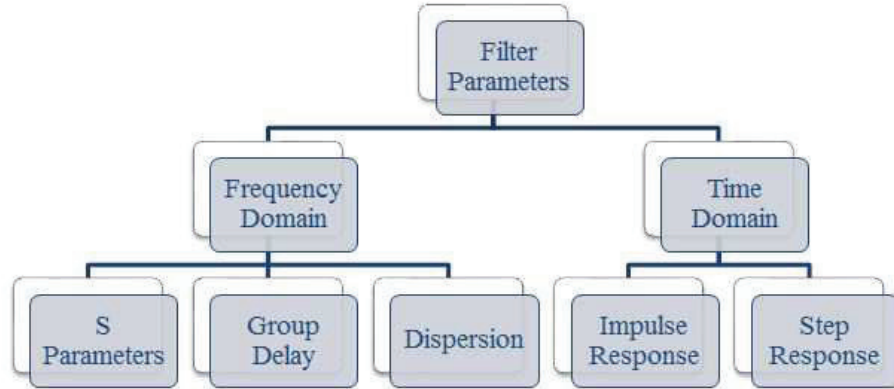


Figure 1.5: Important Filter Parameters

1.4.1 Frequency Domain Parameters

Frequency Domain Parameters indicate how well a filter performs in frequency domain. Focus is given mainly to scattering (S) parameters (transmission and reflection

parameters), group delay and dispersion. These are important factors determining the transmission quality.

S Parameters

Z, Y and H parameters are used for low frequency characterization. At higher frequencies S parameters take precedence which are defined in terms of voltage traveling waves and are easy to measure. S parameters relate traveling waves to a network's reflection and transmission behaviour. This does not require connections to undesirable loads (like open and short circuits required for Z and Y parameters). Moreover Z, Y and H parameters can be derived from S parameters if required.

Performance characteristics like insertion loss, roll off rate, return loss and stopband attenuation of a filter can be obtained from the S parameters.

Group Delay

Group delay is defined as the rate of change of transmission phase angle with respect to frequency.

$$GroupDelay = \frac{-\Delta\phi}{\Delta\omega} \quad (1.1)$$

where ϕ is the phase angle and ω is the frequency. The unit of quantity on LHS works out to time when the angle is in radians and frequency is in radians/time (seconds, nanosecond, picosecond or whatever is convenient, depending on the length of the path).

Group delay evaluates the linear phase nature of the filter. A signal can contain a collection of different frequency components. If the phase of each of these components

suffer a delay proportional to their corresponding frequencies, at any particular instant of time, the signal appears to be constituted of the same components. In other words, the envelope remains the same and there is no distortion. This is the case of flat or constant group delay. The group delay may also be referred to as envelope delay. The difference in group delay for signals spread out over a filter's passband is a measure for the phase distortion introduced by the filter.

Flat and consistent group delay (versus frequency) is important in communication systems and radar systems. In radar systems, distances are to be measured accurately using electromagnetic energy. The radar pulse is complex and its frequency content can span a bandwidth of 1GHz or more. When the pulse is being processed, its spectrum has to be the same over the intended bandwidth of frequencies, otherwise distortion may cause inaccurate radar range measurements. Inductors, capacitors, transistors, amplifiers, transformers etc. can all contribute to eroding the group delay flatness of a network.

Group delay consistency is extremely important in receivers such as mono pulse, where amplitude and phase tracking is required to achieve good null depths. Similar is the case with communication receivers where variation in group delay can cause distortion in received signals.

Group delay can be positive or negative depending on the phase shift over a range of frequency considered. A transmission line loaded with resonators can exhibit combinations of negative and positive group delay. Negative group delay does not violate the principle of causality; instead, it only reshapes the waveform of the pulse. At the resonant frequencies of the resonators, there will be accumulation of charges at

the resonators causing increased delay [15].

Dispersion

The signal energy (as well as the information it carries) is spread across a range of frequencies. Dispersive propagation occurs when phase velocity depends on frequency. If the different frequencies that comprise a signal propagate at different velocities through a microwave filter (i.e., each signal frequency has a different delay, τ), the output signal will be distorted. Alternatively, if the phase constant β is not a linear function of frequency, then the phase velocity $v_p = \omega/\beta$ will vary with frequency. This phenomenon is called signal dispersion. This is not desirable for filters used in communication applications.

The dispersive nature of microstrip transmission line is due to quasi TEM mode of propagation which causes the effective dielectric constant ϵ_{eff} vary with frequency. The computation of the physical parameters of microstrip line presented in section 3.1.1 are based on the quasi-static approximation and are strictly valid only at DC (or very low frequencies). At higher frequencies a number of effects can occur that lead to variations from the quasi-static results for effective dielectric constant, characteristic impedance and attenuation of microstrip line.

The electromagnetic field that exists on microstrip line involves a hybrid coupling of TM and TE modes [14], complicated by the boundary condition imposed by the air and dielectric substrate interface (surface wave mode). In addition, the current on the strip conductor is not uniform across the width of the strip, and this distribution varies with frequency. Although the lowest surface wave mode can propagate at any frequency

(it has no cutoff), its coupling to the quasi-TEM mode of the microstrip only becomes significant at the frequency

$$f_s = \frac{c \tan^{-1}(\epsilon_r)}{\sqrt{2\pi h} \sqrt{\epsilon_r - 1}} \quad (1.2)$$

at which the phase velocities of the two modes are close [16]. The value of f_s is computed as 30.84GHz for $\epsilon_r=4.4$ and $h=1.6\text{mm}$ [16]- [17].

The excitation of higher-order modes in a microstrip can be avoided by operating it below the cutoff frequency of the first higher-order mode, which is given by

$$f_s = \frac{c}{\sqrt{\epsilon_r} (2W + 0.8h)} \quad (1.3)$$

which is evaluated to 19.65 GHz. In practice, the lowest value (the worst case) of the two frequencies given by Eq. 1.2 and Eq. 1.3, is taken as the upper limit of operating frequency of a microstrip line.

In this work the highest frequency is 10.6GHz and hence, the dispersion effects are negligible, which is supported by the dispersion diagrams of the developed filters.

Dispersion of a filter can be checked by plotting the variation of phase with frequency, the $\omega - \beta$ diagram. Due to periodicity of the complex exponential function, the phase of S_{21} generally appears as a curve varying between $-\pi$ and $+\pi$, whereas the dispersion characteristic $\beta(\omega)$ is a continuous function of frequency [18]. It is therefore necessary to unwrap the phase $\phi(S_{21})$ in order to restore the continuous nature of β . Linear phase relationship with frequency also indicates constant group delay.

Performance Parameters in Frequency Domain

The main performance parameters used in the design which are deduced from the S parameters are listed below.

(i) *Insertion Loss*: Insertion loss can be defined as the logarithmic ratio of the power delivered to the load impedance before insertion of the filter to the power delivered to the load impedance after insertion of the filter. This has to be kept as low as possible. The insertion loss can be determined from the transmission characteristics (S_{21}) between the two cut off frequencies. It should be as minimum as possible.

(ii) *Return Loss*: The return loss of a filter is a measure of energy/power reflected at the ports instead of transmitting. Often a constraining value of at least 10 dB in the passband is usually insisted for return loss in most applications. It is extracted from the reflection parameters (S_{11}).

(iii) *Cut Off Frequency*: The passband and stopband boundary points in the filter transmission characteristics are defined by cut-off frequency. The 3dB cut off frequencies chosen are 3.1GHz and 10.6 GHz.

(iv) *Roll Off Rate*: The roll off rate is the slope of the transfer characteristics (S_{21}) at the passband edges or in the transition band. This determines the selectivity of the filter. Higher slope indicates better selectivity. The filters discussed in this thesis are all comparatively of high selectivity and the roll off rate is specified in dB/GHz. A roll off rate steeper than 30dB/GHz is considered reasonable in most of the applications.

(v) *Stopband Attenuation*: This indicates the signal suppression offered by a filter. This should be as high as possible. The FCC spectral mask suggests a stopband attenuation of 10dB on either side for indoor applications and 20dB on either side for

outdoor applications.

1.4.2 Time Domain Parameters

Time Domain analysis of systems such as microwave two-port networks (i.e., filters, amplifiers etc.) or one-port networks (i.e., antennas, resonators etc.) can be of great help to understand their behaviour to improve their functionality, and is widely employed in the research environment.

The physical phenomena actually occurs in time domain, and therefore it is easier to isolate the behaviour of each part of a certain subsystem when studying it in time domain. Usually impulse response or step response of a system is analyzed to get the system behaviour like response time, overall system stability, presence of ringing and overshoot, thus assess its suitability in a particular application.

Impulse Response

Optimized impulse response is required for filters used in modern microwave receivers, radars, satellite systems etc. If the design causes significant time domain overshoots, receiver channels will be saturated and hence will not respond in time [19]. The impulse response of a filter in the time domain is inversely proportional to the bandwidth of the filter in the frequency domain. The narrower the impulse, the wider the bandwidth of the filter.

Step Response

The step response of a filter is the integral of the impulse response. The step response of a filter is useful in determining the envelope distortion of a modulated signal. The two most important parameters of a filter's step response are the overshoot and ringing. Overshoot should be minimal for good pulse response. Ringing should decay as fast as possible, so as not to interfere with subsequent pulses.

Performance Parameters in Time Domain

The performance parameters observed from step response are as follows. These are to be optimized in a design.

(i) *Rise Time and Settling Time:* Rise time T_r is often defined as the time required for the output of a filter to move from 10% to 90% of its steady state value on the initial rise. A short rise time is indicative of a fast response of the filter. Settling time T_s is the time it takes for the output signal to settle within a specified overshoot percentage after the input has been subjected to a step, pulse, impulse, or ramp input. The rise time and settling time should be as small as possible for fast and stable response of the filter. But design trades off are required since reduced rise time will cause increased overshoots and manipulations on settling time by additional damping elements can make the filter response sluggish.

(ii) *Overshoot:* The overshoot is important as it may cause saturation of components when exceeded a specified maximum value. Parametric studies can be used to analyze and identify the components causing overshoot and accordingly compensations can be incorporated. Unit step response and various performance parameters are defined as

shown in Fig. 1.6.

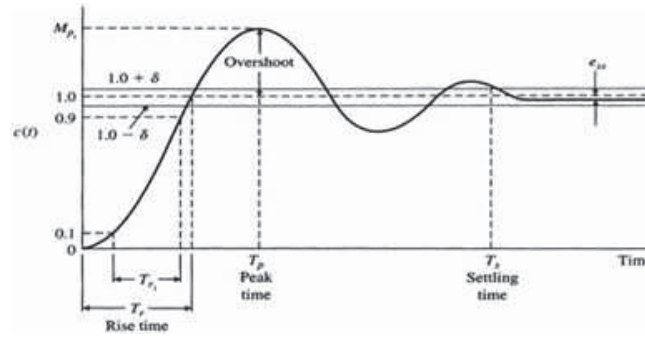


Figure 1.6: Unit Step Response and Various Performance Parameters

1.5 Related Work

A detailed literature survey is conducted on the works reported in the area of planar UWB filters. Different methodologies are available for implementing filters. The most traditional way is to use transmission line stubs of half wavelength and quarter wavelength long in proper combinations. These are simple to design, but occupy more space while trying to achieve steep roll off and reasonable attenuation in stopband. Immediately after the deregulation of the UWB spectrum, several attempts were reported in the field of bandpass filter design. Many researchers have proposed and demonstrated microstrip filter structures using open and short circuited stubs [20]-[42].

Lei Zhu and Wolfgang Menzel suggested [20] a compact microstrip bandpass filter developed using a half-wavelength transmission line resonator with a pair of tap-connected open-ended stubs. The filter had a passband of 4.8 to 5.6GHz. Even though the filter exhibited steep roll off, stopband attenuation was poor. Rui Li et al.

[23] suggested a UWB filter by combining series and short stubs. The bandwidth achieved seemed good, but the structure was not compact and selectivity was poor. Qing-Xin Chu et al proposed [25] a stepped impedance stub loaded resonator to implement UWB filters, in 2010. Y.L Wu, in his work [27], employed stepped impedance resonators for designing a dual passband filter. J. Xu et al. reported a multiband bandpass filter using two-side open-circuit stepped-impedance resonator with short-circuit stubs in its low-impedance sections [29]. The filter exhibited excellent passband characteristics, but stopband attenuation is yet to be improved. Also the structure appeared complex and relatively large. Manidipa Nath reported in [32] an ultra-wide band filter design using half hexagon resonator with five stubs having the range 3.1-10.6GHz, but the insertion loss was as high as 3.5dB. UWB filter using short circuited quarter wavelength stubs is explained in [33]. In 2013, D. Pakiaraj reported filter [34] based on short circuited meandered coupled lines with rectangular shaped slots incorporated in the ground plane. The UWB filter reported by [35] gives a fractional bandwidth of only 42% with centre frequency 3.5GHz.

Works have been reported in the field of bandpass filter design by using different types of coupled resonators [36]-[44]. Yo Shen Lin reported [36] a bandpass filter with lumped inductors placed between coupled lines to realize K inverters. Even though the response was good, the structure was not compact. Jia-Sheng Hong and Hussein Shaman proposed [37] a UWB microstrip-filter having passband from 3.5 to 14.5GHz with design based on a circuit model for an optimum short-circuited stub transmission-line filter. Liang Han et al. reported in their work, demonstrated the integration of UWB filter using wire bonded four line interdigital capacitors in commercial package [39].

The Ground Plane Aperture (GPA) technique reported by Velazquez-Ahumada [45] and Anka Rao Putla [46] which incorporated a microstrip line with a centered slot at the ground plane, found attractive applications in 3 dB edge coupler for tight coupling and bandpass filters for spurious band suppression and enhanced coupling.

Filters with Defected Ground Structures (DGS's) and Complementary Split Ring Resonators (CSRR's) were proposed for microwave applications. In this area several researches were being reported [47]-[84]. Wen-Jeng Lin et al. in 2008 designed a UWB bandpass filter [47] with short-circuited stubs and defected ground structure. Even though the response was reasonably good, the design was not compact. Zheng-Zheng Hou et al. in their work [48], claimed the design of a bandpass filter in 1-2.4GHz range using cascaded SRR. But the attenuation in the lower stopband was not very promising and the structure not compact. M. Shobeyri and M. H. Vadjed Samiei attempted [50] the design of bandpass filter using a combination of lowpass filter using DGS and highpass filter using coupled short circuited stubs. The work, though claims to have achieved the passband it was not compact and stopband attenuation is yet to be improved. Chaudhuri. R et al. reported [51] a UWB filter in 2011, using a cascade of lowpass and highpass filters employing SRR's and defected ground structures. B Xia et al. reported an ultra-wideband filter designed using defected ground structures [53]. The filter uses U-shaped and H-shaped DGS. Yashika Saini et al. proposed a UWB filter with defected ground structures employing a cascade of highpass and lowpass filters. Even though the filter exhibits reasonable performance, the size is not compact.

Amir Reza Dastkhosh et al. exploited [62] the effects of adaptive genetic algorithms (AGA's) and defected ground structures on performance optimization of tapered

microstrip filter. The proposed filter achieved an insertion loss of 0.8 dB from DC up to 4GHz and 21 dB rejection in the stopband. In 2013, Bo Jiang[63] reported a wide band bandpass filter, with centre frequency 3GHz using slotline ring resonator. J. An et al. proposed [66] a coupled defected ground structure synthesized by etching Von Koch fractal shape slot in the ground plane and series capacitive gap in the conductor strip. Unlike the structures loaded with complementary split ring resonators (CSRR's), the proposed structure was claimed to operate at very wide band. A UWB filter using the above structure was fabricated and tested. The relative bandwidth of the 10 dB return loss was 128% and the insertion loss better than 1.5 dB except at high frequencies. I.Tseng Tang et al. proposed in 2008 [68] UWB band-pass filter structure using five short-circuited stubs with reverse double U-shape defected ground structure (RDU-DGS), which exhibits a very wide bandwidth from 3.1 GHz to 10.6 GHz.

The efforts for miniaturization have been reported in lot of works [82]-[86], but not much in ultra wide band area. The authors tried different options like use of fractals, metamaterials, etc. I. A. I. Al-Naib proposed [82] single metal layer metamaterial bandpass filters based on compact complementary u-shaped resonators, a concept that could directly be integrated with a single sided coplanar waveguide. The designed filter was at a center frequency of 3.75 GHz. B. Lopez-Garca et al. designed [86] a bandpass filter with center frequency 2.4GHz using metamaterial inspired Epsilon Near Zero (ENZ) and Mu Near Zero (MNZ) behaviors. The miniaturization achieved by this method can be studied to extend in UWB range.

In coplanar waveguide, some works are reported, [87]- [99] but the roll-off at the lower passband edge were not sharp for most of them. Also the electrical size appeared to

be relatively large. Drawbacks and future scopes in these works are analyzed. Yu-Kang Kuo used bended short-end parallel stubs together with the folded open-end series stubs [90] to design a broadband filter, and slow-wave structures were adopted to implement a narrowband filter. Hang Wang et al. presented [92] a filter design using the hybrid microstrip and coplanar waveguide structure for use in ultra wide band. Even though the authors claimed to have acquired the bandwidth and low insertion loss, the roll off at the lower band edge was not so good.

S.-N.Wang and N.-W Chen proposed [94] CPW-BPF designed by exploiting CPW short stub and open-stub structures that were connected in a cascade topology. The bandwidth achieved was 2.8-10.1GHz. Tsung-Nan Kuo et al. suggested [95] compact ultra-wide band bandpass filters based on the composite microstrip/coplanar waveguide structure. The structure seemed to be quite complex.

Keren Li in his work [99], presented an ultra-wide band bandpass filter using broadside coupled microstrip/coplanar waveguide structure. The 3-section filter demonstrated the UWB performance, 10dB bandwidth from 3.0 GHz to 10.63 GHz. Although the insertion loss and group delay were best suited for filter applications, the bandwidth considered at 10dB instead of 3dB. The author also claimed to have reshaped a step like negative pulse as a Gaussian doublet-like UWB pulse. Shau Gang Mao et al. [100] presented filters composed of two microstrip Conductor-Backed Co-Planar Waveguide (CBCPW) transitions with tunable transmission zeros. Although simulation studies showed good results, the structure was double layered making circuit integration difficult. Zhongbao Wang and Shaojun Fang reported [101] a coplanar waveguide filter using stepped impedance conductor backed structure to realize

controllable dual band bandpass filter.

Notched filters have been studied and reported [12]- [112]. Pankaj Sarkar et al. reported a dual notch band filter [12] with notches at 5.46GHz and 8.04GHz. L. Chen et al. constructed [105] an Ultra Wideband filter with multiple mode resonators with a notch at 5.8GHz. The structure is bit complex and requires dimensions which may impose fabrication problems. P.Y. Hsiao and R.M. Weng tried to develop a UWB filter [106] with notches at 3.5GHz and 5.8GHz for WLAN/WiMAX applications. The band attained was 2.6-9.6GHz and the attenuation at the notches was only 10dB. Moreover the structure was quite complex. Harish Kumar et al. implemented a UWB filter [109] using aperture backed parallel coupled microstrip lines and then used a quarter wave length stub to introduce a notch at 5.8GHz. In 2014, Huaxia Peng [112] reported a UWB filter with triple notch bands centered at 5.2GHz, 5.8GHz and 6.8GHz using triple mode stepped impedance resonators and interdigital coupled lines.

There has been relatively little work being reported on ultra wide band BPFs employing uniplanar , coplanar waveguide (CPW) structures.

1.6 Motivation

Mobile devices are the enabling centerpiece of digital convergence and the digital gateway for the real world to adapt to the ever demanding human needs. The society is now entering the era of ‘wearable’ mobile technology with smart glasses, and smart watches. Addition of mobile network components offers undeniable business benefits, both direct and indirect and wireless networking moves into the mainstream. Wireless

technologies provide considerable savings in networking cost and a degree of flexibility not known in wired systems.

In the present scenario, there is a strong customer desire to have compact, portable, cheap, secured and easy to use devices with high data/video transfer capability within home and office environments. Sensors and embedded wireless controllers are increasingly needed in a variety of appliances and applications. PDA's and mobile computers are regularly connected to e-mail and internet services through wireless communications, and wireless local area networks for computers are becoming common in public areas like universities, airports etc.

With its high data capacity, UWB devices will be the right candidates to meet this demand. UWB communications technology provides a practical means of low power, high-data-rate transmissions over short distances, such as in personal area networks (PAN's). Wireless USB offers high data rates (480Mbps at 3mtrs and 110Mbps at 10mtrs) and a superior power management scheme that will help it prevail over other more power hungry interface technologies. Along with its merits, cost benefits are added as FCC announced deregulation of the UWB band. Thus UWB is expected to have great impact on home networking and entertainment market. Being low power technology, it is best suited for mobile devices. The technology is also suitable for long-range applications, such as radar systems.

All UWB communication systems require key building blocks such as bandpass filters and bandstop filters, consisting of wider bandwidth, low insertion loss and flat group delay properties. High performance filters with adequate bandwidths are essential in order for UWB systems to co-exist with current wireless communications

systems.

The research aims to understand the design trade-offs and build optimum filters for UWB systems. A bottom-up design strategy is followed, wherein the constraining metrics like lower and upper cut off frequencies, are met first, further building on it to meet the optimizing metrics like passband insertion loss, stopband attenuation and roll off rate. Optimizing one metric may adversely affect another, hence requires a trade off in most cases. Lumped element equivalent circuit models are developed for each of the planar filters designed, which helps in identifying the circuit behavior in a better detail. Generalized design equations are developed in all cases to help designing similar filters on different substrates. Dispersion characteristics of the developed filters are studied to ensure their linear phase nature. Time domain behaviour is examined with the help of unit step response of the filters.

Proposed designs are simple, compact, planar, repeatable and reproducible with minimum turnaround time.

1.7 Thesis Organization

The thesis consolidates the entire work carried out into 7 chapters and appendices A and B. The references relevant to each chapter are given after every chapter summary. Pictorial representation of the organization of the thesis is given in Fig. 1.7. Chapter 1 discusses about the wireless communication technology with emphasis on UWB communication and role of filters. It also details the different types and categories of filters used in various applications, design methods, challenges etc. A section is set

Thesis Organization

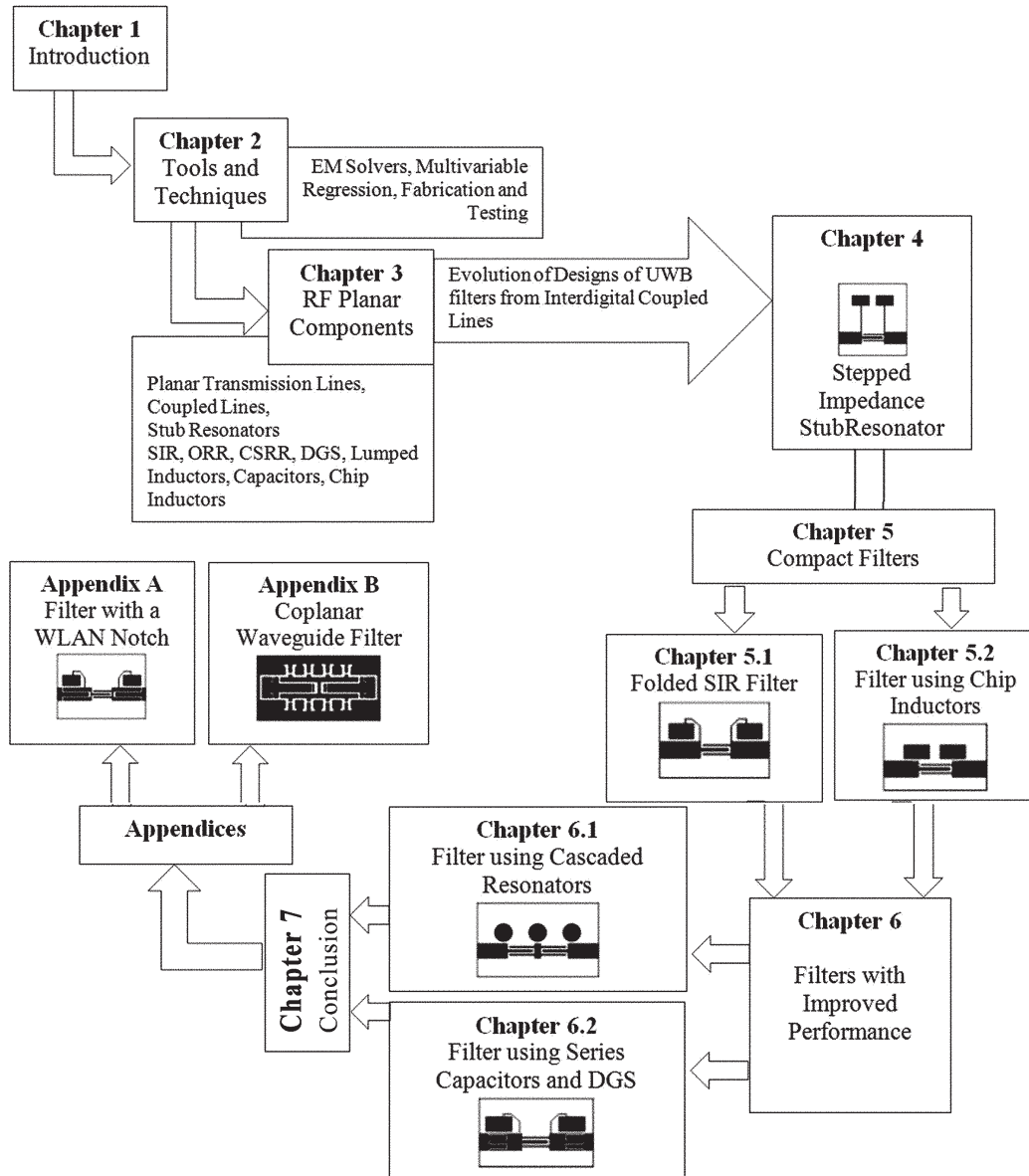


Figure 1.7: Organization of the Thesis

aside for deliberations about important filter parameters in both time and frequency domain which are crucial in the performance analysis and hence looked into while designing. The chapter also includes a review of similar work in literature.

Chapter 2 provides an overview of simulation software and optimization studies used for the design and development, multivariable regression used in formulating design equations, fabrication method adopted and the measurement setup used.

A study of various planar/lumped components which are rendered useful in the design of filters developed is included in Chapter 3. The behavior of these components under varying parameters is analyzed through simulation studies and their use in filter designs is justified.

Chapters 4-6 explain the step by step design and development of various UWB filters. This includes the geometry, simulation studies, field study at various frequencies of interest, analysis and generalized design equations, LC equivalent circuit model and response, dispersion studies, measured results etc. In chapter 4 a stepped impedance stub resonator filter is designed. The response of filter is reasonably good. In chapter 5, attempts are made to reduce the size of the filter without affecting the performance. Two compact filters are designed and explained in two sections of chapter 5.

Chapter 6 describes two more filters with improved performance, mainly roll off rate and stopband attenuation. A filter with cascaded resonators is explained in section 1 of chapter 6. This is the traditional method for improving the filter performance. Section 2 of the chapter explains another filter employing planar components such as series capacitors and DGS. This has the advantage of independently controlling the filter characteristics.

Chapter 7 describes the highlights of the thesis. The inferences from the various studies conducted and proved fruitful in the design are given in this chapter. Salient features of the designed filters are included along with a comparison of parameters of the developed filters. The chapter concludes with suggestions for future research.

Filter designs with a WLAN notch and another on coplanar waveguide are included as two appendices.

Bibliography

- [1] “Ultra-Wideband: Past, Present and Future”, EUWB Consortium; White Paper, June 2011.
- [2] First Report and Order FCC, Federal Communications Commission Revision of Part 15 of the Commission’s Rules Regarding Ultra-Wideband Transmission Systems, Feb. 2002.
- [3] Directive 2004/108/EC of The European Parliament and of The Council, Official Journal of the European Union, Dec. 2004.
- [4] Homayoun Nikookar, Ramjee Prasad, “Introduction to Ultra Wide Band for Wireless Communications”, Springer Science, 2009, e-ISBN: 978-1-4020-6633-7.
- [5] Faranak Nekoogar, “Ultra-Wideband Communications: Fundamentals and Applications”, Prentice Hall, ISBN :0-13-146326-8.
- [6] Maria Gabriella Di Benedetto, Thomas Kaiser, Andreas F Molisch, Ian Oppermann, Christian Politano, and Domenico Porcino, “UWB Communication Systems: A Comprehensive Overview”, Hindawi Publishing Corporation, New York, ISBN 977-5945-10-0.
- [7] Cam Nguyen, Jeongwoo Han, Time Domain Ultra Wide Band Radar, Sensor and Components Theory Analysis and Design”, Springer, USA, ISBN 978-1-4614-9578-9 (ebook)
- [8] Robert Aiello, Anuj Batra, “Ultra Wideband Systems Technologies and Applications”, Elsevier Inc. USA, 2006, ISBN 13:978-0-7506-7893-3.
- [9] Ismael Pele, Marie Crespin, Yann Mahe, and Serge Toutain, “Association of a UWB Filter with a UWB Antenna : Control of Antenna Characteristics”, IEEE Antennas and Propagation Society International Symposium, pp.1425-1428, June 2007.

-
- [10] "Preferred Channel Arrangements for Fixed Service Systems Operating in the Frequency Band 10.7 - 11.7 GHz", CEPT/ERC/Recommendation 12-06 E, Rome 1996, Revised, Rottach Egern, February 2010.
- [11] Andreas Antoniou, "Digital Signal Processing: Signals, Systems and Filters", Mc Graw-Hill, ISBN- 978-0071454247.
- [12] M.Makimoto and S Yamashita, "Microwave Resonators and Filters for Wireless Communication; Theory, Design and Applications", Springer, ISBN-13: 978-3540675358.
- [13] Jorge A. Ruiz-Cruz, Chi Wang and Kawthar A. Zaki, "Advances in Microwave Filter Design Techniques", Microwave Journal, pp. 26-44, Nov. 2008
- [14] David M. Pozar, "Microwave Engineering", Second Edition, John Wiley & Sons Inc., USA, ISBN 0-471-17096-8.
- [15] Ernst. C, Postoyalko. V, Khan, N.G, "Relationship between group delay and stored energy in microwave filters", IEEE Transactions on Microwave Theory and Techniques, Vol. 49, pp.192-196, Jan. 2001.
- [16] Inder Bahl "Lumped Elements for RF and Microwave Circuits", Artech House Inc., London, ISBN 1-58053-309-4.
- [17] T. C. Edwards, M. B. Steer, "Foundations of Interconnect and Microstrip Design", Third Edition, John Wiley & Sons, Ltd. NewYork, ISBN 0-471-60701-0.
- [18] Christophe Caloz, Tatsuo Itoh, "Electromagnetic Metamaterials: Transmission Line Theory and Microwave Applications- The Engineering Approach", John Wiley & Sons Inc., ISBN-10: 0-471-66985-7.
- [19] Milka M. Potrebi, "Microwave Filters with Concentrated Impulse Response in Microstrip Technology", 17th Telecommunications forum TELFOR, pp.883-890, Nov.2009.

- [20] Lei Zhu and Wolfgang Menzel, "Compact Microstrip Bandpass Filter with Two Transmission Zeros Using a Stub-Tapped Half-Wavelength Line Resonator", *IEEE Microwave and Wireless Components Letters*, Vol.13, No.1, pp.16-18, Jan.2003.
- [21] Wen-Hua Tu and Kai Chang, "Compact Second Harmonic-Suppressed Bandstop and Bandpass Filters Using Open Stubs", *IEEE Transactions on Microwave Theory and Techniques*, Vol.54, No. 6, pp.2497-2502, June 2006.
- [22] Pramod K. Singh, Sarbani Basu and Yeong-Her Wang, "Planar Ultra-Wideband Bandpass Filter Using Edge Coupled Microstrip Lines and Stepped Impedance Open Stub", *IEEE Microwave and Wireless Components Letters*, Vol.17, No.9, pp.649-651, Sep.2007.
- [23] Rui Li, Sheng Sun and Lei Zhu, "Synthesis Design of Ultra-Wideband Bandpass Filters with Composite Series and Shunt Stubs", *IEEE Transactions on Microwave Theory and Techniques*, Vol. 57, No. 3, pp.284-286, Mar.2009.
- [24] K.-S. Chin and D.-J. Chen, "Novel Microstrip Bandpass Filters Using Direct Coupled Triangular Stepped Impedance Resonators for Spurious Suppression", *Progress in Electromagnetics Research*, Vol.12, pp. 11-20, 2009.
- [25] Qing-Xin Chu and Xu-Kun Tian, "Design of UWB Bandpass Filter Using Stepped-Impedance Stub-Loaded Resonator", *IEEE Microwave and Wireless Components Letters*, Vol.20, No.9, pp.501-503, Sep. 2010.
- [26] A. Namsang and P. Akkaraekthalin, "Microstrip Bandpass Filters Using End-Coupled Asymmetrical Step-Impedance Resonators for Wide-Spurious Response", *Progress in Electromagnetics Research C*, Vol. 14, pp.53-65, 2010.
- [27] Y.-L. Wu, C. Liao and X.-Z. Xiong, "A Dual-Wideband Bandpass Filter Based on E-Shaped Microstrip SIR with Improved Upper- Stopband Performance", *Progress in Electromagnetics Research*, Vol.108, pp.141-153, 2010.

- [28] Y.-C. Chiou and P.-S. Yang, "Transmission Zero Design Graph for Dual Mode Dual Band Filter with Periodic Stepped Impedance Ring Resonator", *Progress in Electromagnetics Research*, Vol.108, pp.23-36, 2010.
- [29] J. Xu, C. Miao, L. Cui, Y.-X. Ji and W. Wu, "Compact high isolation quad-band bandpass filter using quad-mode resonator", *Electronics Letters*, Vol. 48, No. 1, Jan. 2012.
- [30] W.-Y. Chen, M.-H. Weng, S.-J. Chang, H. Kuan and Y.-H. Su, "A New Tri-Band Bandpass Filter for GSM, WiMAX and Ultra-Wideband Responses By Using Asymmetric Stepped Impedance Resonators", *Progress in Electromagnetics Research*, Vol.124, pp.365-381, 2012.
- [31] C. G. Tan and K. M. Lum, "Ultra-wideband Bandpass Filter Using Symmetrical Step Impedance Resonators", *PIERS Proceedings, Moscow, Russia*, pp.1488-1490, Aug. 2012.
- [32] Manidipa Nath, "A Compact UWB Filter for Wireless Communication", *International Journal of Scientific Research Engineering and Technology (IJSRET)*, Vol.1, Issue2, pp.004-010, May 2012.
- [33] Sonu Raman, Amita Soni, "UWB Bandpass Filter With Quarter Short Circuited Stubs", *International Journal of Scientific and Engineering Research*, Vol.4, No.6, pp.1345-1348, May.2013.
- [34] D. Packiaraj, K. J. Vinoy, M. Ramesh and A. T. Kalghatgi, "Miniaturized Ultra Wide Band Filter with Extended Stopband", *Microwave and Optical Technology Letters*, Vol. 55, No.4, pp. 703-705, Apr. 2013.
- [35] Neelam Thakur and Ajay Kumar Yadav, "Design of Novel UWB Coupled Line Band Pass Filter with Improved Stop Band Performance", *International Journal of Engineering and Advanced Technology (IJEAT)*, Vol.3, June 2014.
- [36] Yo-Shen Lin, Chi-Hsueh Wang, Chao-Huang Wu and Chun Hsiung Chen, "Novel Compact Parallel Coupled Microstrip Bandpass Filters With Lumped-Element K-Inverters", *IEEE Transactions on Microwave Theory and Techniques*, Vol.53, No.7, pp.2324-2328, July 2005.

- [37] Jia-Sheng Hong and Hussein Shaman, "An Optimum Ultra-Wideband Microstrip Filter", *Microwave and Optical Technology Letters*, Vol.47, No.3, pp.230-233, Nov.2005.
- [38] J. Marimuthu and M. Esa, "Compact UWB PCML Bandpass Filter with L- and C-shaped Resonator", *Electronics Letters*, Vol.44, No.6, pp.419-420, Mar.2008.
- [39] Liang Han, Ke Wu and Xiupu Zhang, "Development of Packaged Ultra-Wideband Bandpass Filters", *IEEE Transactions on Microwave Theory and Techniques*, Vol.58, No.1, pp.220-228, Jan. 2010.
- [40] H.-W. Wu, S.-K. Liu, M.-H. Weng and C.-H. Hung, "Compact Microstrip Bandpass Filter with Multispurious Suppression", *Progress in Electromagnetics Research*, Vol.107, pp.21-30, 2010.
- [41] Sinia P. Jovanovi, "An Overview of Microwave Bandpass Filters with Capacitive Coupled Resonators", *Microwave Review*, pp.29-36, Dec.2010.
- [42] L. Chen, F. Wei, X.-W. Shi and C.-J. Gao, "An Ultra-Wideband Bandpass Filter with a Notch-Band and Wide Stopband Using Dumbbell Stubs", *Progress in Electromagnetics Research Letters*, Vol.17, pp.47-53, 2010.
- [43] Kaijun Song, and Quan Xue, "Ultra-Wideband (UWB) Bandpass Filters with Multiple Notched Bands Using Asymmetric Dual-Line Coupling Structure", *Proc., Asia-Pacific Microwave Conference*, pp.978-984, 2010.
- [44] Ram Krishna Maharjan and Nam-Young Kim, "Microstrip Even-mode Half-wavelength SIR Based I-band interdigital Bandpass Filter", *Indian Journal of Engineering Materials Science*, Vol. 19, pp. 299-303, Oct. 2012.
- [45] Velazquez-Ahumada, M. C, J. Martel and F. Medina, "Parallel Coupled Microstrip Filters with Ground-Plane Aperture for Spurious Band Suppression and Enhanced Coupling", *IEEE Transactions on Microwave Theory and Techniques*, Vol.52, pp.1082-1086, 2004.

- [46] Anka Rao Putla, S. S. Karthikeyan and Rakesh Singh Kshetrimayum, "Design of UWB Bandpass Filter using Ground Plane Aperture", *International Journal of Recent Trends in Engineering*, Vol. 1, No. 3, pp.271-273, May 2009.
- [47] Wen-Jeng Lin, I-Tseng Tang, Ding-Bing Lin Chi-Min Li, Min-Yuan Chiu and Mau-Phon Houn, "A Compact Ultra-Wideband Bandpass Filter with Low Insertion Loss Using Stub Circuits with Defected Ground Structure", *PIERS Proceedings, Cambridge*, pp.562-565, July 2008.
- [48] Zheng-Zheng Hou, Xing-Xing Li and Chao-Kun Hao, "Design of Wideband Filter Using Splitting Resonator DGS", *Progress in Electromagnetics Research Symposium, Hangzhou*, pp.33-36, Mar. 2008.
- [49] L. H. Weng, Y. C. Guo, X. W. Shi and X. Q. Chen, "An Overview on Defected Ground Structure", *Progress in Electromagnetics Research B*, Vol.7, pp.173-189, 2008.
- [50] M. Shobeyri and M. H. VadjedSamiei, "Compact Ultra-Wideband Bandpass Filter with Defected Ground Structure", *Progress in Electromagnetics Research Letters*, Vol.4, pp.25-31, 2008.
- [51] Chaudhuri. R, Mukherjee. S and Saha. C, "Design of UWB filter using DGS and Slot SRR array with band rejection for IEEE 802.11a WLAN", *IEEE Applied Electromagnetics Conference (AEMC), Kolkata*, pp. 1-2, Dec. 2011.
- [52] Keskin, A.K, Yildiz and Partal, H.P, "An UWB High-Q Bandpass Filter with Wide Rejection Band using Defected Ground Structures", *IEEE International Conference on Ultra-Wideband (ICUWB), Syracuse, NY*, pp.99-102, Sep. 2012.
- [53] B. Xia, L.-S. Wu and J. F. Mao, "An Ultra-Wide band Balanced Bandpass Filter Based on Defected Ground Structures", *Progress in Electromagnetics Research C*, Vol. 25, pp.133-144, 2012.
- [54] Maryam Jaldi and Majid Tayarni, "Design of Ultra Wideband Bandpass Dual Band Filter Using Defected Ground Structures", *International Journal of Information and Electronics Engineering*, Vol. 3, No. 1, pp.59-62, Jan. 2013.

- [55] Shraddha Sharma, Raj Kumar, Raghupatruni V. S. R. Krishna³ and Rajas Khokle, "Design Of Defected Ground Band Pass Filters Using Stepped Impedance Resonators", *Progress in Electromagnetics Research B*, Vol. 54, pp.203225, 2013.
- [56] Neelamegam, Nakkeeran R and Thirumalaivasan K, "Development of Compact Bandpass Filter using Defected Ground Structure for UWB Systems", *International Journal of Microwaves Applications*, Vol. 2, No. 1, pp.28-31, Jan. 2013.
- [57] Yashika Saini and Mithilesh Kumar, "Design and Analysis of Compact UWB Bandpass Filter with Wide Passband Using Defected Ground Structure", *American Journal of Engineering Research (AJER)*, Vol. 03, No. 8, pp-267-272, 2014.
- [58] M. Kazerooni, A. Cheldavi and M. Kamarei, "A Novel Bandpass Defected Microstrip Structure (DMS) Filter for Planar Circuits", *PIERS Proceedings, Moscow*, pp.1214-1217, Aug.2009.
- [59] I.Gil, R. Fernandez, Y. Vives, R. Jauregui and F. Silva, "Characterization of EMI Filters Based On Metamaterials", *Electromagnetic Compatibility - EMC Europe, International Symposium*, pp.1-3, June.2009.
- [60] Anjini Kumar Thiwari and Nisha Gupta, "Performance of Microstrip Lowpass Filter on Electromagnetic Band Gap Ground Plane", *IETE Journal of Research*, Vol. 56, pp.230-234, Sep.2010.
- [61] Mudrik Alaydrus, "Designing Microstrip Bandpass Filter at 3.2 GHz", *International Journal on Electrical Engineering and Informatics*, Vol. 2, No. 2, pp.71-83, 2010.
- [62] Amir Reza Dastkhosh, Gholamreza Dadashzadeh and Mohammad Hossein Sedaaghi, "New Design Method of UWB Microstrip Filters Using Adaptive Genetic Algorithms with Defected Ground Structures", *International Journal of Microwave Science and Technology*, Vol. 2010, pp.1-9, Mar.2010.

- [63] Bo Jiang, Lei Zhu and Dong Chen, "A Novel Wide Band Bandpass Filter Using Triple Mode Slotline Ring Resonator", *Progress in Electromagnetics Research Letters*, Vol. 40, pp.163-170, 2013.
- [64] Bian Wu, Bin Li, Tao Su and Chang-Hong Liang, "Study on Transmission Characteristic of Splitting Resonator Defected Ground Structure", *PIERS Online*, Vol.2, No.6, pp.710-714, 2006.
- [65] Si-Weng Fok, Pedro Cheong, Kam-Weng Tam and Rui P. Martins, "A Novel Microstrip Square-Loop Dual-Mode Bandpass Filter With Simultaneous Size Reduction and Spurious Response Suppression", *IEEE Transactions on Microwave Theory and Techniques*, Vol.54, No.5, pp.2033-2041, May 2006.
- [66] J. An, G.-M. Wang, W.-D. Zeng and L.-X. Ma, "UWB Filter Using Defected Ground Structure of Von Koch Fractal Shape Slot", *Progress in Electromagnetics Research Letters*, Vol. 6, pp. 61-66, 2009.
- [67] Ji-Chyun Liu, Hsieh-Chih Lin et al., "An Improved Equivalent Circuit Model for CSRR-Based Bandpass Filter Design With Even and Odd Modes", *IEEE Microwave and Wireless Components Letters*, Vol. 20, No. 4, pp.193-195, Apr. 2010
- [68] I.Tseng Tang, Ding-Bing Lin, Chi-Min Li and Min-Yuan Chiu, "A Novel Ultra-wideband Bandpass Filter", *Progress in Electromagnetics Research Symposium, Cambridge*, pp. 91-94, July 2008.
- [69] Isaias Zagoya-Mellado, Alonso Corona-Chavez and Ignacio Llamas-Garro, "Miniaturized Metamaterial Filters Using Ring Resonators", *IEEE MTT-S International Microwave Workshop*, pp.45-49, Feb. 2009.
- [70] R.N Baral and P.K Singhal, "Miniaturized Microstrip Bandpass Filter Using Coupled Metamaterial Resonators", *International Journal of Microwave and Optical Technology*, Vol.4, No.2, pp.115-118, Mar. 2009.

- [71] S. S. Karthikeyan and Rakshesh Singh Kshetrimayum, "Performance Enhancement of Microstrip Bandpass Filter using CSSRR", International Conference on Advances in Computing, Control and Telecommunication Technologies, pp.67-70, Dec. 2009.
- [72] J. C. Liu and H. C. Lin, "Complementary Split Ring Resonators with Dual Mesh-Shaped Couplings and Defected Ground Structures for Wide Pass-Band and Stop-Band BPF Design", Progress in Electromagnetics Research Letters, Vol.10, pp.19-28, 2009.
- [73] Cherinet Seboka Ambaye, Guoping Zhang and Yunhu Wu, "Ultra Wide Band Filter from Defected Ground Structures as Complementary Split Ring Resonator by with Simultaneously Double Negative Permittivity ϵ and permeability μ ", International Journal of Engineering Research and General Science, Vol. 2, No. 4, June-July, 2014.
- [74] Wen-Ling Chen and Guang-Ming Wang, "Effective Design of Novel Compact Fractal-Shaped Microstrip Coupled-Line Bandpass Filters for Suppression of the Second Harmonic", IEEE Microwave and Wireless Components Letters, Vol.19, No.2, pp.74-76, Feb. 2009.
- [75] Miguel Durn-Sindreu, Adolfo Vlez, Francisco Aznar, Gerard Sis, Jordi Bonache and Ferran Martn, "Applications of Open Split Ring Resonators and Open Complementary Split Ring Resonators to the Synthesis of Artificial Transmission Lines and Microwave Passive Components," IEEE Transactions on Microwave Theory and Techniques, Vol.57, No.12, pp.3395-3403, Dec. 2009.
- [76] A.R. H. Alhawari and A. Ismail, "Compact Wideband Bandpass Filter Using Single Corners-Cut Isosceles Triangular Patch Resonator", Progress in Electromagnetics Research C, Vol.14, pp.227-237, 2010.
- [77] Hung-Wei Wu and Cheng-Yuan Hung, "Equivalent Circuit Model of the Slotted Ground Structures (SGS's) Underneath the Microstrip Line", Proc., International Multiconference of Engineers and Computer Scientists, Vol.2, Mar. 2010.

- [78] L. Borja, J. Carbonell, V. E. Boria, J. Cascon and D. Lippens, "A 2% Bandwidth C-Band Filter Using Cascaded Split Ring Resonators", *IEEE Antennas and Wireless Propagation Letters*, Vol.9, pp.256-259, Mar. 2010.
- [79] J.-K. Xiao, H.-F. Huang and Jeffrey S. Fu, "Single Trapezoidal Patch Resonator Bandpass Filter", *Proc., IEEE International Conference on Ultra-Wideband ICUWB*, pp.1-4, Sep. 2010.
- [80] Masaya Tamura, Toshio Ishizaki and Michael Hft, "Design and Analysis of Vertical Split Ring Resonator and its Application to Unbalanced Balanced Filter", *IEEE Transactions on Microwave Theory and Techniques*, Vol.58, No. 1, pp.157-164, Jan. 2010.
- [81] B. Ghahremani and M. Kamyab, "The Design of a Novel Compact CRLH Bandpass Filter with Harmonics Suppression", *Progress in Electromagnetics Research C*, Vol.16, pp.99-110, 2010.
- [82] I.A I-Naib, C. Jansen and M. Koch, "Single Metal Layer CPW Metamaterial Bandpass Filter", *Progress in Electromagnetics Research Letters*, Vol.17, pp.153-161, 2010.
- [83] S. Y. Zheng, W. S. Chan and K. F. Man, "Multi-Function Patch Element", *Progress in Electromagnetics Research*, Vol.109, pp.159-174, 2010.
- [84] Deena A. Salem, Ashraf. S. Mohra and A. Sebak, "A compact ultra wideband bandpass filter using arrow coupled lines with defected ground structure", *Vol. 1, Issue 1*, pp. 3644, May 2014.
- [85] G. Jang and S. Kahng, "Design of a Dual-Band Metamaterial Bandpass Filter Using Zeroth Order Resonance", *Progress in Electromagnetics Research C*, Vol.12, pp.149-162, 2010.
- [86] B. Lopez-Garca, D. V. B. Murthy and A. Corona-Chavez, "Design of A Dual-Band Metamaterial Band Pass Filter Using Zeroth Order Resonance", *Progress in Electromagnetics Research*, Vol.113, pp.379-393, 2011.
- [87] Rizwan Masood and Syed A. Mohsin, "Characterization of a Coplanar Waveguide Open Stub-Based Discontinuity for MMICs and Filter Applications", *International Journal of Antennas and Propagation*, 2012.

- [88] Junding Zhao, Jianpeng Wang and Jia-Lin Li, "Compact Microstrip UWB Bandpass Filter with Triple-Notched Bands", *Progress in Electromagnetics Research C*, Vol. 44, pp.1326, 2013.
- [89] Thomas M. Weller, "Edge-Coupled Coplanar Waveguide Bandpass Filter Design", *IEEE Transactions on Microwave Theory and Techniques*, Vol.48, No.12, pp.2453-2458, Dec. 2000.
- [90] Yu-Kang Kuo, Chi-Hsueh Wang and Chun Hsiung Chen, "Novel Reduced-Size Coplanar Waveguide Bandpass Filters", *IEEE Microwave and Wireless Components Letters*, Vol. 11, No. 2, pp. 65-67, Feb. 2001.
- [91] S.K. Menon, K. Vasudevan, C.K. Aanandan and P. Mohanan, "Compact Asymmetric Coplanar Waveguide Filter", *Electronics Letters online*, Vol.41, No.11, May 2005.
- [92] Hang Wang, Lei Zhu and Wolfgang Menzel, "Ultra-Wideband Bandpass Filter with Hybrid Microstrip/CPW Structure", *IEEE Microwave and Wireless Components Letters*, Vol.15, No.12, pp.844-846, Dec. 2005.
- [93] Chao-Huang Wu, Chi-Hsueh Wang, Yo-Shen Lin and Chun Hsiung Chen, "Parallel Coupled Coplanar Waveguide Bandpass Filter with Multiple Transmission Zeros", *IEEE Microwave and Wireless Components Letters*, Vol.17, No.2, pp.118-120, Feb. 2007.
- [94] S.-N. Wang and N.-W. Chen, "Compact Ultra-Broadband Coplanar-Waveguide Bandpass Filter with Excellent Stopband Rejection", *Progress in Electromagnetics Research B*, Vol. 17, pp.15-28, 2009.
- [95] Tsung-Nan Kuo, Shih-Cheng Lin and Chun Hsiung Chen, "Compact Ultra-Wideband Bandpass Filters Using Composite MicrostripCoplanar-Waveguide Structure", *IEEE Transactions on Microwave Theory and Techniques*, Vol.54, No.10, pp.3772-3778, Oct. 2006.
- [96] Chin-Hsiung Chen, Ching-Ku Liao and Chi-Yang Chang, "Novel Multifold Finite-Ground-Width CPW Quarter-Wavelength Filters With Attenuation Poles", *IEEE Transactions on Microwave Theory and Techniques*, Vol.55, No.1, pp.128-136, Jan. 2007.

- [97] Jin-Won No and Hee-Yong Hwang, "A Design of Cascaded CPW Low-Pass Filter with Broad Stopband", *IEEE Microwave and Wireless Components Letters*, Vol. 17, No. 6, pp. 427-429, June 2007.
- [98] Jiunn-Jye Chang and Chih-Hong Sie, "Inductively/Capacitively Coupled Conductor-Backed Coplanar Waveguide Bandpass Filters Using Slow-Wave Stepped-Impedance Resonators", *Journal of Marine Science and Technology*, Vol. 17, No. 2, pp.137-144, 2009.
- [99] Keren Li, Kurita D and Matsui. T, "A novel UWB bandpass filter and its application to UWB pulse generation", *IEEE International Conference on Ultra Wide Band*, pp.446-451, Sep. 2005.
- [100] Shau-Gang Mao, Yu-Zhi Chueh, Chia-Hsien Chen and Min-Chun Hsieh, "Compact Ultra-Wideband Conductor-Backed Coplanar Waveguide Bandpass Filter with a Dual Band-Notched Response", *IEEE Microwave and Wireless Components Letters*, Vol.19, No.3, pp.149-151, Mar.2009.
- [101] Zhongbao Wang, Shaojun Fang, "A CPW Dual-Band Bandpass Filter with Independently Controllable Transmission Zeros", *Radio Engineering*, Vol. 22, No. 3, pp.739-744, Sep. 2013.
- [102] Pankaj Sarkar, Manimala Pal, Rowdra Ghatak and Dipak R. Poddar, "Miniaturized UWB Bandpass Filter with Dual Notch Bands and Wide Upper Stopband", *Progress in Electromagnetics Research Letters*, Vol. 38, pp.161-170, 2013.
- [103] Chun-Ping Chen, Yoshinori Takakura, Hiroshige Nihie, Zhewang MA and Tetsuo Ananda, "Design of Compact Notched UWB Filter Using Coupled External Stepped-Impedance Resonator", *Asia Pacific Microwave Conference*, pp. 945-948, Dec. 2009.
- [104] Zhang-Cheng Hao, Jia-Sheng Hong, Jonathan P. Parry and Duncan P. Hand, "Ultra-Wideband Bandpass Filter with Multiple Notch Bands Using Non uniform Periodical Slotted Ground Structure", *IEEE Transactions on Microwave Theory and Techniques*, Vol.57, No. 12, pp.3080-3088, Dec. 2009.

- [105] L. Chen, Y. Shang and Y.L. Zhang and F. Wei, "Design of a UWB Bandpass Filter with a Notched Band and Wide Stopband", *Microwave Journal*, Vol. 52, No.11, pp.96-105, Nov. 2009.
- [106] P.-Y. Hsiao and R.-M. Weng, "Compact Tri-Layer Ultra-Wideband Bandpass Filter with Dual Notch Bands", *Progress in Electromagnetics Research*, Vol.106, pp.49-60, 2010.
- [107] C. Y. Liu, T. Jiang, Y. S. Li and J. Zhang, "A Novel UWB Filter with Dual-notch-bands Characteristic Using Radial-multimode Loaded Stub Resonator", *Progress in Electromagnetics Research Symposium Proceedings, China*, pp.1119-1121, Sept. 2011.
- [108] L. Chen, F. Wei, X.-W. Shi and C.-J. Gao, "An Ultra-Wideband Bandpass Filter with a Notch-Band and Wide Stopband Using Dumbbell Stubs", *Progress in Electromagnetics Research Letters*, Vol.17, pp.47-53, 2010.
- [109] Harish Kumar, Vibhor Kumar Bhardwaj and Upadhayay M.D, "UWB Band Pass Filter with WLAN Notch", *ACEEE International Journal on Communications*, Vol.3, No.1, pp.45-47, Mar. 2012.
- [110] Fu, W.Y, Sun, C.M and Dong. Y.L, "Ultra-wideband Bandpass Filter with Multiple Notched Band", *Computational Problem-Solving (ICCP), International Conference*, pp.269-271, Oct. 2011.
- [111] Anil Kamma, Swapnil R. Gupta, Gopi S. Reddy and Jayanta Mukherjee, "Multi-Band Notch UWB Band Pass Filter with Novel Contiguous Split Rings Embedded In Symmetrically Tapered Elliptic Rings", *Progress in Electromagnetics Research C*, Vol. 39, pp.133-148, 2013.
- [112] Huaxia Peng, Junding Zhao and Bing Wang, "Compact Microstrip UWB Bandpass Filter with Triple-Notched Bands and Wide Upper Stopband ", *Progress in Electromagnetics Research*, Vol. 144, pp.185191, 2014.

2 Tools and Techniques

Contents

- ★ *Simulation and Optimization*
- ★ *Multivariable Regression*
- ★ *Fabrication and Testing*

This chapter introduces the different tools and techniques used in the design of various UWB filters. The classification of popular electromagnetic field solvers is given with emphasis on HFSSTM from ANSYS[®], which is used in the simulation studies. A brief explanation of multivariable regression used in the formulation of design equations for the developed filters is given in the chapter along with fabrication methods and the measurement setup used in the work.

Various types of tools and techniques used in the work is elaborated in this chapter. This include the tools for simulation and optimization, measurement techniques and methods used for developing generalized design equations for the various filters designed.

2.1 Simulation and Optimization

Designing and prototyping are made easy with the availability of a wide variety of commercially available Electromagnetic (EM) field solvers. They optimize the design and help to reduce the cost of production. Fig. 2.1 shows classifications of popular EM solvers. EM simulation has long been an essential modeling tool for RF/microwave

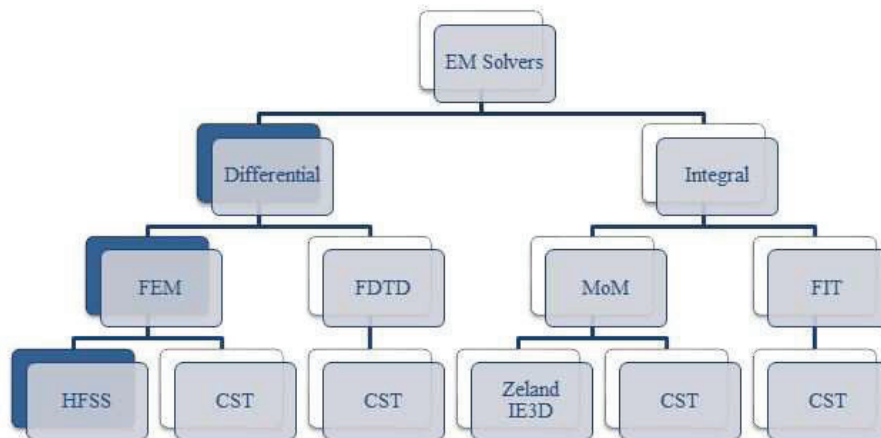


Figure 2.1: Classifications of Popular EM solvers

design. Electromagnetic field solvers simulate the structure behavior by solving (a subset of) Maxwell's equations directly. They are commonly used in the design of MMIC's and printed circuit boards when a solution from first principles is needed, or

the highest accuracy is required. They help to learn the circuit behavior under varying design aspects and thus save costly prototyping. All these CAD products provide analysis tools of unparalleled power and flexibility and can be selected based on the structure at hand.

Depending on the formulation of Maxwell's equations (differential/integral) there are two classes of solution methods. Differential equation based and Integral equation based [1]-[3].

Finite Element Method (FEM) is a good choice for solving partial differential equations over complex domains. FEM algorithms are suited to the problems that are electrically not large because of the necessity to use too much memory. Also the method can accurately model complex structures with curved boundaries. In FEM, the full problem space is divided into smaller regions (tetrahedral) forming a finite element mesh and the field in each region is represented by a local function. It stores the components of the fields at each vertex tangential to the three edges and the field at the midpoint of each edge. The value of field inside the tetrahedron is interpolated from these values. Maxwell's equations are formed from these field values. The accuracy depends on the size of the finite element. The smaller the mesh size, the better the accuracy, but more computing time and resources.

High Frequency Structure Simulator (HFSSTM) from ANSYS[®] Inc. is used in this work. It employs adaptive refining of mesh in error prone areas automatically. Also, the designer can define the mesh manually if desired. Since H field is computed from E field, the solution is more accurate for E field. The analysis is done by selecting a frequency sweep in the desired range of frequencies. For excitation, each port is assumed to be

connected to a uniform waveguide that has the same cross section as the port [4]. The software is used to observe the S parameters, group delay and step response for the various filters designed. It is also used to plot the electric and magnetic field distribution in various components in the structure at different frequencies. The Smith chart utility enabled the study of impedance variation at different frequency points.

ANSYS® Designer™ is used for the lumped model analysis of the designed filters. The Schematic Editor in the ANSYS® Designer™ tool is used to create circuit schematics, wherein the components, ports, connectors and wires are placed and analyzed in the frequency range of interest.

2.2 Multivariable Regression

The lower and upper cut off frequencies of the planar filter are dependent on a number of physical dimensions of the filter. Thus formulating the design equations necessitates relating the various dimensions of the filter to the required design parameters. Regression analysis is the best tool for relating multiple independent variables to a dependent variable.

The generalized design equations for lower and upper cut off frequencies for the various filter structures are formulated using the regression tool in Microsoft Excel [5]. This is a statistical tool that relates multiple independent variables to a dependent variable. Once it is identified how these multiple variables relate to the dependent variable, the information about all of the independent variables can be used to make much more powerful and accurate predictions about why things are the way they are.

This method is referred to as Multiple (or multivariate) Regression.

The accuracy of the method depends on the fitness of the data set chosen. Analysts must have a prior knowledge of the variables to be identified as independent variables in the model. For this, parametric analyses are conducted on the simulated transmission parameters by varying the dimensions of crucial elements in the filter structure. In the cases described in this thesis, the dependent variable is the parameter dominantly controlling the lower/upper cut off frequencies. The independent variables are other parameters such as substrate permittivity, thickness, and other dimensions. The data set is prepared by running simulations varying each of the independent variables keeping others constant.

2.3 Fabrication and Testing

The designed filters are fabricated on copper cladded substrate materials after forming suitable masks. Different aspects are to be considered in the selection of substrate materials as elaborated in following section.

2.3.1 Substrate Material

Selection of the most suitable substrate for an application is a matter of prime importance. The dielectric constant, loss tangent and slab thickness of the substrate have a pronounced effect on the fabricated filter performance. Right material chosen can provide excellent performance [6]-[7].

The dimensions of the transmission lines and distributed filter elements is inversely

proportional to the square root of the material's dielectric constant; in short, materials with higher dielectric constants make it possible to design and fabricate smaller filters for a given frequency.

Dielectric loss tangent is another important circuit material parameter for filter circuits. Quite simply, low values of loss tangent indicate materials capable of achieving low insertion loss. This also means high quality factor (Q), which translates into the potential for a filter with sharper transitions from passband to stopband [8].

In this work, FR4 and its low loss variants (obtained from Centre for Materials for Electronics Technology (C-MET), Thrissur) are used for fabricating the filter prototypes. FR-4 is the most commonly used substrate material possessing considerable mechanical strength. It is well proven and relatively low cost.

Negative photolithography is used for filter prototype fabrication.

2.3.2 Testing

Vector network analyzers are used for the measurement of parameters of the fabricated filter prototype. The measurements are taken utilizing the facilities at Centre for Research in Electromagnetics and Antenna (CREMA), under the Department of Electronics, CUSAT. The vector network analyzers used are the Agilent (HP) 8510 and E8362B PNA. These analyzers can make measurements from 45MHz to 50GHz and 10 MHz to 20 GHz respectively [9].

Fig. 2.2 shows the experimental setup. Network analysis is concerned with accurate measurement of ratios of the reflected signal to the incident signal and the transmitted signal to the incident signal. The accuracy of measurements depends on how well we

terminate the load port. It is to be terminated in perfect Z_0 . The characteristic impedance of 50Ω is chosen for microwave systems as an average value between those corresponding to minimum loss/length (77Ω) and maximum power handling (30Ω) of a 10mm coaxial cable. When DUT is connected to the network analyzer, the imperfect



Figure 2.2: Experimental Setup

matching of the test port should be carefully accounted for. One port calibration is done for reflection measurements and two port calibration for transmission measurements. This is done in the frequency range of interest. For filter measurements, both test ports are to be calibrated for reflection and transmission, so as to measure full two-port scattering matrices (S-parameters) for the device. For two port calibration measurement of known standards is taken. There are four standards; Short, Open, Load and Through. The definitions for these standards are available with the calibration kit.

The measurements for insertion loss, return loss, group delay, magnitude and phase are taken for all the fabricated prototype filters using this. Fig. 2.3 shows the generalized internal block diagram of a network analyzer.

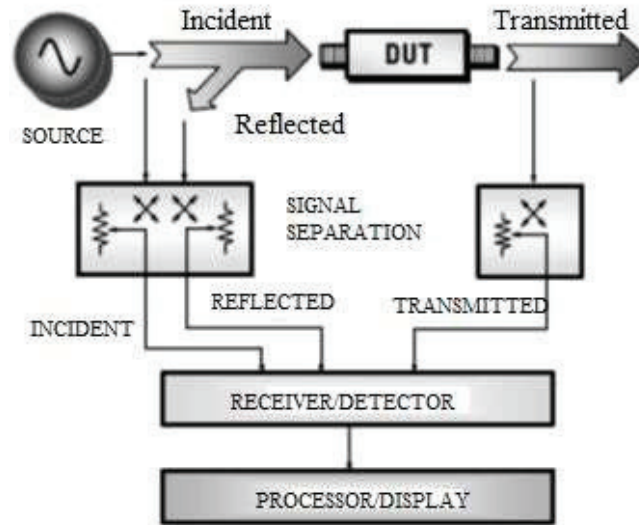


Figure 2.3: Network Analyzer-Generalized Internal Block Diagram

2.4 Summary

The chapter details the tools and techniques used in the research. It begins with a briefing of the various EM simulation softwares available in the market with emphasis on HFSSTM and its FEM method. The discussion about multivariable regression used for developing the design equations of the filters is included next. The role of substrate materials on the performance and the different fabrication methods adopted in this work are elaborated in the subsequent sections and finally the vector network analyzer and the measurement set up used are explained.

Bibliography

- [1] A Vasylichenko, Y Schols, W De Raedt and G.A.E Vandenbosch, “Quality Assessment of Computational Techniques and Software Tools for Planar-Antenna Analysis”, Antennas and Propagation Magazine, IEEE Vol.51 , pp.23-28, Feb.2009.
- [2] Guy A. E. Vandenbosch and Alexander Vasylichenko, “A Practical Guide to 3D Electromagnetic Software Tools Katholieke Universiteit Leuven, Belgium, www.intechopen.com.
- [3] Luca Pierantoni, Marco Farina et.al, “Comparison of the Efficiency of Electromagnetic Solvers in the Time-and Frequency-Domain for the Accurate Modeling of Planar Circuits and MEMS”, IEEE MTT-S Digest, pp. 891-894.
- [4] “Ansoft-HFSS Technical Notes”, Ansoft Corporation 1996-2001
- [5] Dan Remenyi, Gorge Onofrei and Joe English, “An Introduction to Statistics using Microsoft Excel”, ISBN 978-1-906638-55-9, Academic Publishing Ltd. 2009.
- [6] John Coonrod, “Choosing Circuit Materials for Millimeter wave Applications”, High Frequency Electronics, July 2013.www.highfrequencyelectronics.com.
- [7] John Coonrod, “Understanding When To Use FR-4 or High Frequency Laminates”, www.rogerscorp.com/documents/2122/acm/articles.
- [8] Russell Hornung, “Insertion Loss and Loss Tangent”, Application Notes, www.arlon-med.com.
- [9] www.agilent.com

3 RF Planar Components

★ ***Planar Transmission Lines***

Microstrip Line

Coplanar Waveguide

Coupled Lines

Interdigital Coupled Lines

★ ***Resonators***

Stub Resonators

Open Ring Resonators

Complementary Split Ring Resonators

Defected Ground Structures

★ ***Lumped/Semi Lumped Elements***

Inductors

Chip Inductors

Capacitors

This chapter discusses different planar components used in the design of UWB filters. Their behaviour is analyzed in support of their candidature in the design. These include planar transmission lines, coupled lines, half wavelength and quarter wavelength resonators, stepped impedance resonators, open ring resonators, split ring resonators, defected ground structures, lumped inductors and capacitors.

A microwave circuit consists of a number of components whose functions depend on the specific application intended. Engineering these components for a desired frequency response is often difficult and cost prohibitive, and usually the required frequency response may be obtained by the use of filters. Filters can be fabricated from lumped or distributed elements or a combination of both and can usually be designed for the precise frequency response required, at low cost [1]. Thus, they have been used for a very long time and are popular microwave components, present in virtually every microwave subsystem.

This section deals with different planar components used in the development of various filter structures. Most of the network lumped elements like inductors, capacitors, transformers etc. have their planar counterparts. The main difference between the lumped element and their planar counterpart is that the latter shows repetitive nature and distributed parameters. But these microstrip components have higher thermal stability compared to lumped element counterparts [2].

3.1 Planar Transmission Lines

The planar UWB filters presented in the thesis are developed from planar transmission lines formed by printing conducting strips on the surface of substrates.

Commonly used planar transmission lines include Microstrip, Strip line, Suspended Stripline, Finline, Coplanar Waveguide etc. Each has its own advantages and disadvantages and depending on the circuit types, any of these can be chosen. In some cases a hybrid combination may yield optimum performance [3]. Microstrip lines and

coplanar wave guides are the most popular guided wave structures used in the transmission of microwave signals. They support quasi-TEM mode of propagation.

3.1.1 Microstrip Line

The widespread use of microstrip line in microwave circuits owes greatly to its simple geometry, small size and ease of integration with printed circuit boards. It consists of a track of copper or other conductor (width W and thickness t) on an insulating substrate with dielectric constant ϵ_r and permeability μ_r and thickness h . (In this work, the dielectric material is evaluated as ferro-magnetic; $\mu_r = 1$). There is a backplane on the other side of the insulating substrate, formed from a similar conductor which acts as a return path. A microstrip configuration is illustrated in Fig. 3.1.

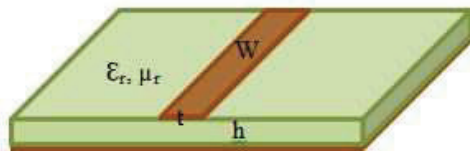


Figure 3.1: Microstrip Configuration

The fields in the microstrip extend within two media (air and dielectric) so that the structure is inhomogeneous. Due to this inhomogeneous nature, the microstrip does not support a pure TEM wave [4]. A pure TEM wave has only transverse components, and its propagation velocity depends only on the material properties, namely the permittivity and the permeability. However, with the presence of the two guided-wave media (the dielectric substrate and the air), the waves in a microstrip line will have longitudinal

components of electric and magnetic fields, and their propagation velocities will depend not only on the material properties, but also on the physical dimensions of the microstrip.

When the longitudinal components of the fields for the dominant mode of a microstrip line remain very much smaller than the transverse components, they may be neglected. In this case, the dominant mode then behaves like a TEM mode, and the TEM transmission line theory is applicable for the microstrip line as well. This is called the quasi-TEM approximation and it is valid over most of the operating frequency ranges of microstrip.

Fig. 3.2 shows the electric and magnetic field lines for fundamental quasi TEM mode in a microstrip. For transmission lines placed in inhomogeneous medium like

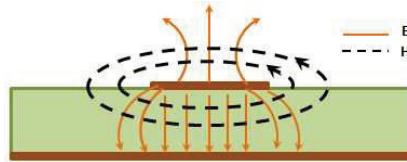


Figure 3.2: Electric and Magnetic Field Lines for Fundamental Quasi TEM in Microstrip

microstrip, the relative distribution of electric energy in the various regions of the inhomogeneous medium is taken into account by the effective dielectric constant ϵ_{re} . Closed form expressions have been developed by earlier researchers for evaluating the effective dielectric constant and characteristic impedance for a microstrip line.

$$\epsilon_{re} = \frac{\epsilon_r + 1}{2} + \frac{\epsilon_r - 1}{2} \frac{1}{\sqrt{1 + \frac{12h}{W}}} \quad (3.1)$$

$$\begin{aligned}
Z_0 &= \begin{cases} \frac{60}{\epsilon_{re}} \ln\left(\frac{8h}{W} + \frac{W}{4h}\right) & \text{for } \frac{W}{h} \leq 1 \\ \frac{120\pi}{\sqrt{\epsilon_{re}}\left(\frac{W}{h} + 1.393 + 0.667 \ln\left(\frac{W}{h} + 1.444\right)\right)} & \text{for } \frac{W}{h} \geq 1 \end{cases} \quad (3.2)
\end{aligned}$$

This expression for ϵ_{re} is based on the quasi-TEM or quasi-static approximation, and therefore is rigorous only with DC. At low microwave frequencies, these expressions provide a good approximation. At higher frequencies the effect of dispersion has to be considered. The effective dielectric constant ϵ_{re} is a function of frequency and can in general be defined as the frequency dependent effective dielectric constant $\epsilon_{re}(f)$. Approximate expressions for W/h in terms of Z_0 and ϵ_r , derived by Wheeler and Hammerstad are available [4].

$$\text{With } A = \frac{Z_0}{60} \sqrt{\frac{\epsilon_r + 1}{2}} + \frac{\epsilon_r - 1}{\epsilon_r + 1} \left(0.23 + \frac{0.11}{\epsilon_r}\right) \quad ; \quad B = \frac{377\pi}{2Z_0\sqrt{\epsilon_r}}$$

$$\begin{aligned}
\frac{W}{h} &= \begin{cases} \frac{2}{\pi} \left[(B-1) - \ln(2B-1) + \frac{\epsilon_r - 1}{2\epsilon_r} \left\{ \ln(B-1) + 0.39 - \frac{0.61}{\epsilon_r} \right\} \right] & \text{for } \frac{W}{h} \geq 2 \\ \frac{8e^A}{e^{2A} - 1} & \text{for } \frac{W}{h} \leq 2 \end{cases} \quad (3.3)
\end{aligned}$$

These equations are employed to compute the dimensions of various microstrip segments of the filter sections for achieving the desired frequency response and proper impedance matching. These expressions provide accuracy better than one percent. For more accurate results, an iterative or optimization process based on analysis models is employed. By the judicious choice of the substrate material, the size of the circuit can be reduced considerably.

Microstrip lines have a Q factor of about 250. The ground plane can be modified to improve electrical performance and reduce the size of the microstrip circuit. Modifications of the ground plane can be divided into the following categories: physical dimensions variance, use of defected ground plane structures (DGS) and ground plane apertures (GPA).

Transmission Characteristics of Microstrip Transmission Line

A simple transmission line behaves as a low pass filter [5]. Wave propagation through any medium requires time varying electric and magnetic fields. Requirement of electric field implies the existence of capacitor in the equivalent circuit model and requirement of magnetic field implies the existence of inductor. Fig. 3.3 shows the HFSS model of a microstrip transmission line, its equivalent circuit and transmission characteristics. In actual case the series impedance include a distributed resistance element and the shunt admittance include a distributed conductance element. The length of the transmission

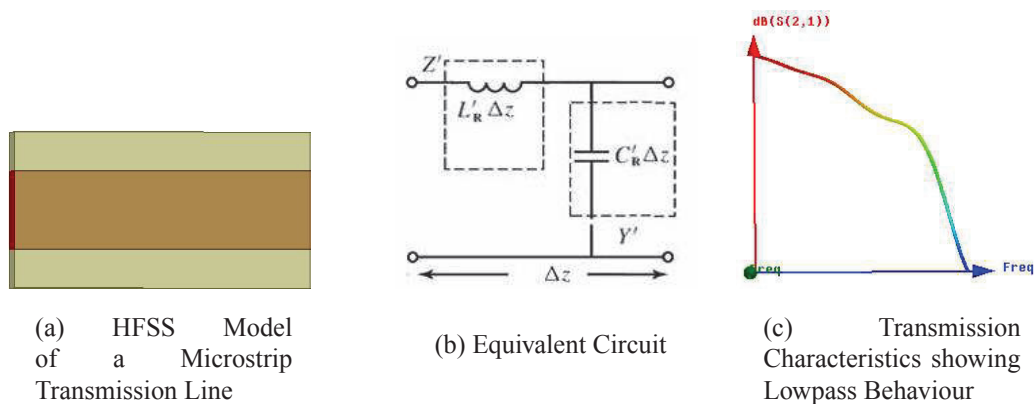


Figure 3.3: Microstrip Transmission Line, Equivalent Circuit & Transmission Characteristics

line is not of much importance in low frequency circuits. But it is important when the signal includes frequency components with corresponding wavelengths comparable to or less than the length of the wire.

Simulation studies are carried out to analyze the behaviour of microstrip transmission lines and other planar components. Dielectric substrate with relative permittivity $\epsilon_r=4.4$ and thickness 1.6mm is used for the simulations to follow. The frequency is chosen as 6.85GHz, the centre frequency of the UWB band under consideration.

In a quarter wavelength line, the current density plot shows maximum at one end and minimum at the other end. In the case of a half wavelength line there will be current maximum at both ends with minimum at the middle or vice versa, as depicted by the surface current distribution in Fig. 3.4. Here the guide wavelength is chosen for the center frequency 6.85GHz of the UWB band under study.

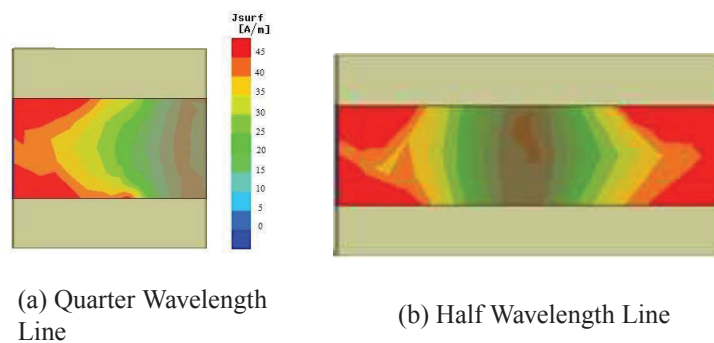


Figure 3.4: Surface Current Distribution of Transmission Line Sections

3.1.2 Coplanar Waveguide

In a coplanar waveguide all conducting elements, including the ground planes, are on the same side of a dielectric substrate. In conventional coplanar waveguide the conductors form a center strip separated by a narrow gap from two lateral ground planes on either side as shown in Fig. 3.5. The dimensions of the center conductor strip, the gap between conductor strip and ground planes, the thickness and permittivity of the dielectric substrate determine the effective dielectric constant, characteristic impedance and the attenuation of the line. Closed form expressions and iterative techniques for calculating the characteristic impedance and effective dielectric constant are given in [6]. The thickness of the dielectric substrate becomes less critical with higher relative dielectric constants. The gap in the coplanar waveguide is usually very small and supports electric fields primarily concentrated in the dielectric. Characteristic impedance depends on the ratio $W/(W+2s)$. This introduces considerable design flexibility. Due to the presence of ground plane between any two conductors, cross talk is minimized. Hence CPW circuits can be made denser compared to other planar circuits.

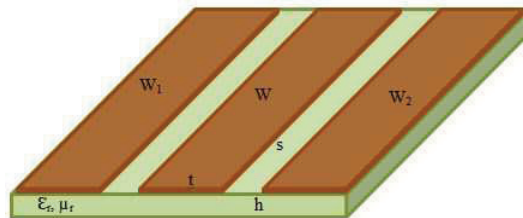


Figure 3.5: Coplanar Waveguide Configuration

With little fringing field in the air space, the coplanar waveguide exhibits low

dispersion. The expression for effective permittivity of CPW is given as

$$\epsilon_{re} = \frac{\epsilon_r + 1}{2} \quad (3.4)$$

In order to concentrate the fields in the substrate area and to minimize radiation, the dielectric substrate thickness is usually set to more than twice the gap width [7]. CPW has a zero cut-off frequency (suitable for wideband), but its low order propagation mode is approximated as Quasi-TEM. At higher frequencies ($\approx 20\text{GHz}$), the field becomes less-TEM, and more TE in nature with its magnetic field elliptically polarized [8]. The ground planes must be maintained at the same potential to prevent unwanted modes from propagating. The ideal CPW structure is conveniently considered as a pair of coupled slotlines with odd and even normal modes. The coplanar line has basically two dominant modes of propagation. The odd mode or quasi TEM mode referred to as the CPW mode and the even mode or non TEM mode referred to as slot line mode [6]. In CPW microwave circuits, CPW mode is the preferred mode due to low radiation properties. Excitation of unwanted slotline mode can be eliminated by either maintaining symmetry of the structure or by introducing air bridges to connect the ground planes of CPW. Fig. 3.6 shows the electric and magnetic field lines in CPW (odd) mode. The electric and magnetic field lines in slotline (even) mode are shown in Fig. 3.7. If the grounds are at different potentials, the CPW mode will become uneven, with a higher field in one gap than the other. Signal propagation through more than one mode is not desired since this causes signal loss and distortion at the receiver end. Air bridges between ground planes have to be applied to suppress the undesired slotline mode. CPW offers several advantages over conventional microstrip line. It simplifies

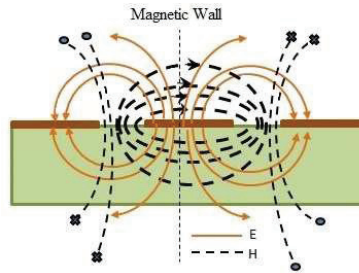


Figure 3.6: Electric and Magnetic Field Lines in CPW Mode (Odd)

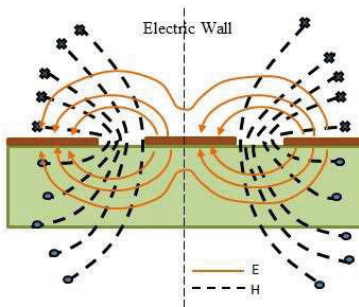


Figure 3.7: Electric and Magnetic Field Lines in Slotline Mode (Even)

fabrication and allows easy mounting of shunt and series active and passive components. It eliminates wraparounds and via holes and reduces radiation losses [6]. Coplanar waveguides are broadly classified into Conventional CPW, Conductor Backed CPW and Micro-machined CPW.

Microstrip and CPW formats are often selected over other high-frequency transmission line options, such as stripline, due to their simplicity. In spite of the many advantages listed above, CPW circuits can be lossier than comparable microstrip circuits, if a compact layout is needed. In terms of circuit size, CPW is at a disadvantage compared to a microstrip circuit, because its effective dielectric constant is lower.

The work done in this research is based on microstrip lines. The components described in this chapter are microstrip components unless specified otherwise.

3.1.3 Coupled Lines

Coupled lines may generally consist of two or more transmission lines. The lines are placed in close proximity such that the electromagnetic fields interact. When one port is excited with a known signal, a part of this signal appears at other ports. This interaction effect (coupling) is used in realizing several important microwave circuit functions such as directional couplers, filters and baluns, with the coupled line length usually being approximately a quarter-wave long.

Coupled lines can be symmetric (with lines of equal widths) or asymmetric (with lines of unequal widths). Due to the interaction of electromagnetic fields, they can support two distinct modes of propagation. In symmetric coupled lines, the electromagnetic waves propagate in general even and odd modes, which are two fundamental independent modes, whereas in asymmetrical coupled lines they are c & π modes. The c - mode is an even-like mode, while the π - mode is an odd-like mode. They exhibit bandpass characteristics as opposed to lowpass characteristics of a simple transmission line.

The electrical and magnetic fields of coupled lines with even and odd modes of propagation is shown in Fig. 3.8. The coupling between symmetrical lines can be determined in terms of phase velocities and characteristic impedances of the even and odd modes of coupled lines. Even mode wave propagates in lines if voltages in the signal strips are equal in magnitude and sign. Odd-mode wave propagates in case

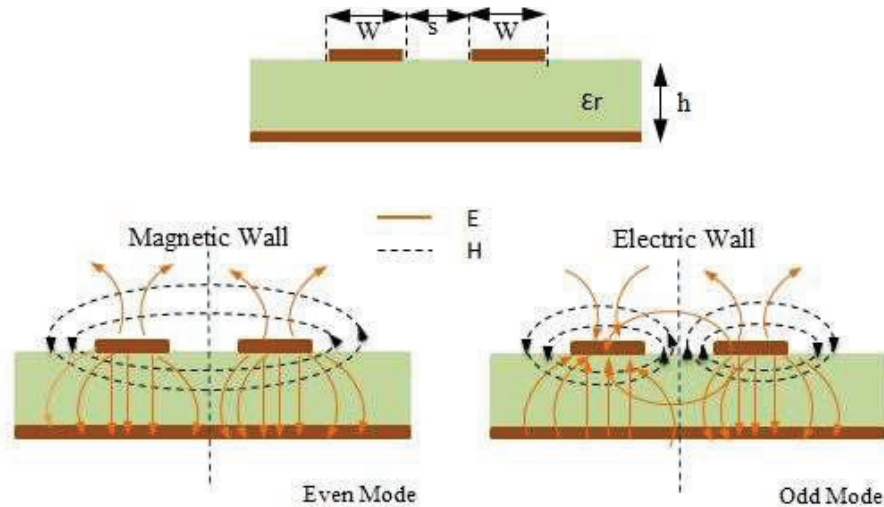


Figure 3.8: Electrical and Magnetic Fields of Coupled Microstrip Lines with Even and Odd Mode Propagation

voltages are equal in magnitude and opposite in sign. An arbitrary excitation of coupled line can always be treated as a superposition of appropriate amplitudes of even and odd modes [9]-[10]. Since the propagation mode is not purely TEM, the phase velocities and hence the effective permittivity in even and odd modes will be different. In general, a transmission line with n conductors in an inhomogeneous dielectric and a ground conductor supports n distinct normal quasi-TEM modes, each with distinct phase velocity and with distinct characteristic impedance. Equations for the frequency dependence of the even- and odd-mode effective dielectric constants and characteristic impedances are given by Kirschning and Jansen [1]. The characteristic impedance of the combined lines can also be obtained by using the Green's function [9]. The coupled line parameters are specified as W/h , S/h and the relative permittivity ϵ_r . A single microstrip line can be considered as a special case of coupled line structure where

$S/h \rightarrow 0$.

A two-port network can be formed from a coupled line section by terminating two of the four ports with either open or short circuits, or by connecting two ends. Fig. 3.9(a-c) show the canonical coupled line circuits with an electrical length $\theta = \pi/2$, yielding bandpass characteristics (The ports are marked as 1,2,3 and 4). The circuit in Fig. 3.9(b) with open circuit (at port 2 and 4) is easy to fabricate and hence used in the UWB filter designs.

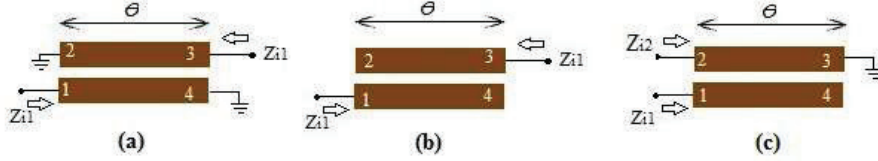


Figure 3.9: Canonical Coupled Line Circuits Forming Bandpass Characteristics

The filter characteristics of coupled lines can be analyzed by calculating the image impedance. The image impedance Z_{i1} is input impedance at port 1 when port 2 is terminated with Z_{i2} and Z_{i2} is input impedance at port 2 when port 1 is terminated with Z_{i1} . Thus both ports are matched when terminated in their image impedances [13]. For symmetrical networks, $Z_{i1} = Z_{i2} = Z_0$, the characteristic impedance of the network. The image impedance Z_{i1} in this case is given by Eq. 3.5.

$$Z_{i1} = \frac{\sqrt{(Z_{oe} - Z_{oo})^2 - (Z_{oe} + Z_{oo})^2 \cos^2 \theta}}{2 \sin \theta} \quad (3.5)$$

At lower frequencies, value of θ will be less than $\pi/2$ (*i.e.* $\theta \rightarrow 0$), indicating high value for Z_{i1} . At higher frequencies, θ value will be greater than $\pi/2$ (*i.e.* $\theta \rightarrow \pi$) and yields large value for Z_{i1} . At mid frequency θ value is equal to $\pi/2$ giving a minimum value

for Z_{i1} . A high value of image impedance indicates a stopband.

The behavior of the coupled lines in Fig. 3.9(b) studied by analyzing field distributions in the UWB band. The even and odd modes are excited at lower and upper frequencies respectively as illustrated by the surface current vector plots in Fig. 3.10.

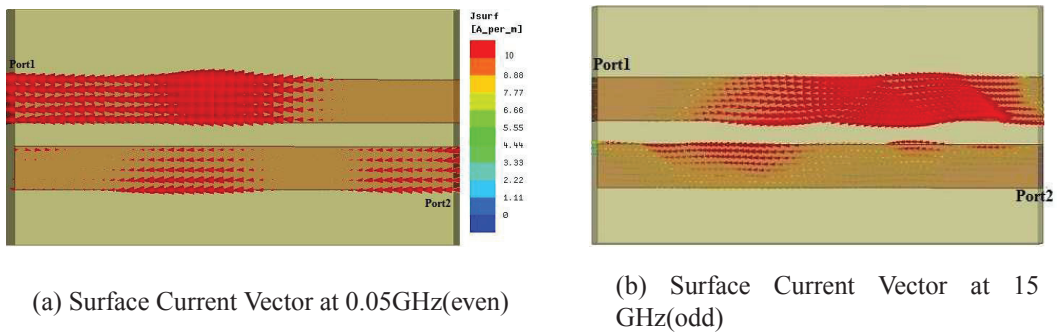


Figure 3.10: Surface Current Vectors Revealing the Excitation of Even and Odd Modes in Coupled Lines

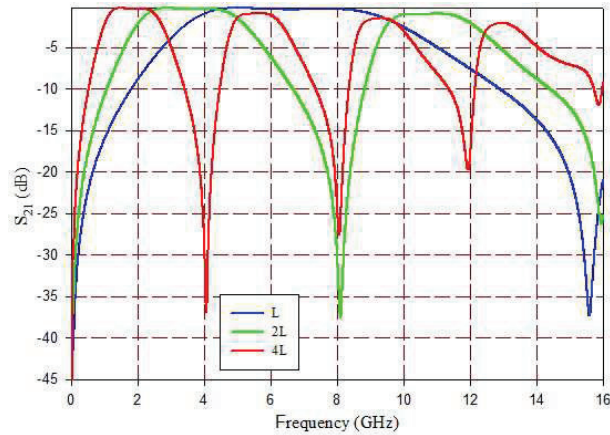


Figure 3.11: The variation of Responses with Variation of Coupled line Length : L Stands for $\theta = \pi/2$ at 6.85 GHz

The variation of transmission parameters with length is shown in Fig. 3.11. As the

length doubles the frequency at which the transmission zeros are introduced is halved.

3.1.4 Interdigital Coupled Lines

The coupling between lines can be increased if three lines are used instead of two. Symmetrical configuration of three coupled lines (equal widths for all three lines) are reported in earlier works. But later on it is numerically proved that the design will be simplified if asymmetrical lines are used [11]-[12]. This is due to the fact that when three lines of equal widths are used the center line will have a greater characteristic impedance than the other two, leading to two extra modes of propagation, which may complicate the design of other components in the system. To compensate for this, middle line is made to have a larger width compared to the side lines. Such a structure will have only three different modes and the design is much more stable compared to those using equal width coupled lines. The relationship between widths of coupled lines is given in [11].

Fig. 3.12 shows the structure and transmission characteristics of interdigital transmission line. It is observed that there is improvement in characteristics as compared to that of a simple coupled line [12].

An analysis of field distribution of the interdigital coupled line is done. Fig. 3.13 shows the surface current distributions of the interdigital coupled line at different frequencies in the UWB band illustrating the excitation of even and odd modes.

Even mode is excited at 1 GHz as shown by the surface current vector in Fig. 3.13(a). This is evident from the current directions in center and side limbs. Mode changes as frequency increases and at 14 GHz, excitation of odd mode occurs as can be observed in

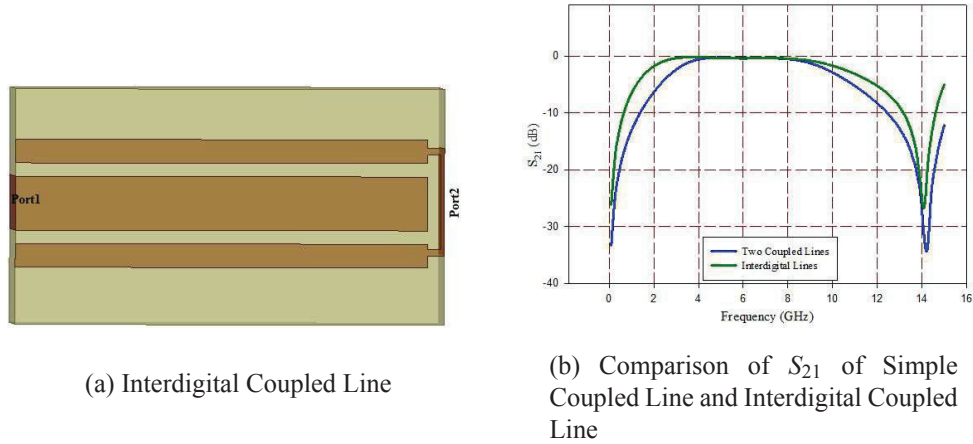


Figure 3.12: Structure and Characteristics of Interdigital Transmission Line

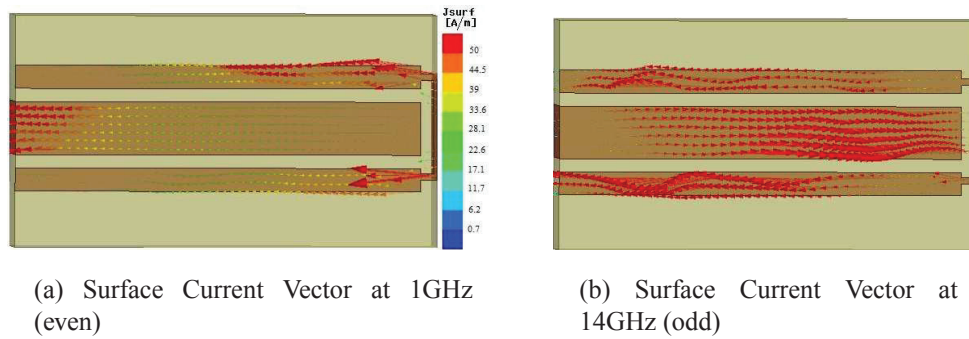


Figure 3.13: Surface Current Distributions of the Interdigital Coupled Line at Different Frequencies Illustrating the Excitation of Even and Odd Modes

Fig. 3.13(b).

A larger portion of the surface current of signals propagating in the odd mode is located in the ambient air, outside the relatively high dielectric substrate than that of signals propagating in the even mode. Because of this propagation difference of signals in even and odd mode and because of the dielectric difference between the substrate

and the ambient air, the phase velocity of the signal traveling in the odd mode is different from that in the even mode. This establishes the varying values of characteristic impedance.

At low frequencies Z_{0e} is higher; at high frequencies Z_{0o} is higher. $Z_0 = \sqrt{Z_{0e}Z_{0o}}$. So Z_0 is high for lower and upper frequencies which accounts for the bandpass nature of the interdigital coupled lines.

In this work the coupled lines are used in the form of asymmetric interdigital transmission line to achieve maximum fractional bandwidth in the 3.1-10.6GHz band.

3.2 Resonators

The filter configurations presented in the thesis incorporates planar resonators to introduce transmission zeros at the passband edges of the UWB band.

The most important and unavoidable planar components are resonators. These find applications in filters, directional couplers, baluns, antennas etc. A microstrip resonator is any structure that is able to contain atleast one oscillating electromagnetic field [4]. In general, microstrip resonators for filter designs may be classified as lumped-element or quasi-lumped element resonators and distributed line or patch resonators. The Q of the resonator depends on the geometry of the resonator as well as the substrate materials.

There are different types of resonators used in microwave circuits, such as cavity resonators, dielectric resonators, acoustic wave resonators, lumped/semi-lumped resonators, transmission line resonators (stub resonators), metamaterial resonators etc. However, the present discussion is limited to those resonators which are used in the

development of various filters in this work.

Other than transmission line resonators, focus is given to electrically small semi-lumped and lumped element resonators, with dimensions much smaller than the signal wavelength at their fundamental resonance frequency.

3.2.1 Stub Resonators

In microwave circuits which deal with distributed components, resonators can be realized by using transmission line sections in proper terminations (open and short) with dimensions comparable with the wavelength; namely half wavelength and quarter wavelength resonators [13]. Fig. 3.14 shows the normalized impedance variation along a transmission line under different terminations.

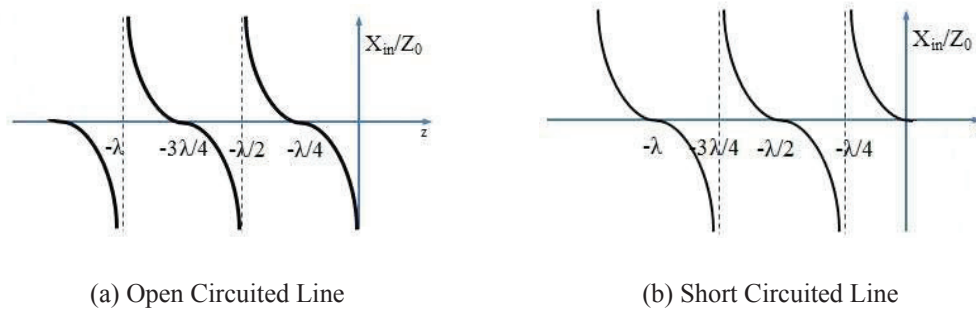


Figure 3.14: Impedance Variation along a Transmission Line under Different Terminations

Half Wavelength Stubs

Half wavelength stubs act as shunt RLC when open circuited and series RLC when short circuited. They are the best suited for filter design as they can introduce transmission

zeros at desired frequencies. Open circuited half wavelength lines are used in this work. The design does not require any via hole to ground as in the case of short circuited line. Fig. 3.15(a-c) show the transmission characteristics of a transmission line loaded with a half wavelength (open/short) stub at the centre frequency f_0 (6.85GHz) of the UWB band. Transmission line loaded with half wavelength stub is shown in Fig. 3.15(a). The

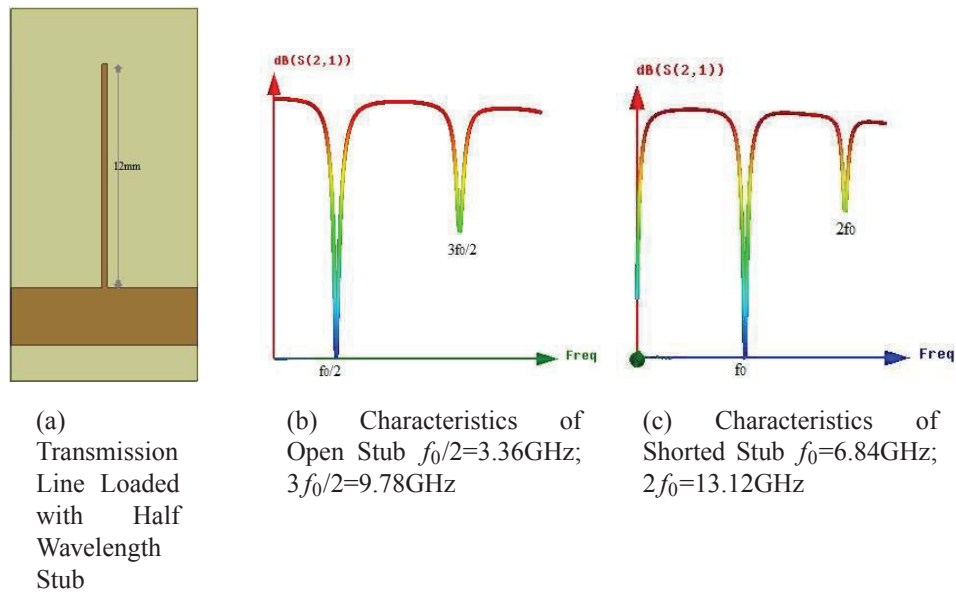


Figure 3.15: Half Wavelength Stub and Transmission Characteristics

transmission characteristics in Fig. 3.15(b-c) illustrate the formation of two transmission zeros at $f_0/2$ and $3f_0/2$ for an open circuited stub and at zero, f_0 and $2f_0$ for shorted half wavelength stub.

Smith chart in Fig. 3.16(a-b) show the impedances at the transmission zeros of half wavelength open stub and shorted stub respectively. At frequencies lesser than the center frequency, the effective physical lengths will be lesser than half wavelength and

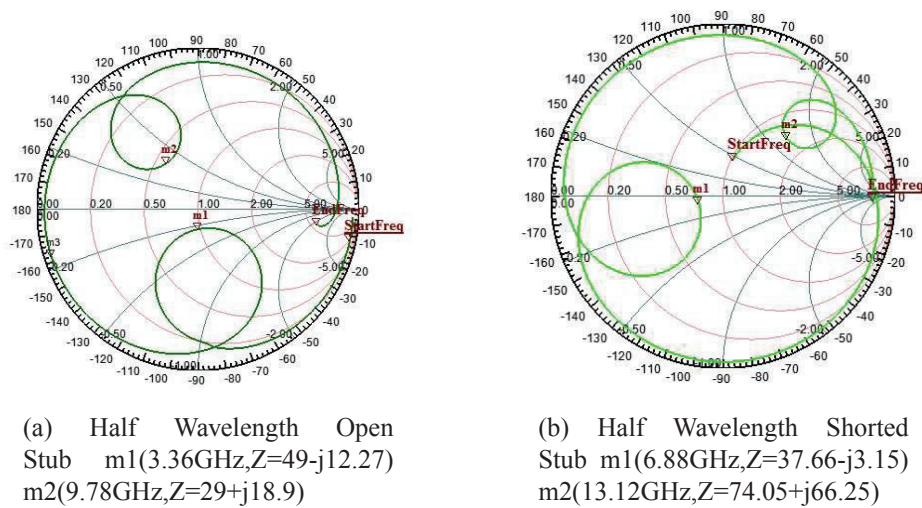


Figure 3.16: Smith Chart Showing the Impedances at Transmission Zeros of Half Wavelength Stub

the reactance will be capacitive in nature as can be observed from corresponding Smith charts. Similarly for frequencies above center frequency, the reactance will be inductive. The electric field distributions of half wavelength open stub at these transmission zeros are shown in Fig. 3.17(a-b), and magnetic field in Fig. 3.17(c-d). At the lower side transmission zero, the electric field is concentrated near the open end and magnetic field at the bottom end of the stub which identifies the prominent capacitive behavior near the open end and inductive behavior at the lower portion of the stub. This is made use of while designing the stepped impedance open stubs.

In this work half wavelength open stubs in the form of stepped impedance resonators are used to achieve transmission zeros at 3.1GHz and 10.6GHz.

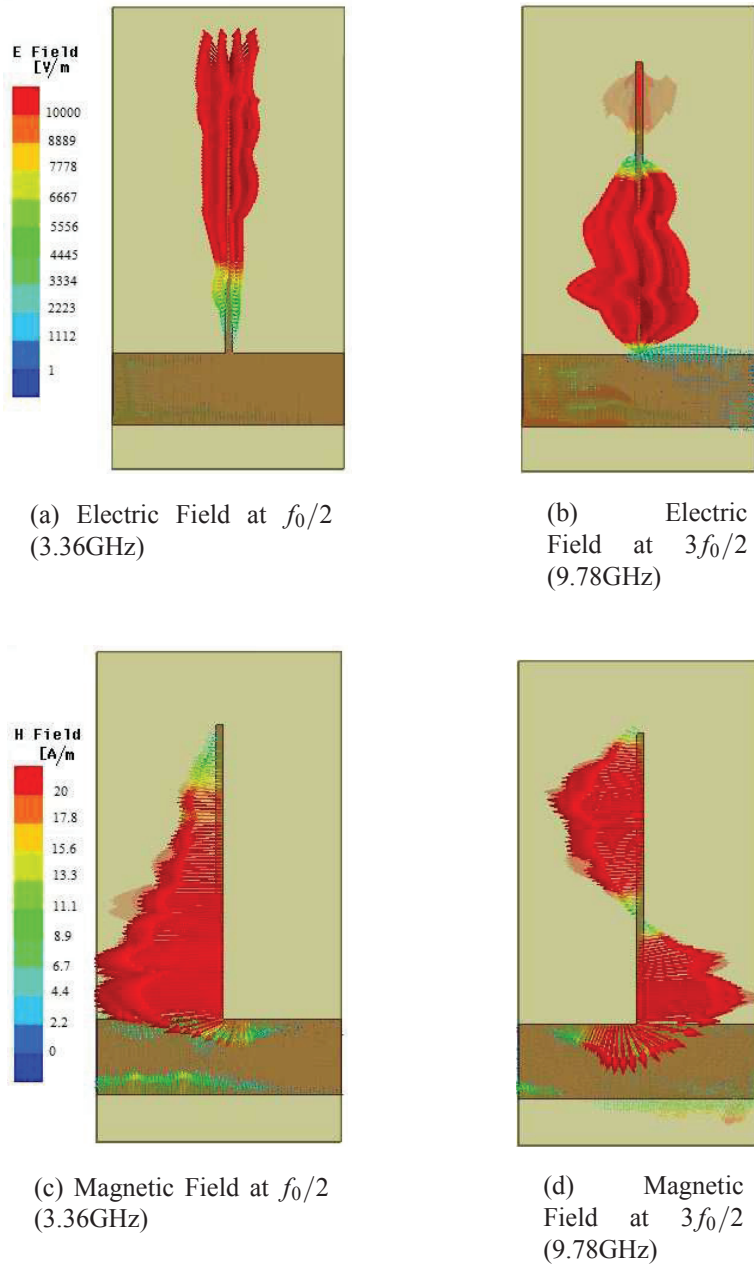


Figure 3.17: Electric and Magnetic Field of Half Wavelength Open Stub at Transmission Zeros

Quarter Wavelength Stubs

Parallel resonant circuit is formed by short circuited quarter wavelength line. It is mainly used as impedance transformer. On the other hand, the open circuited quarter wave line acts like a series resonant circuit. Transmission line loaded with quarter wavelength stub is shown in Fig. 3.18(a). The transmission characteristics in Fig. 3.18(b-c) illustrate the formation of a transmission zero at f_0 for an open circuited stub and at zero and $2f_0$ for shorted stub.

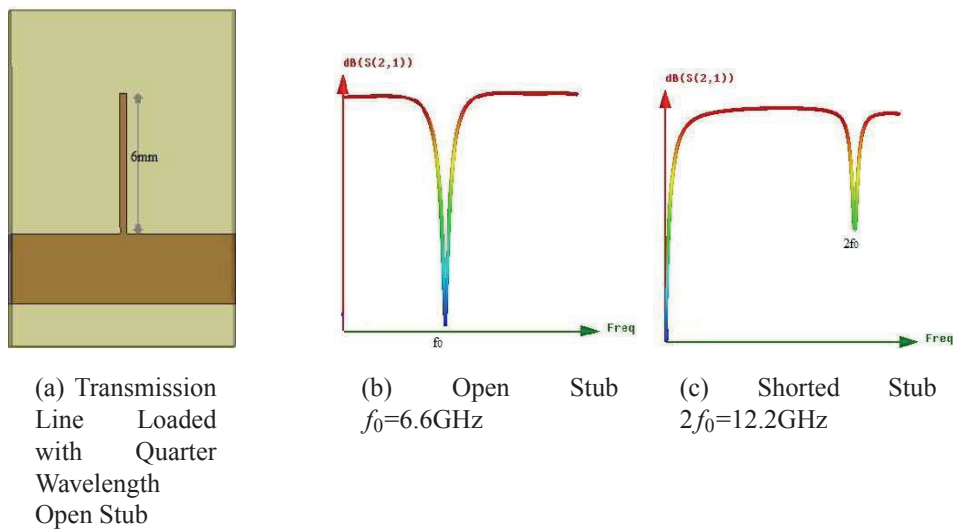


Figure 3.18: Quarter Wavelength Stub and Transmission Characteristics

Smith chart in Fig. 3.19(a-b) show the impedances at the transmission zeros of quarter wavelength open stub and shorted stub respectively. At frequencies lesser than the resonant frequency, the effective physical lengths will be lesser than quarter wavelength and the reactance will be capacitive in nature as can be observed from corresponding Smith charts. Similarly for frequencies above center frequency, the

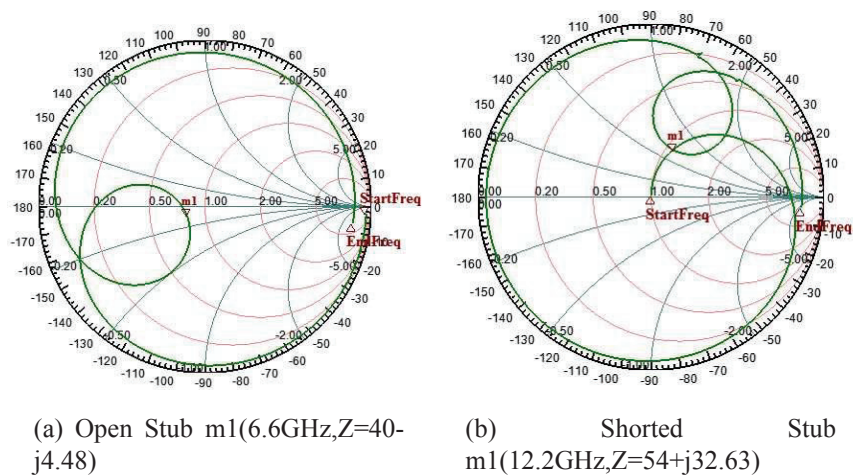


Figure 3.19: Smith Chart Showing the Impedances at Transmission Zeros of Quarter Wavelength Stub

reactance will be inductive. The electric field and magnetic field vectors of quarter wavelength open stub at the transmission zeros are shown in Fig. 3.20(a-b). At the transmission zero (at 6.6GHz), the electric field is concentrated at the open end and magnetic field at the bottom end of the quarter wavelength open stub. This implies the capacitive nature of the open end and inductive nature of the bottom end. The surface current vector on the quarter wavelength open stub in Fig. 3.21 reveals that the current is concentrated at the stubs thus producing a transmission zero at that frequency. A shorted quarter wavelength line behaves similar to an open half wavelength line as observed from the field studies. Fig. 3.22(a-b) show the surface current magnitude on the quarter wavelength shorted stub at transmission zeros. In Fig. 3.22(a) current is circulating through the shorted stub at lower transmission zero. At the upper transmission zero, half wavelength behavior is revealed as observed in Fig. 3.22(b),

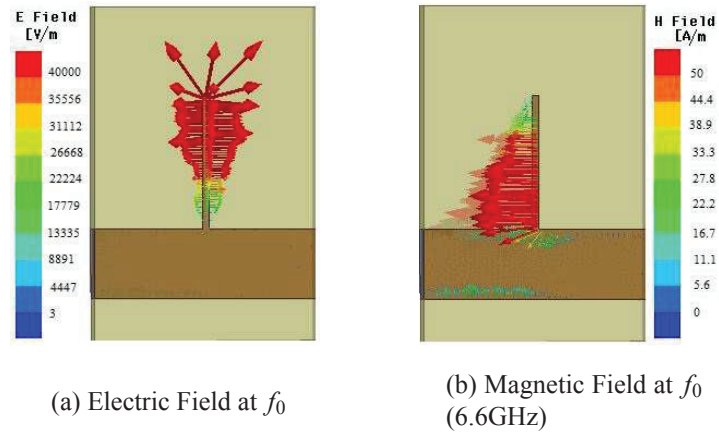


Figure 3.20: Electric/Magnetic Field Vectors for Quarter Wavelength Open Stub at Transmission Zero(6.6GHz)

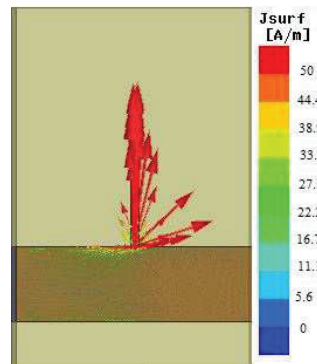


Figure 3.21: Surface Current Vector on Quarter Wavelength Open Stub at Transmission Zero(6.6GHz)

with two current maxima at the ends and a minimum at the centre.

In this work quarter wavelength open and short stubs are used in coplanar waveguide filter as detailed in Appendix B.

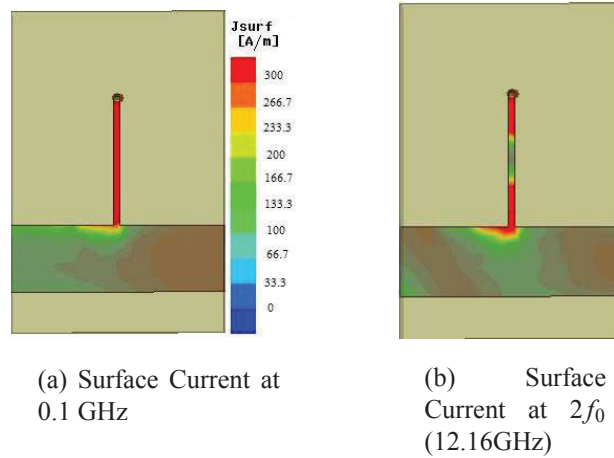


Figure 3.22: Surface Current on Quarter Wavelength Shorted Stub at Transmission Zeros

Stepped Impedance Resonators

Stepped Impedance Resonators (SIR) are employed in this work to reduce the stub size resulting in compact filters. Moreover, there is fine control over the transmission zeros.

An open ended stepped impedance resonator shown in Fig. 3.23 is formed by joining together two microstrip transmission lines with different characteristic impedance Z_1 and Z_2 [14]. This can be considered as both transmission line/semi lumped resonators. In semi lumped resonators the inductance and capacitance can be associated to a certain element of the resonator topology. Half wave length or quarter wave length resonator behavior can be realized using stepped impedance resonators in a much reduced size. In order to realize a half wavelength stub in stepped impedance resonators, two quarter wavelength stubs are connected end on end making a half wavelength line. Each quarter wavelength section is made of different characteristic impedances, achieved by using different widths for each sections. As the width varies, the effective permittivity and

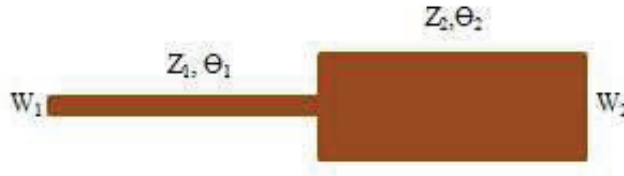


Figure 3.23: An Open Ended SIR

guide wavelength varies which in turn forms a quarter wavelength line at a lesser length than the earlier case.

A stepped impedance resonator can be connected in series or shunt to a transmission line or it can transform the transmission line as such into sections of low and high impedances as in the case of low pass filter realization [14]-[18]. Z_1 and Z_2 are the characteristics impedances of the two cascaded sections and θ_1 and θ_2 are the corresponding electrical lengths ($\theta_1 + \theta_2 = \pi$ for a half wavelength SIR). The resonance condition of the SIR can be varied by changing the width and length of transmission line sections. The stepped impedance stub can be made to give a larger fractional bandwidth as compared to uniform open stub. The resonant frequency can be varied by varying the impedance ratio, $R_z = Z_2/Z_1$. This is implemented by varying the width ratio [19] of the two sections, $W_r = W_1/W_2$. Separation between the resonant frequencies can be varied by varying the electrical length ratio $U_z = \theta_2/(\theta_1 + \theta_2)$.

A transmission line loaded with an SIR open stub is shown in Fig. 3.24(a). Fig. 3.24(b) shows the transmission characteristics of a stepped impedance open stub in comparison with that of a uniform half wavelength open stub of Fig. 3.15(a). The reduction in stub length is evident(8.5mm against 12mm of uniform stub). Variation in

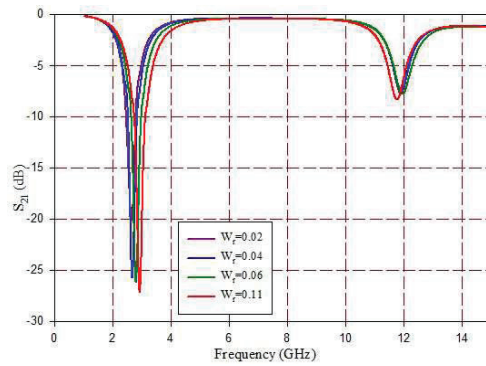
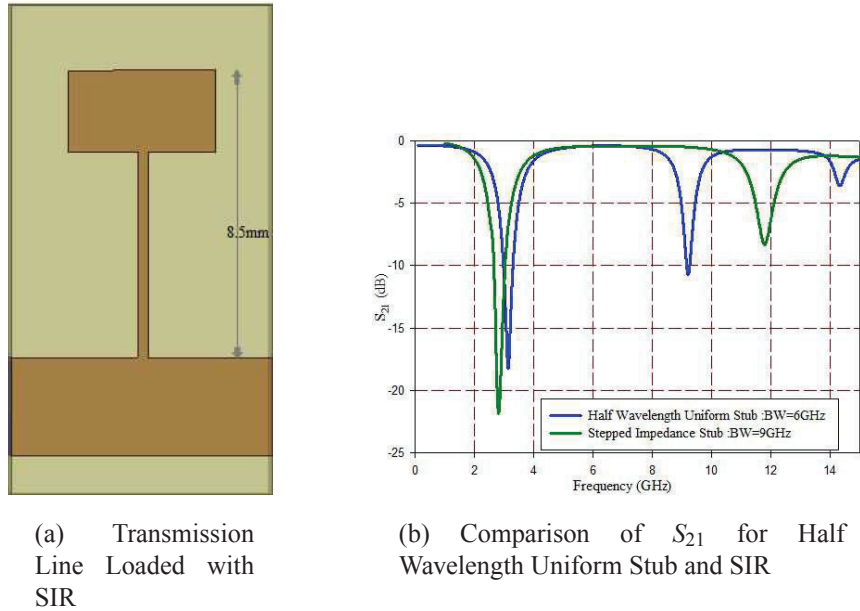


Figure 3.24: Stepped Impedance Resonator and its Characteristics

the resonant frequency with variation of W_r is illustrated in Fig. 3.24(c). As W_r increases the resonant frequency also increases.

The surface current vectors at various frequencies (the first and second resonance

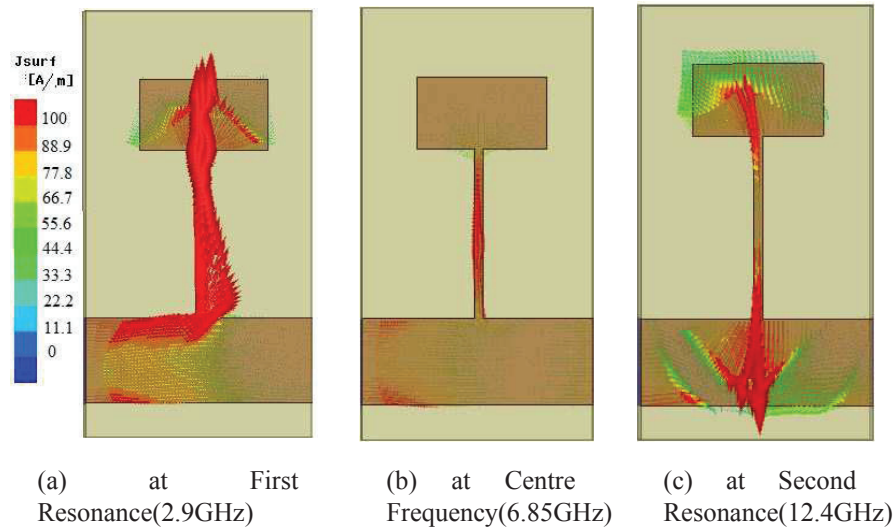


Figure 3.25: Surface Current Vector at Various Frequencies of Interest in the UWB Band

and at center frequency) in the UWB band are shown in Fig. 3.25(a-c). There is current crowding on the SIR at 2.9GHz and 12.4GHz, revealing the role of SIR in producing the transmission zeros. This analysis helps in deciding SIR dimensions for the required positions of transmission zeros.

In this work, half wavelength stubs are implemented using stepped impedance resonators for realizing the transmission zeros in the UWB band.

3.2.2 Open Ring Resonators

There is a need to introduce notch band(s) within UWB band to avoid interference from existing wireless communication systems such as WiMAX, WLAN etc. This can be achieved by using open ring resonators (ORR's) with sharp notch characteristics.

An ORR is a $\lambda/2$ transmission line in a ring configuration [20]-[22]. The

configurations of various ring resonators are shown in Fig.3.26.

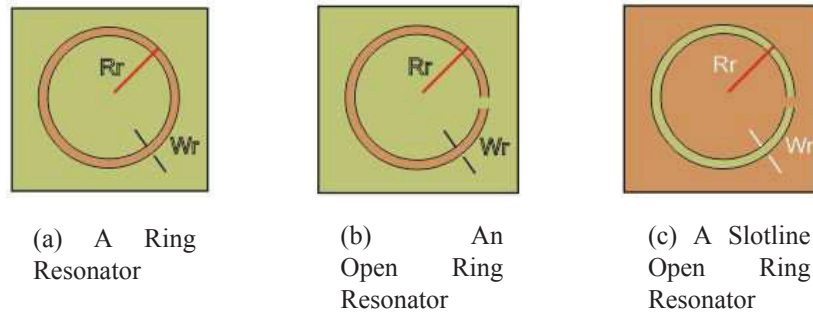


Figure 3.26: Configurations of Various Ring Resonators

Slotline open ring resonator is the complement structure of the open ring resonator and is etched on the ground plane, to form an anti-resonant structure. This can be used to produce a frequency notch. Fig. 3.27 shows a transmission line with ORR etched in ground plane and its transmission characteristics. As can be seen from the transmission

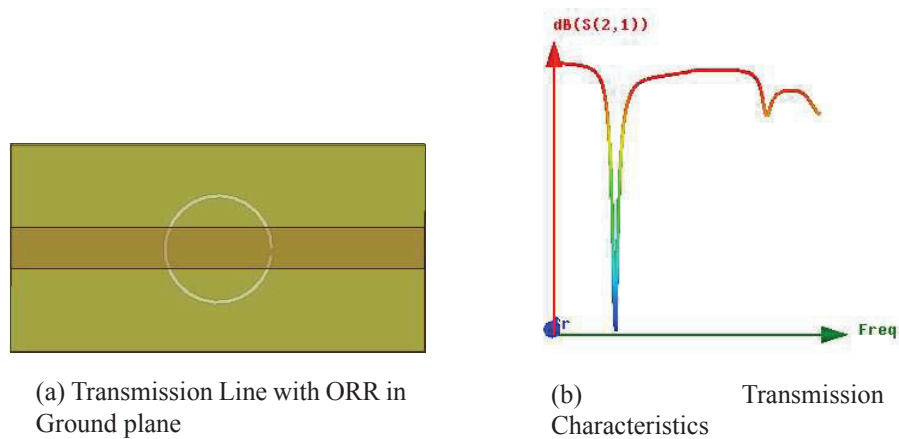


Figure 3.27: Slotline ORR and its Transmission Characteristics

characteristics in Fig. 3.27(b), the second resonance of the slotline ORR is not so sharp

leaving the rest of the transmission characteristics unaffected. The resonant frequency is dependent on the diameter of the ring. Variation of notch frequency and notch bandwidth with dimensions of slotline ORR is shown in Fig. 3.28. The variation of resonant frequency with radius is depicted in Fig. 3.28(a). A larger radius corresponds to a smaller resonant frequency. The notch bandwidth depends on the width of the ring. Thinner rings cause narrow rejection bands as shown in Fig. 3.28(b). The field

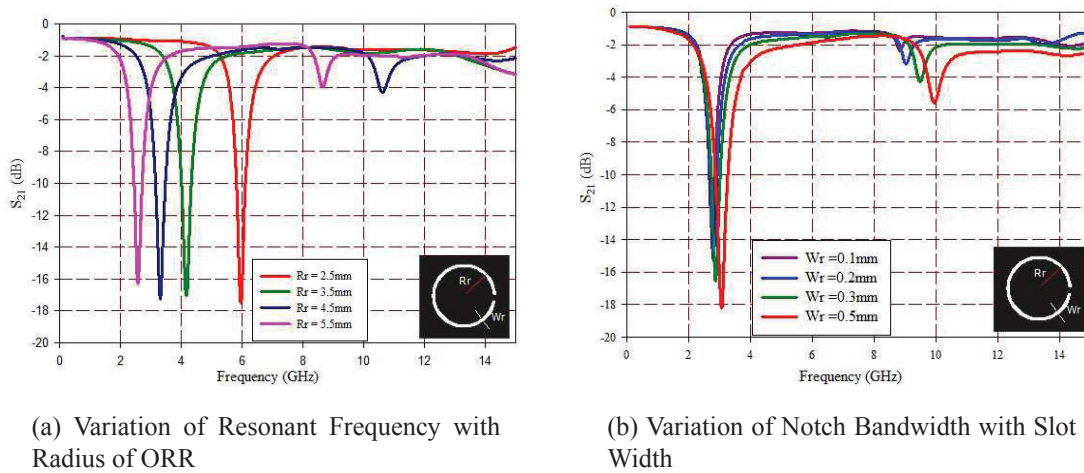


Figure 3.28: Variation of Notch Frequency and Notch Bandwidth with Dimensions of Slotline ORR

distributions of slotline ORR excited by an axial electric field are analyzed at first resonant frequency and shown in Fig. 3.29. In the magnetic field vector, it is observed that there are two maxima at both sides of the slit, and a null centered at the opposite side of slotline ORR, thus exhibiting a half-wavelength resonator behaviour.

Considerable enhancement of resonant characteristics can be achieved by using an array of resonators. The resonator array can be formed so as to have electric, magnetic or electromagnetic coupling between individual resonators, based on orientations of open

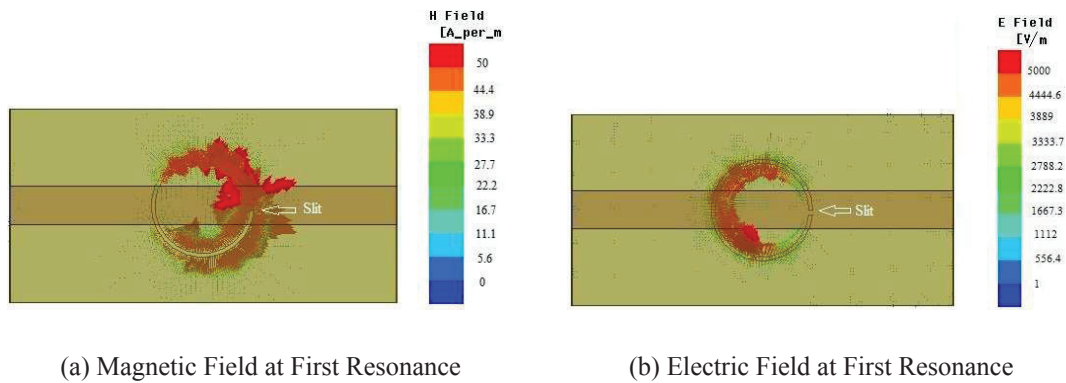


Figure 3.29: Electric and Magnetic Field Distributions

ring resonators as shown in Fig. 3.30(a-c).

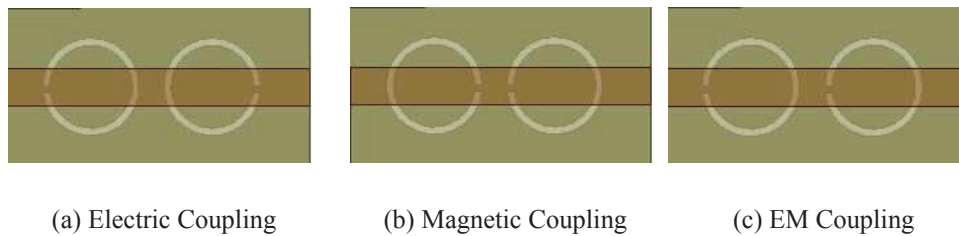


Figure 3.30: Electric and Magnetic Coupling Configurations

The coupling behavior is analyzed and shown in Fig. 3.31. It is obvious that coupling in these structures is proximity coupling through fringe fields. The nature and the extent of the fringe fields determine the nature and the strength of the coupling. It can be shown that at the fundamental mode of resonance, each of the slotline open ring resonators has maximum magnetic field density at the open slit, and maximum electric field density at the opposite side. Because the fringe field exhibits an exponentially decaying character outside the region, the electric fringe field is stronger near the side having the maximum

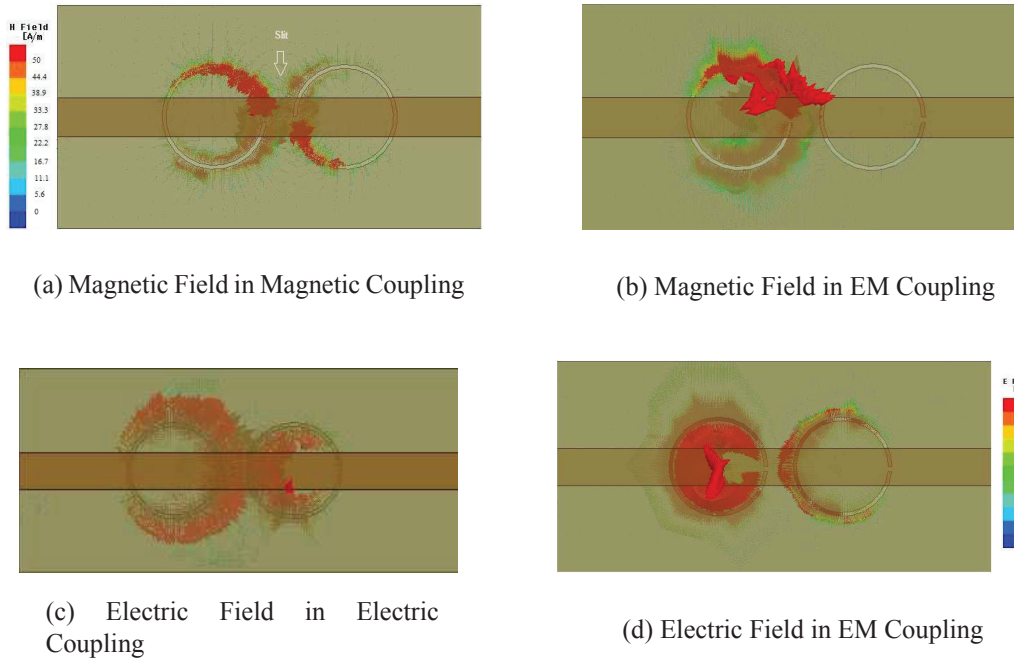


Figure 3.31: Magnetic and Electric Field Vectors for Different Coupling Configurations

electric field distribution, whereas the magnetic fringe field is stronger near the side having the maximum magnetic field distribution. It follows that the magnetic coupling can be obtained if the slit sides of two coupled resonators are closely placed, as shown in Fig. 3.31(a), and the electric coupling can be obtained if the sides with the maximum electric field are closely placed, as shown in Fig. 3.31(c). For the coupling structures in Fig. 3.31(b-d), the electric and magnetic fringe fields at the coupled sides may have comparative distributions, so that both electric and the magnetic coupling (EM coupling) occur.

Deep rejection achieved using two slotline ORR's is illustrated in Fig. 3.32(a). Transmission characteristics under different coupling configurations are compared in

Fig. 3.32(b).

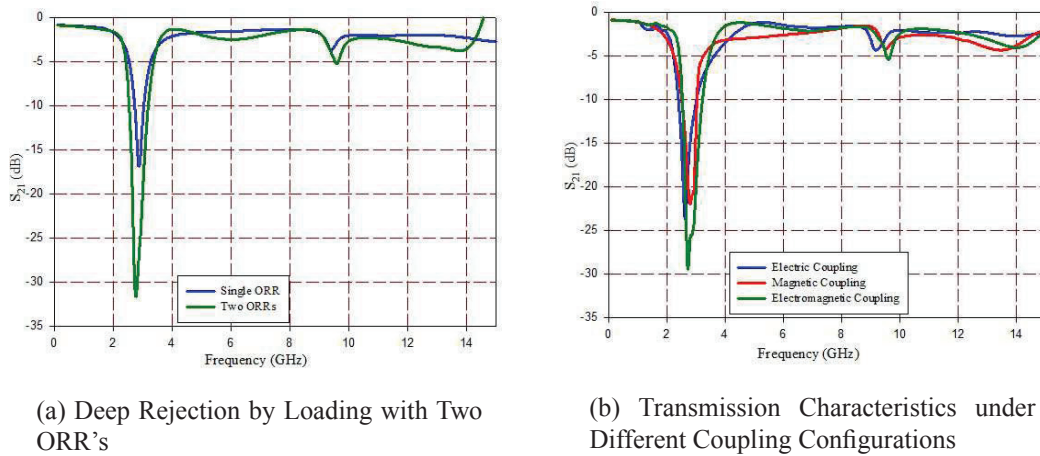


Figure 3.32: Transmission Characteristics of an Array of ORR's

The UWB filter incorporating WLAN notch presented in Appendix A employs two EM coupled slotline ORR's to achieve the required notch band characteristics.

3.2.3 Complementary Split Ring Resonators

Sharp roll off of the UWB filter at the upper passband edge can be achieved using Complementary Split Ring Resonators(CSRR) etched on the ground plane of the planar filter structure.

The CSRR is a complementary structure of Split Ring Resonator (SRR) obtained by adding an inner ring to the slotline ORR as shown in Fig. 3.33(a). By virtue of the mutual coupling between both rings, the fundamental resonant frequency of the resulting structure is lower than that of any individual rings, and thus the structure is electrically smaller than a single ring resonator[22]. SRR's were proposed by Pendry et

al. in 1995 [23] and CSRR's by F. Falcone et al. in 2004 [24]. Fig. 3.33(b) shows a

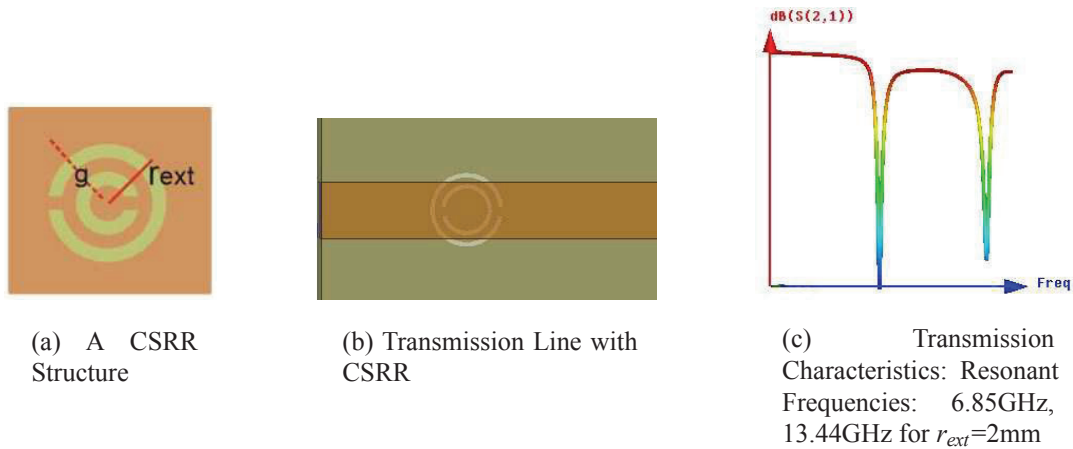


Figure 3.33: Complementary Split Ring Resonator

microstrip transmission line with a CSRR etched in the ground plane. Since the diameter can be made much smaller than the wavelength, this structure is useful for the implementation of effective media with controllable electromagnetic properties, also called metamaterials. Two prominent resonances are exhibited by the structure as shown in the transmission characteristics in Fig. 3.33(c).

The notch characteristics is obtained by virtue of the negative permittivity introduced by the CSRR[25]. Above resonant frequency, the electric field generated in the CSRR is opposite to the incident electric field. This is useful for the synthesis of negative effective permittivity media. Fig. 3.34(a-b) show the electric field of CSRR in the vicinity of the first resonant frequency (6.85GHz) of the CSRR. The field direction in Fig. 3.34(a) is oriented inwards in the CSRR whereas in Fig. 3.34(b) it is outwards showing the reversal of permittivity and hence electric field at resonance.

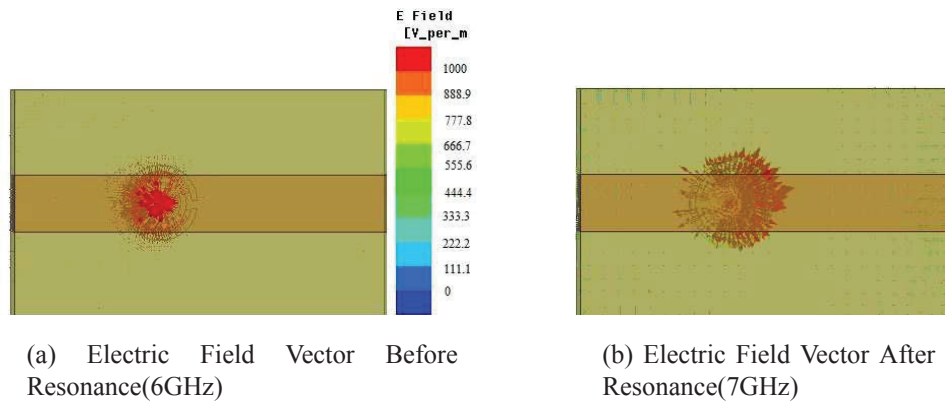
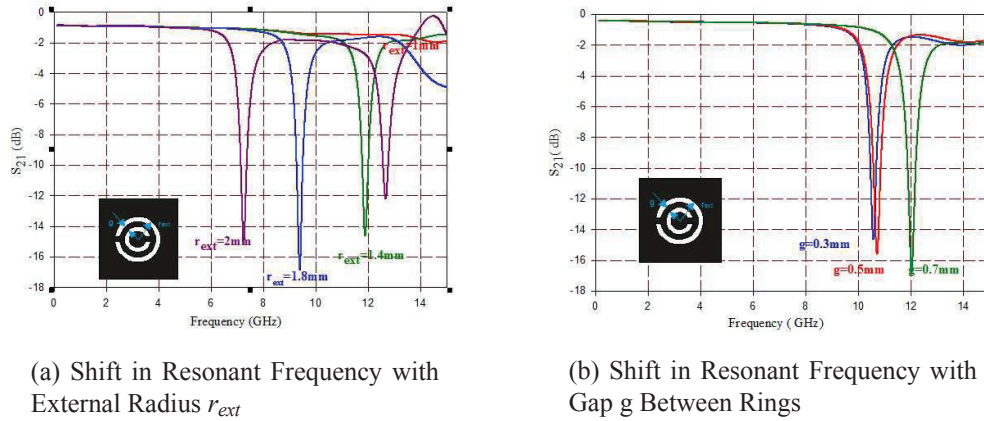


Figure 3.34: Electric Field of CSRR in the Vicinity of the First Resonant Frequency (6.85GHz)

The resonant frequency of the CSRR is dependent on the dimensions of the ring. The dependence is established with the help of the transmission characteristics for varying radius of the external ring as shown in Fig. 3.35(a). As the radius increases, the inductance offered by the CSRR increases ($L=2\pi rL_{pul}$) and hence resonant frequency decreases. As the gap between rings is increased keeping external radius constant, the effective capacitance due to CSRR decreases causing the resonant frequency to increase as observed in Fig. 3.35(b). Prominent second resonance makes CSRR's unfit for use in lower frequencies in UWB filter design.

In this work, CSRR is employed to sharpen the upper roll off rate and suppress the higher frequencies in the upper stop band ($\geq 10.6\text{GHz}$) of the two filters presented in section 5.1, section 5.2 and section 6.1.



(a) Shift in Resonant Frequency with External Radius r_{ext}

(b) Shift in Resonant Frequency with Gap g Between Rings

Figure 3.35: Variation of Resonant Behaviour with Dimensions of CSRR

3.2.4 Defected Ground Structures

Defected Ground Structures (DGS) exhibit notch characteristics with more degrees of freedom with respect to CSRR's. These structures can be incorporated into UWB filter designs to achieve better filter performance.

Defected ground structures (DGS) are realized by etching a defective pattern in the ground plane as shown in Fig. 3.36, which disturbs the shield current distribution. This

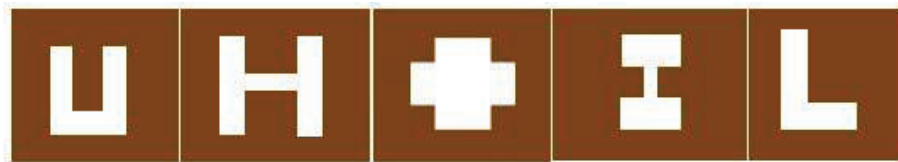


Figure 3.36: Different shapes of Defected Ground Structures

disturbance can cause much higher impedance as compared to conventional transmission lines [26]-[27]. Also it enables unwanted frequency rejection, spurious and leakage

transmission and helps in circuit size reduction. Microstrip designs with DGS exhibit well-defined transmission characteristics, and as such they find many applications in microwave printed circuits. The DGS beneath a microstrip line creates a resonance in the circuit with the resonant frequency controllable by changing the size and shape of the defect. The DGS helps to get sharp resonances without increasing the size of the circuit.

Fig. 3.37(a) shows a dumb bell DGS structure. Fig.3.37(b-c) show a transmission line with DGS etched on the ground plane and its transmission characteristics.

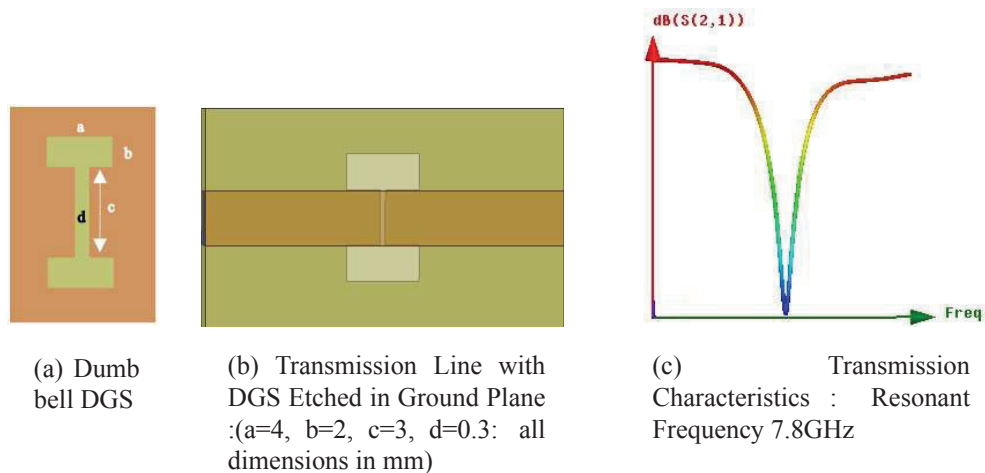


Figure 3.37: Dumb bell DGS and its Transmission Characteristics

Electric field distribution shown in Fig. 3.38(a) reveals the capacitive nature of middle slot portion (represented by dimensions 'c' and 'd') and the magnetic field in Fig. 3.38(b) reveals the inductive nature of dumb bell heads (represented by dimensions 'a' and 'b'). DGS thus form a series connected parallel LC resonant circuit. Larger value of dimensions 'a' and 'b' increases the inductance and hence reduces the

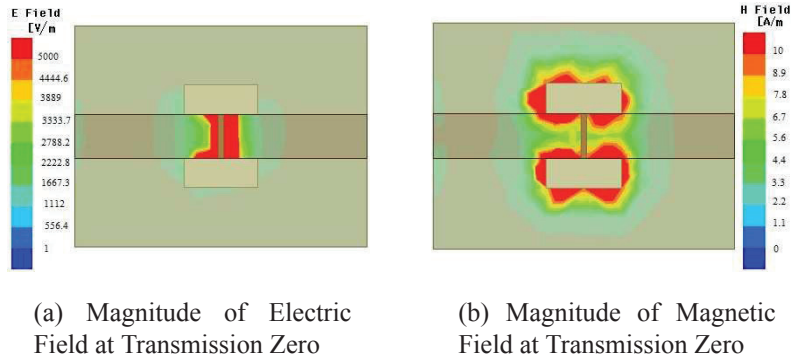


Figure 3.38: Field Distribution revealing DGS Behaviour

resonant frequency. An increase in length 'c' corresponds to an increased capacitance causing reduced resonant frequency. Increase in thickness 'd' of the slot reduces capacitance and thus increases resonance frequency. Variation of resonant frequency with dimensions of DGS is illustrated in Fig. 3.39.

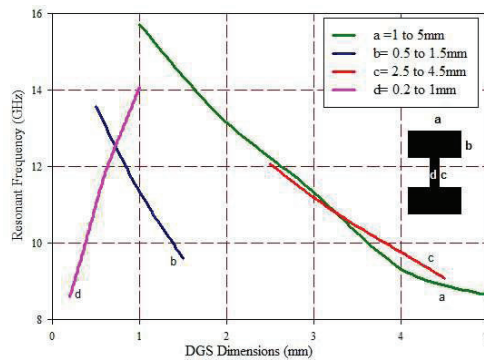


Figure 3.39: Variation of Resonant Frequency with Dimensions of DGS

Dumb bell shaped DGS is employed in filter designs discussed in section 6.2 and Appendix A.

3.3 Lumped/Semi Lumped Elements

Lumped/semi lumped elements find use in the design of compact planar filters.

A passive component whose maximum dimension is smaller than $\lambda/20$ is considered as a lumped element [28]. Lumped-element design using inductors, capacitors, and resistors is a key technique for reducing MMIC chip area resulting in more chips per wafer and thus lower cost.

3.3.1 Inductors

Inductors can take the form of single or multiple bond wires, wire-bound chip inductors, or lumped inductors made using hybrid and MIC fabrication technologies. Various inductor configurations are shown in Fig. 3.40.

MIC fabricated lumped microstrip inductors can be of different forms like straight ribbon, single turn or multi turn rectangular or circular spiral inductors. A high-impedance, straight-line section is the simplest form of inductor, used for low inductance values (typically up to 3nH), whereas the spiral inductor (circular or rectangular) can provide higher inductance values, typically up to 10nH. The innermost turn of the spiral inductor can be connected to outside circuit through a dielectric-spaced underpass or using a wire-bond air bridge crossover.

Expressions for computing the value of the inductance of these microstrip inductors are available [28]. The lumped element approach uses frequency-independent formulas for free-space inductance with ground plane effects. These formulas are useful only when the total length of the inductor is a small fraction of the operating wavelength. In

the inductance expressions, a correction factor K_g is considered to take into account the effect of a ground plane, which tends to decrease the inductance value. When ground plane apertures are employed this ground factor is eliminated thus increasing the effective inductance.

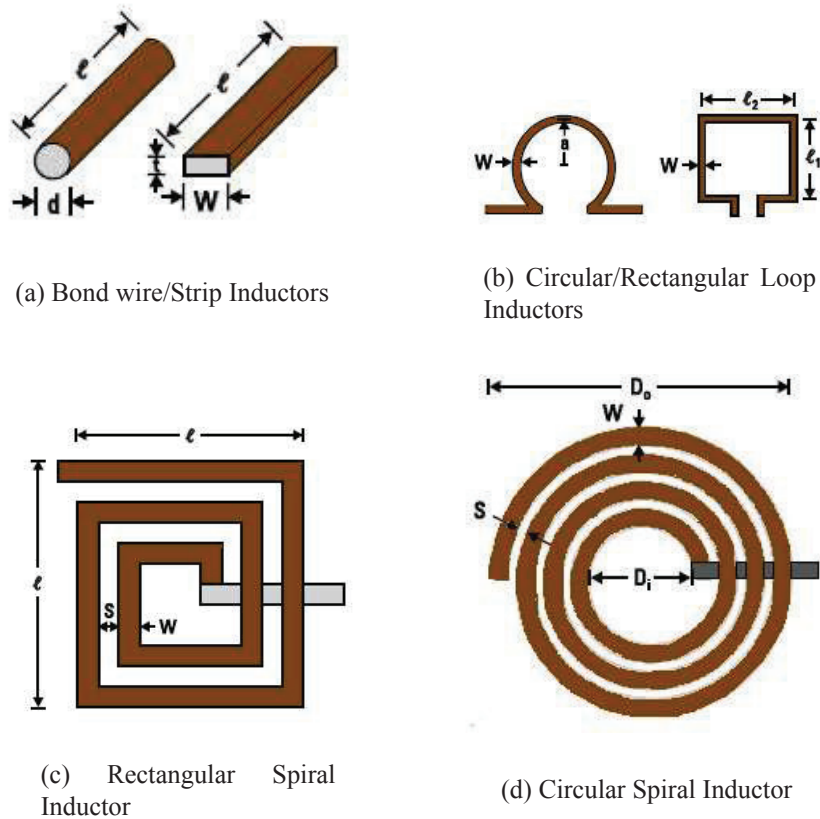


Figure 3.40: Various Inductor Configurations

Each inductor configuration will have its associated parasitic shunt capacitance which gives rise to a resonance at some frequency namely the self-resonant frequency (SRF). The SRF is defined as the frequency at which the imaginary portion of the

inductor impedance $Z_L(\omega_0)$ reaches zero. While designing/choosing the inductor for an application, care should be taken so that the SRF value is well outside the required band. Of the inductor configurations mentioned, circular spiral has the highest SRF, followed by hexagonal spiral and rectangular spiral respectively.

Wire-wound inductors can be realized in several forms of coil including rectangular, circular, solenoid, and toroid. The inductance of a coil can be increased by wrapping it around a magnetic material core such as a ferrite rod.

3.3.2 Chip Inductors

Chip inductors widely used in RF circuits are wire wound inductors with ceramic core having Q value up to 100. Fig. 3.41 shows electrical parameters of chip inductor as a function of frequency. It is observed that chip inductors exhibit almost steady inductance

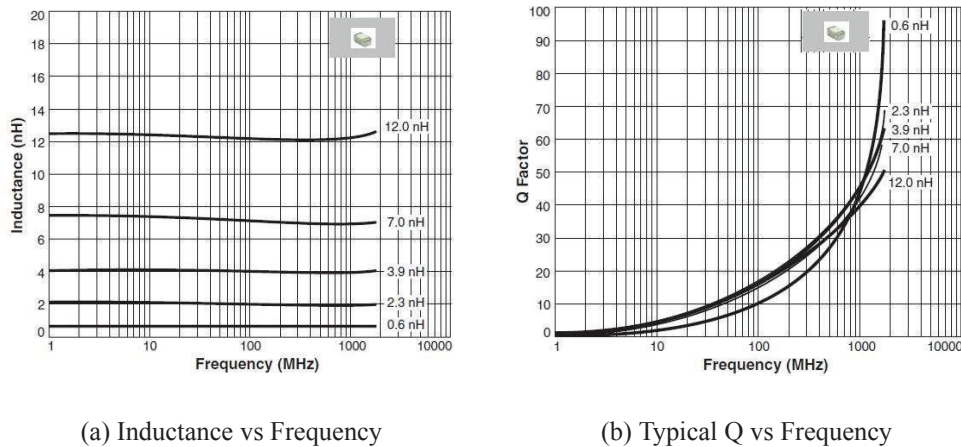


Figure 3.41: Electrical Parameters of Chip Inductor as a Function of Frequency [29]

value over a wide range of frequencies. They can be used as RF chokes for biasing solid-

state devices and in realizing passive components and matching networks. Requirements for applications in passive and matching circuits are high Q , high SRF and low parasitic capacitance, whereas RF chokes need higher current-handling capability and lower dc resistance values. Also, low cost RF front-ends need low profiles or compact size and inexpensive components. Miniature chip coil inductors having inductance values from 1 to 4,700nH with SRF ranging from 90 MHz to 23.5 GHz are commercially available [29]. For chip inductors, a maximum Q -value of 100 can be obtained.

In this work chip inductors are employed in the design of UWB filters discussed in section 5.2 and section 6.1.

3.3.3 Capacitors

Microstrip capacitors can be realized in any arbitrary shape [28]. Various capacitor configurations are shown in Fig. 3.42. The rectangular shape is the most popular, but

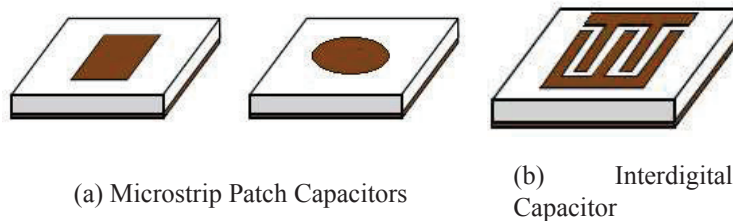


Figure 3.42: Various Capacitor Configurations

has a drawback of high electrostatic discharge due to the sharp edges which is eliminated in circular capacitors.

In addition to the above, interdigital or interdigitated capacitors can be used as lumped circuit elements in microwave circuits, especially at higher microwave

frequencies. The interdigital capacitor is a multifinger periodic structure and they are more suitable for applications where low values of capacitance (less than 1.0pF) are required. Typically, values range from 0.05 to about 0.5pF. The capacitance can be increased by increasing the number of fingers, or by using a thin layer of high dielectric constant material between the conductors and the substrate.

Rectangular and Circular patch capacitors and interdigital capacitors are employed in the design of filter structures presented in sections 5.2, section 6.1, section 6.2 and Appendix A.

3.4 Summary

The chapter discusses different planar components which are instrumental in various filter structures designed. Their characterization in frequency domain is also presented to establish their effectiveness in achieving the desired filter response.

Bibliography

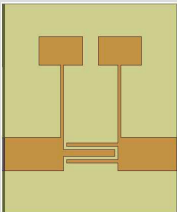
- [1] R K Mongia, I J bahl, P Bhartia, J Hong, “RF and Microwave Coupled-Line Circuits”, Artech House, Inc., London ISBN-13: 978-1-59693-156-5.
- [2] Franco Di Paolo, “Networks and Devices Using Planar Transmission Lines”, CRC Press, ISBN 0-8493-1835-1.
- [3] Cam Nguyen, “Analysis Methods for RF, Microwave and Millimeter-Wave Planar Transmission Line Structures”, John Wiley & Sons Inc., ISBN 0-471-20067-0.
- [4] Jia Sheng, M J Lancaster, “Microstrip Filters for RF/Microwave Applications”, John Wiley & Sons Inc., ISBN 0-471-22161-9.
- [5] Christophe Caloz, Tatsuo Itoh, “Electromagnetic Metamaterials: Transmission Line Theory and Microwave Applications- The Engineering Approach”, John Wiley & Sons Inc., ISBN-10: 0-471-66985-7.
- [6] Rainee N Simons “Coplanar Waveguide Circuits, Components and Systems”, John Wiley & Sons Inc., ISBN 0-471-16121-7.
- [7] Cheng P. Wen, “Coplanar Waveguide: A Surface Strip Transmission Line Suitable for Nonreciprocal Gyromagnetic Device Applications”, IEEE Transactions on Microwave Theory and Techniques, Vol. MTT-17, No. 12, pp. 1087-1090, Dec. 1969.
- [8] Majid Riaziat, Reza Majidi-Ahy and I-Jaung Feng, “Propagation Modes and Dispersion Characteristics of Coplanar Waveguides”, IEEE Transactions on Microwave Theory and Techniques, Vol.38, No.3. Mar.1990.

- [9] Thomas G. Bryant, Jerald A. Weiss, "Parameters of Microstrip Transmission Lines and of Coupled Pairs of Microstrip Lines", IEEE Transactions on Microwave Theory and Techniques, 1, pp.1021-1027, Dec.1968.
- [10] V. Urbanavicius, . Mikuionis, R. Martavius, "Model of the Coupled Transmission Lines with a Non-uniform Dielectric", Electronics and Electrical Engineering. Kaunas: Technologija, No. 5(77) pp. 23-28, 2007.
- [11] Esmat A. F. Abdallah and Nabil A. El-Deeb, "On the Analysis and Design of Three Coupled Microstrip Lines", IEEE Transactions on Microwave Theory and Techniques, Vol. MTT-33, No.11, pp.1217-1222, Nov.1985.
- [12] Rasool Keshavarza, Masoud Movahhedia and Abdolali Abdipour, "A Broadband and Compact Asymmetrical Backward Coupled-Line Coupler with High Coupling Level", International Journal of Electronics and Communications (*AE*), pp.569-574, 2012.
- [13] David M Pozar, "Microwave Engineering", John Wiley & Sons Inc., ISBN 0-471-17096-8.
- [14] M.Makimoto and S Yamashita, "Microwave Resonators and Filters for Wireless Communication; Theory, Design and Applications", ISBN-13: 978-3540675358, Springer.
- [15] Jen-Tsai Kuo and Eric Shih, "Microstrip Stepped Impedance Resonator Bandpass Filter with an Extended Optimal Rejection Bandwidth", IEEE Transactions on Microwave Theory and Techniques, Vol. 51, No. 5, pp.1554-1559, May 2003.
- [16] Kongpop U-yen, Edward J. Wollack, Terence Doiron, John Papapolymerou and Joy Laskar, "A Bandpass Filter Design Using Half-Wavelength Stepped Impedance Resonators with Internal Couplings", IEEE Microwave and Wireless Components Letters, Vol. 16, No. 8, pp.443-445, Aug 2006.
- [17] Kamaljeet Singh and K. Nagachenchaiah, "Compact Ultra-Wideband Microstrip Bandpass Filter Using SIR Approach", High Frequency Electronics, pp.46-49, Jul. 2009.

- [18] L. Guo, Z.-Y. Yu and L. Zhang, "Design Of A Dual-Mode Dual-Band Filter Using Stepped Impedance Resonators", *Progress in Electromagnetics Research Letters*, Vol. 14, pp.147-154, 2010.
- [19] Pramod K. Singh, Sarbani Basu and Yeong-Her Wang, "Planar Ultra-Wideband Bandpass Filter Using Edge Coupled Microstrip Lines and Stepped Impedance Open Stub", *IEEE Microwave and Wireless Components Letters*, Vol. 17, No. 9, pp.649-651, Sep. 2007.
- [20] Kai Chang, Lung-Hwa Hsieh, "Microwave Ring Circuits and Related Structures", John Wiley & Sons, Inc., ISBN 0-471-44474-X.
- [21] Miguel Durn-Sindreu, Jordi Naqui, Ferran Paredes, Jordi Bonache and Ferran Martn, "Electrically Small Resonators for Planar Metamaterial, Microwave Circuit and Antenna Design: A Comparative Analysis", *Applied Sciences*, 2, pp.375-395, 2012.
- [22] L.J. Rogla, J. Carbonell and V.E. Boria, "Study Of Equivalent Circuits for Open-Ring and Split-Ring Resonators in Coplanar Waveguide Technology", *IET Microwave Antennas Propagation*, Vol. 1, (1), pp.170-176, 2007.
- [23] J. B. Pendry, J. Holden, D.J. Robbins, W.J. Stewart, "Magnetism from Conductors and Enhanced Nonlinear Phenomena", *IEEE Transactions on Microwave Theory and Techniques*, Vol.47, No. 11, pp.2075-2084, 1999.
- [24] F. Falcone, T. Lopetegi, J. D. Baena, R. Marquis, F. Martn and M. Sorolla, "Effective Negative Stopband Microstrip Lines Based on Complementary Split Ring Resonators", *IEEE Microwave and Wireless Component Letters*, Vol.14, pp.280-282, 2004.
- [25] Juan Domingo Baena, Jordi Bonache et. al, "Equivalent-Circuit Models for Split-Ring Resonators and Complementary Split-Ring Resonators Coupled to Planar Transmission Lines", *IEEE Transactions on Microwave Theory and Techniques*, Vol.53, No. 4, pp.1451-1460, Apr.2005.
- [26] Hang Wang and Lei Zhu, "Aperture-Backed Microstrip Line Multiple-Mode Resonator for Design of a Novel UWB Bandpass Filter", *Proc. APMC*,2005.

-
- [27] Leo G Maloratsky "Microstrip Circuits with a Modified Ground Plane", High Frequency Electronics, pp.38-47,Dec.2009.
- [28] Inder Bahl "Lumped Elements for RF and Microwave Circuits", Artech House, Inc., ISBN 1-58053-309-4.
- [29] "Coilcraft Chip Inductors ", 0201DS Series (0603) (datasheet), 2 pages. Available at: <http://www.coilcraft.com/0201ds.cfm>

4 Stepped Impedance Stub Resonator Filter

	Contents	<ul style="list-style-type: none">★ <i>Geometry</i>★ <i>Simulation Studies</i>★ <i>Analysis and Design</i>★ <i>Lumped Element Model</i>★ <i>Dispersion Studies</i>★ <i>Time Domain Analysis</i>★ <i>Measurement Results</i>
--	-----------------	---

This chapter introduces a planar UWB filter developed using two half wavelength stepped impedance open stub resonators on interdigital coupled lines. The structure is simple having low insertion loss in its passband, sharp roll off rates at its lower and upper stopband edges and a reasonably good attenuation in both stopbands. The filter has an overall dimension of 17mm x 19mm on a substrate with $\epsilon_r = 4.4$ and thickness 1.6mm. ¹

¹Bindu C J, S Mridula and P Mohanan, *Design of Compact Planar Ultra Wide Band Filter*, International Joint Colloquiums on Computer Electronics Electrical Mechanical and Civil, CEMC-ILAHIA College of Engineering and Technology (ICET), Muvattupuzha, Kerala, India, pp 114-117, Sep.,2011

The work aims at the design of compact planar ultra wide band filters with an operating bandwidth of 3.1-10.6GHz. Design approach followed and the various planar components identified for the design are elaborated in detail in chapters 1-3. Analyses show that asymmetrical interdigital coupled lines form a good candidate for obtaining a large fractional bandwidth (section 3.1.4) and stepped impedance resonators are best suited to give controllable transmission zeros (section 3.2.1). The planar components analyzed in chapter 3 are suitably employed in various filter designs to follow.

4.1 Geometry

The filter uses two stepped impedance open stub resonators on asymmetrical interdigital coupled lines to achieve the desired UWB response. Asymmetrical interdigital coupled lines have a middle line thicker than the side lines for a stable design [1]. They give better coupling and an increased fractional bandwidth compared to a simple coupled line structure, as illustrated in section 3.1.4 and hence used in the design. The coupled lines are made a quarter wavelength long at the center frequency f_0 (6.85GHz) of the UWB spectrum extending from 3.1 GHz to 10.6 GHz. Layout of the filter structure coupled to a 50Ω transmission line section is shown in Fig. 4.1(a). The structure is very simple to fabricate and has an area of 17mm x 19mm. The simulated S parameters of the structure is shown in Fig. 4.1(b). Double sided substrate with relative permittivity of 4.4, dielectric loss tangent of 0.02 and a thickness of 1.6mm is used. Dimensions of the stepped impedance stubs are obtained from transmission line theory as explained in

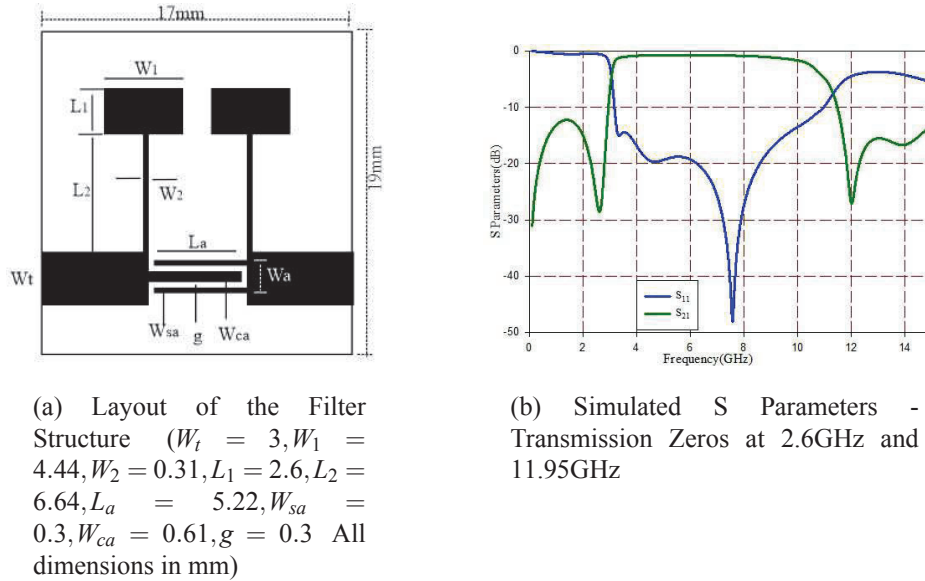


Figure 4.1: Layout of the Filter and Simulated S Parameters

section 4.3.

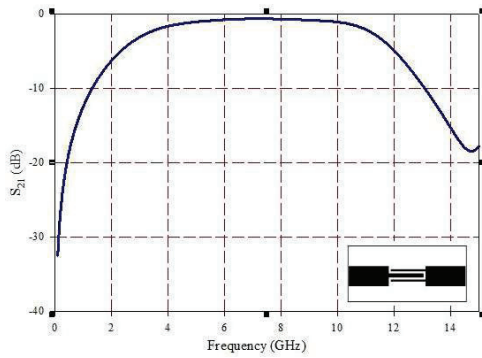
Simulated insertion loss for the filter is well within 0.5dB. Also there is sharp rejection at lower and upper cut off frequencies. Stop band attenuation is 12-15dB, which can be further reduced by cascading another section, at the cost of still higher insertion loss and increased chip area. The insertion loss can be minimized by using a less lossy dielectric.

Design Evolution

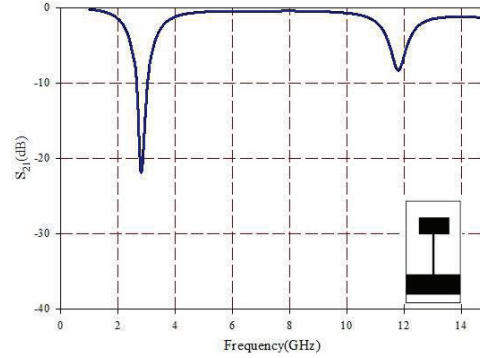
The design evolution is shown in Fig. 4.2. The interdigital coupled lines inherently possess bandpass characteristics as detailed in section 3.1.4. An interdigital coupled line (of length $\lambda/4$ at center frequency f_0 , 6.85GHz of the UWB band) and its

transmission characteristics are shown in Fig. 4.2(a).

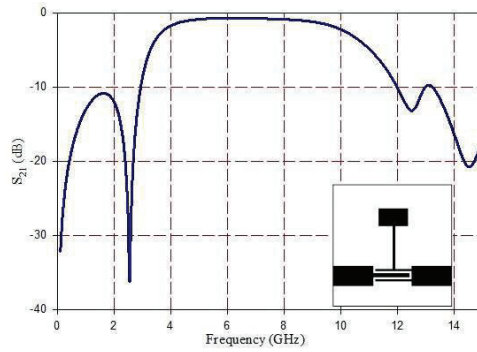
The transmission zeros are formed at zero and $2f_0$. This has to be tuned to the



(a) Interdigital Coupled Line and Simulated S_{21}



(b) SIR Open Stub and Simulated S_{21}



(c) Interdigital Line with Single SIR Open Stub and Simulated S_{21}

Figure 4.2: Design Evolution

requirements of a UWB band. As per transmission line theory, half wavelength uniform open stubs act as parallel LC resonant circuits and thus can be used to introduce fixed transmission zeros at $f_0/2$ and $3f_0/2$ as explained in section 3.2.1. Accordingly, stubs

designed for half wavelength at 6.85GHz will have transmission zeros at 3.4GHz and 10.2GHz. However, this has to be tuned to the required UWB band of 3.1-10.6GHz. Hence stepped impedance stubs which gives controllable transmission zeros by varying the widths and lengths of the stub sections are used instead of uniform thickness stubs. Moreover, this results in a compact filter.

Each of the impedance sections in the SIR is one quarter wavelength long connected end to end forming effectively a half wavelength stub. Stepped impedance stubs reduce the overall stub length. This is due to the fact that a change in width of the stub and hence effective permittivity (ϵ_{eff}) causes a change in guide wavelength. A larger width causes a larger value for ϵ_{eff} thus reducing the guide wavelength. The transmission zeros can be adjusted according to the requirements by adjusting the width ratio of the stepped impedance sections which in turn corresponds to the impedance ratio [2]-[5].

The theory of stepped impedance resonators and comparison of their characteristics with those of uniform stubs are explained in detail in section 3.2.1. The transmission characteristics of a stepped impedance open stub (length $\lambda/2$ at center frequency of the UWB band) is shown in Fig. 4.2(b).

The effect of addition of a single stepped impedance open stub on the interdigital coupled line transmission characteristics is shown in Fig. 4.2(c). Attenuation and roll off characteristics at the upper stopband are not so promising for this structure. To improve the performance, one more stub is added to obtain the final layout of Fig. 4.1(a). The overall size is not affected.

4.2 Simulation Studies

Surface current vector of the structure at various frequencies of interest are shown in Fig. 4.3(a-d). It can be observed that there exists a current crowding at the stepped impedance resonator at lower cut off frequency 3.1GHz, indicating a power loss occurring in these elements. This reveals that the lower cut off frequency is controlled by the stepped impedance resonators. Surface current vector at 6.85 GHz shows the beginning of odd mode currents through the interdigital coupled line. At 10.6 GHz, it is shown that the odd mode current is strengthened in the interdigital coupled lines. The upper transmission zero at 11.95GHz is due to the combined effect of the coupled line length and the second resonance of the stepped impedance stubs as visualized in Fig. 4.3(d). Electric field at 2.6GHz (lower side transmission zero) in Fig. 4.3(e) indicates that the field is concentrated on the low impedance stub indicating its capacitive nature. The magnetic field at 2.6GHz shown in Fig. 4.3(f) establishes the inductive nature of the high impedance stub of SIR.

4.3 Analysis and Design

A parametric analysis is carried out to analyze the filter behavior on varying the dimensions of the constituent elements. Fig. 4.4(a-d) show the results of parametric analysis of the filter. The width ratio W_1/W_2 of the stepped impedance open stub controls the lower cut off frequency. Larger ratio corresponds to a lesser lower cut off frequency as can be observed in Fig. 4.4(a), while upper cut off remains almost

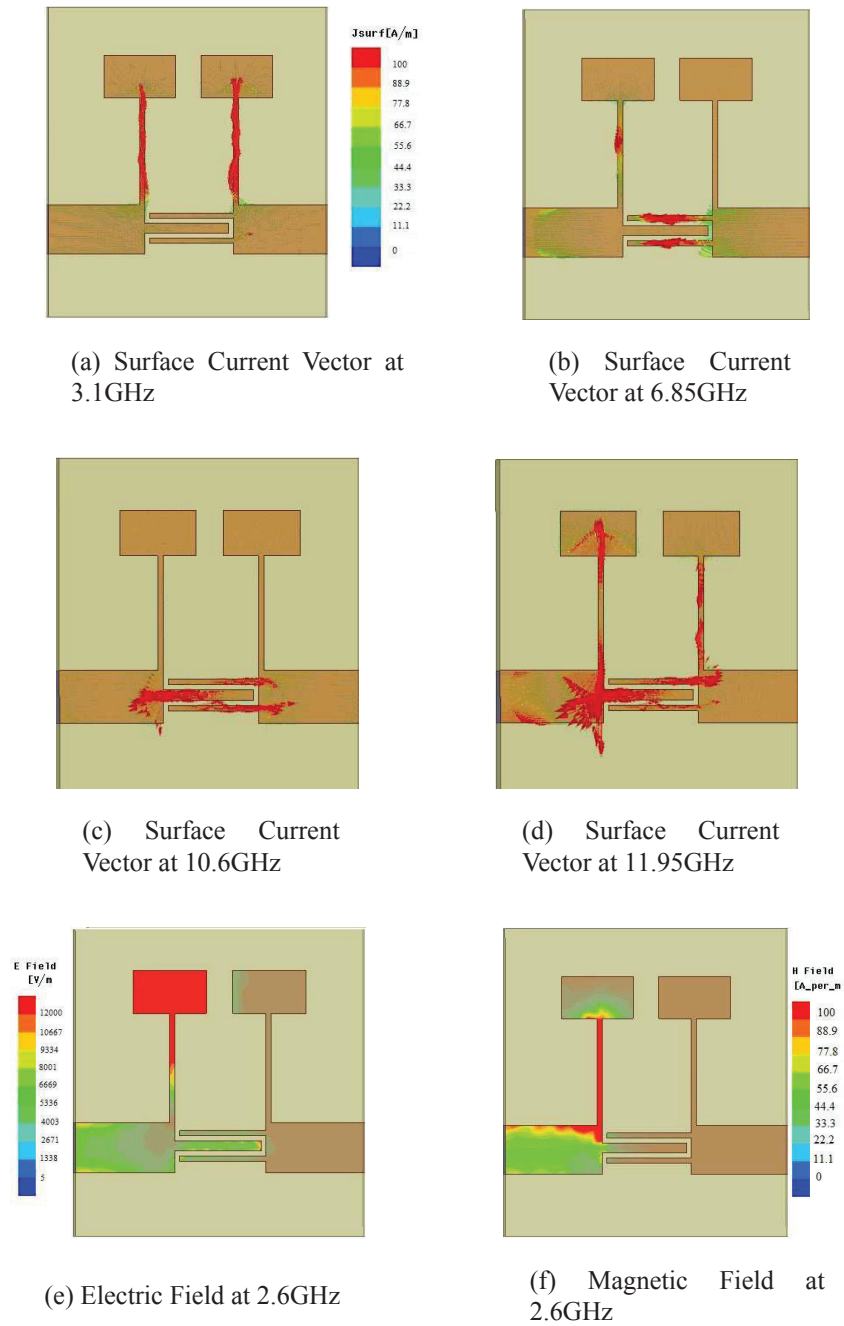


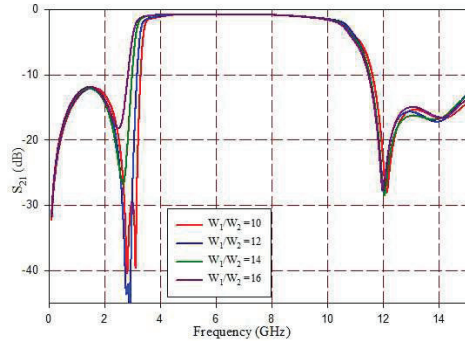
Figure 4.3: Field Distributions at Frequencies of Interest

unaffected. The lengths of the stub sections (L_1 and L_2) are made one quarter wavelength (slightly less than a quarter wavelength after accounting for the fringing field) at the centre frequency (6.85GHz) so that the stepped impedance stubs ($L_{stub}=L_1+L_2$) act as half wavelength stubs. Hence considerable change in the lengths can cause variation of centre frequency which in turn cause a shift in the entire band. Parametric studies show that the variation of L_{stub} cause shifting of the entire band as in Fig. 4.4(c). However shift at the lower band edge is comparatively less than that at the upper edge. Also for equal variations of capacitive (L_1) and inductive (L_2) stub lengths, the frequency shift is more prominent for variations in inductive stub length as observed in Fig. 4.4(d).

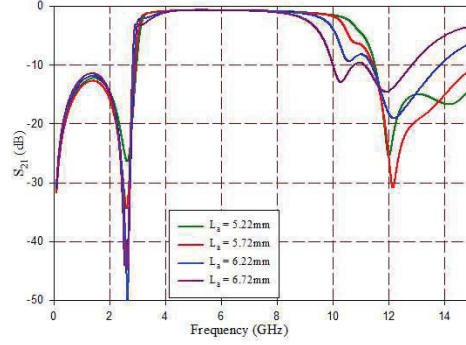
The upper cut off can be varied by varying the length of the coupled line and it can be seen that lower cut off remains unaffected, as evident in Fig. 4.4(b). Hence by properly adjusting the lengths of the stubs, the position of transmission zero due to the coupled line and that due to the second resonance of the open stubs can be aligned to occur at the same frequency point to get sharper cut off in the upper band edge. These factors are taken into consideration while formulating the generalized design equations for the filter. However, the variation of width of any section causes variation in effective permittivity which in turn affects the electrical length. Thus all variations are interdependent.

Generalized design equations for the filter are formulated using multivariable regression. The dataset is generated through numerous parametric iterations on different substrates.

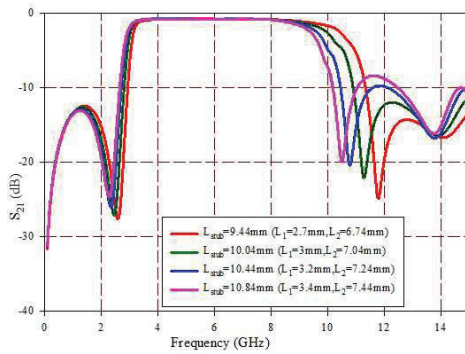
Table 4.1-4.3 show the results of parametric analysis of the filter on a substrate with $\epsilon_r=4.4$ and thickness 1.6mm. It is identified that lower cut off frequency f_1 is dependent



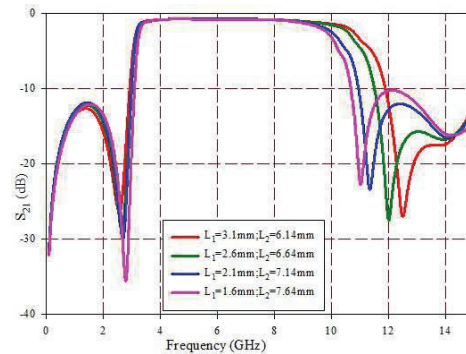
(a) Variation of Lower Cutoff Frequency with Width Ratio W_1/W_2 of SIR



(b) Variation of Upper Cutoff Frequency with Coupled Line Length L_a



(c) Shifting of the band for varying Stub Length L_{stub}



(d) Shifting of the band for varying Lengths of L_1 and L_2 ($L_1+L_2=\text{constant}$)

Figure 4.4: Results of Parametric Analysis of the Filter

on the impedance ratio of the stepped impedance stubs, which is interpreted as width ratio W_r of the stubs. Larger W_r corresponds to a lower f_1 as can be observed in Table 4.1, while upper cut off f_2 remains almost unaffected. The width ratio W_r required for the lower cut off frequency f_1 (GHz) may be computed using Eq. 4.1. The narrow width

Table 4.1: Variation of Cut off Frequencies with Width Ratio W_r of Stubs

$W_r = W_1/W_2$	f_1 (GHz)	f_2 (GHz)
10	3.42	10.79
12	3.3	10.78
14	3.15	10.74
16	3.06	10.67

W_2 may be fixed for fabrication convenience and W_1 calculated from W_r .

$$W_r = 46.12 - 6.36f_1 - 1.67\epsilon_r - 2.87h \quad (4.1)$$

where ϵ_r is the relative permittivity and h is the slab thickness (mm) of the substrate chosen.

The upper cut off frequency f_2 can be varied by varying the length of the coupled line (L_a) as observed in Table 4.2. The variation in f_1 in this case is negligible. Upper cutoff

Table 4.2: Variation of Cut off Frequencies with Coupled line Length L_a

L_a	f_1 (GHz)	f_2 (GHz)
5	3.10	10.75
5.5	3.10	10.50
6	3.09	10.074
6.5	2.99	9.56
7	2.98	9.04

is also affected by SIR stub length. Individual variations of lengths L_1 and L_2 give an inverse relationship between length and f_2 as seen in first two sections of Table 4.3. But when both L_1 and L_2 are varied the inverse relationship holds good for variations in L_2 as

observed in section3 of Table 4.3. It is inferred from the above regression analysis that

Table 4.3: Variation of cut off frequencies with stub lengths L_1 and L_2

L_1 (mm)	L_2 (mm)	f_1 (GHz)	f_2 (GHz)	Remarks
2.2	6.64	3.15	10.78	L_1, f_2 inversely related
3.4	6.64	2.97	10.30	
2.6	5.8	3.12	10.96	L_2, f_2 inversely related
2.6	7.0	3.20	10.40	
3.6	5.64	3.13	11.07	L_1, f_2 directly related; L_2, f_2 inversely related; L_{stub} constant
3.1	6.14	3.06	10.8	
2.6	6.64	3.10	10.67	
2.1	7.14	3.10	10.30	

f_2 is dependent on both coupled line length L_a and the length of high impedance stub (L_2). The influence of L_1 is negligible. Accordingly the design equation is formulated as

$$L_a = 20.39 - 0.72f_2 - 0.42L_2 - 1.13\epsilon_r + 0.17h \quad (4.2)$$

The equations 4.1 and 4.2 are verified on various substrates. Table 4.4 shows the computed values of W_r, L_a and UWB Bands obtained on various substrates.

4.4 Lumped Element Model

The lumped element model of the filter shown in Fig. 4.5 is deduced by computing the values of microstrip components based on transmission line theory. These lumped-element approximations are not to be taken as equivalent circuits but rather as a guide to the behaviour of the distributed elements. The model gives insight into the inherent

Table 4.4: Computed Values of W_r and L_a and UWB bands Obtained

Substrate (ϵ_r/h mm)	W_r	L_a (mm)	Band (GHz)	Obtained	%error (lower)	%error (upper)
2.2/0.787	20.47	7.1	3.2-10.8		3.2	1.8
2.94/0.76	19.3	6.6	3.0-10.7		3.2	0.9
3.48/0.762	18.4	6.27	3.14-10.7		1.2	0.9
3.7/1.6	15.63	6	3.1-10.9		0	2.8
4.4/1.6	14.3	5.2	3.06-10.67		1.2	0.6

behavior of the distributed elements over the given frequency range. A half wavelength

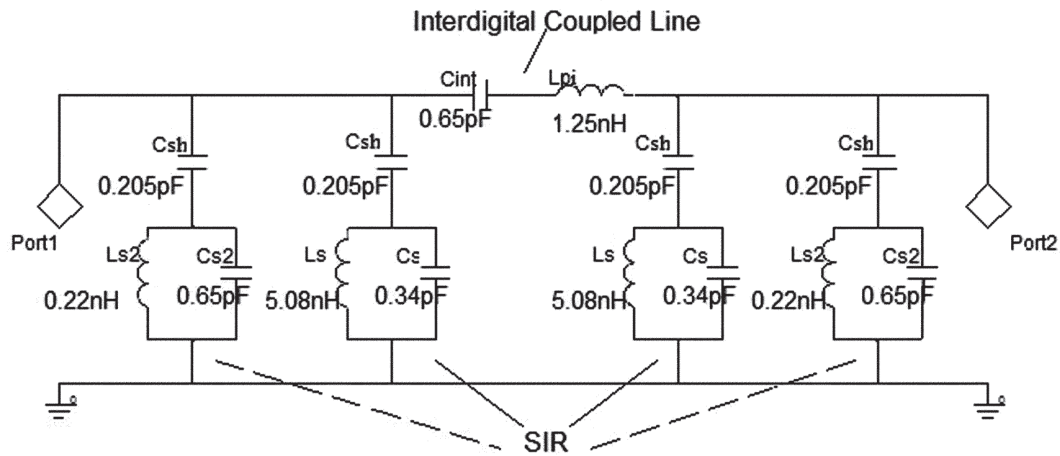


Figure 4.5: Lumped Element Model of the Filter

open stub behaves like a shunt connected parallel LC resonator as detailed in section 3.2.1. This fact is considered in modeling the circuit. L_s and C_s represent the equivalent inductance and capacitance of the SIR. C_{int} and L_{pi} represent the interdigital coupled line.

Z_1 of 40 Ω and Z_2 of 130 Ω are the stepped impedance values corresponding to W_1

and W_2 . The value of capacitance C_s corresponding to length L_1 is computed using the relation, $L_1 = f_c \lambda_{g1} Z_1 C_s$ [6], as 0.34pF. The inductance L_s for length L_2 is evaluated using the expression $L_2 = f_c \lambda_{g2} L_s / Z_2$, as 5.08nH. C_{int} and L_{pi} represent the capacitance and parasitic inductance of the interdigital coupled line ($L_a = 5.22\text{mm}$). C_{int} of the interdigital coupled line is evaluated using Eq. 4.3 [7]. The unequal finger widths are accounted for by taking average of capacitances of two different finger widths W_{ca} and W_{sa} [8].

$$C_{int} = \frac{\epsilon_{re} 10^{-3}}{18\pi} \frac{K(k)}{K'(k)} (N-1) L_a (\text{pF}) \quad (4.3)$$

where L_a is the length of the finger in microns, N the number of fingers, ϵ_{re} the effective dielectric constant of the microstrip line of width $W = W_{ca}$ or W_{sa} . The ratio

$$\frac{K(k)}{K'(k)} = \frac{\pi}{\ln \left[2 \frac{1+\sqrt{k'}}{1-\sqrt{k'}} \right]}; k = \tan^2 \left(\frac{a\pi}{4b} \right);$$

$$a = \frac{W}{2}; b = \frac{W+g}{2}; k' = \sqrt{1-k^2}$$

The parasitic inductance and capacitance L_{pi} and C_{pi} represent conventional series inductance and shunt capacitance in microstrip transmission line. The values of L_{pi} and C_{pi} are evaluated as in Eq. 4.4 [7],

$$L_{pi} = \frac{Z_0 \sqrt{\epsilon_{re}}}{c} L_a; C_{pi} = \frac{1}{2} \frac{\sqrt{\epsilon_{re}}}{Z_0 c} L_a \quad (4.4)$$

where ϵ_{re} is effective relative permittivity of the microstrip transmission line whose strip width is W_a (marked in Fig. 4.1(a)), Z_0 is characteristic impedance of a microstrip

transmission line with strip width W_a and c is the velocity of light in free space. The distributed shunt capacitance C_{sh} also accounts for the parasitic shunt capacitance C_{pi} of the interdigital line. The inherent property of the half wavelength open stub producing a second resonance is taken into consideration by introducing another parallel LC circuit (L_{s2} and C_{s2}) resonating at $3f_c/2$.

The model is simulated using ANSYS® Designer™ and a comparison of measured and simulated transmission parameters is shown in Fig. 4.6.²

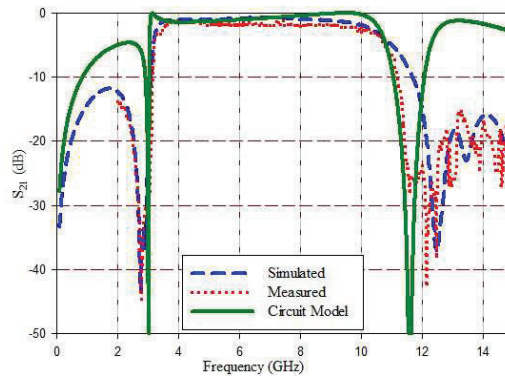


Figure 4.6: Comparison of Transmission Parameters

4.5 Dispersion Studies

The variation of phase with frequency is examined for the designed filter. A linear phase variation over the passband dictates a constant group velocity which is a basic

²Bindu C J, S Mridula and P.Mohanam, *Equivalent Circuit Modeling of a Microstrip UWB Filter*, Ninth Asia International Conference on Mathematical Modelling and Computer Simulation- Kuala Lumpur, Malaysia, pp. 175- 178, Sep.,2015

requirement of filters used in communication applications. This ensures distortionless transmission of signals.

Propagation constant of the filter structure can be computed from transmission parameters. Fig. 4.7 shows the $\omega - \beta$ diagram for the filter. ω is the frequency ($2\pi f$ rad/sec, where f is in GHz) and β is the unwrapped phase of S_{21} . It is seen that the phase variation is linear in the passband extending from 3.1GHz to 10.6GHz.

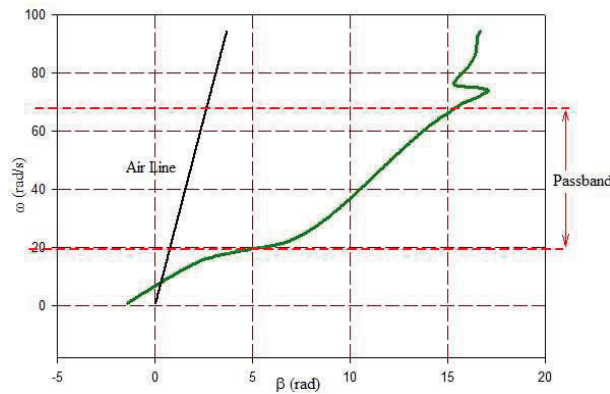


Figure 4.7: $\omega - \beta$ diagram

Air line corresponds to the dispersion of a uniform microstrip line. Plotting the air line divides this diagram into two distinct regions known as the fast wave region (lying to the left of the air line) and the slow wave region (lying to the right of the air line).

As seen in the Fig. 4.7, the β value for the designed filter increases with frequency and the increase is higher when compared to that of simple uniform microstrip line. The slope of the air line marks the propagation velocity. For the waves bound by the substrate, the velocity is less than that of light propagating in a homogeneous medium. The left side of the air line represents region where the propagating modes are not bound

to the surface and are radiative in nature. For the filter, the entire frequency range lies in the slow wave region (to the right of the air line), where the waves are bound to the substrate.

4.6 Time Domain Analysis

Optimized time response is required for filters used in modern microwave receivers, radar, satellite systems etc. If the design causes considerable overshoots, receiver channels will be saturated and may not respond in time. As frequency discrimination is increased, Q of the individual sections tends to increase which in turn increases overshoot and ringing.

The filter response in time domain is examined. Fig. 4.8 shows the simulated unit step response of the filter.

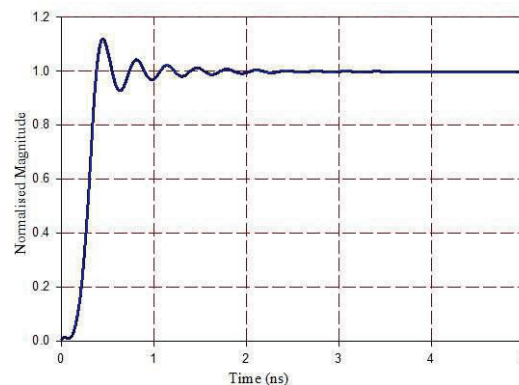


Figure 4.8: Simulated Unit Step Response of the filter

As can be observed the rise time is 0.18ns indicating the fast response of the filter. The overshoot reaches upto 116% and the filter is well damped to get a steady output

with 2% accuracy in 1.4ns (settling time) thus establishing the stability of the system.

4.7 Measurement Results

Fig. 4.9 shows the photograph of the prototype filter along with the SMA connectors. The structure is compact as can be seen in figure. Standard photolithography is used for the fabrication process and the S parameter measurements are taken using HP8510C Vector Network Analyzer.

The measured results in Fig. 4.10 (a-c) agree well with the simulated results. Small

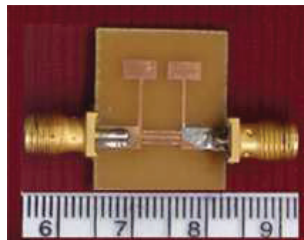


Figure 4.9: Photograph of the Prototype Filter

discrepancies in the results can be attributed to the inaccuracies in the fabrication process and/or numerical errors in simulation.

Measured S_{21} characteristics in Fig.4.10(a) show an average insertion loss of 1.6dB including that introduced by the SMA connectors. Attenuation in the lower stopband is 13dB and upper stopband is better than 14dB. Roll-off rate at lower band edge is 76dB/GHz and 26 dB/GHz at upper band edge. Fractional bandwidth attained is 109%. Measured reflection characteristics of the filter shown in Fig. 4.10(b) is well below 10dB for the entire bandwidth.

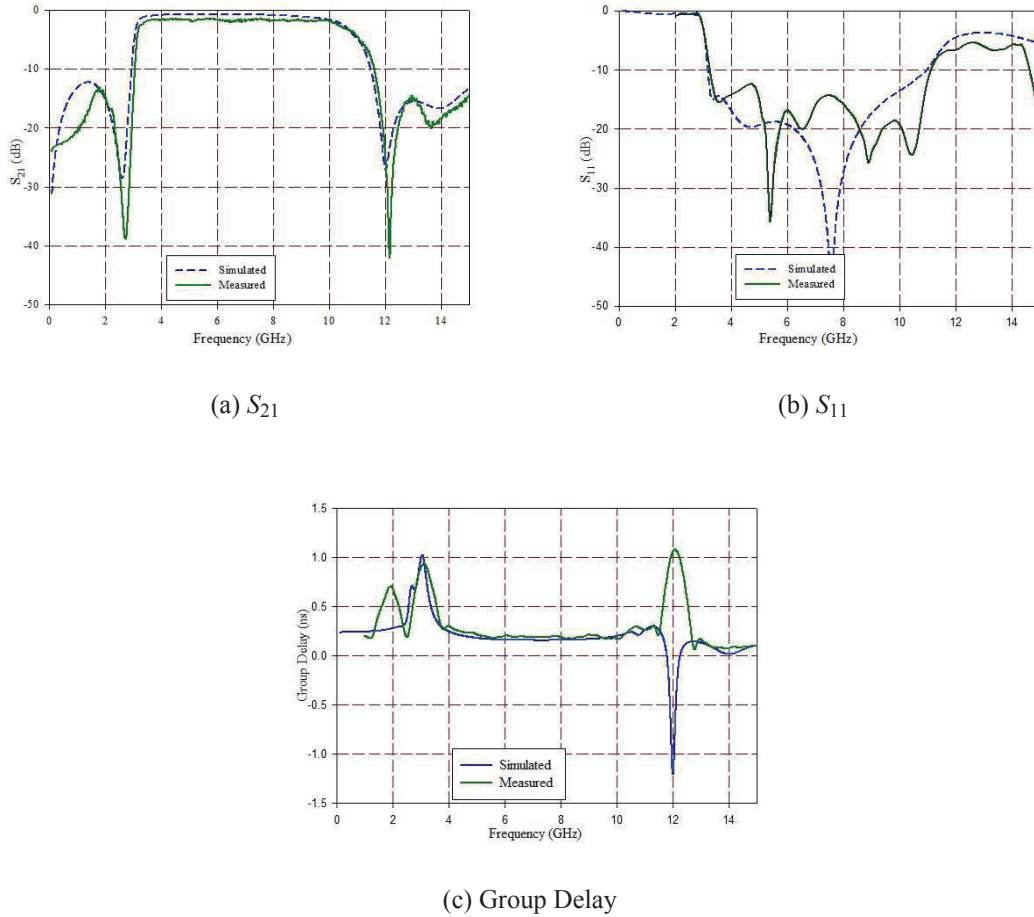


Figure 4.10: Measured Results of the Fabricated Filter

Flat group delay in Fig. 4.10(c) reveals that the designed filter has good linear phase characteristics making it suitable for a variety of communication applications. The group delay is almost flat in the passband and variation is less than 0.06ns. Abrupt change in group delay near the cut off frequencies indicates the presence of resonators which tend to store energy, rather than passing it out. Table 4.5 gives a comparison of filter parameters with similar reported work.

4.8 Summary

The filter designed is a stepping stone for future implementations. The design is simple and can be tuned to any required bandwidth, by varying the width ratio of open stubs and length of coupled lines. The roll off achieved is steep and the attenuation in the stop bands is sufficient to make it suitable for indoor UWB applications. It can be further improved by cascading more sections as desired. However, there is a limitation that the structure may become complex and occupy more real estate as more sections are incorporated. Attempts are made to improve the performance without increasing the size as detailed in the subsequent chapters.

Table 4.5: Comparison of Filter Parameters with Similar Reported Work

Parameters/ References	Passband (GHz)	Insertion Loss (dB)	Roll off Rate- Lower, Upper (dB/ GHz)	Stopband Attenuation- Lower, Upper (dB)	Group Delay Variation (ns)	Size (mm ²)	Substrate [ϵ_r / h (mm)]
[Jia Sheng et al., 2005]	3.5-14.5	0.75	14,9	16	0.23	34 x 6	6.15/1.27
[Pramod K. Singh et al., 2007]	3.1-10.6	0.5	50,30	35,15	0.21	18.6 x 13.5	3.38/0.81
[M. S. Razalli et al., 2008]	3.06-10.43	0.85	10,20	13,13	0.15	25 x 20	2.2/0.508
[K. Song and Q. Xue, 2010]	3.3-10.4	≤ 1	20,13	-,32	0.22	16.2 x 8.8	2.2/0.127
[Marjan Mokhtaari et al., 2010]	2.8-8.2	2	36,65	21,8	0.5	20 x 17	6.15/0.635
[Proposed Filter]	3.1-10.6	1.6	76,26	13,14	0.06	17 x 19	4.4/1.6

Bibliography

- [1] Esmat A. F. Abdallah and Nabil A. El-Deeb, "On the Analysis and Design of Three Coupled Microstrip Lines", IEEE Transactions on Microwave Theory and Techniques, Vol. MTT-33, No. 11, pp.1217-1222, Nov.1985.
- [2] Mitsuo Makimoto and Sadahiko Yamashita, "Bandpass Filters Using Parallel Coupled Stripline Stepped Impedance Resonators", IEEE Transactions on Microwave Theory and Techniques, Vol. MTT-28, No.12, pp.1413-1417, Dec.1980.
- [3] Jia-Sheng Hong, M. J. Lancaster, "Microstrip Filters for RF/Microwave Applications", John Wiley & Sons Inc., ISBN 0-471-22161-9, 2010.
- [4] Kongpop U-yen, Edward J. Wollack, Terence Doiron, John Papapolymerou and Joy Laskar, "A Bandpass Filter Design Using Half-Wavelength Stepped Impedance Resonators with Internal Couplings", IEEE Microwave and Wireless Components Letters, Vol.16, No.8, pp.443-445, Aug. 2006.
- [5] Pramod K. Singh, Sarbani Basu and Yeong-Her Wang, "Planar Ultra-Wideband Bandpass Filter Using Edge Coupled Microstrip Lines and Stepped Impedance Open Stub", IEEE Microwave and Wireless Components Letters, Vol.17, No.9, pp.649-651, Sep.2007.
- [6] David M. Pozar, "Microwave Engineering", John Wiley & Sons Inc., USA, ISBN 0-471-17096-8, Second Edition.
- [7] Inder Bahl, "Lumped Elements for RF and Microwave Circuits", International Journal of RF and Microwave Computer-Aided Engineering, Artech House, Norwood, MA, USA, 2003.

- [8] Mahdi Ali, et.al, "Novel Method for Planar Microstrip Antenna Matching Impedance", *Journal of Telecommunications*, Vol.2, pp.131-138, 2010.
- [9] M. S. Razalli, A. Ismail and M. A. Mahdi, "Novel Compact Microstrip Ultra-Wideband Filter Utilizing Short-Circuited Stubs With Less Vias", *Progress in Electromagnetics Research*, PIER 88, pp.91104, 2008.
- [10] Jia-Sheng Hong and Hussein Shaman, "An Optimum Ultra-Wideband Microstrip Filter", *Microwave and Optical Technology letters*, Vol. 47, No.3, pp.230-233, Nov. 2005.
- [11] K. Song and Q. Xue, "Inductance Loaded Y Shaped Resonators and their Applications to Filters", *IEEE Transactions on Microwave Theory and Techniques*, Vol.58, No.4, pp.978-984, Apr.2010.
- [12] Marjan Mokhtaari, Jens Bornemann and Smain Amari, "A Modified Design Approach for Compact Ultra-Wideband Microstrip Filters", *International Journal of RF and Microwave Computer-Aided Engineering*, Vol.20, No.1, pp.66-75, Jan.2010.

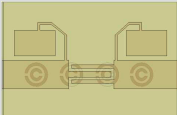
5 Compact UWB Filters

Contents

- ★ *Filter Using Folded SIR's and CSRR's*
- ★ *Filter Using Chip Inductors and CSRR's*

The chapter discusses two different methods employed to reduce the size of the filter presented in the previous chapter without affecting the performance. The first method folds the inductive stub of the SIR thus reducing the filter real estate. The second method replaces the inductive stub with chip inductor. However these methods affect the inherent properties of transmission line stubs which are accounted for by other means as elaborated in this chapter.

5.1 Filter Using Folded Stepped Impedance Resonators and Complementary Split Ring Resonators

	<i>Contents</i>	<ul style="list-style-type: none">★ <i>Geometry</i>★ <i>Simulation Studies</i>★ <i>Analysis and Design</i>★ <i>Lumped Element Model</i>★ <i>Dispersion Studies</i>★ <i>Time Domain Analysis</i>★ <i>Measurement Results</i>
---	-----------------	---

*This section presents a planar UWB filter employing folded Stepped Impedance Resonators to reduce the size. Complementary Split Ring Resonators etched in the ground plane improve the upper stopband performance. Compared to the SIR filter discussed in chapter 4, the overall dimension of the filter is 18mm x 12mm on a substrate with $\epsilon_r = 4.4$ and thickness 1.6mm, without degrading the performance.*¹

¹Bindu C J, S Mridula, *Folded SIR Filter with CSRR's for Ultra Wide Band Applications, International Symposium on Electronic System Design organized by the IEEE Computer Society at NTU, Singapore, pp. 182-185, Dec. 12-13, 2013.*

A UWB filter employing half wavelength SIR's on interdigital coupled lines was discussed in chapter 4. The compact UWB filter presented here is obtained by folding the inductive stub of the SIR. CSRR's on the ground plane serve to optimize the filter characteristics. SIR's and CSRR's are discussed in detail in chapter 3.

5.1.1 Geometry

The proposed filter uses folded stepped impedance resonators (SIR) on asymmetrical interdigital coupled lines to obtain the required UWB response. The interdigital coupled lines are quarter wavelength long at 6.85 GHz, the centre frequency of the UWB band extending from 3.1-10.6GHz. The transmission zero at the lower band edge is introduced by LC resonant circuits realized using folded half wavelength SIR's to reduce the chip area. However folding affects the inherent properties of transmission line stubs. Hence complementary split ring resonators are used to optimize the filter performance. Top and bottom view of the filter structure coupled to a 50Ω transmission line section on a substrate of dielectric constant 4.4, thickness 1.6mm and loss tangent 0.0018 are shown in Figure 5.1.1(a-b).

Design Evolution

The design evolution is shown in Fig. 5.1.2. Fig. 5.1.2(a) shows the layout of the filter with stub SIR and Fig. 5.1.2(b) shows the filter where the stub SIR is replaced with its folded counterpart. Care is taken to avoid sharp bends while folding, as there may occur current crowding at the sharp edges. On folding the inductive stub, the lengths of individual sections of the stub are reduced to much smaller than quarter wavelength. The

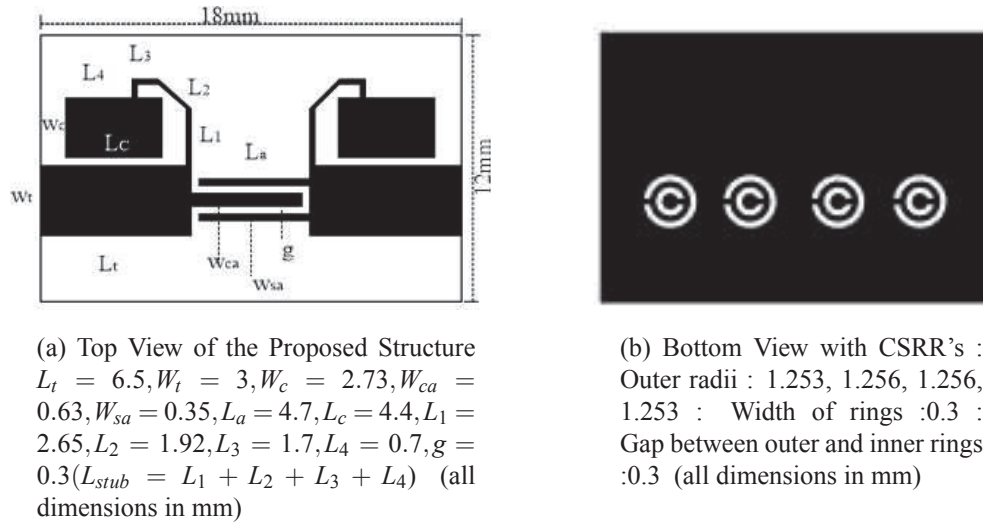
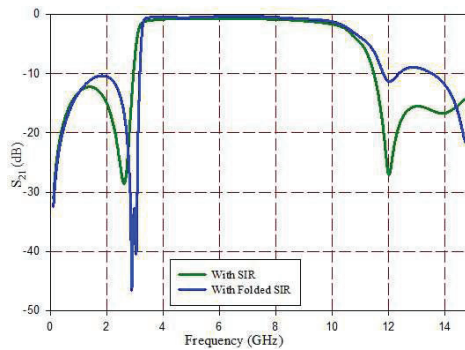
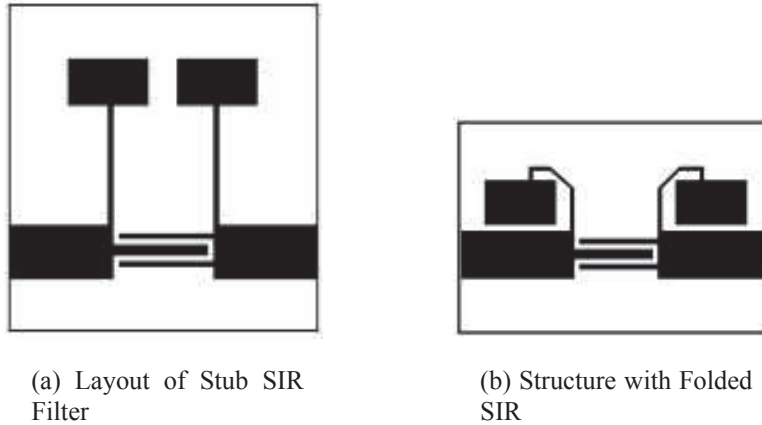


Figure 5.1.1: Top and Bottom View of the Filter Structure

inductive stub thus loses its transmission line property and behaves like a lumped element. The contribution from the second resonance of the half wavelength SIR is therefore absent. The upper band edge in the transmission characteristics is thus adversely affected as evident in Fig. 5.1.2(c). Hence additional measures are to be taken to get a steep roll off at the upper band edge.

The conventional method of improving the roll off rate is to increase the filter order by adding more number of resonators. This will increase the size and complexity of the structure. Hence the introduction of sub wavelength resonators in the ground plane is explored. The band notch property of the complementary split ring resonators (CSRR) is exploited to get the sharp roll off at the upper band edge. The behaviour of CSRR's is analyzed in detail in section 3.2.3. CSRR's behave like shunt connected parallel LC resonant circuits [1]-[3] and can be tuned to desired frequencies by varying the



(c) Comparison of Transmission Characteristics

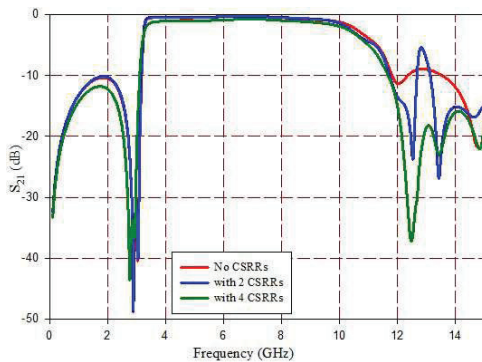
Figure 5.1.2: Design Evolution

dimensions. The main attraction is that CSRR's can be added without increasing the overall chip area of the filter structure.

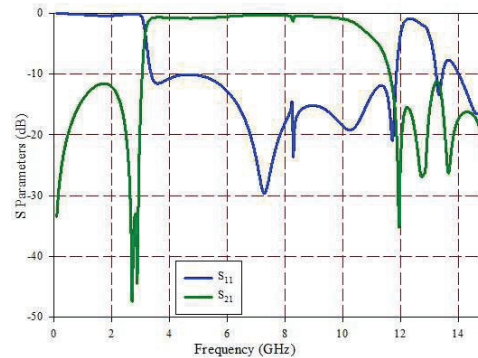
The CSRR's etched on the ground plane are aligned exactly below the transmission line portion for better performance. These resonators have inherent sharp resonances. The radii of the CSRR rings are selected so as to suppress the higher frequencies in the upper stopband. A parametric study on the dimensions of CSRR's is given in section

3.2.3. The outer radii of the outer rings of the four CSRR's are optimized as 1.253, 1.256, 1.256 and 1.253mm respectively. All the rings are of width 0.3 mm and are separated by a gap of 0.3 mm. The structure is compact with an optimized dimension of 18mm x 12mm.

Simulated responses of the filter are shown in Fig. 5.1.3. The variation in S_{21} for different number of CSRR's etched in the ground plane is shown in Fig. 5.1.3(a), thus justifying the use of four CSRR's in the ground plane. Simulated S parameters of the proposed filter in Fig. 5.1.3(b) reveal the sharp rejection at lower and upper cut off frequencies. Out of band rejection obtained is 11dB. Roll off rate at the lower band edge is 175dB/GHz and at upper band edge is 30dB/GHz. The average insertion loss is 0.5dB, but can be reduced further by using a low loss dielectric material. Return loss is below 10dB for the entire band.



(a) Variation in S_{21} for Different Number of CSRR's



(b) Simulated S Parameters of the Proposed Filter: Transmission Zeros- 2.87GHz, 11.95GHz, 12.76GHz, 13.65GHz

Figure 5.1.3: Simulated Responses of the Filter Structure

5.1.2 Simulation Studies

Detailed analysis of the circuit behavior is done by examining the field distributions at various frequencies in the UWB band. The surface current vectors on the top surface of the filter are shown in Fig. 5.1.4(a-c). At the lower cut off frequency 3.1GHz, the surface

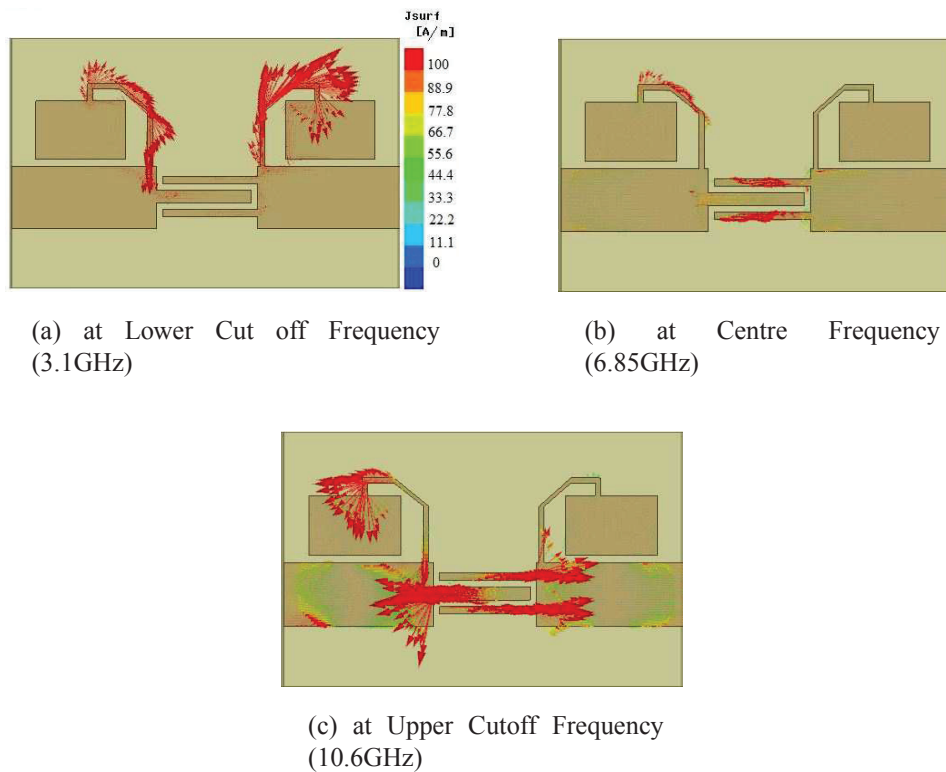


Figure 5.1.4: Surface Current Vectors on the Top Surface

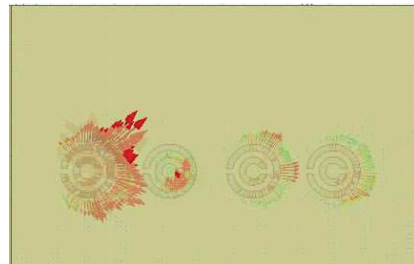
current is concentrated in the folded SIR's. At centre frequency 6.85GHz, the entire signal is coupled to the output port along the interdigital coupled lines. At the upper cut off frequency 10.6GHz, the current direction changes and the odd mode currents are

seen crowded in the filter with minimal flow towards the output port as shown in Fig. 5.1.4(c).

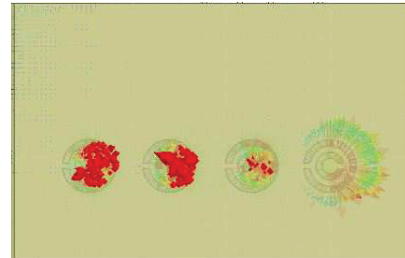
Although the resonant frequency of the CSRR depends on the external radius, the interactive nature of the CSRR array influences the resonant behaviour. The electric field vector in CSRR reverses its orientation at the transmission zeros in the upper stopband as shown in Fig. 5.1.5. CSRR's 1 and 3 contribute to the transmission zero at 11.95GHz. This is evident from the reversal of orientation of electric field at two frequencies on either side of the transmission zero (Fig. 5.1.5(a-b)). Transmission Zero at 12.7GHz is due to CSRR's 1 and 2, as evident from Fig. 5.1.5(c-d). Similarly transmission zero at 13.6GHz is due to CSRR's 1 and 4 (Fig. 5.1.5(e-f)).

5.1.3 Analysis and Design

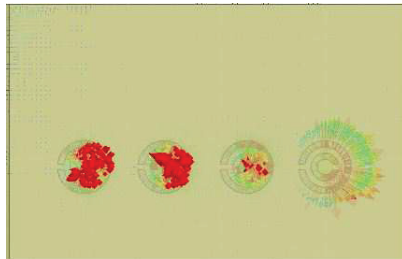
Results of parametric analysis in Fig. 5.1.6 reveals the dependence of the lower and upper cut off frequencies on the dimensions of the filter. Variation of the length of the inductive stub, $L_{stub} = L_1 + L_2 + L_3 + L_4$ from 5.85mm to 6.85mm results in a lower cut off frequency variation from 3.8 to 3.5 GHz (Fig. 5.1.6(a)). The upper cut off frequency is not affected significantly. Variation of upper cut off frequency with the coupled arm length (L_a) is shown in Fig. 5.1.6(b). As the coupled arm length decreases, the upper band edge increases, while the lower band edge remains almost unaffected. The results are shown for coupled arm length variation from 5.3mm to 4.5mm varying the upper cut off from 10.11GHz to 10.7GHz. Due to the inter dependent nature of resonators and the change in effective permittivity of the entire structure with change in individual dimensions, the lower and upper band edges cannot be controlled independently



(a) at 10.9GHz



(b) at 12.2GHz



(c) at 12.2GHz



(d) at 13.2GHz



(e) at 13.2GHz



(f) at 14.5GHz

Figure 5.1.5: Electric Field Vectors in CSRR's in the Vicinity of Upper Stopband Transmission Zeros :(a-b) Transmission zero at 11.95GHz: (c-d) Transmission zero at 12.76GHz :(e-f) Transmission zero at 13.65GHz

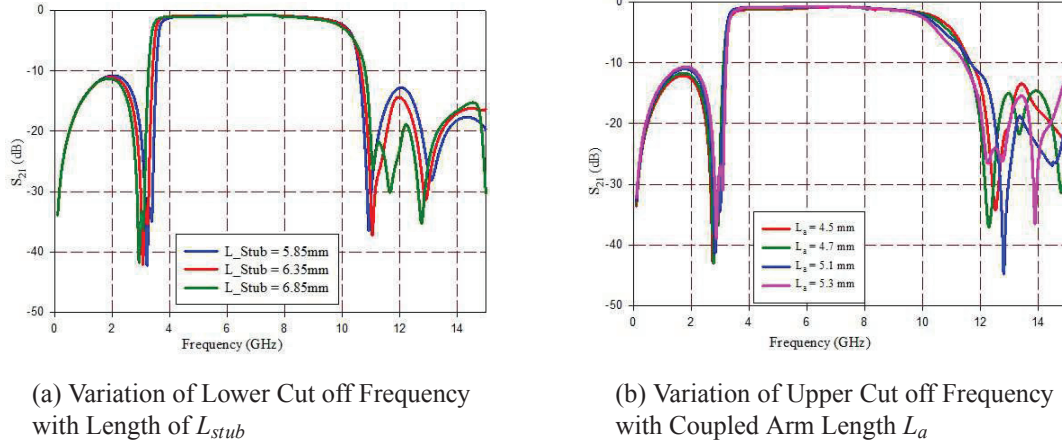


Figure 5.1.6: Results of Parametric Analysis

beyond a limit. But this can be used as a guideline for designing the filter for different bandwidths.

Based on the parametric studies and field distributions, the controlling elements for lower and upper cut off frequencies are identified. Simulations are carried out for different values of these elements on different substrates to form a database.

Multivariable regression analysis is carried out on this data to evaluate the influence of each parameter and thus formulate design equations. For a substrate with relative permittivity ϵ_r and slab thickness h (mm), the required length of inductive stub L_{stub} (mm) for a lower cut off frequency f_1 (GHz) is calculated using Eq. 5.1.1.

$$L_{stub} = 12.41 - 2.71f_1 - 0.26\epsilon_r + 2.51h \quad (5.1.1)$$

Similarly, the coupled arm length L_a required for an upper cut off frequency f_2 is

calculated using Eq. 5.1.2.

$$L_a = 13.97 - 1.15f_2 - 0.35\epsilon_r + 3.11h \quad (5.1.2)$$

The equations are verified on different substrates. Computed values of inductive stub length L_{stub} and coupled arm length L_a along with UWB bands obtained are shown in Table 5.1.1. The equations are valid for $2.2 \leq \epsilon_r \leq 5.7$; $0.8 \leq h \leq 1.6$.

Table 5.1.1: Computed Values of L_{stub} and L_a with the UWB bands Obtained

Substrate ϵ_r/h	L_{stub} (mm)	L_a (mm)	Band Obtained (GHz)	%Error (Lower)	%Error (Upper)
2.2/1	5.98	4.12	3.15-10.61	1.6	0.09
3.5/0.8	5.11	3.04	3.06-10.57	1.2	0.28
3.8/1.6	7.04	5.43	3.08-10.52	0.6	0.75
5.7/1.25	5.66	3.67	3.2-10.5	3.2	0.94

5.1.4 Lumped Element Model

Lumped element model for the filter is deduced as explained in chapter 4 and shown in Fig. 5.1.7. The folded SIRs are represented by two shunt connected parallel LC resonant circuits with values $L_s = 5.08\text{nH}$ and $C_s = 0.34\text{pF}$. The interdigital coupled line is represented by capacitance C_{int} and parasitic inductance L_{pi} , with values 0.6pF and 2.5nH respectively. The CSRR's are represented by four shunt connected parallel LC circuits resonating at 16.96GHz ($L_{c1} = 0.1\text{nH}$, $C_{c1} = 0.88\text{pF}$) and 15.53GHz ($L_{c2} =$

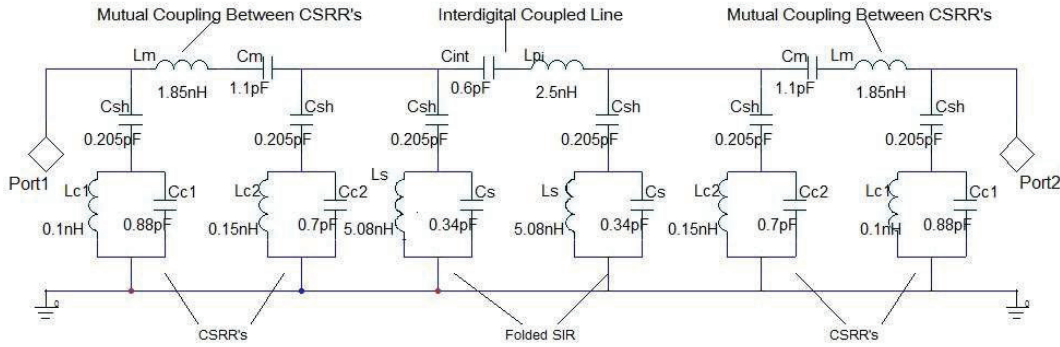


Figure 5.1.7: Lumped Element Model

0.15nH , $C_{c2} = 0.7\text{pF}$), corresponding to outer radii 1.253mm and 1.256mm respectively [4]. The distributed shunt capacitance C_{sh} also accounts for the parasitic shunt capacitance of the interdigital line. L_m and C_m account for the mutual coupling between CSRR's.

Comparison of transmission parameters of simulated, measured and circuit model of the filter is shown in Fig. 5.1.8.

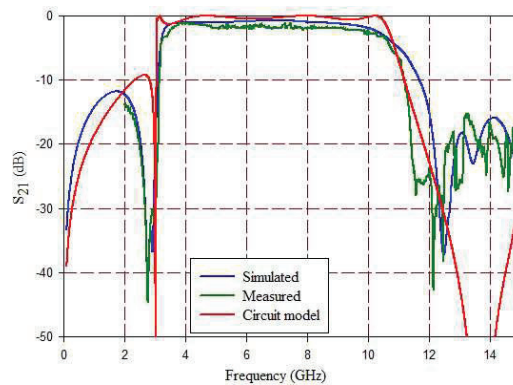


Figure 5.1.8: Comparison of Transmission Parameters

5.1.5 Dispersion Studies

The variation of phase with frequency is examined for the designed filter. A linear phase variation over the passband dictates a constant group velocity which is a basic requirement of filters used in communication applications for distortionless transmission of signals.

Fig. 5.1.9 shows the $\omega - \beta$ diagram for the filter. It is seen that the phase variation is

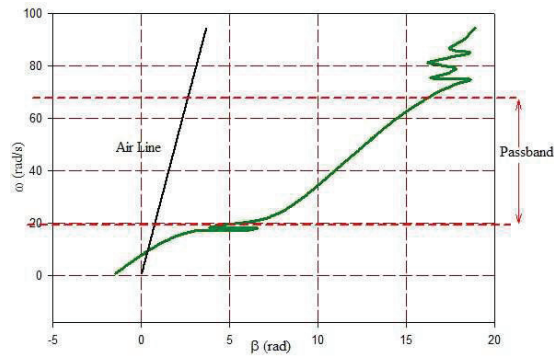


Figure 5.1.9: $\omega - \beta$ diagram

linear in the passband extending from 3.1GHz to 10.6GHz. As explained in section 4.5, the operating band of the filter lies in the slow wave region lying to the right of the air line.

5.1.6 Time Domain Analysis

The simulated time response of the filter for a unit step input is obtained as shown in Fig. 5.1.10. The response shows a fast response with a rise time of 0.19ns and the output settles down to 2% tolerance limit within 1.6ns. The maximum overshoot is

119%. However the response is slightly degraded when compared with that of the SIR filter discussed in chapter 4. This may be attributed to the slightly complex structure involving folded stubs and CSRR's.

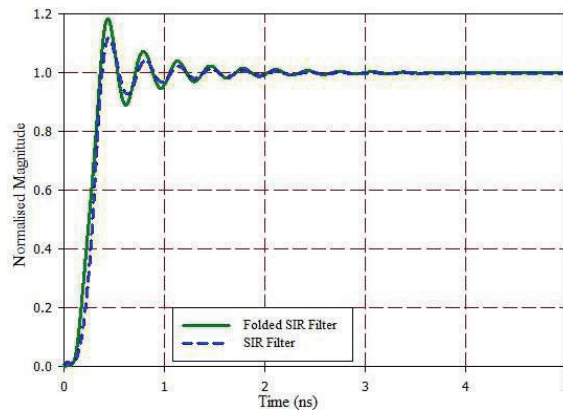
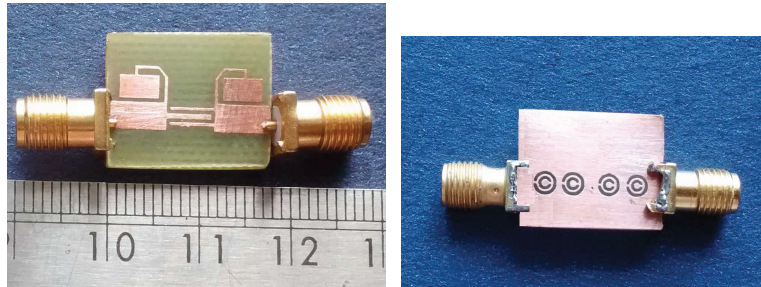


Figure 5.1.10: Simulated Unit Step Response of the Filter in Comparison with SIR Filter

5.1.7 Measurement Results

Fig. 5.1.11(a-b) show the photograph of the prototype filter along with the SMA connectors. The structure is compact with an overall dimension of 18mm x 12mm. Standard photolithography is used for the fabrication process and S parameter measurements are taken using Agilent 8753ES Vector Network Analyzer.

Measured results in Fig. 5.1.12 agree well with simulated results. Average insertion loss is 1.5dB including those introduced by the SMA connectors. The tolerance of the substrate material may also contribute. Attenuation in the lower stopband is less than 13dB and upper stopband is less than 15dB. Roll off rate is sharp with 85dB/GHz at lower and 26dB/GHz at upper band edges and the fractional bandwidth attained is

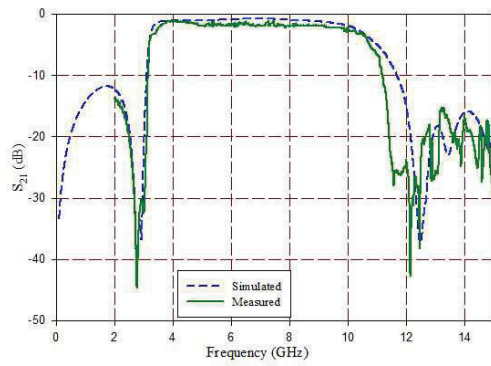
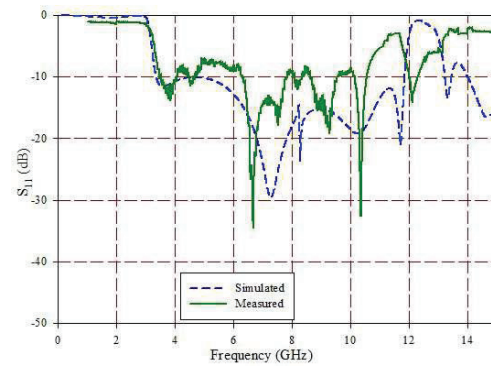
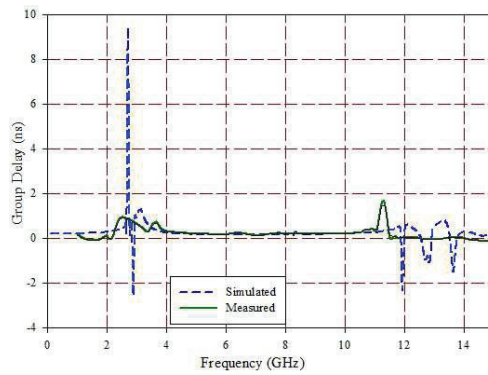


(a) Top View

(b) Bottom View

Figure 5.1.11: Photograph of the Prototype Filter

109%. The group delay is flat in the entire passband and variation is less than 0.04ns thus making the filter suitable for communication applications. Table 5.1.2 gives a comparison of the filter performance with other reported work [7]-[10]. As can be observed from the table the filter is superior in terms of roll off rate and group delay.

(a) S_{21} (b) S_{11} 

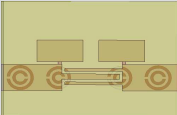
(c) Group Delay

Figure 5.1.12: Measured Results

Table 5.1.2: Comparison of Parameters of Similar Works

Parameters/ References	Passband (GHz)	Insertion Loss (dB)	Roll off Rate- Lower, Upper (dB/ GHz)	Stopband Attenuation- Lower, Upper (dB)	Group Delay Variation (ns)	Size (mm^2)	Substrate [ϵ_r , $h(mm)$]
[Pramod K. Singh et al., 2007]	3.1-10.6	0.5	50,30	35,15	0.21	18.6 x 13.5	3.38/0.81
[K. Song, and Q. Xue, 2010]	3.3-10.4	≤ 1	20,13	-,32	0.22	16.2 x 8.8	2.2/0.127
[B. Xia et al., 2012]	3.54-10.6	0.15-2.5	45,45	14.3,15.4	Not Specified	26.2 x 11.9	4.3/0.41
[Marjan Mokhtaari et al., 2010]	2.8-8.2	2	36,65	21,8	0.5	20 x 17	6.15/0.635
[Proposed Filter]	3.1-10.6	1.5	85,26	13,15	0.04	18 x 12	4.4/1.6

5.2 Filter Using Chip Inductors and Complementary Split Ring Resonators

	<i>Contents</i>	<ul style="list-style-type: none"> ★ <i>Geometry</i> ★ <i>Simulation Studies</i> ★ <i>Analysis and Design</i> ★ <i>Lumped Element Model</i> ★ <i>Dispersion Studies</i> ★ <i>Time Domain Analysis</i> ★ <i>Measurement Results</i>
---	-----------------	---

Planar UWB filter using stepped impedance resonators (SIR's) and quarter wavelength coupled lines has been presented in Chapter 4. Further in section 5.1, filter employing folded SIR's was discussed to reduce the filter real estate. As a different approach for size reduction, the stub inductors in SIR's are replaced with chip inductors. Sharp attenuation is achieved by the introduction of suitably tuned CSRR's etched in cascade in the bottom ground plane. The proposed filter has a much reduced footprint compared to the one discussed in chapter 4, occupying only 17mm x 12mm on a substrate with $\epsilon_r = 3.7$ and thickness 1.6mm. ²

²Bindu C J, Anju Pradeep, S Mridula, Compact Ultra Wide Band Filter Using Chip Inductors and CSRR's, National Symposium on Antennas and Propagation, CUSAT, Kochi, India, pp.90-93 Dec., 2012.

The compact UWB filter presented here is obtained by replacing the inductive stubs of SIR with chip inductors while retaining the capacitive stubs as rectangular patch capacitors. However the use of chip inductors affects the upper stopband performance. This is compensated by incorporating complementary split ring resonators in the ground plane. The details are elaborated in subsequent sections.

5.2.1 Geometry

The filter consists of two LC resonators on quarter wavelength asymmetrical interdigital coupled lines. The top and bottom layout of the filter on a substrate with relative permittivity $\epsilon_r = 3.7$ and thickness $h = 1.6\text{mm}$, is given in Fig. 5.2.1(a-b). The optimized dimension of the structure is $17\text{mm} \times 12\text{mm}$.

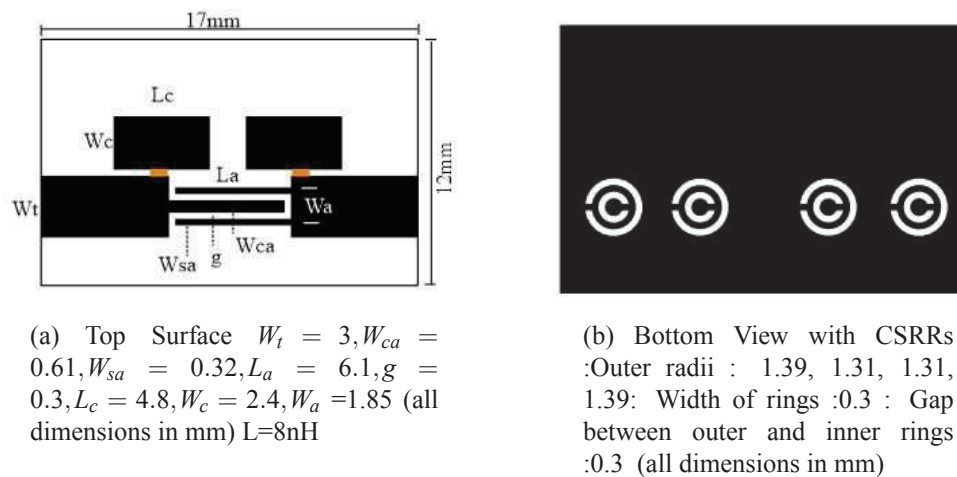


Figure 5.2.1: Top and Bottom Layout of the Filter

The transmission zeros at lower cut off frequency are introduced with the help of LC resonators, where the inductance is realized using chip inductors, while low impedance

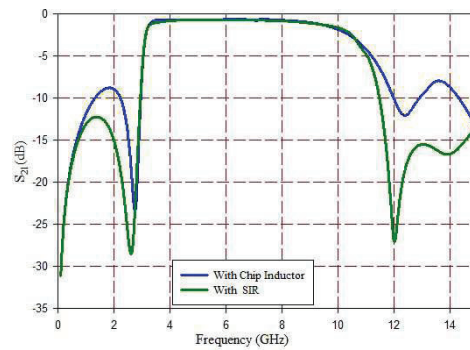
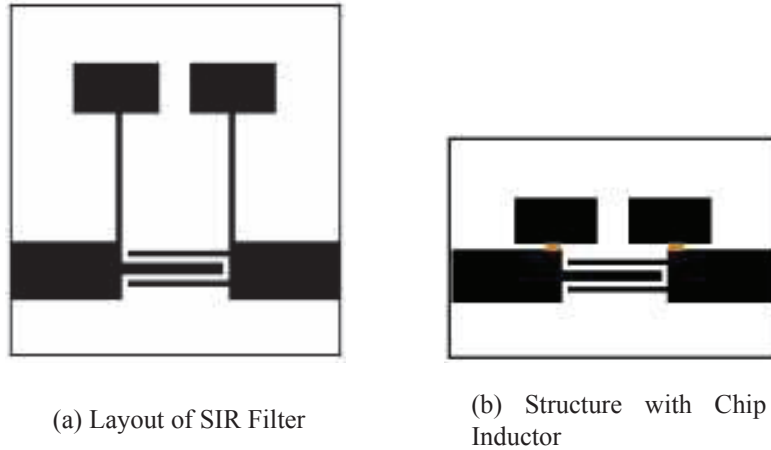
open stubs (of the stepped impedance resonators) are retained as capacitors, *i.e.* the LC resonators required for the desired transmission zeros are implemented using chip inductors and rectangular patch capacitors. Complementary split ring resonators on the ground plane are used to optimize filter performance as discussed in section 5.1.1.

Design Evolution

Figure 5.2.2 (a-c) show the design evolution of the proposed filter from a stub SIR filter. Chip inductors can effectively minimize the chip area [11]-[12] and are thus used in place of stub inductors. Further, the design is quite easy as chip inductors are available in discrete values over a wide range. Chip inductors are seen to have high Q value as frequency increases. So the performance of the filter will not be affected [13]. While choosing the inductor, it is made sure that the self-resonant frequency (SRF) is well outside the operating band. Also, the electrical characteristics like variation of inductance value with frequency must be nominal.

Fig. 5.2.2(c) shows a comparison of simulated S_{21} plots of stub SIR filter and filter with chip inductors. From the plot, it is seen that the response has a sharp roll off at lower band edge and a low insertion loss in the passband, but the higher band edge is not very attractive compared to that of the stub SIR filter in Fig. 5.2.2(a). This can be attributed to the absence of second resonance of SIR, which contribute to the sharp roll off in the upper band edge along with the influence of coupled lines.

The possibility of incorporating metamaterial/sub-wavelength resonators to improve the upper roll off rate is explored so as not to affect the chip area adversely. Fig. 5.2.3(a-b) shows the modified ground plane with two CSRR's incorporated. Performance of



(c) Comparison of Transmission Characteristics

Figure 5.2.2: Design Evolution

CSRR's is analyzed in section 3.2.3. CSRR is already proved to greatly help in achieving steeper roll off rate at the upper band edge in the previous work employing folded SIR discussed in section 5.1. Thus the required performance is obtained by etching CSRR's in the ground plane. From the transmission characteristics, it is seen that the roll off in the upper edge is made sharp by the introduction of the CSRR's etched in the ground

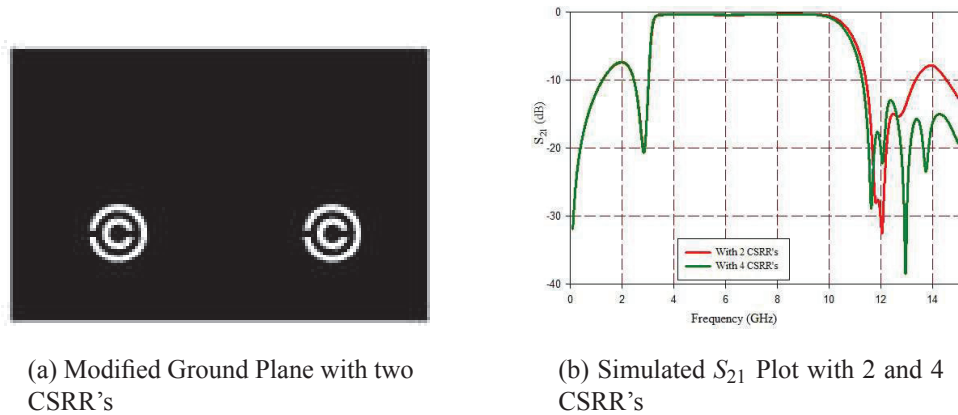


Figure 5.2.3: Modified Ground Plane and Improved Transmission Characteristics

plane. Stopband attenuation is improved by providing a cascade of 4 CSRR's tuned so as to suppress the higher frequencies. A comparison of transmission characteristics with 2 and 4 CSRR's is given in Fig. 5.2.3(b).

The outer radii of the CSRR's from left to right are 1.39mm, 1.31mm, 1.31mm and 1.39mm respectively. Thickness of the rings and the gap between the rings is 0.3mm.

5.2.2 Simulation Studies

Simulated S_{21} plot in Fig. 5.2.4(a) reveals that the additional CSRR's contribute to improved upper stopband attenuation. The insertion loss for the filter is well within 0.5dB. Also there is sharp rejection at lower and upper cut off frequencies. Transmission Zeros in the upper stopband are at 11.62GHz, 12.07GHz, 12.94GHz and 13.75GHz. Simulated group delay in Fig. 5.2.4(b) reveals the linear phase nature of the filter.

Field distributions at various frequencies are plotted to analyze the obtained transmission characteristics. The surface current vector on the top surface at the lower

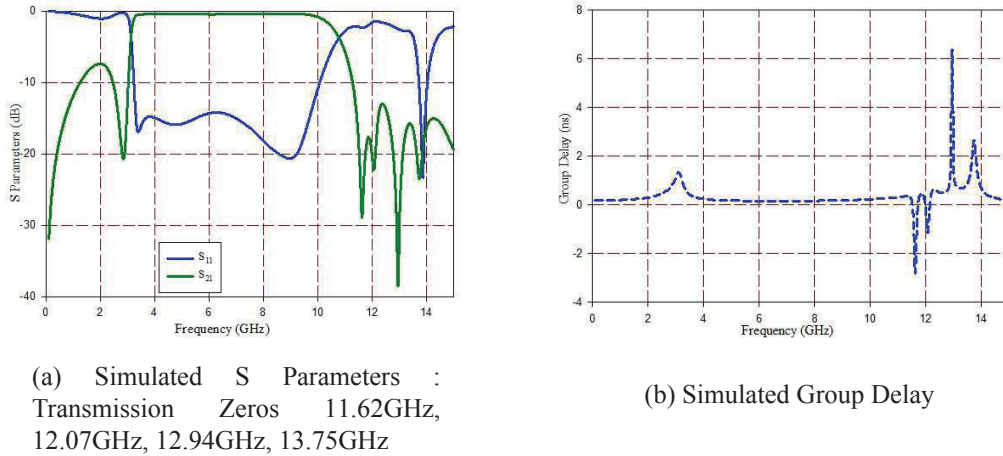


Figure 5.2.4: Simulated S Parameters and Group Delay

cut off frequency, centre frequency and upper cut off frequency are plotted in Fig. 5.2.5. At lower cut off frequency 3.1GHz, the current is concentrated in the LC resonator and it is identified as the contributing element (Fig. 5.2.5(a)). At the centre frequency 6.85GHz the surface current vector along the interdigital coupled line shows the beginning of odd mode currents of smaller magnitudes. At 10.6GHz, upper cut off frequency, strong odd mode currents flow which contribute towards a transmission zero. These are shown in Fig. 5.2.5(b-c). The influence of CSRR's is evident from the electric field vectors in the ground plane at frequencies on either sides of upper transmission zeros.

At the first transmission zero in the upper stopband (11.62GHz), the electric field vector orients outwards from the right most CSRR. Immediately after the transmission zero, the direction of electric field reverses. This is evident from the reversal of orientation of electric field at two frequencies on either side of the transmission zero as

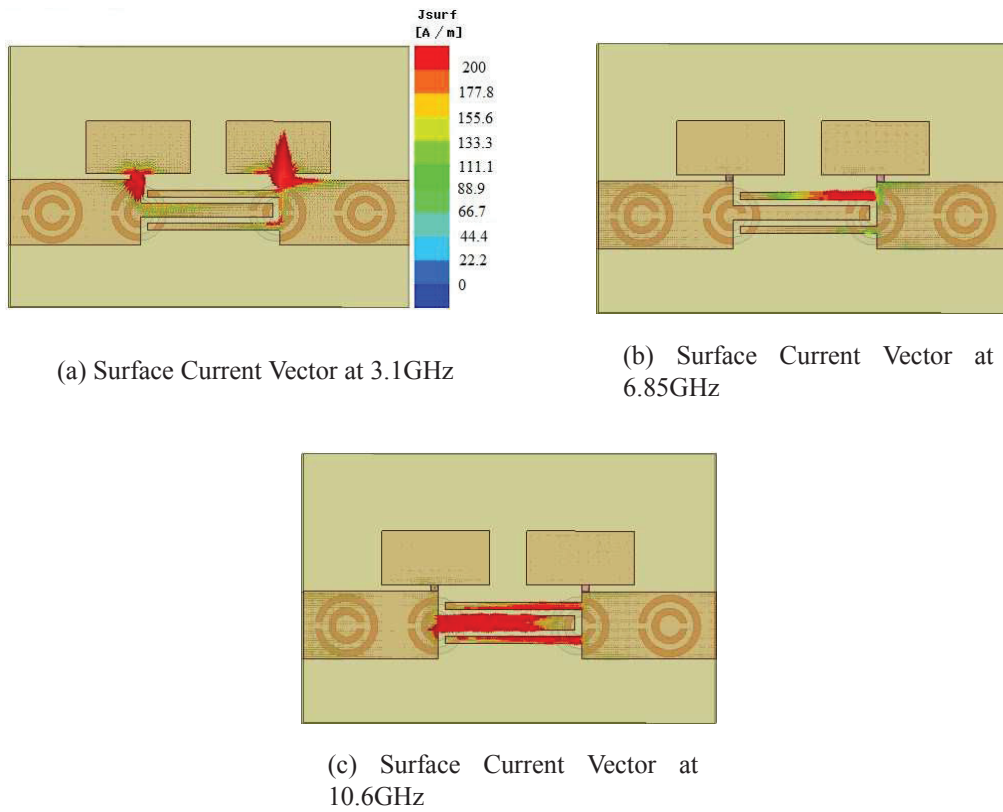


Figure 5.2.5: Surface Current Vector on Top Surface

shown in Fig. 5.2.6(a-b), thus identifying it as causing the phase reversal and hence the transmission zero. Similar behavior is observed in Fig. 5.2.6(c-d), near the left most CSRR for the second transmission zero at 12GHz. Third transmission zero is due to CSRR third from left as seen from Fig. 5.2.7(a-b). A combined effect of second and third CSRR from left, is seen in the fourth transmission zero as observed in Fig. 5.2.7(c-d). Even though transmission zeros are associated individually to different CSRR's, the effect of the entire array on the effective impedance of the structure is responsible for the obtained transmission characteristics. However these findings help

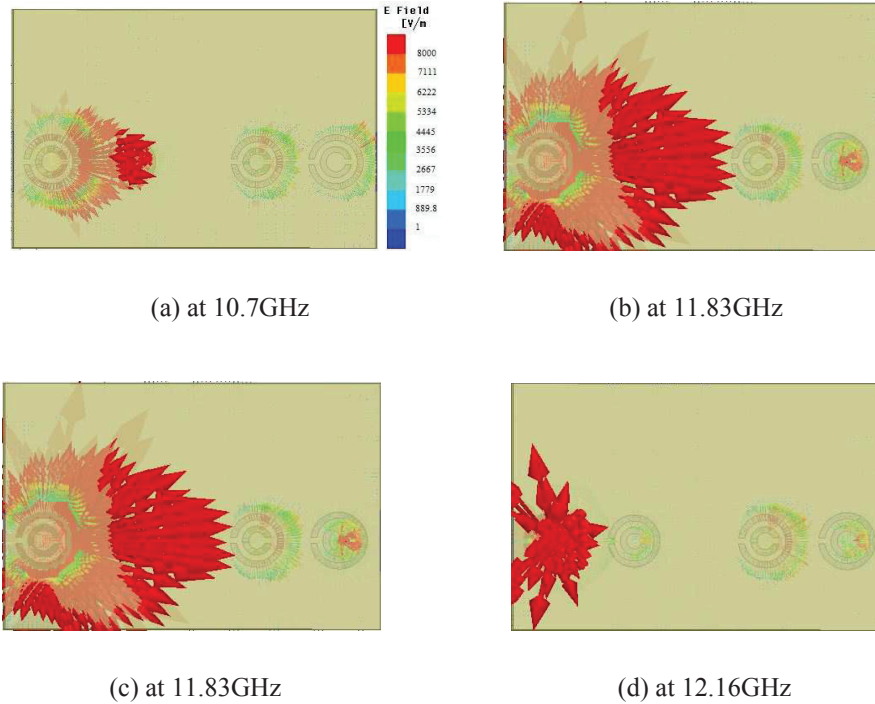


Figure 5.2.6: Electric Field Vectors in CSRR's in the Vicinity of Upper Stopband Transmission Zeros :(a-b) Transmission zero at 11.62GHz: (c-d) Transmission zero at 12.07GHz

in fine tuning of CSRR dimensions to get the required characteristics.

5.2.3 Analysis and Design

Parametric analysis is carried out by varying the chip inductor values as illustrated in Fig. 5.2.8. As expected, the lower cut off frequency decreases as the chip inductor value increases (Fig. 5.2.8(a)). However, varying width of the rectangular patch capacitor (W_c) does not cause a significant change in lower cut off frequency.

But, there occurs shift of the entire band for varying lengths (L_c) of rectangular

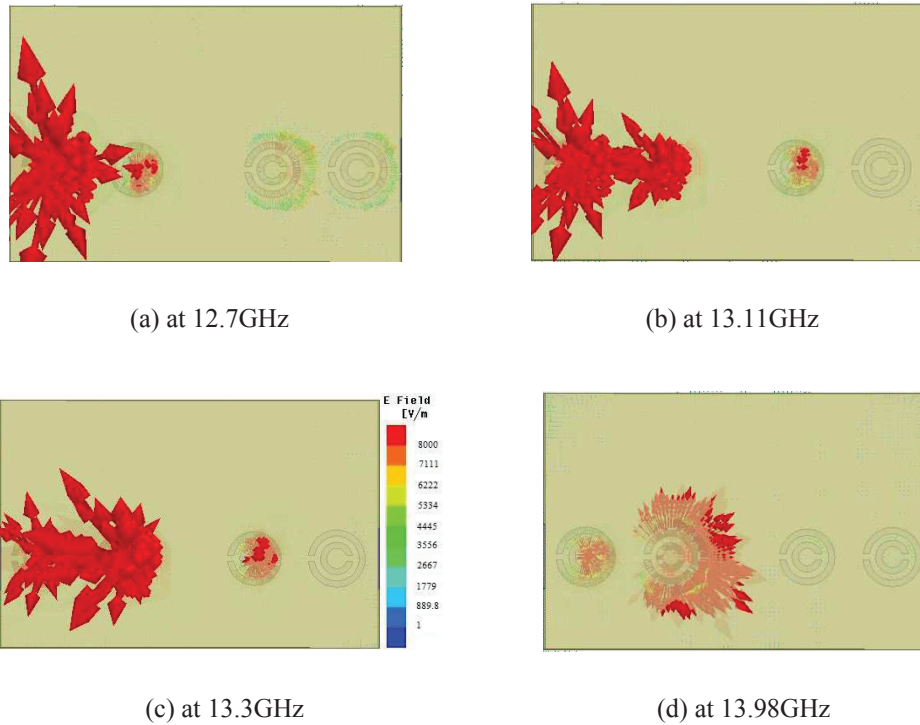
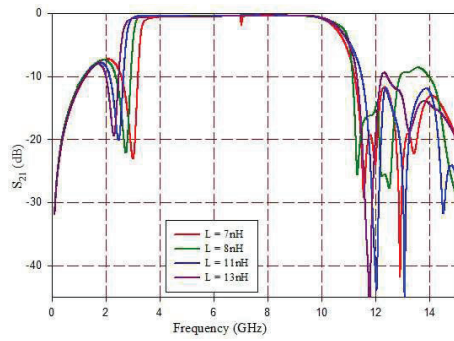


Figure 5.2.7: Electric Field Vectors in CSRR's in the Vicinity of Upper Stopband Transmission Zeros :(a-b) Transmission zero at 12.94GHz: (c-d) Transmission zero at 13.75GHz

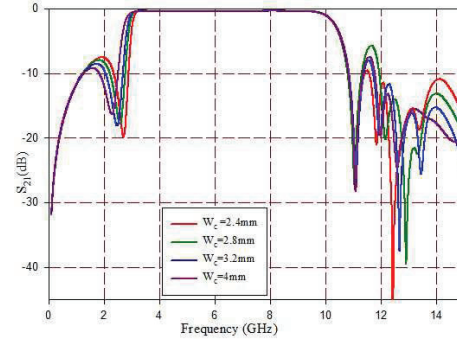
patch capacitor as seen in Fig. 5.2.8(c). Fig. 5.2.8(d) shows the variation of upper cut off frequency with coupled line length L_a . As length increases, frequency decreases.

Based on the above facts revealed from the parametric studies, generalized design equations for obtaining the required bandwidth on various substrates are developed applying multivariable regression on the database formed from simulation studies.

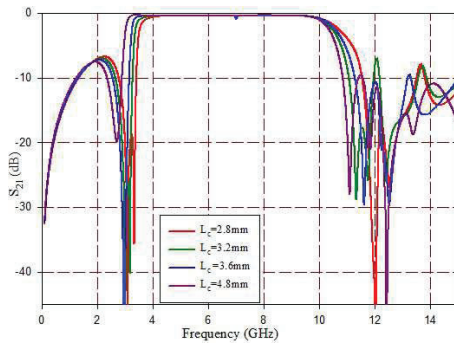
The chip inductor value L (nH) required for a lower cut off frequency f_1 (GHz) can



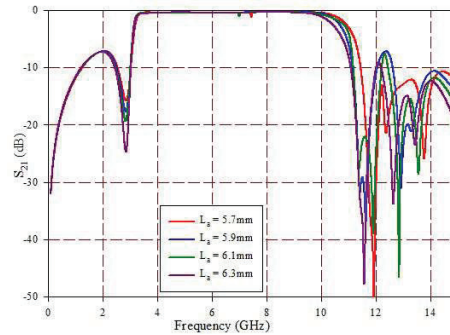
(a) Variation of Lower Cutoff Frequency with Chip Inductor Values



(b) Variation of Lower Cutoff Frequency with Varying Widths of Rectangular Patch Capacitor



(c) Shift in Band Observed with Variation of Length of Rectangular Patch Capacitor



(d) Variation of Upper Cut off Frequency with Coupled Arm length

Figure 5.2.8: Parametric Analysis

be calculated for a substrate with permittivity ϵ_r and thickness h (mm) using Eq. 5.2.1.

$$L = 30.73 - 5.45f_1 - 2.12\epsilon_r + 2.47h \quad (5.2.1)$$

Similarly the coupled line length L_a (mm) required for an upper cutoff frequency

f_2 (GHz) can be obtained using Eq. 5.2.2.

$$L_a = 23.75 - 1.2f_2 - 1.6\epsilon_r + 0.06h \quad (5.2.2)$$

The equations are verified for different substrates. The computed values of chip inductor L , coupled line length L_a and the UWB bands obtained on different substrates are given in Table. 5.2.1.

Table 5.2.1: Computed Values of L and L_a and UWB bands Obtained

Substrate (ϵ_r/h)	L (nH)	L_a (mm)	Band Obtained (GHz)	%error (lower)	%error (upper)
2.2/1	11.7	7.6	3.08-10.6	0.6	0
3.5/0.8	8.3	6.1	3.14-10.5	1.2	4.7
4.4/1.6	8.4	4.7	3.08-10.5	0.6	4.7
5.7/1.25	4.8	2.1	3-10.5	3.2	4.7

5.2.4 Lumped Element Model

Lumped element model for the filter shown in Fig. 5.2.9 is deduced as explained in section 4.4 and section 5.1.4. In the lumped element model, L_s and C_s represent the equivalent inductance and capacitance of the resonators comprising the chip inductor and rectangular patch capacitor. C_{int} represents the capacitance of the interdigital coupled line, L_{pi} forms its parasitic inductance. Four CSRR's are represented by four parallel LC resonant circuits with L_c and C_c . L_m and C_m represent the mutual coupling between CSRR's. The distributed shunt capacitance C_{sh} also accounts for the parasitic

shunt capacitance of the interdigital line. A comparison of transmission characteristics

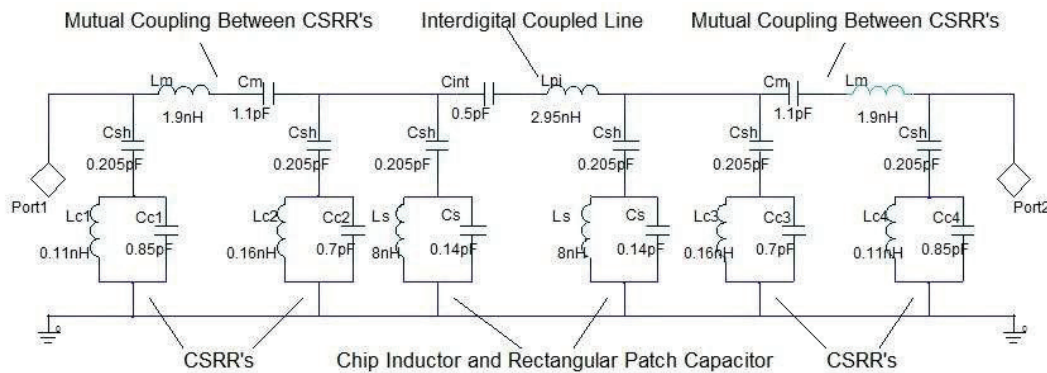


Figure 5.2.9: Lumped Element Model

is shown in Fig. 5.2.10.

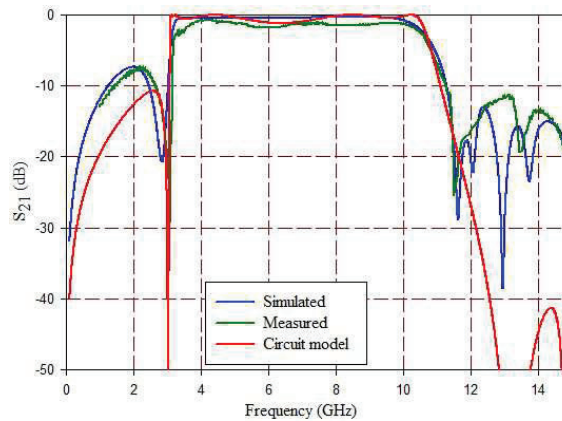


Figure 5.2.10: Comparison of Transmission Characteristics

5.2.5 Dispersion Studies

The variation of phase with frequency is examined for the designed filter. Fig. 5.2.11 shows the $\omega - \beta$ diagram for the filter. It is seen that the phase variation is linear in

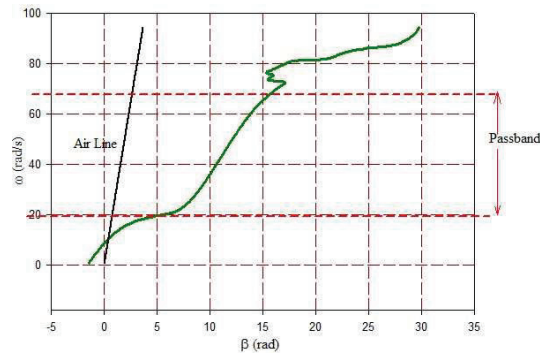


Figure 5.2.11: $\omega - \beta$ diagram

the passband extending from 3.1GHz to 10.6GHz. A linear phase variation over the passband dictates a constant group velocity which is a basic requirement of filters used in communication applications. This ensures distortionless transmission of signals. As explained in section 4.5, the operating band of the filter lies in the slow wave region lying to the right of the air line.

5.2.6 Time Domain Analysis

The response of the filter to a step input or impulse input gives necessary information about the system behavior in time domain. As can be observed the rise time is 0.2ns indicating the fast response of the filter. The overshoot reaches upto 117% and the filter is well damped to get a steady output with 2% accuracy in 1.8ns (settling time) thus establishing the stability of the system. Fig. 5.2.12 shows a comparison of simulated

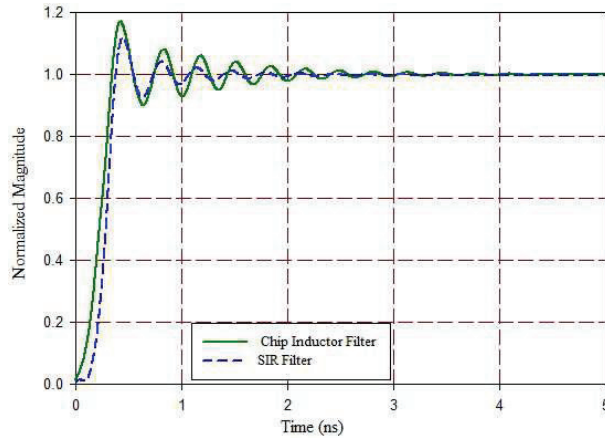


Figure 5.2.12: Simulated Unit Step Response of the Filter in Comparison with SIR Filter

unit step response of the filter with that of the SIR filter discussed in the chapter 4. It is observed that the overshoot is slightly higher in the former. This can be attributed to the high Q of the chip inductor at higher frequencies. However, the stability is not affected and the response settles down in 1.8ns.

5.2.7 Measurement Results

The filter structure is fabricated on a substrate with relative permittivity of 3.7, dielectric loss tangent of 0.003 and a thickness of 1.6mm. Fig. 5.2.13 shows the photograph of the prototype filter along with SMA connectors. The structure is compact as can be seen in figure. Standard photolithography is used for the fabrication process and S parameter and group delay measurements are taken using Agilent 8753ES Vector Network Analyzer.

Measured results in Fig. 5.2.14(a-c) agree well with the simulated results. Average insertion loss is less than 1.5 dB including those introduced by the SMA connectors. Measured roll-off rate is 130dB/GHz on lower and 26dB/GHz on upper band edges and

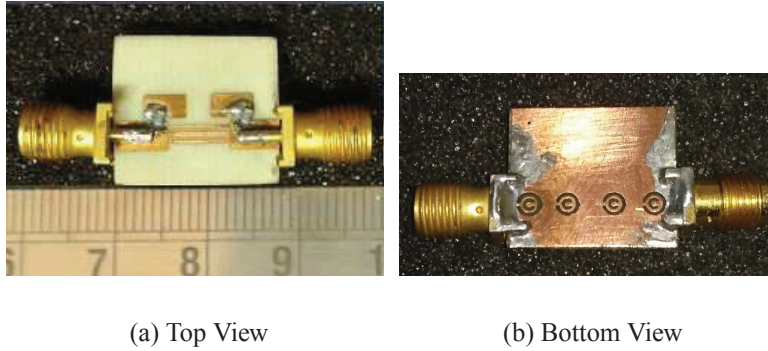


Figure 5.2.13: Photograph of the Prototype Filter

the fractional bandwidth attained is 109%. Group delay plot in Fig. 5.2.14(c) reveals that the filter exhibit good linear phase characteristics making it suitable for a variety of communication applications. Group delay is flat in the passband in agreement with simulated result and variation is less than 0.14ns. Table 5.2.2 gives a comparison of filter parameters with similar reported work.

5.3 Summary

The filters discussed in this chapter are compact. Designs are simple, straight forward and dimensions facilitate easy fabrication. They can be re-designed for any bandwidth of interest. Design with chip inductors is limited only by the availability of suitable chip inductors with sufficiently large values of self- resonant frequency.

Roll off rate achieved is steep and attenuation in the stopbands is reasonable. It can be further improved by cascading more sections as desired. This is the traditional way. However, there is a limitation that the structure may become complex as more sections

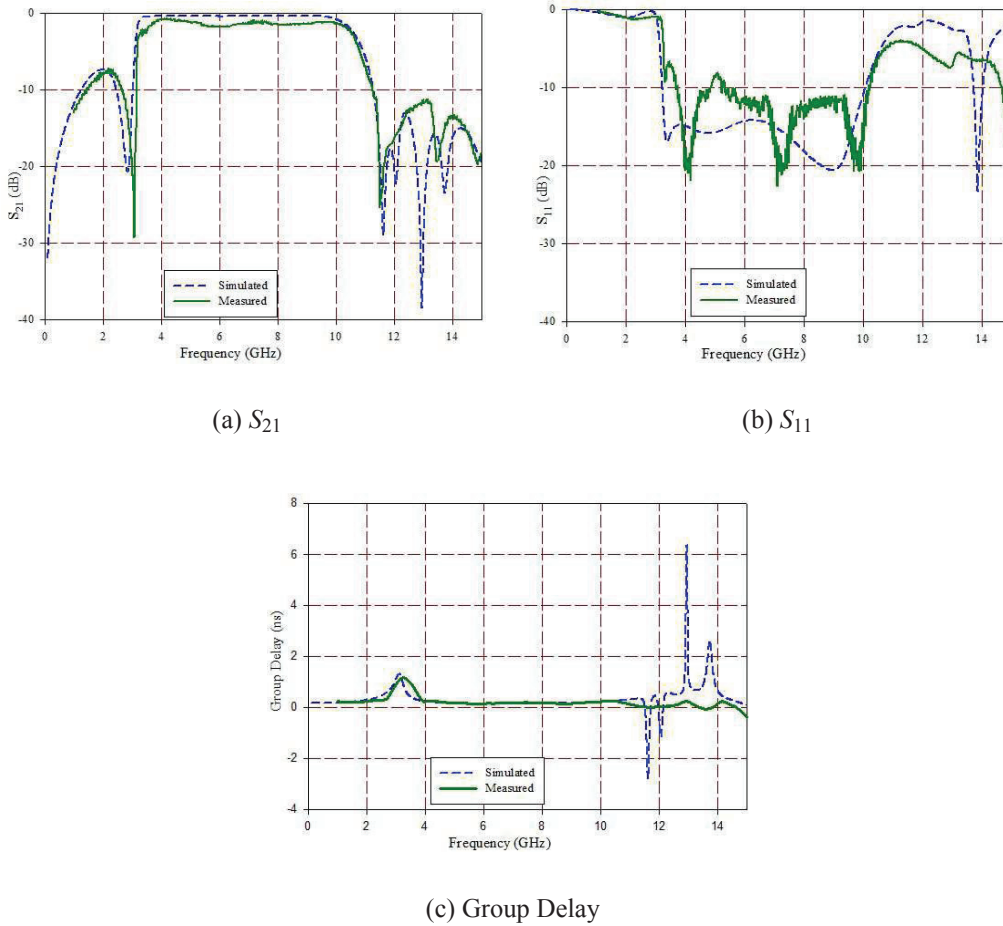


Figure 5.2.14: Measured Results

are incorporated. Another method to improve the performance is to control the lower and upper stopband characteristics separately using lumped elements/resonators without increasing the filter real estate. These methods are explored in the next chapter.

Table 5.2.2: Comparison of Parameters of Similar Works

Parameters/ References	Passband (GHz)	Insertion Loss (dB)	Roll off Rate-Lower, Upper(dB/ GHz)	Stopband Attenuation- Lower, Upper (dB)	Group Delay Variation(ns)	Size (mm^2)	Substrate [ϵ_r , $h(mm)$]
[Yasuhisa Yamamoto et al., 2007]	2-9.5	0.26	58,19	Narrow stopband 1-2 GHz; 9.5-11GHz	0.13	20 x 25	2.17/0.508
[Pramod K. Singh et al., 2007]	3.1-10.6	0.5	50,30	35,15	0.21	18.6 x 13.5	3.38/0.81
[K. Song, and Q. Xue, 2010]	3.3-10.4	≤ 1	20,13	-,32	0.22	16.2 x 8.8	2.2/0.127
[Marjan Mokhtari et al., 2010]	2.8-8.2	2	36,65	21,8	0.5	20 x 17	6.15/0.635
[B. Xia et al., 2012]	3.54- 10.6	0.15-2.5	45,45	14.3,15.4	Not Specified	26.2 x 11.9	4.3/0.41
[Proposed Filter]	3.12- 10.6	≤ 1.5	130,26	7,11	0.14	17 x 12	3.7/1.6

Bibliography

- [1] F. Zhang, Q. Zhao et.al, “Coupling Effect of Split Ring Resonator and its Mirror Image”, Progress in Electromagnetics Research, Vol. 124, pp.233-247, 2012.
- [2] Miguel Durn-Sindreu, Jordi Naqui, Ferran Paredes, Jordi Bonache and Ferran Martn, “Electrically Small Resonators for Planar Metamaterial, Microwave Circuit and Antenna Design: A Comparative Analysis”, Applied Sciences, 2, pp.375-395, 2012.
- [3] Joan Garca-Garca, Ferran Martn, et.al, “Spurious Passband Suppression in Microstrip Coupled Line Band Pass Filters by Means of Split Ring Resonators”, IEEE Microwave and Wireless Components Letters, Vol.14, No.9, pp.416-418, Sep. 2004.
- [4] Juan Domingo Baena, Jordi Bonache et. al., “Equivalent-Circuit Models for Split-Ring Resonators and Complementary Split-Ring Resonators Coupled to Planar Transmission Lines”, IEEE Transactions on Microwave Theory and Techniques, Vol.53, No.4, pp.1451-1461, Apr.2005.
- [5] Inder Bahl, Prakash Bhartia, “Microwave Solid State Circuit Design”, ISBN-0-471-83189-1, John Wiley & Sons, Inc.
- [6] Jia-Sheng Hong, M.J.Lancaster, “Microstrip Filters for RF/Microwave Applications”, ISBN 0-471-38877-7, John Wiley & Sons, Inc.
- [7] K. Song and Q. Xue, “Inductance-Loaded Y-Shaped Resonators and Their Applications to Filters”, IEEE Transactions on Microwave Theory and Techniques, Vol.58, No.4, pp.978-984, Apr. 2010.
- [8] Jia-Sheng Hong and Hussein Shaman, “An Optimum Ultra-wideband Microstrip Filter”, Microwave and Optical Technology Letters, Vol. 47, No. 3, Nov. 2005.

- [9] Marjan Mokhtaari, Jens Bornemann and Smain Amari, "A Modified Design Approach for Compact Ultra-Wideband Microstrip Filters", *International Journal of RF and Microwave Computer Aided Engineering*, Vol. 20, No. 1, pp.66-75, Jan. 2010.
- [10] Pramod K. Singh, Sarbani Basu and Yeong-Her Wang, "Planar Ultra-Wideband Bandpass Filter Using Edge Coupled Microstrip Lines and Stepped Impedance Open Stub", *IEEE Microwave and Wireless Components Letters*, Vol.17, No.9, pp.649-651, Sep.2007.
- [11] GiMoon Lee, Wu Seong Lee et al., "A Compact and Wide Stop-Band Low-Pass Filter Using a Wire Wound Chip-Inductor", *Microwave Symposium (MMS)*, pp.156-159, Aug.25-27, 2010.
- [12] Ting-Wei Kang and Kin-Lu Wong, "Chip Inductor Embedded Small-Size Printed Strip Monopole for WWAN Operation in The Mobile Phone", *Microwave and Optical Technology Letters*, Vol.51, No.4, pp.966-971, Apr.2009.
- [13] Coilcraft Chip Inductors - 0201DS Series (0603) (datasheet), 2 pages, Available at: <http://www.coilcraft.com/0201ds.cfm>.
- [14] Bindu.C J, Anju Pradeep and S. Mridula, "Compact Ultra Wide Band Filter Using Chip Inductors and CSRR's", *Proc., National Symposium on Antennas and Propagation*, pp.90-93, Dec.2012.

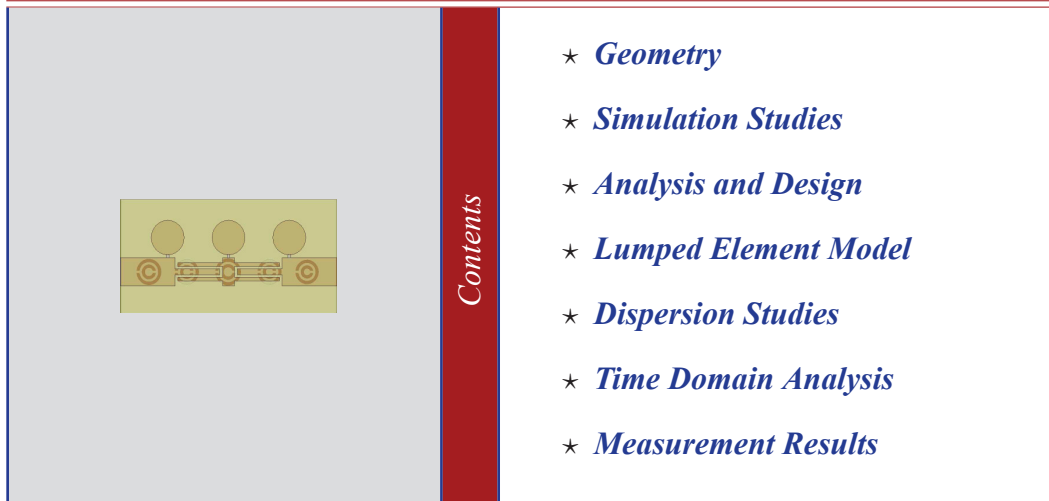
6 UWB Filters with Improved Performance

Contents

- ★ *Filter Using Cascaded Resonators*
- ★ *Filter Using Series Capacitors and Defected Ground Structures*

The chapter introduces methods to further improve the performance of filters discussed in previous chapters. The major drawback in earlier designs is the comparatively poor stopband performance. Two methods are explored. One is the conventional method of cascading additional resonators and the other is suppressing frequencies in lower and upper stopbands independently using suitable planar components.

6.1 Filter using Cascaded Resonators



This section discusses a planar UWB filter employing cascaded sections of interdigital quarter wavelength coupled lines and three shunt connected LC resonators comprising chip inductors and circular patch capacitors. The filter is suitable for both indoor and outdoor UWB applications. The overall dimension is 24mm x 12mm on a substrate with $\epsilon_r = 4.3$ and thickness 1.6mm. ¹

¹Bindu C J, Anju Pradeep, S Mridula and P Mohanan, Compact Planar UWB Filter Using Cascaded Resonators, International Journal of Ultra Wideband Communications and Systems (Accepted).

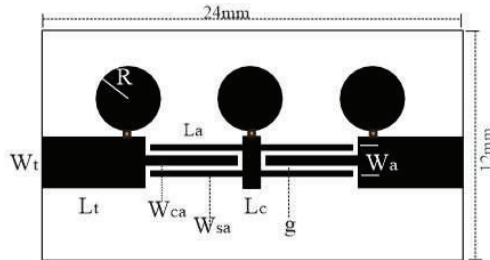
UWB filters employing stepped impedance resonators on interdigital coupled lines were presented in chapters 4 & 5. The filter presented here makes use of the traditional way of cascading additional resonators to improve the performance. This is detailed in the following sections.

6.1.1 Geometry

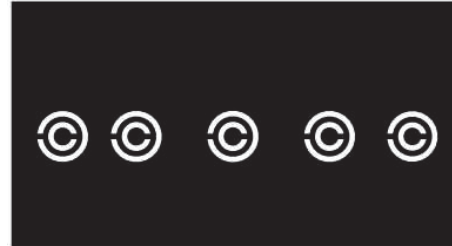
The proposed filter comprises two asymmetrical interdigital coupled lines and three LC resonators made of wire wound chip inductors and circular patch capacitors. Top and bottom view of the designed structure coupled to a 50Ω transmission line section fabricated on a substrate of dielectric constant 4.3, thickness 1.6mm and loss tangent 0.0018 are shown in Fig. 6.1.1(a-b).

The interdigital coupled lines, quarter of guide wavelength long at 6.85 GHz, the mid frequency of the UWB spectrum, provides the required bandpass characteristics. Upper cut off frequency is determined by the coupled line length (L_a). The LC resonators determine the lower cut off frequency. Sharp resonance of Complementary Split Ring Resonators on the ground plane is found to improve the upper stopband characteristics from the studies given in section 3.2.3.

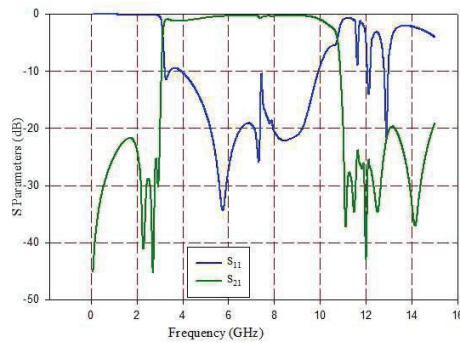
Five CSRR's with slightly varying resonant frequencies above the upper cut off frequency are etched on the ground plane and aligned exactly below the transmission line portion for better upper stopband performance. CSRR's affect the inductance and capacitance of the transmission line and greatly help to achieve steeper roll off rate at the upper band edge.



(a) Top View of the Proposed Structure
 $L_t = 6, W_t = 3, W_{ca} = 0.6, W_{sa} = 0.39, L_a = 4.99, L_c = 1.3, W_a = 1.98, g = 0.3, R = 1.83$, Chip Inductor=5.2nH)(All dimensions in mm)



(b) Bottom View with CSRR's :
 Outer radii : 1.36, 1.32, 1.4, 1.32, 1.28 : Width of rings :0.3 : Gap between outer and inner rings :0.3 (all dimensions in mm)



(c) Simulated S Parameters
 : Transmission Zeros
 2.27GHz, 2.72GHz,
 11.1GHz,11.4GHz,12GHz,12.5GHz

Figure 6.1.1: Layout of the Filter Structure and Simulated S Parameters

Design Evolution

The filter with an interdigital coupled line and two LC resonators comprising chip inductors and rectangular patch capacitors discussed in section 5.2 exhibits an

attenuation of 7dB in the lower stopband and 11 dB in the upper stopband respectively. An improvement in performance is attained by introducing one more cascaded section. The occupied chip area is reduced considerably with the use of circular patch capacitors instead of rectangular patch capacitors.

The lower cut off frequency for the filter is 3.1GHz. An inductor value (5.2nH) is chosen from the available range of inductors. The corresponding capacitance is computed using Eq. 6.1.1 [9].

$$f_1 = \frac{1}{2\pi\sqrt{LC}} \quad (6.1.1)$$

where f_1 is the desired lower cut off frequency and L is the chip inductor value chosen. For the substrate chosen, the radius R for the patch is calculated using Eq. 6.1.2.

$$C = \epsilon R \left[\frac{\pi R}{h} + \ln \left(\frac{16\pi R}{h} \right) - 1 \right] \quad (6.1.2)$$

where ϵ is the absolute permittivity of the substrate material and h is the thickness of the dielectric slab [2]. Fine tuning of the patch radius is required when the effective permittivity (ϵ_{eff}) of the entire structure is considered. Design equations are developed in Section 6.1.3.

The radii of the CSRR rings are selected for the required roll off rate and also for improved upper stopband performance. The outer radii of the outer rings of the five CSRR's are 1.36, 1.32, 1.4, 1.32, and 1.28mm respectively. All the rings are of width 0.3 mm and inner and outer rings are separated by a gap of 0.3 mm. Optimized values for the length L_a and widths W_{ca} and W_{sa} , of center and side limbs of the interdigital coupled arm are 4.99mm, 0.6mm and 0.39mm respectively. These dimensions also contribute to

the effective inductance of the structure. The gap (g) between the coupled lines is 0.3mm and it contributes to the effective capacitance. The structure has an overall dimension of 24mm x 12mm.

Simulated transmission and reflection characteristics in Fig. 6.1.1(c) reveal the sharp rejection at lower and upper cut off frequencies. The passband extends from 3.1-10.65GHz. Average out of band rejection obtained is 20dB in both stopbands. Roll off rate at the lower band edge is 126dB/GHz. The upper roll off rate is 76dB/GHz. Average insertion loss in the passband is 0.63dB, which can be justified by the presence of additional cascaded sections.

6.1.2 Simulation Studies

Surface current vectors on the top surface of the structure at various frequencies in lower stopband region and in the passband are shown in Fig. 6.1.2 & Fig. 6.1.3 respectively. Current distributions at the lower side transmission zeros in Fig. 6.1.2(a-c) show current crowding near the LC resonators thus identifying them as causing the transmission zeros. At lower transmission zero 2.27GHz, well below the lower cut off frequency all three resonators are involved as seen in Fig. 6.1.2(a) with reduced magnitudes of surface current towards second and third resonators. This justifies the improved stopband performance due to increased number of resonators. Near the cut off frequency, at 2.72GHz and 2.94GHz, only two resonators are mainly contributing to the transmission zeros.

The surface current vector on the top surface at 3.1GHz, 6.85GHz and 10.6GHz in the passband is shown in Fig. 6.1.3. At the lower cutoff (3.1GHz), the influence of the

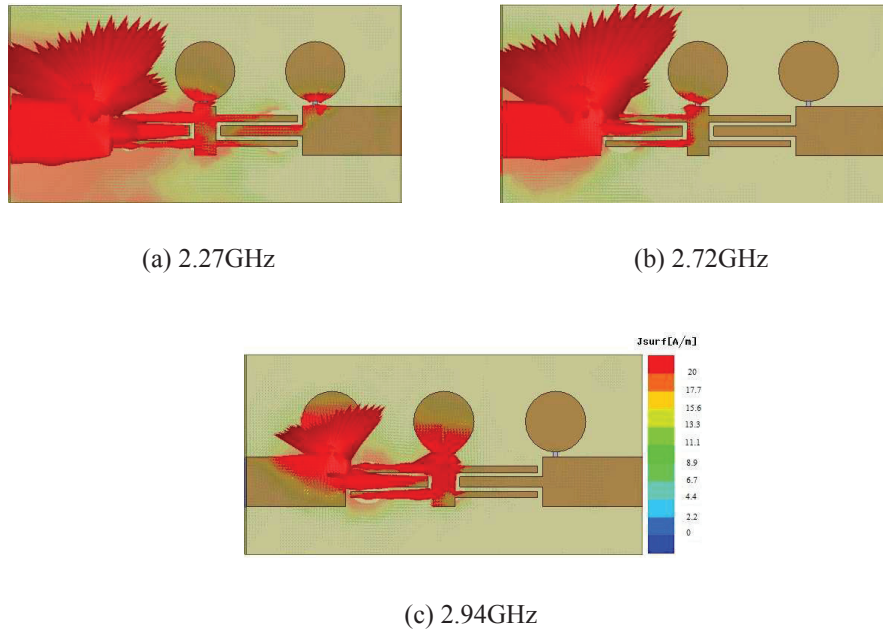


Figure 6.1.2: Surface Current Vectors on the Top Surface in Lower Stopband

LC resonators are prominent. The current direction in the coupled lines reveals even mode wave propagation which gradually changes, showing the beginning of odd mode at 6.85GHz and strong odd mode currents at 10.6GHz. This contributes to the bandpass behaviour of interdigital coupled lines as detailed in section 3.1.4. Fig. 6.1.4(a-h) show the electric field vectors in the vicinity of upper stopband transmission zeros. They reveal the effect of varying dimensions of CSRR's upon the upper stopband characteristics. CSRR's cause the structure to behave as an effective medium with negative permittivity in a narrow band above resonance where the wave propagation is inhibited [3]. This can be observed by the reversal of electric field vector on either side of the transmission zeros. At 10.7GHz the electric field vector is oriented outwards in CSRR's 1 and 3 and

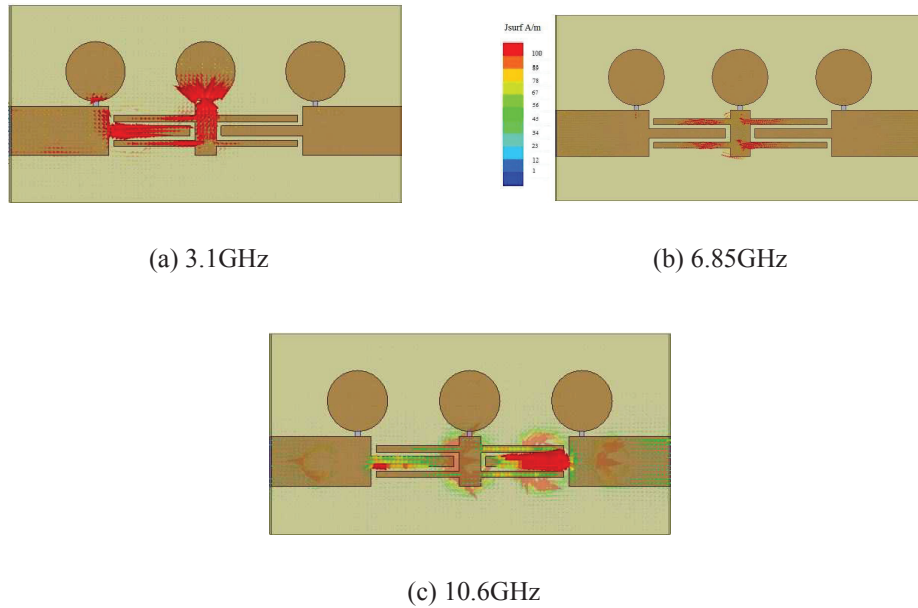


Figure 6.1.3: Surface Current Vectors on the Top Surface in the Passband

at 11.2GHz the field vector is oriented inwards. Thus the transmission zero at 11.1 GHz is contributed by CSRR's 1 and 3. In a similar manner, CSRR's 3 and 4 are identified responsible for transmission zero at 11.48GHz. The transmission zero at 12 GHz is due to CSRR's 2 and 4 and transmission zero at 12.59GHz is due to CSRR 1.

6.1.3 Analysis and Design

Parametric study as shown in Fig. 6.1.5(a) confirms the dependence of lower cut off frequency on the inductor value of the LC resonator. Variation of inductance L from 4nH to 6nH results in a lower cut off frequency shift from 3.4 to 3GHz while upper cut off frequency is unaffected. Distortions are seen in the passband characteristics in the



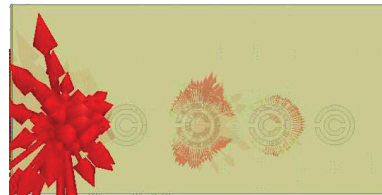
(a) Electric Field Vector at 10.9GHz



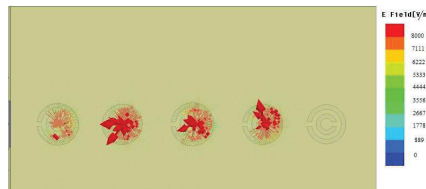
(b) Electric Field Vector at 11.2GHz



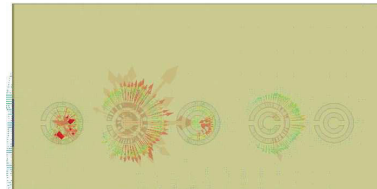
(c) Electric Field Vector at 11.3GHz



(d) Electric Field Vector at 11.5GHz



(e) Electric Field Vector at 11.9GHz



(f) Electric Field Vector at 12.2GHz



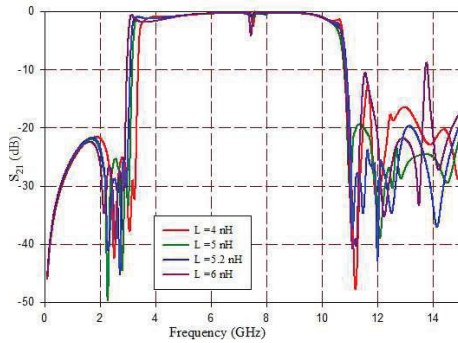
(g) Electric Field Vector at 12.4GHz



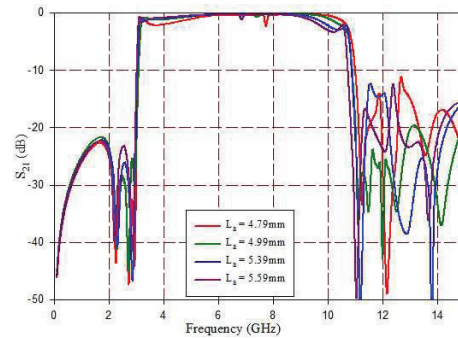
(h) Electric Field Vector at 13GHz

Figure 6.1.4: Electric Field Vectors in CSRR's in the Vicinity of Upper Stopband Transmission Zeros :(a-b) Transmission zero at 11.1GHz: (c-d) Transmission zero at 11.4GHz :(e-f) Transmission zero at 12GHz :(g-h) Transmission zero at 12.5GHz

mid band region as the inductor value is varied. However the effective inductance is also influenced by both the length and width of the coupled arm and CSRR dimensions. So these distortions can be countered by varying the dimensions of the CSRR's. The



(a) Variation of lower cut off Frequency with Varying Chip Inductor values



(b) Variation of the Upper cut off Frequency with Coupled Arm length L_a

Figure 6.1.5: Parametric Study

upper cut off frequency is mainly dependent on the coupled arm length (L_a). Variation of upper cut off frequency with the coupled arm length is shown in Fig. 6.1.5(b). As the length decreases, the upper cut off frequency increases, while the lower band edge remains unaffected. The results are shown for lengths varying from 4.79mm to 5.59mm causing the upper cut off to shift from 10.7 to 9.9GHz. The prototype is developed with $L=5.2\text{nH}$ and $L_a=4.99\text{mm}$.

Due to the interdependent nature of resonators and the change in the effective permittivity of the entire structure with the change in individual dimensions, the lower and upper band edges cannot be controlled independently beyond a limit. But this can be used as a guideline for designing the filter for different bandwidths. Table 6.1.1

shows the various bands achieved by the variation of coupled arm length L_a and the chip inductor value. Multivariable regression analysis is carried out on simulation

Table 6.1.1: Computed Values of L_{stub} and L_a with the UWB bands Obtained

Chip Inductor Value L (nH)	Arm Length L_a (mm)	Frequency Band (GHz)
4	4.79	3.1-10.7
5	4.79	3.3-10.7
5.2	4.79	3.1-10.7
4	4.99	3.6-10.6
5	4.99	3.3-10.6
5.2	4.99	3.1-10.6
6	4.99	2.9-10.6
5	5.39	3.3-10.3
6	5.39	2.9-10.3
7	5.39	2.8-10.3

results. Generalized design equations are thus developed. The equations are validated on various substrates having different values of permittivity and slab thickness. The chip inductor value for the lower cut off frequency can be determined using Eq. 6.1.3.

$$L = 25.131 - 0.6618\epsilon_r - 1.035h - 2.767R - 3.145f_1 \quad (6.1.3)$$

Here L is the chip inductor value in nH, ϵ_r is the relative permittivity of the substrate material, h is the thickness of the dielectric slab in mm, R is the radius of the circular disc capacitor in mm and f_1 is the lower cut off frequency in GHz. The expression for the coupled arm length L_a required for the upper cut off frequency f_2 is given by Eq.

6.1.4.

$$L_a = 21.917 - 1.191\epsilon_r - 2.626h - 0.739f_2 \quad (6.1.4)$$

Table 6.1.2 illustrates the UWB bands obtained by using the designed values of L and L_a as per Eq. 6.1.3 and Eq. 6.1.4 on various substrates. The equations are valid for the range $3.7 \leq \epsilon_r \leq 6.15$; $1.32 \leq h \leq 1.7$.

Table 6.1.2: Computed Values of Chip Inductor L and L_a with the UWB bands Obtained

Substrate ϵ_r/h	L (nH)	L_a (mm)	Band Obtained (GHz)	%Error (Lower)	%Error (Upper)
3.7/1.6	6.2	5.47	3.12-10.67	0.6	0.6
4.3/1.6	5.11	5.2	4.99	0.6	0.4
5/1.7	5.25	3.6	3.16-10.61	1.9	0.09
6.15/1.32	5.25	3.3	3.05-10.5	1.6	0.9

6.1.4 Lumped Element Model

Fig. 6.1.6 shows the lumped element model. Lumped element model consists of

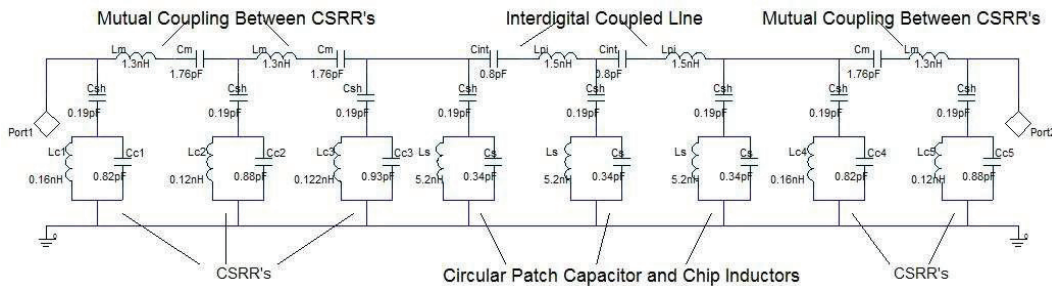


Figure 6.1.6: Lumped Element Model

resonant circuits due to the combined effect of chip inductor and circular patch

capacitors, interdigital coupled arm and the five CSRR's in the ground plane. The component values are deduced as explained in section 4.4 and section 5.1.4. L_S and C_S

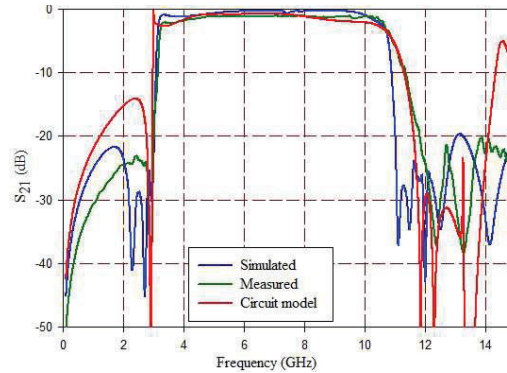


Figure 6.1.7: Comparison of Transmission Characteristics

represent the equivalent inductance and capacitance of the resonator comprising the chip inductor (5.2nH) and circular patch capacitor (0.34pF). C_{int} and L_{pi} represent the capacitance and parasitic inductance of interdigital coupled lines. Five CSRR's are represented by five parallel LC resonant circuits with L_c and C_c resonating at different upper stopband frequencies 14.8GHz, 14.5GHz, 13GHz and 12.8GHz. Mutual coupling between CSRR's is represented by L_m and C_m . C_{sh} is the distributed shunt capacitance which also accounts for the parasitic shunt capacitance of interdigital coupled lines. The comparison of transmission characteristics of the lumped model with that of simulated and fabricated models is shown in Fig. 6.1.7.

6.1.5 Dispersion Studies

The variation of phase with frequency is examined for the designed filter. Fig. 6.1.8 shows the $\omega - \beta$ diagram for the filter. A linear phase variation over the passband

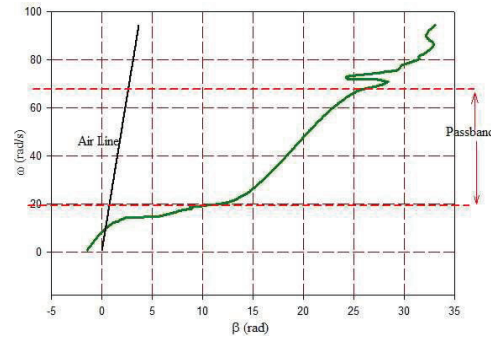


Figure 6.1.8: $\omega - \beta$ diagram

dictates a constant group velocity which is a basic requirement of filters used in communication applications. This ensures distortionless transmission of signals. It is seen that the phase variation is linear in the passband extending from 3.1GHz to 10.6GHz. As explained in section 4.5, the operating band of the filter lies in the slow wave region lying to the right of the air line.

6.1.6 Time Domain Analysis

Optimized time response is required for filters used in modern microwave receivers, radars, satellite systems etc. If the design causes significant time domain overshoots, receiver channels will be saturated and hence will not respond in time. As the number of cascaded sections increases, there is a tendency for the time domain response to degrade. More cascaded sections result in increased frequency discrimination which in turn increases the Q of individual sections. This may cause increased overshoots and ringing. Simulated unit step response in Fig. 6.1.9 is reasonably good and shows that the filter is stable. In spite of the cascaded sections, the filter exhibits a sharp rise time of 0.2 nanoseconds. The maximum overshoot is 120% and the filter is well damped

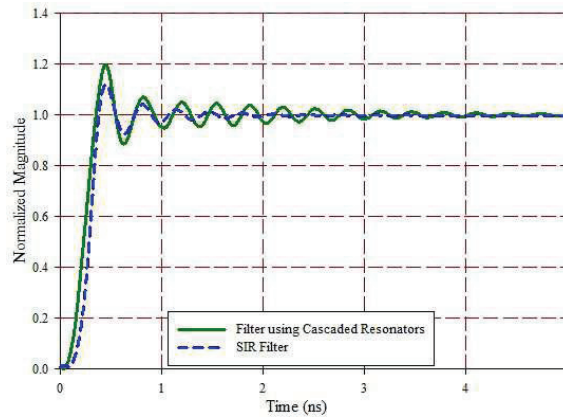


Figure 6.1.9: Simulated Unit Step Response of the Filter in Comparison with SIR Filter with ringing subsiding to the 2% tolerance limit in 2.45 nanoseconds. From simulation studies, it is seen that the overshoot increases as the coupled arm length increases.

6.1.7 Measurement Results

Fig. 6.1.10(a-b) shows the photograph of the prototype filter along with the SMA connectors. The structure is compact as can be seen in figure. Standard photolithography is used for the fabrication process and the measurements are done using Agilent 8753ES Vector Network Analyzer.

The measured results shown in Fig. 6.1.11(a-c) agree reasonably well with the simulated results. Small discrepancies in the result can be attributed to the inaccuracies in fabrication and/or numerical errors in simulations. Measured average insertion loss in the passband is less than 1.6dB. This may include the contribution due to the SMA connectors. The 3dB fractional bandwidth attained is 110% and measured roll-off rate is sharp with 146dB/GHz at lower and 20dB/GHz at upper band edges. The flat group

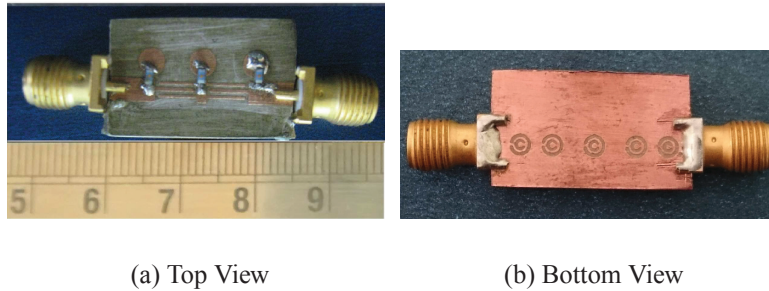
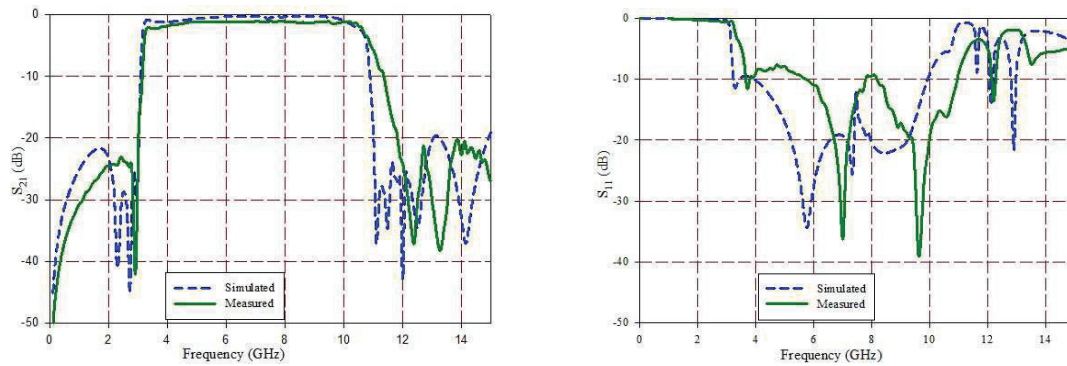
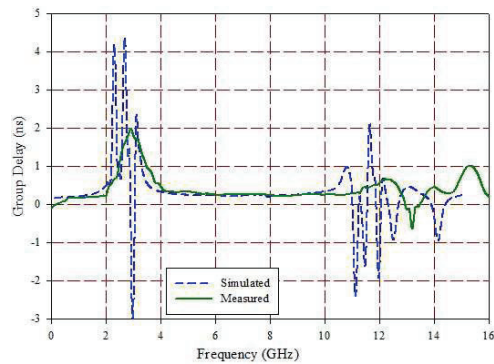


Figure 6.1.10: Photograph of the Prototype Filter

delay characteristics in Fig. 6.1.11(c) reveal the linear phase nature of the filter making it suitable for most of the communication applications. Group delay is 0.26ns and the variation is less than 0.08ns over the entire passband. Abrupt change in group delay at cut off frequencies is by the influence of resonators.

Table 6.1.3 gives a comparison of the filter performance with other reported UWB filters. As can be observed from the table, the proposed filter is compact and superior in performance with respect to roll off rate, stopband attenuation and group delay. The actual size neglecting substrate dimension is 24mm x 6.96mm.

(a) S_{21} (b) S_{11} 

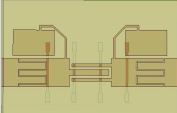
(c) Group Delay

Figure 6.1.11: Measured Results

Table 6.1.3: Comparison of Parameters of Similar Works

Parameters/ References	Passband (GHz)	Insertion Loss (dB)	Roll off Rate- Lower, Upper (dB/ GHz)	Stopband Attenuation- Lower, Upper (dB)	Group Delay Variation (ns)	Size (mm^2)	Substrate [ϵ_r , $h(mm)$]
[Pramod K. Singh et al., 2007]	3.1-10.6	0.5	50,30	35,15	0.21	18.6 x 13.5	3.38/0.81
[K. Song, and Q. Xue, 2010]	3.3-10.4	≤ 1	20,13	-,32	0.22	16.2 x 8.8	2.2/0.127
[Marjan Mokhtaari et al., 2010]	2.8-8.2	2	36,65	21,8	0.5	20 x 17	6.15/0.635
[B. Xia et al., 2012]	3.54-10.6	0.15-2.5	45,45	14.3,15.4	Not Specified	26.2 x 11.9	4.3/0.41
[Proposed Filter]	3.12-10.68	≤ 1.6	146,20	22,20	0.08	24 x 12	4.4/1.6

6.2 Filter Using Series Capacitors and Defected Ground Structures

	<i>Contents</i>	<ul style="list-style-type: none">★ <i>Geometry</i>★ <i>Simulation Studies</i>★ <i>Analysis and Design</i>★ <i>Lumped Element Model</i>★ <i>Dispersion Studies</i>★ <i>Time Domain Analysis</i>★ <i>Measurement Results</i>
---	-----------------	---

This section presents a planar UWB filter using series interdigital capacitor and defected ground structures for achieving improved performance. The filter has good attenuation in its lower and upper stop bands. The overall dimension is 20mm x 12mm on a substrate with $\epsilon_r = 4.4$ and thickness 1.6mm.²

²Chettiparampil J. Bindu, Shanta Mridula, and Pezhohil Mohanan, *High Selectivity Filter Employing Stepped Impedance Resonators, Series Capacitors and Defected Ground Structures for Ultra Wide Band Applications*, *Progress in Electromagnetics Research C*, Vol. 49, pp.123-131, 2014.

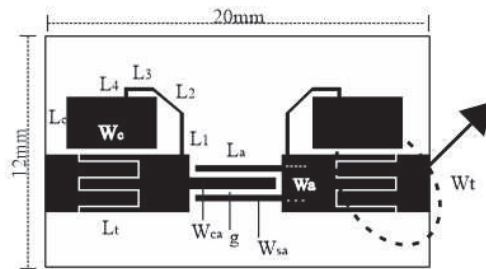
Planar UWB filter using cascaded sections for performance enhancement was presented in section 6.1. The filter presented here uses a different approach to improve the stopband characteristics. Attenuation in lower and upper stopbands is improved with the help of series interdigital capacitor and defected ground structures respectively. This is elaborated in subsequent sections.

6.2.1 Geometry

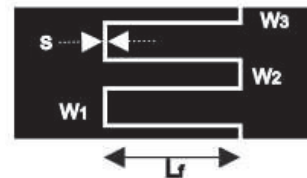
The proposed filter uses folded SIR's on interdigital coupled lines quarter guide wavelength ($\lambda_d/4$) long at 6.85GHz, the centre frequency of the UWB spectrum extending from 3.1-10.6GHz. The upper edge of the passband is determined by the length of the coupled arm (L_a) and lower edge by dimensions of folded SIR. An interdigital series capacitor is embedded in the 50Ω transmission line to improve the lower stopband attenuation. Dumb bell shaped defected ground structures serve to improve the upper stopband attenuation.

Fig. 6.2.1 shows the top and bottom view of the proposed filter structure on a substrate with $\epsilon_r = 4.4$ and thickness 1.6mm. Overall dimension of the structure including substrate is 20mm x 12mm.

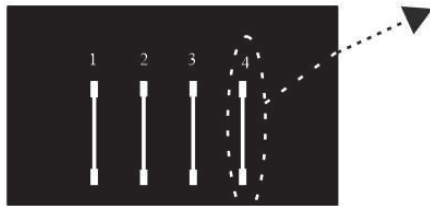
Simulated transmission and reflection characteristics in Fig. 6.2.1(e) reveal that the average insertion loss for the filter is within 1dB except for 1.2dB at 3.68GHz. Roll off rate is 215dB/GHz at lower edge and 34dB/GHz at the upper edge. Out of band rejection obtained is better than 18dB at lower and 23dB at upper bands. Insertion loss is minimized by optimizing the gap (g) between the coupled lines.



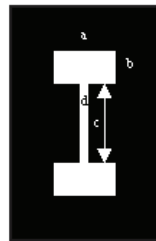
(a) Top view of the structure- ($L_t=7.5, W_t=3, W_{ca}=0.61, W_{sa}=0.32, W_c=4.7, L_a=4.5, L_1=2.15, L_2=1.95, L_3=1.5, L_4=0.7, L_c=2.6, W'=1.85, g=0.3; L_{stub}=L_1+L_2+L_3+L_4$)



(b) Enlarged View - Interdigital Capacitor ($L_f=3.2, W_1=0.8, W_2=0.6$)

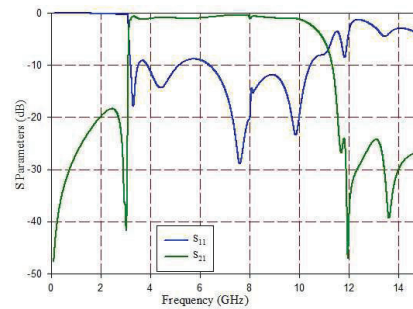


(c) Bottom View- Ground Plane with DGS



(d) Enlarged View- Dumbbell DGS

($a=0.46, b=1, c=4.3, d=0.244(1\&4)$
 $(a=0.46, b=0.95, c=4.4, d=0.244(2\&3))$)



(e) Simulated S Parameters : Transmission Zeros- 2.9GHz, 11.7GHz, 11.9GHz, 13.6GHz

Figure 6.2.1: Structural Layout (all dimensions in mm)

Design Evolution

The drawback of the folded SIR filter presented in section 5.1 is the comparatively poor passband attenuation. Methods to improve the filter performance without compromising

the size and complexity are analyzed here.

A series capacitor acts as high pass element. Thus by suppressing lower frequencies below 3.1 GHz using an interdigital series capacitor embedded in the transmission line, the lower stopband attenuation can be improved. The series capacitance of the interdigital capacitor C_s is evaluated as follows [9].

$$C_s = \frac{\epsilon_{re} 10^{-3}}{18\pi} \frac{K(k)}{K'(k)} (N-1) L_f (pF) \quad (6.2.1)$$

where L_f is the length of the finger in microns, N the number of fingers, ϵ_{re} the effective dielectric constant of the microstrip line of width W_f . The ratio

$$\frac{K(k)}{K'(k)} = \frac{\pi}{\ln \left[2 \frac{1+\sqrt{k'}}{1-\sqrt{k'}} \right]}; k = \tan^2 \left(\frac{a\pi}{4b} \right);$$

$$a = \frac{W_f}{2}; b = \frac{W_f + s}{2}; k' = \sqrt{1 - k^2}$$

The unequal finger widths (W_1, W_2) are accounted for by taking average of capacitances of two different finger widths W_1 and W_2 [10]. The parasitic inductance and capacitance are calculated as given in Eq. 6.1.6. However, fine tuning of the band requires changes in the dimensions of the capacitor, resulting in an asymmetric structure. The actual dimensions of the interdigital capacitor are shown in Fig. 6.2.1(b).

The introduction of series capacitor seriously affects the insertion loss in the passband due to its parasitic resistance, whose value is given by the expression

$$R = \frac{4}{3} \frac{L_f}{W_f N} R_s \text{ ohms}; \quad (6.2.2)$$

where R_s is the sheet resistivity of copper. Exhaustive simulation studies show that the alignment of the series interdigital capacitors does not affect the passband frequency response, but alters the stopband attenuation considerably. The position is so chosen as to optimize the stopband attenuation.

In order to compensate for the insertion loss and to get better rejection in the upper stopband, the use of Defected Ground Structures (DGS) is exploited. Dumb bell shaped DGS is employed in this work. Dimensions of various parts of dumb bell DGS are shown in the enlarged view of Fig. 6.2.1(d). The function of DGS is multifold. It functions as a series connected parallel LC resonant circuit, providing independent control of inductance and capacitance of the entire structure.

The dimensions 'a', 'b' of the dumb bell affect the route length of current and hence change the effective inductance while 'c' and 'd' affect the accumulation of charge and thus vary the capacitance. The behaviour of dumb bell shaped DGS is analyzed in detail in section 3.2.4. The dimensions and spacing of dumb bells are optimized to achieve the required upper stopband characteristics.

6.2.2 Simulation Studies

Simulation studies are carried out to observe the influence of various components used in the structure. The influence of series interdigital capacitor in suppressing lower frequencies is evident in the electric field distribution at 2GHz (in the lower attenuation band) shown in Fig. 6.2.2.

Surface current vector at the top surfaces of the structure at various frequencies in the passband are shown in Fig. 6.2.3. At 3.1GHz surface current is concentrated in

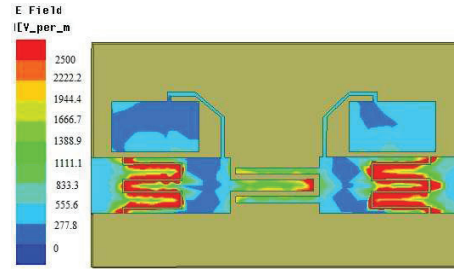


Figure 6.2.2: Electric Field Distribution at 2GHz

the LC resonator thus establishing its role in the lower cut off (Fig. 6.2.3(a)). Surface current vector in Fig. 6.2.3(b) shows that the entire signal is coupled to the output port at 6.85GHz. At 10.6GHz, the upper cut off frequency, the transmission zero is produced due to the phase reversal in odd mode propagation, as seen by the surface current vector in Fig. 6.2.3(c).

Upper side transmission zeros at 11.7GHz, 11.9GHz and 13.6GHz are due to the presence of DGS with varying dimensions as can be observed from the electric fields in the ground plane shown in Fig. 6.2.4(a-c).

The role played by the series capacitor and the DGS in improving the filter response can be seen from the simulated plots in Fig. 6.2.5(a-b). The series capacitor suppresses the signal below the lower cut off frequency and DGS improves the passband insertion loss along with upper stopband performance.

6.2.3 Analysis and Design

Results of parametric analysis carried out for varying lengths of inductive stub L_{stub} and coupled arm L_a as shown in Fig. 6.2.6. As the length of the inductive stub ($L_{stub} = L_1 + L_2 + L_3 + L_4$) is varied from 5.3mm to 6.8mm, the structure shows a shift in lower cut

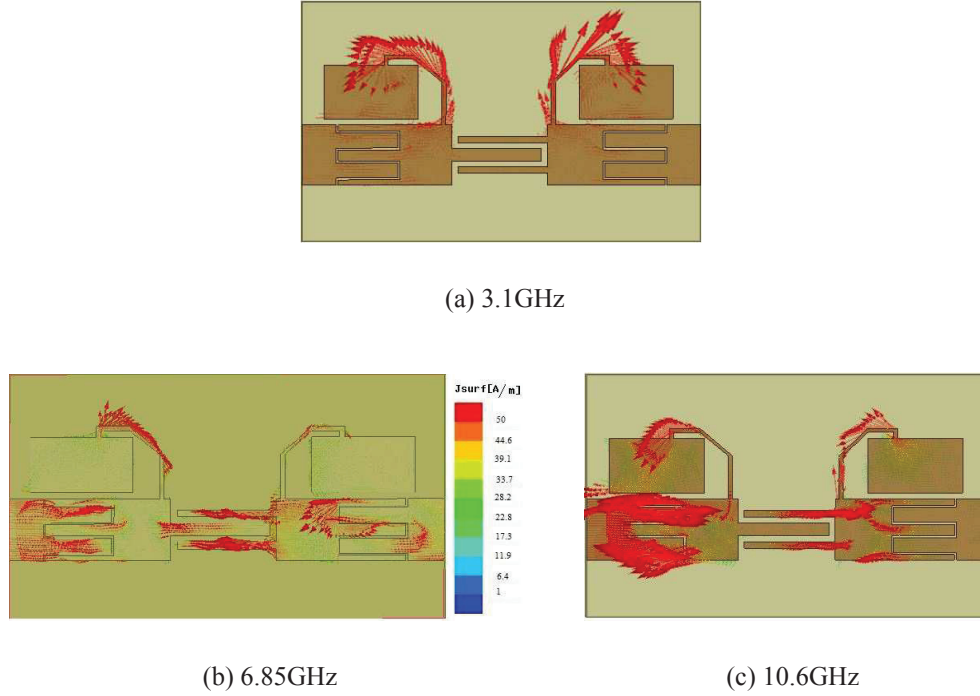
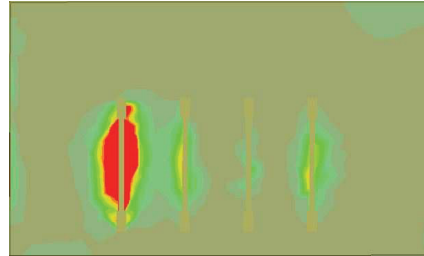


Figure 6.2.3: Surface Current Vector on Top Surface at Various Frequencies in the Passband

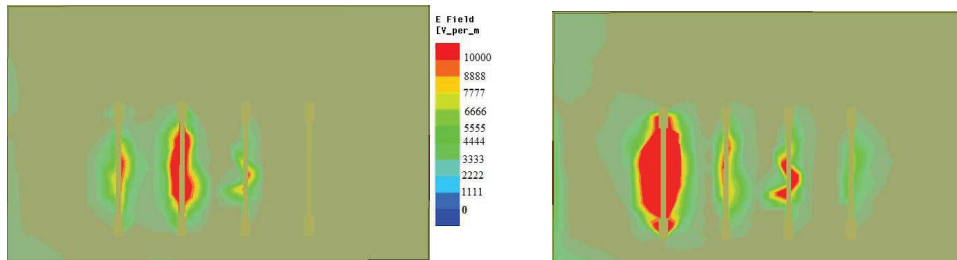
off frequency from 3.4 to 3.08GHz, as illustrated in Fig. 6.2.6(a). The variation of upper cut off frequency with coupled arm length is illustrated in Fig. 6.2.6(b).

Multivariable regression analysis is carried out on simulation results. Generalized design equations are developed and validated on substrates having different values of permittivity and thickness. The length of the folded inductive stub L_{stub} (mm) of the SIR for the desired lower cut off frequency f_1 (GHz) on a substrate with relative permittivity ϵ_r and thickness h (mm) can be determined by using the relation,

$$L_{stub} = 33.73 - 1.62\epsilon_r - 3.51h - 4.71f_1 \quad (6.2.3)$$



(a) Electric Field at 11.7GHz



(b) Electric Field at 11.9GHz

(c) Electric Field at 13.6GHz

Figure 6.2.4: Electric Field Distributions in the Ground Plane

The expression for the coupled arm length L_a (mm) required for an upper cut off frequency f_2 (GHz) is given by

$$L_a = 22.59 - 1.1\epsilon_r - 1.35h - f_2 \quad (6.2.4)$$

Table 6.2.1 illustrates the designed values of L_{stub} and L_a on different substrates as per Eq. 6.2.3 and Eq. 6.2.4 and the UWB bandwidth obtained. The dimensions of DGS and interdigital capacitor are kept unaltered except for substrates which require considerable change in the width of transmission line for proper impedance matching. For these

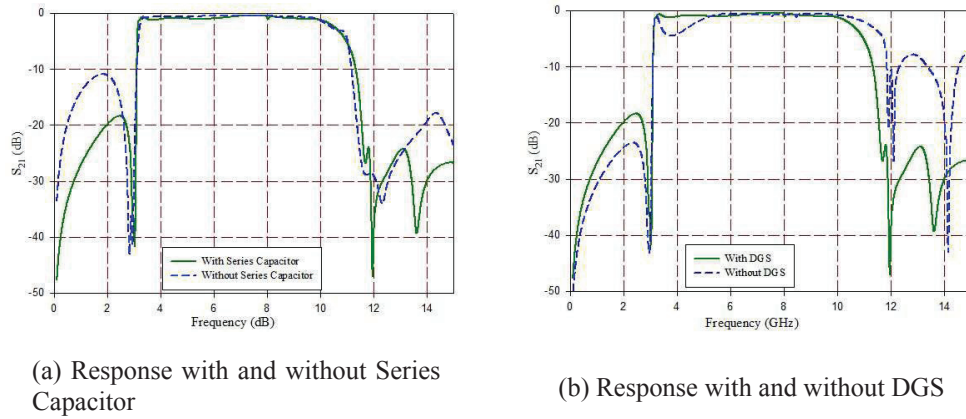


Figure 6.2.5: Influence of Series Capacitor and DGS on Filter Response

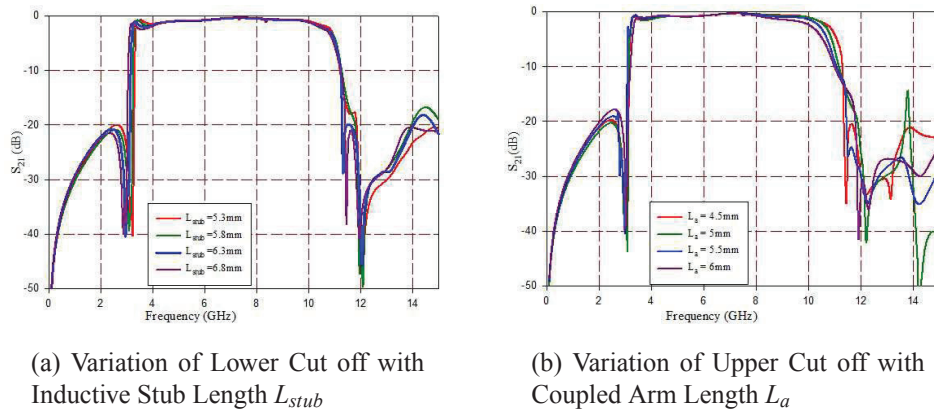


Figure 6.2.6: Results of Parametric Analysis

cases, $\pm 10\%$ change is required in the dimensions of the interdigital finger width. The equations are valid for the range $3.7 \leq \epsilon_r \leq 5.7$; $1.5 \leq h \leq 1.6$.

Table 6.2.1: Computed Values of L_{stub} and L_a with the UWB bands Obtained

Substrate ϵ_r/h	L_{stub} (mm)	L_a (mm)	Band Obtained (GHz)	%Error (Lower)	%Error (Upper)
3.7/1.6	7.51	5.7	3.04-10.5	1.9	0.9
4.2/1.6	6.7	5.3	3.07-10.5	0.9	0.9
5.2/1.5	5.44	4.2	3.12-10.6	0.6	0
5.7/1.5	4.63	3.6	3.1-10.5	0	0.9

6.2.4 Lumped Element Model

Fig. 6.2.7 shows the lumped element model of the filter. The values L_s and C_s represent the parallel LC resonators introduced by the folded SIR. C_{int} is the capacitance of the interdigital coupled arm and L_{pi} its parasitic inductance.

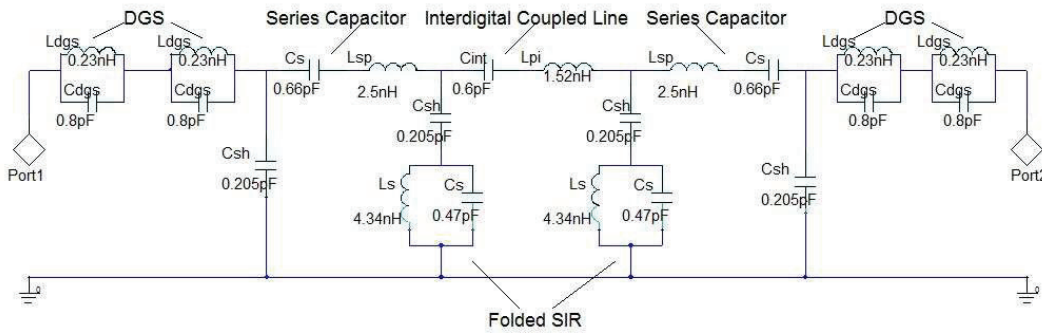


Figure 6.2.7: Lumped Element Model

C_s represents the series capacitance introduced due to the series interdigital capacitor and L_{sp} its parasitic inductance. L_{dgs} & C_{dgs} represent the inductance and capacitance values due to the defected ground structures. C_{sh} represents the distributed shunt capacitance of

the entire structure which is inclusive of the parasitic capacitance of the series capacitor.

For stepped impedance resonator, a high impedance (Z_{0l}) of 150Ω and low impedance (Z_{0c}) of 40Ω are chosen. Inductance (L_s) is 4.34nH and capacitance (C_s) is 0.47pF for the SIR used in this structure. The computation of inductance and capacitance is done as explained in Section 4.4. The capacitance (C_{int}) of coupled arm is 0.6pF and its parasitic inductance is 1.52nH . These are evaluated using Eq. 4.3 and Eq. 4.4 in section 4.4.

The capacitance and parasitic inductance of series interdigital capacitor (C_s & L_{sp}) are 0.66pF and 2.5nH respectively [9] -[10]. Distributed shunt capacitance of the circuit is 0.205pF , which also accounts for the parasitic shunt capacitance of the interdigital coupled line and series capacitor.

The values of inductance and capacitance of DGS (L_{dgs} and C_{dgs}), are computed based on the desired frequency values using Eq. 6.2.5.

$$C_{dgs} = \frac{\omega_c}{2Z_0(\omega_0^2 - \omega_c^2)} ; L_{dgs} = \frac{1}{\omega_0^2 C} \quad (6.2.5)$$

where ω_c is the required 3dB cut off frequency (10.6GHz), ω_0 is the resonant frequency of the DGS (selected as 11.5GHz , slightly above cut off frequency) and Z_0 the characteristic impedance[11]. The computed values are 0.23nH and 0.8pF . Comparison of transmission characteristics is shown in Fig. 6.2.8.

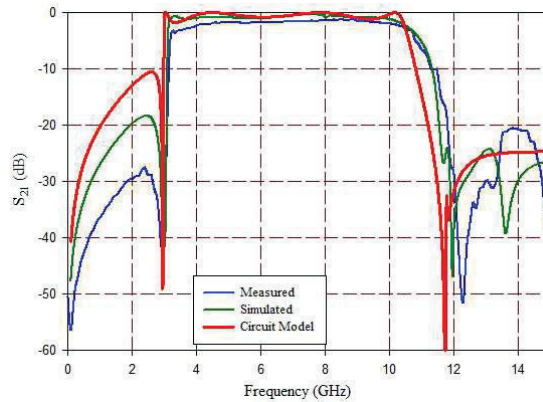


Figure 6.2.8: Comparison of Transmission Characteristics

6.2.5 Dispersion Studies

The variation of phase with frequency is examined for the designed filter. Fig. 6.2.9 shows the $\omega - \beta$ diagram for the filter. It is seen that the phase variation is linear in the passband extending from 3.1GHz to 10.6GHz. As explained in section 4.5, the operating band of the filter lies in the slow wave region lying to the right of the air line.

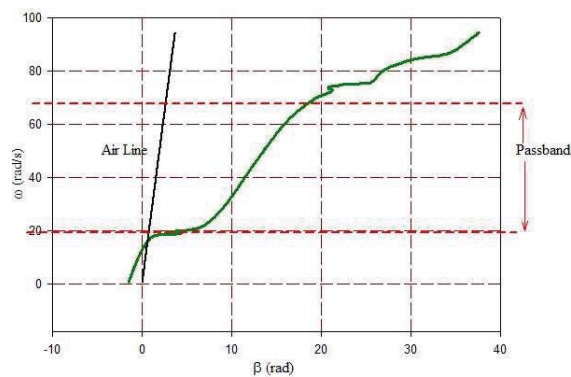


Figure 6.2.9: $\omega - \beta$ diagram

6.2.6 Time Domain Analysis

Simulated unit step response of the filter in comparison with SIR filter discussed in section 4.6 is plotted and shown in Fig. 6.2.10. The step response of this filter shows better time response comparing with filter discussed in section 6.1 also. The rise time is reduced considerably to 0.14ns, while the overshoot is 112%. The settling time for a 2% tolerance limit is 1.5ns.

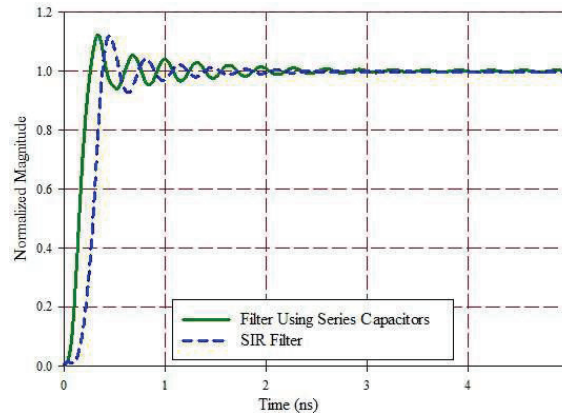


Figure 6.2.10: Simulated Unit Step Response of the Filter in Comparison with SIR Filter

6.2.7 Measurement Results

Filter structure is fabricated on a substrate with relative permittivity of 4.4, dielectric loss tangent of 0.02 and thickness of 1.6mm. Fig. 6.2.11 shows the photograph of the prototype filter along with the SMA connectors. The structure is compact with an overall dimension of 20mm x 12mm. Standard photolithography is used for the fabrication process and the filter characteristics are measured with Agilent 8362B PNA Network Analyzer.

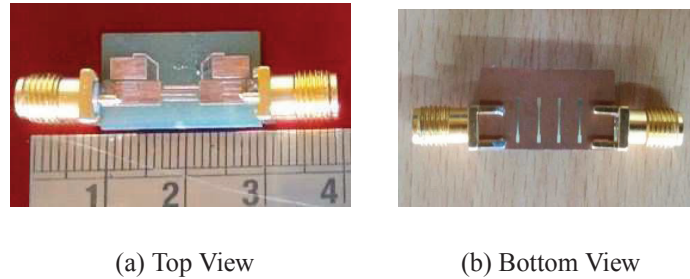


Figure 6.2.11: Photograph of the Prototype Filter

Measured results in Fig. 6.2.12(a-c) show good agreement with the simulated results. Small discrepancies in the result can be attributed to the inaccuracies in the fabrication process. Since the filter contains sub wavelength structures minute change in dimension while fabricating can cause severe change in the response. Average insertion loss for the fabricated filter in the passband is less than 1.4dB, except at the lower band edge. This can be brought down by using a low loss substrate material. Measured attenuation is better than 28dB in the lower stopband and 20dB in upper stopband. Roll off rate is sharp with 130dB/GHz at lower and 30dB/GHz at upper band edge and the fractional bandwidth attained is 109%. Group delay is flat in the passband with variation less than 0.06ns. This reveals the linear phase nature of the filter making it suitable for communication applications. The filter behavior at frequencies in upper band edge and above is controlled by DGS having sub wavelength dimensions.

Table 6.2.2 gives a comparison of the filter performance with other reported UWB filters. As can be observed from the table, the proposed filter is compact and superior in performance with respect to roll off rate and group delay. The actual size neglecting substrate dimension is 20mm x 6.6mm.

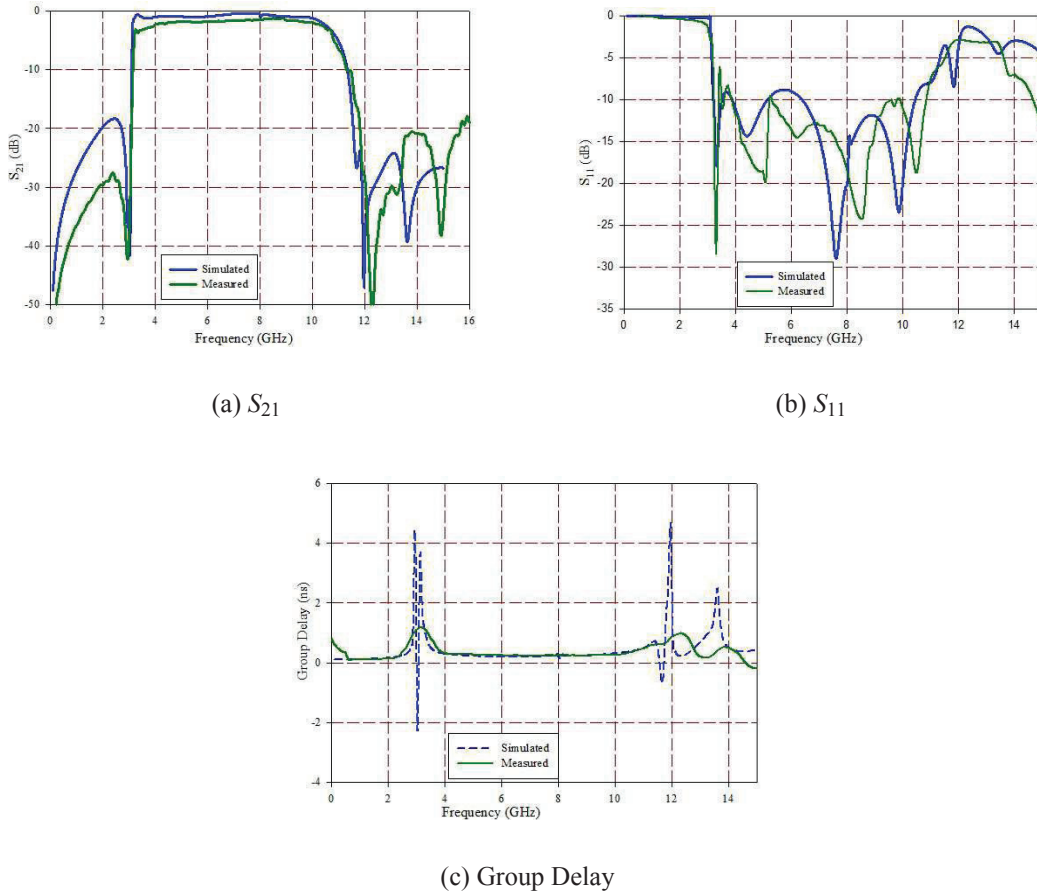


Figure 6.2.12: Measured Results

6.3 Summary

The filters discussed in this chapter have improved performance like high selectivity and good stopband attenuation. These are simple and can be designed with different substrates using the empirical relations given. These filters are well suited for both indoor and outdoor UWB applications and can be easily integrated to UWB transceivers,

several mass produced consumer items, spectrum/frequency analyzers, converters used with satellite television dishes etc.

Table 6.2.2: Comparison of Parameters of Similar Works

Parameters/ References	Passband (GHz)	Insertion Loss (dB)	Roll off Rate- Lower, Upper (dB/ GHz)	Attenuation :Lower,Upper (dB)	Group Delay Variation (ns)	Size (mm^2)	Substrate [ϵ_r , $h(mm)$]
[Weiyu Zong et al., 2009]	3.1-10.6	≤ 1	28,22	26,16	Not Specified	34.2 x 29	2.2/0.508
[K Song and Q Xue, 2010]	3.6-9.45	1-2	26,16	20	0.28	16.4 x 6.6	2.94/0.76
[Z -C Hao and J -S Hong, 2011]	3.3-9.9	0.9	44,34	60,36.1	0.3	25.48 x6.42	LCP
[B. Xia et al., 2012]	3.54- 10.6	0.15-2.5	45,45	14.3,15.4	Not Specified	26.2 x 11.9	4.3/0.41
[Proposed Filter]	3.17- 10.6	1.4	130,30	28,20	0.06	20 x 6.6	4.4/1.6

Bibliography

- [1] Bindu. C. J, Anju Pradeep and S. Mridula, "Compact Ultra Wide Band Filter Using Chip Inductors and CSRR's", Proc., National Symposium on Antennas and Propagation, pp.90-93 Dec.2012.
- [2] Edward F Kuester, "Explicit Approximations for the Static Capacitance of a Microstrip Patch of Arbitrary Shape", Scientific Report No. 82, Electromagnetics Laboratory, Department of Electrical and Computer Engineering, University of Colorado, pp.1-3, Mar.1986.
- [3] Juan Domingo Baena, Jordi Bonache et al, "Equivalent-Circuit Models for Split-Ring Resonators and Complementary Split-Ring Resonators Coupled to Planar Transmission Lines", IEEE Transactions on Microwave Theory and Techniques, Vol.53, No.4, pp.1451-1461, Apr.2005.
- [4] K. Song and Q. Xue, "Inductance Loaded Y Shaped Resonators and their Applications to Filters", IEEE Transactions on Microwave Theory and Techniques, Vol.58, No.4, pp.978-984, Apr.2010.
- [5] Marjan Mokhtaari, Jens Bornemann and Smain Amari, "A Modified Design Approach for Compact Ultra Wideband Microstrip Filters", International Journal of RF and Microwave Computer Aided Engineering, Vol.20, No.1, pp.66-75, Jan.2010.
- [6] Jia-Sheng Hong and Hussein Shaman, "An Optimum Ultra-wideband Microstrip Filter", Microwave and Optical Technology Letters, Vol.47, No.3, pp.230-233, Nov.2005.
- [7] Pramod. K. Singh, Sarbani Basu and Yeong-Her Wang, "Planar Ultra-Wideband Bandpass Filter Using Edge Coupled Microstrip Lines and Stepped Impedance Open Stub", IEEE Microwave and Wireless Components Letters, Vol.17, No.9, pp. 649-651, Sept.2007.
- [8] Bindu. C. J and S. Mridula, "Folded SIR Filter with CSRR's for Ultra Wide Band Applications", Proc., International Symposium on Electronic System Design, pp.182-185, Dec.12-13, 2013.

-
- [9] Bahl I. J, "Lumped elements for RF and microwave circuits", Artech House, London, ISBN 1-58053-309-4, pp.230-233.
- [10] Mahdi Ali, Abdennacer Kachouri and Mounir Samet, "Novel Method For Planar Microstrip Antenna Matching Impedance", Journal of Telecommunications, Vol.2, pp.131-138, 2010.
- [11] Yuchun Guo and Quin Wang, "An Improved Parameters Extraction Method for Dumb bell Shaped Defected Ground Structure", Scientific Research Engineering Online Journal, Vol. 2, pp.197-200, 2010.
- [12] B. Xia, L.-S. Wu and J. F. Mao, "An Ultra-Wide band Balanced Bandpass Filter Based on Defected Ground Structures", Progress in Electromagnetics Research C, Vol. 25, pp.133-144, 2012.
- [13] Weiyu Zong, Xiaowei Zhu et al, "Design and Implementation of Compact UWB Bandpass Filter with a Frequency Notch by Consisting of Coupled Microstrip Line Structure, DGS and EOS", Proc., The 2009 International Conference on Advanced Technologies for Communications, pp.179-182, 2009.
- [14] Z.-C. Hao and J.-S. Hong, "Highly Selective Ultra Wideband Bandpass Filters with Quasi-Elliptic Function Response", IET Microwaves, Antennas and Propagation, Vol. 5, pp.1103-1108, 2011.

7 Conclusion

Contents

- ★ *Thesis Highlights*
- ★ *Comparison of Salient Features of Various Filters Developed*
- ★ *Suggestions for Future Work*

The chapter concludes the thesis by pointing out the highlights of the work carried out. Inferences derived from the investigations carried out on the design and development of planar UWB filters are presented in this chapter. It also gives a comparison of the developed filters on the basis of their performance and size. Suggestions for future implementations are also included.

7.1 Thesis Highlights

The thesis is the outcome of a comprehensive study on the design and development of five planar UWB filter configurations. Detailed analysis carried out on all the filters are presented in chapters 4-6. The studies and results included in the thesis establish the efficiency of the procedure adopted for the design of ultra wide band filters. The thesis highlights are as follows.

- ★ Evaluation of filter parameters in frequency domain to ensure the effectiveness of the design
- ★ Formulation of design equations which can be used as a guideline for the design of filters in the UWB frequency band on desired substrates
- ★ Lumped element model to provide a better understanding of the two port system represented by filters
- ★ Dispersion studies for analyzing the suitability of the filters in communication applications
- ★ Time domain analysis to give insight into the response time, overshoot and ringing of the filters when subjected to a step input
- ★ Experimental results to validate the designs

A brief introduction of ultra wide band technology, design considerations for UWB filters, various tools and techniques used in the design and development of UWB filters are discussed in the first two chapters.

Chapter 3 gives an overview of planar components used in the design of UWB filters. The behaviour of different planar components described here justifies their use in improving the filter performance. From the analyses carried out, it is seen that interdigital coupled lines can provide better coupling as compared with ordinary coupled lines and hence used in all the filters designed. Stepped impedance resonators provide required fractional bandwidth with properly chosen width and length ratios with compact dimensions and hence have found their place in the designs (chapter 4, sections 5.1, 6.2 & Appendix A).

Open ring resonators are capable of producing notch bands with less dominant second resonances whereas notch bands produced by CSRR's are followed by dominant second resonances. Hence ORR's are effectively used in introducing notch bands within the UWB band (Appendix A) while CSRR's are best in suppressing unwanted frequencies in the upper stopband. The sharp resonances of the CSRR's are utilized in designing high selectivity filters (sections 5.1, 5.2 & 6.1).

Defected ground structures act like series connected parallel LC circuits with independent control of L and C values. This fact is utilized in getting better upper stopband characteristics in the filter designs (section 6.2 & Appendix A). Ground plane apertures are found to improve the passband characteristics (Appendix A). Chip inductors discussed here are used in the design of compact filters (sections 5.2 & 6.1). Interdigital capacitors serve to improve the stopband attenuation (section 6.2 & Appendix A)

Chapters 4-6 discuss the design and analysis of the UWB filters developed. The design of a stepped impedance stub resonator filter is described in chapter 4. This filter

can be tuned for any bandwidth of interest by varying the width ratio of stepped impedance stubs and length of the interdigital coupled lines. Chapter 5 illustrates two compact UWB filters, one using folded SIR (section 5.1) and other using chip inductors (section 5.2). Considerable reduction in filter real estate is achieved in these designs. CSRR's are incorporated in both these designs to improve the upper stopband characteristics.

Filters with improved performance are discussed in chapter 6. Two methods are employed for improving the performance. Section 6.1 presents a filter using cascaded resonators thereby improving the overall performance like selectivity and stopband attenuation. CSRR's on the ground plane also contribute to the enhanced stopband attenuation. The filter discussed in section 6.2 adopts the use of series interdigital capacitors and defected ground structures to independently improve the lower and upper stopband performance and selectivity. The planar components are chosen such that the overall filter dimensions are not increased.

Chapters (4-6) include the structural layout of the filters with dimensional details. Parametric analyses carried out on these filters are also included based on which the design equations are formulated. Lumped element model maps each planar component to LC circuit. The lumped models are analyzed using ANSYSTM Designer[®] and results are compared with simulation and experiment. The linear phase nature of the filters is validated from the $\omega - \beta$ diagrams and constant group delay plots. Step response of the filters are also examined to study the filter behaviour in time domain. Measured results are in agreement with simulated results thus ascertaining the suitability of the design. Finally the chapters conclude with comparison of parameters of similar reported work

in literature.

The coexistence of other wireless communication standards necessitates the use of notched filters. Appendix A describes a UWB filter with WLAN notch. The design is flexible allowing different notch bands at different radii of slotline open ring resonators. In Appendix B a UWB filter designed using open and shorted stub resonators in coplanar waveguide is explained.

7.2 Comparison of Salient Features of Various Filters Developed

Table 7.1 summarizes the salient features of the developed filters.

The work starts with the design of a stub SIR filter employing interdigital coupled lines and stepped impedance half wavelength open stub resonators. It is simple and gives reasonably good filter response except for slightly low stopband attenuation (12dB). The indoor FCC restriction in the stopband limit is 10dB on either side of the passband and hence this filter can very well be employed for indoor UWB applications.

Folded SIR filter and chip inductor filter are designed in an attempt to make compact filters without compromising the performance.

Stopband performance is the only limiting factor for the above filters which discourages their use in outdoor applications. Two methods are used for improving the performance, one employing conventional method of cascaded resonators and other using series capacitors and defected ground structures.

All the above filters are developed based on a microstrip topology exploiting the

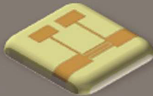
Comparison of Developed Filters							
Filter Structures	Passband (GHz)	Measured Insertion Loss(dB)	Stopband Attenuation (dB)	Roll off Rate (dB/GHz)	Group Delay Variation (ns)	Rise Time (ns)	Size mm x mm
 Stub SIR Filter	3.1-10.6	1.6	13,14	76,26	<0.06	0.18	17 x 19
 Filter Using Folded SIR and CSRR's	3.16-10.6	1.5	13,15	85,26	<0.04	0.19	18 x 12
 Filter Using Chip Inductors and CSRR's	3.12-10.6	1.5	7,11	130,26	<0.14	0.2	17 x 12
 Filter Using Cascaded Resonators	3.12-10.67	1.6	22,20	146,20	<0.08	0.2	24 x 12
 Filter Using Series Capacitor and DGS	3.17-10.6	1.4	28,20	130,30	<0.06	0.14	20 x 12

Figure 7.1: Salient Features of Developed Filters

properties of different types of resonators on interdigital coupled lines. Based on their peculiar characteristics, different resonators are added to improve the filter performance. The designs are simple and straight forward with almost independent control of lower and upper cut off frequencies. Thus any requirements can be moulded onto these designs by properly choosing the dimensions of the resonators for desired frequencies, without considerable increase in size and complexity. The design equations developed for each of the structure serve as a guideline for future designs on any substrate.

7.3 Suggestions for Future Work

The defected ground structures and complementary split ring resonators incorporated in the ground plane to improve the stopband characteristics of the filters are suitable only for the UWB band (3.1 - 10.6GHz). However the filter geometry is tunable for any desired band. The designs are tested as stand alone prototype filters. The issues related to actual PCB integration and shielding/packaging are yet to be addressed.

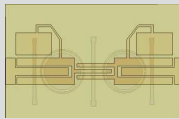
Appendix

Contents

- ★ *Filter with WLAN Notch*
- ★ *Coplanar Waveguide Filter Using Stub Resonators*

Two UWB filter designs, one with a WLAN notch and another using coplanar waveguide technology instead of microstrip - are included as two appendices, Appendix A and B.

A - Filter with WLAN Notch



Contents

- ★ **Geometry**
- ★ **Simulation Studies**
- ★ **Measurement Results**

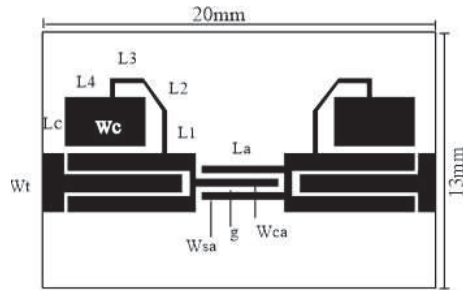
This section presents a UWB filter with WLAN notch. The filter structure consists of an interdigital coupled line with folded SIR's to realize the UWB band. The notch for WLAN band is introduced by two half wavelength open ring resonators etched in the ground plane. The overall dimension is 20mm x 13mm on a substrate with $\epsilon_r = 4.4$ and thickness 1.6mm. ¹

¹Bindu C J, Binu Paul, S Mridula and P Mohanan, *Compact Band Notched UWB Filter for Wireless Communication Applications, International Conference on Advances in Computing and Communications (ICACC-2015), pp. 318-321, Kochi, India.*

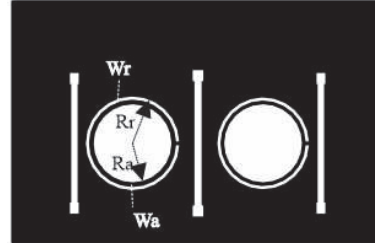
Strong narrow band signals such as WLAN links may severely disturb UWB communication and sensor networks. More over, portable devices such as smart phones and tablets operating in WLAN/WiMAX band have emerged as the vast contemporary technologies. Hence there is a need to introduce notch band(s) within UWB band to avoid interference from existing wireless communication systems such as WiMAX, WLAN etc. [1]-[10]. The UWB filter presented here exhibits notch characteristics in the WLAN band (5.2-5.8GHz). The geometry is derived from the filter discussed in section 6.2.

A.1 Geometry

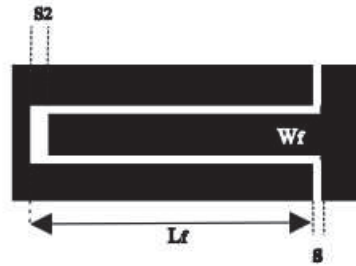
Layout of the top and bottom surfaces of the proposed filter is shown in Fig. A.1. Asymmetrical interdigital coupled line quarter of guide wavelength ($\lambda_d/4$) long at the mid frequency (6.85GHz) of the UWB band ensures maximum coupling and wide band width. Lower band edge is determined by the half wavelength open stubs implemented in the form of folded SIR, while upper band edge by the coupled arm length (L_a). Improvement in lower stopband attenuation is achieved by series interdigital capacitor etched on the transmission line and in upper stopband by the introduction of dumb bell shaped Defected Ground Structure (DGS) in the ground plane. Sharp rejection of WLAN signals is achieved by two slotline Open Ring Resonators (ORR) etched in the ground plane. ORR's are discussed in detail in section 3.2.2. ORR represents a curved open-end stub, and when the length is made equal to half of guide wavelength at a given frequency of interest; it represents an LC parallel resonant circuit, with a



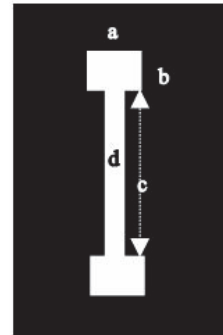
(a) Top View of the Proposed Structure $W_t = 3, W_{ca} = 0.4, W_{sa} = 0.39, L_a = 4.2, L_1 = 2.15, L_2 = 1.87, L_3 = 1.7, L_4 = 0.7, g = 0.28, L_c = 2.5, W_c = 4.1$



(b) Bottom View with ORR's, DGS's and Circular Apertures ($R_r = 2.52, W_r = 0.17, R_a = 2.1, W_a = 0.25$)



(c) Enlarged View of Interdigital Capacitor ($L_f = 6.4, W_f = 0.9, s = 0.18, s_2 = 0.4$)



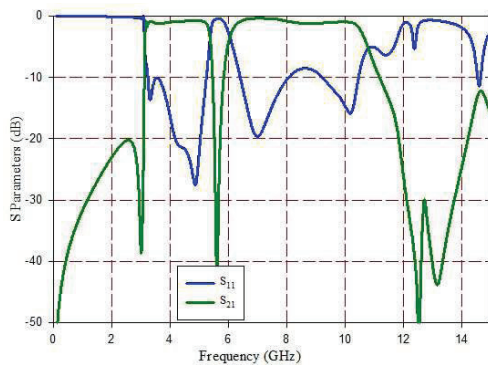
(d) Enlarged View of DGS ($a = 0.48, b = 0.6, c = 6.38, d = 0.35$ (side) $a = 0.58, b = 0.6, c = 6.68, d = 0.39$ (middle))

Figure A.1: Layout of the Filter Structure (all dimensions in mm)

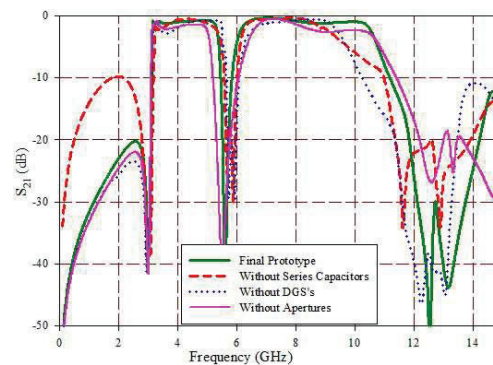
transmission zero at that frequency [11]. The guide wavelength at centre frequency of the notch band (5.5 GHz) is 31mm. Thus to introduce a notch at 5.5GHz, the radius (R_r) of ORR is 2.5mm leading to a perimeter of 15.5mm, half of guide wavelength.

Introduction of ORR's slightly affects the insertion loss in the passband. In order to compensate for the insertion loss and to get better rejection in the upper stopband, the use of circular apertures in the ground plane is exploited. Ground plane apertures (GPA) contribute to strong magnetic coupling between coupled lines, higher impedance and less parasitic capacitance between microstrip conductor and ground plane. The presence of apertures actually nullifies the effect of ground plane thus causing an increase in the inductance value of components. With the introduction of GPA below the strip, line properties can be changed as characteristic impedance varies with the dimensions of the GPA. The final dimensions are selected after exhaustive simulation iterations.

Simulated S parameters are shown in Fig. A.2(a). Average insertion loss for the



(a) Simulated S Parameters of the Filter
: Transmission Zeros-2.99GHz, 5.58GHz,
12.5GHz, 13.2GHz



(b) S_{21} without Series Capacitors,
DGS, Apertures

Figure A.2: Simulated S Parameters

simulated filter is 1dB. Out of band rejection obtained is better than 20dB in lower and upper (up to 14.2 GHz) stopbands. Roll off rate is 256dB/GHz at the lower band edge and 25dB/GHz at the upper band edge. 40dB rejection is achieved in the notch band

extending from 5.18 GHz to 6 GHz. Fig. A.2(b) ascertains the roles of series capacitors, DGS and circular apertures.

A.2 Simulation Studies

The field distributions of the structure at various frequencies in lower and upper stopband regions, in the passband and at the notch frequency, are plotted to analyze the transmission characteristics. The magnitude of electric field on the top surface, at 2 GHz in the lower stopband (Fig. A.3) illustrates the influence of series capacitor. Surface current vector on the top surface at lower cut off frequency (3.1GHz) in Fig.

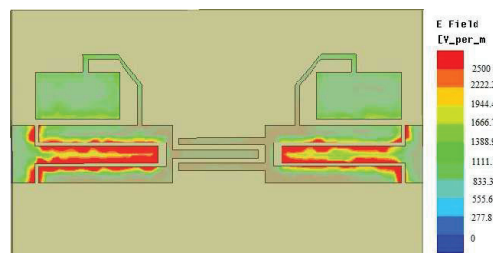
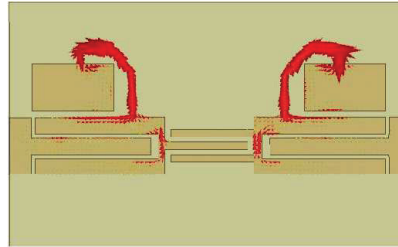


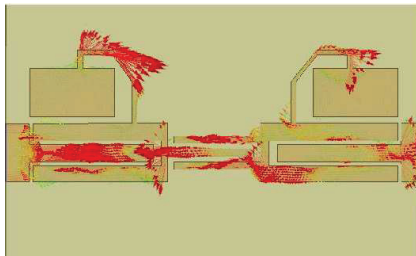
Figure A.3: Magnitude of Electric Field at 2GHz

A.4(a) shows current crowding on the folded SIR's identifying them as responsible for lower cut off frequency. Surface current vector at centre frequency 6.85GHz shows even mode currents in the coupled arm (Fig. A.4(b)) which gradually take a phase reversal and at upper cut off frequency 10.6GHz, the wave mode becomes odd (Fig. A.4(c)).

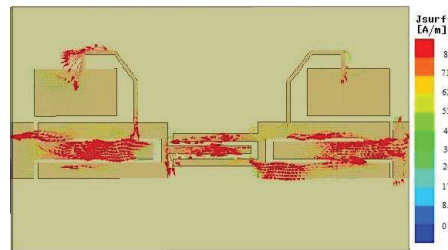
Electric field vector in the notch band edges (5.18GHz and 6GHz) in Fig. A.5(a-b) show the reversal of orientation of the field vector in the slotline ORR's, indicating



(a) Surface Current Vector at 3.1GHz



(b) Surface Current Vector at 6.85GHz



(c) Surface Current Vector at 10.6GHz

Figure A.4: Surface Current Vector on Top Surface

their role in introducing the notch. Electric field vector at the transmission zeros in the upper stopband at 12.5GHz and 13.16GHz (Fig. A.5(c-d)), reveal the role of DGS in the ground plane as shown in figure. Even though there is presence of electric field in the slotline ORRs, their orientation is in the same direction and hence they are not contributing to the transmission zeros.

Dimensional behavior of slotline ORR which is utilized in this design is discussed in detail in section 3.2.2. The notch frequency can be varied by variation of the radius of slotline ORR as indicated in Fig. A.6.

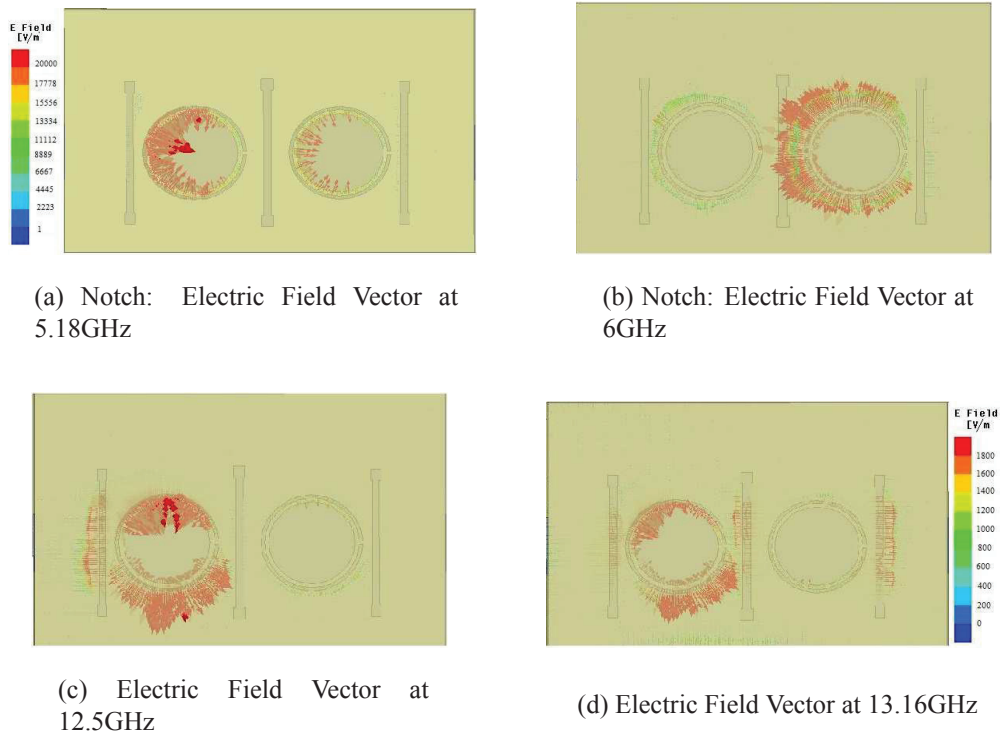


Figure A.5: Electric Field in Ground Plane

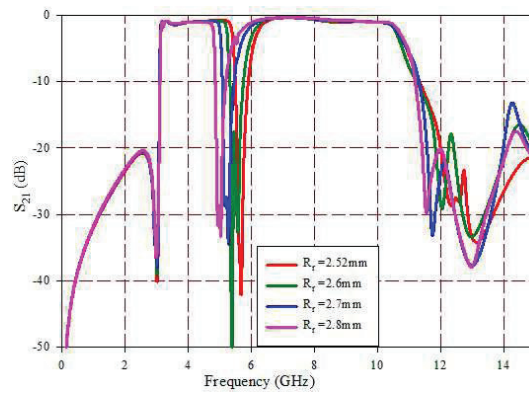
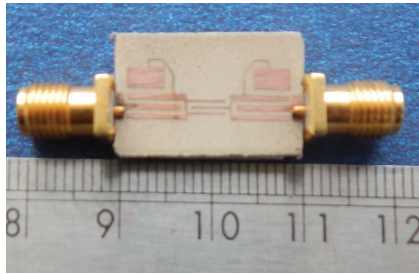


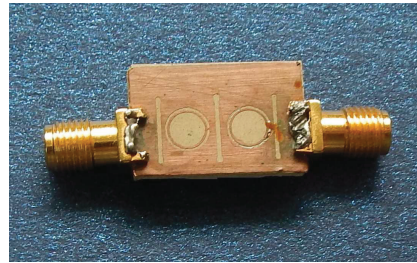
Figure A.6: Variation of Notch Frequency with Radius R_r of Slotline ORR

A.3 Measurement Results

The filter structure is fabricated on a substrate with relative permittivity of 4.4 and thickness 1.6mm. S parameter measurements are taken using HP 8362B PNA. Fig. A.7 shows the photograph of the prototype filter along with the SMA connectors. The structure is compact with an overall dimension of 20mm x 13mm.



(a) Top View



(b) Bottom View

Figure A.7: Photograph of the Prototype Filter

Measured results in Fig. A.8(a-c) agree well with the simulated results. Small discrepancies in the result can be attributed to the inaccuracies in the fabrication process and/or numerical errors in simulation. Insertion loss is less than 1.8dB including those introduced by the SMA connectors. Attenuation in the lower stopband is better than 35dB while it is 15dB, in the upper stopband. Roll off rate is 140dB/GHz at lower band edge and 18dB/GHz at upper band edge.

The flat group delay characteristics (Fig. A.8(c)) in the passband reveal the linear phase nature of the filter, making it suitable for communication applications. Group delay variation is less than 0.25ns over the entire passband. The abrupt change in group

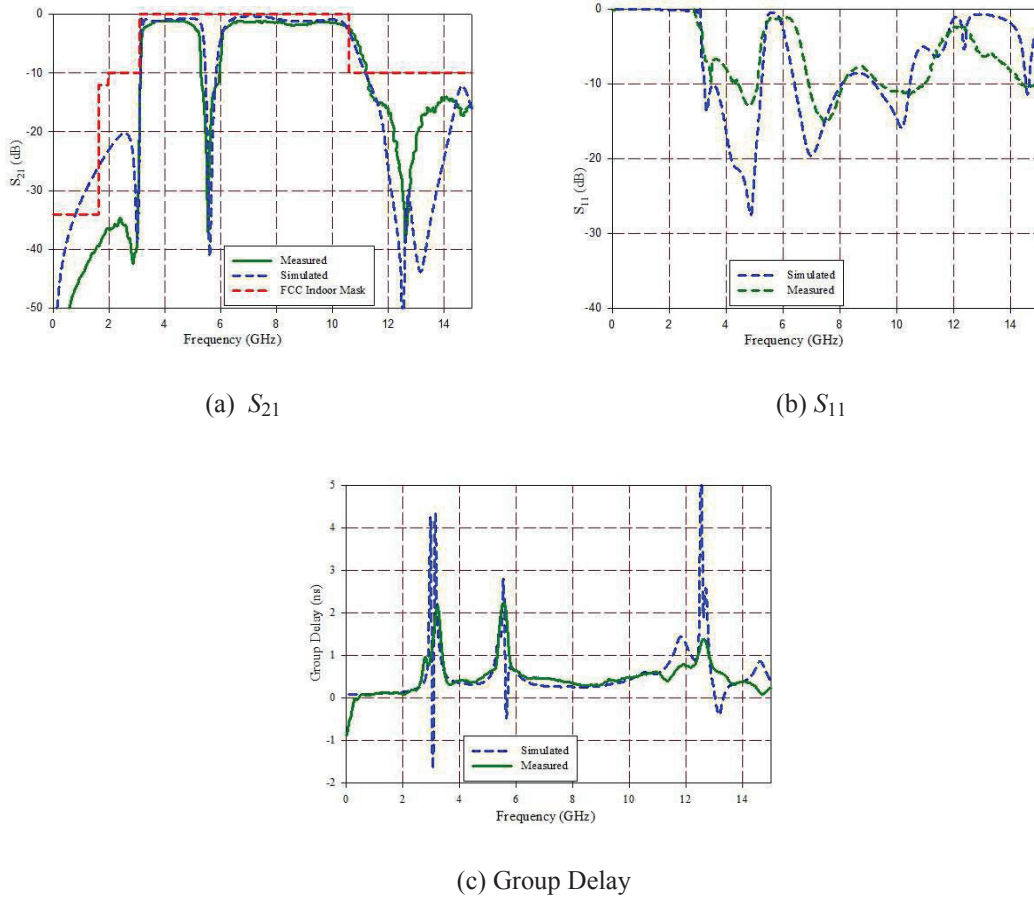


Figure A.8: Measured Results of the Fabricated Filter

delay at the cut off frequencies is by the influence of the resonators.

Table A.1 gives a comparison of the filter performance with other reported UWB notch filters. As can be observed from the table, the proposed filter is superior in performance in terms of notch frequency rejection, roll off rate, stopband attenuation and group delay.

A.4 Summary

The filter designed is compact. Notch band can be varied by varying the radius and width of slotline ORR. Roll off achieved is steep and attenuation in the stop bands is reasonable. Measured rejection at the notch frequency is 37dB.

Table A.1: Comparison with Similar Works

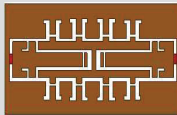
Parameters/ Reference	Passband (GHz)	Notch Frequency/ Band (GHz)	Rejection at Notch Frequency (dB)	Insertion Loss (dB)	Roll off Rate: Lower, Upper (dB/GHz)	Group Delay Variations (ns)	Size (mm^2)	Substrate (ϵ_r/hmm)
[Zhang- Cheng Hao et al., 2009]	3.89- 10.4 (10dB)	6.05	32.64	0.66	13.8,35.7	0.2	23.4 x 17.34	LCP
[Wei Qin et al.,2009]	3.1-10.6	5.8/(5.8-6.4)	31	1	15.6,14.2	-	30 x 60	2.2/0.508
[L. Chen et al.,2010]	3.2-10.6	5.8/(5.25- 6.25)	30	1.6	14,35	0.15	25 x 10	2.2/1.08
[L.-N. Chen et al., 2011]	2.7-10.7	5.8	28	1	11,50	1.23	40 x 20	2.65/1
[Chengyuan Liu et al.,2012]	3-10.8	5.8/(5.2-6.2)	25	0.5	13,26	0.6	12 x 12	10.8/0.635
[Proposed Filter]	3.1-10.6	5.8/(5.18-6)	37	≤ 1.8	148,18	0.25	20 x 13	4.4/1.6

Bibliography

- [1] FCC 15.407 as of June 23, 2011 hallikainen.com, paragraph 'h'.
- [2] Zhang-Cheng Hao, Jia-Sheng Hong, Jonathan P. Parry and Duncan P. Hand, "Ultra-Wideband Bandpass Filter With Multiple Notch Bands Using Nonuniform Periodical Slotted Ground Structure", IEEE Transactions on Microwave Theory and Techniques, Vol.57, pp.3080-3088, No. 12, Dec. 2009.
- [3] P.-Y. Hsiao and R.-M. Weng, "Compact Tri-Layer Ultra Wide Band Band Pass Filter with Dual Notch Bands", Progress in Electromagnetics Research Letters, Vol.106, pp.49-60, 2010.
- [4] L. Chen, F. Wei, X.-W. Shi and C.-J. Gao, "An Ultra-Wideband Bandpass Filter with a Notch-Band and Wide Stopband Using Dumbbell Stubs", Progress in Electromagnetics Research Letters, Vol. 17, pp.47-53, 2010.
- [5] Harish Kumar, Vibhor Kumar Bhardwaj and Upadhyay M.D, "UWB Band Pass Filter with WLAN Notch", ACEEE International Journal on Communications, Vol.3, No.1, pp.45-47, Mar. 2012.
- [6] Chengyuan Liu, Tao Jiang, Yingsong Li and Jing Zhang, "A Novel UWB Filter with WLAN and RFID Stop-Band Rejection Characteristic using Tri-Stage Radial Loaded Stub Resonators", ACES Journal, Vol. 27, No. 9, pp.749-758, Sep.2012.
- [7] C. Y. Liu, T. Jiang, Y. S. Li and J. Zhang, "A Novel UWB Filter with Dual-Notch-Bands Characteristic Using Radial-Multimode Loaded Stub Resonator", Progress in Electromagnetics Research Symposium Proceedings, Suzhou, China, pp.1119-1121, Sep. 2011.

-
- [8] Weiyu Zong, Xiaowei Zhu et. al, "Design and Implement of Compact UWB Bandpass Filter with a Frequency Notch by Consisting of Coupled Microstrip Line Structure, DGS and EOS ", Proc., The 2009 International Conference on Advanced Technologies for Communications, pp.179-182, 2009.
- [9] L.-N. Chen, Y.-C. Jiao, H.-H. Xie and F.-S. Zhang, "A Novel G-shaped Slot Ultra-wideband Bandpass Filter with Narrow Notched Band", Progress in Electromagnetics Research Letters, Vol. 20, pp.77-86, 2011.
- [10] Wei Qin, Wei Hong, Hong Jun Tang and Jing Wang, "Design and Implementation of UWB Bandpass Filter with a Frequency Notch for Choking Back the Interference from Narrow Band Wireless Communication Systems", ICUWB, pp.521-524, Sept.2009.
- [11] L.J. Rogla, J. Carbonell and V.E. Boria, "Study of Equivalent Circuits for Open-Ring and Split-Ring Resonators in Coplanar Waveguide Technology", IET Microwave Antennas and Propagation, Vol.1, pp.170-176, 2007.
- [12] Pankaj Sarkar, Manimala Pal, Rowdra Ghatak and Dipak R. Poddar, "Miniaturized UWB Bandpass Filter with Dual Notch Bands and Wide Upper Stopband", Progress in Electromagnetics Research Letters, Vol. 38, pp.161-170, 2013.

B - Coplanar Waveguide Filter Using Stub Resonators



Contents

- ★ *Geometry*
- ★ *Simulation Studies*
- ★ *Measurement Results*

This section presents a compact coplanar waveguide filter employing stub resonators for ultra wide band applications. A cascade connection of series and shunt stubs quarter wavelength long is used for achieving bandpass characteristics. The filter has an overall dimension of 22mm x 11.5mm on a substrate with $\epsilon_r = 4.4$ and thickness 1.6mm. ¹

¹Bindu C J, S Mridula, P Mohanan, Coplanar Waveguide Filter using Stub Resonators for Ultra Wideband Applications, International Conference on Information and Communication Technologies, Dec.3-5, 2014, Kochi, India, vol.46, pp. 12301237, 2015

Filters discussed in previous sections use stub resonators on microstrip interdigital transmission lines. This section presents the design and development of a UWB filter on coplanar waveguide (CPW). The coplanar waveguide is explained in detail in section 3.1.2. The use of stub resonators for filtering applications originates from transmission line theory, which equates an open circuited and short circuited half wavelength line to a parallel LC and series LC circuit respectively. Hence, a bandpass filter which is a ladder structure of series and parallel LC circuits can very well be realized using such stub resonators. In the recent past different CPW filter configurations have been reported for ultra-wideband applications [1]-[4]. But the issues such as size reduction and simultaneous performance enhancement have not necessarily been addressed in most of the filter designs.

B.1 Geometry

The filter structure consists of a cascade connection of series open stubs and shunt short stubs as shown in Fig. B.1(a), to realize the desired UWB bandwidth (3.1 - 10.6 GHz). The lower side transmission zeros are produced using a pair of shunt short stubs quarter wavelength long at the centre frequency (6.85GHz). Upper side transmission zeros are produced using quarter wavelength long series open stubs. Air bridges are used across these stubs to eliminate unwanted slotline mode propagation. Series short stubs of length much smaller than quarter wavelength long, acting as series inductors are used for performance optimization.

The simulated S parameters are shown in Fig. B.1(b). The average insertion loss for

the filter is 1dB. The roll off rate is 15dB/GHz at both band edges.

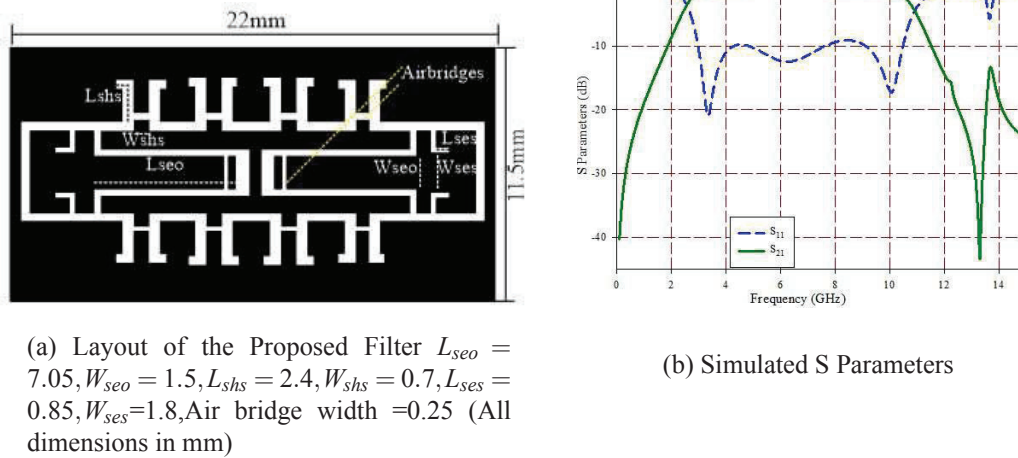
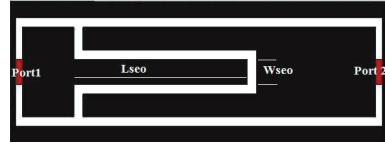


Figure B.1: Layout of the Proposed Filter and Simulated S Parameters

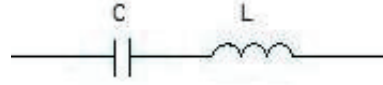
Design Evolution

As per transmission line theory, short circuited and open circuited half wavelength lines act as series and parallel resonant circuits respectively. Similarly short circuited and open circuited quarter wavelength lines act as parallel and series resonant circuits respectively. When length of a series open stub is less than $\lambda_g/4$ it behaves like a series capacitor. Similarly when length of a series short stub is less than $\lambda_g/4$ it acts as a series inductor [5]. A CPW series open stub quarter wavelength long at centre frequency 6.85GHz of the UWB band, its equivalent circuit model and variation of simulated S_{21} with varying length (L_{seo}) and width (W_{seo}) are shown in Fig. B.2(a-d).

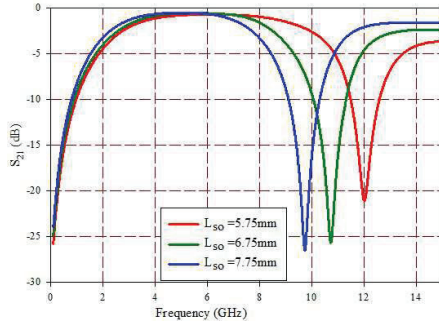
The resonant frequency varies with length of the stubs. As the width of the stub affects the guide wavelength stubs having same length may have slightly different



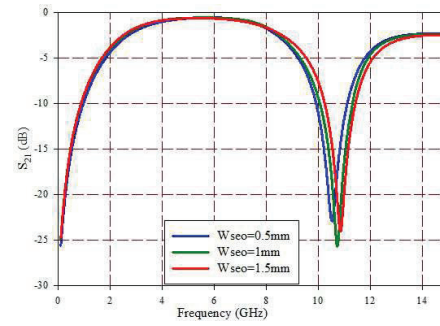
(a) CPW series open(SEO) stub
($\lambda_g/4$ at 6.85GHz)



(b) Equivalent LC Circuit



(c) Simulated S_{21} for varying Lengths($W_{seo}=1$ mm)

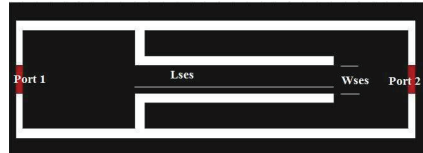


(d) Simulated S_{21} for varying Widths($L_{seo}=6.75$ mm)

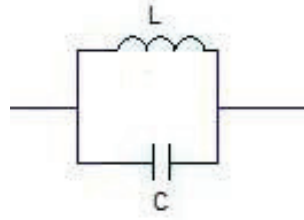
Figure B.2: CPW Series Open Stub and Simulated Responses

resonant frequencies for different widths. However the variation is not significant for varying widths, but can be used for fine tuning of the band. A quarter wavelength series short stub, its equivalent circuit and simulated S_{21} for varying lengths and widths are shown in Fig. B.3 (a-d). CPW layout with a pair of shunt short stub and its transmission characteristics for varying lengths (L_{shs}) and widths (W_{shs}) of stub are shown in Fig. B.4(a-c).

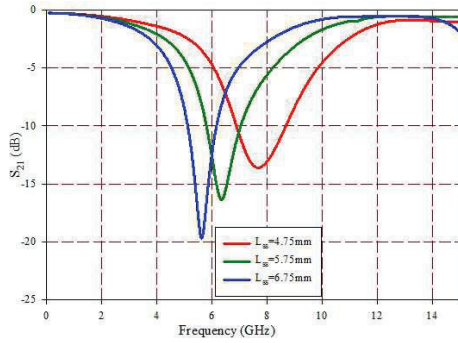
Basic circuit model of a bandpass filter has a parallel resonant circuit controlling its lower cutoff frequency and a series resonant circuit controlling the upper cutoff frequency. A half wavelength open stub or a quarter wavelength short stub will act as



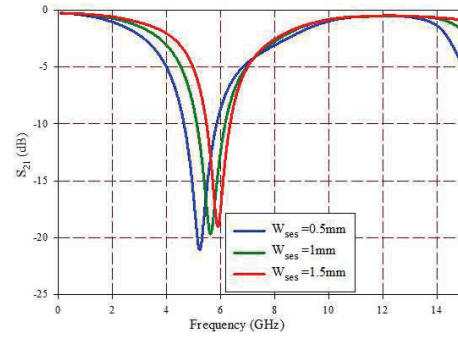
(a) CPW series short(SSES) stub
($\lambda_g/4$ at 6.85GHz)



(b) Equivalent LC
Circuit



(c) Simulated S_{21} for varying
Lengths($W_{ses}=1\text{mm}$)

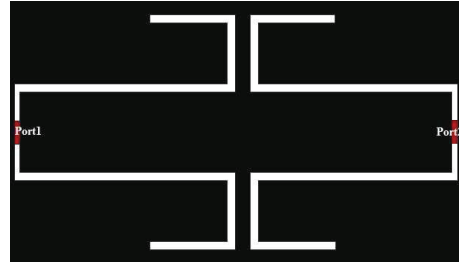


(d) Simulated S_{21} for varying
Widths($L_{ses}=6.75\text{mm}$)

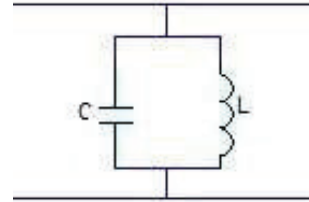
Figure B.3: CPW Series Short Stub and Simulated Responses

parallel LC resonator. Since it is easy to realize shorted stubs in CPW, the choice is for shunt short stubs, which make the structure compact. In the proposed filter, required series resonant circuit is realized with quarter wavelength series open stub and shunt resonant circuit is realized with quarter wavelength shunt short stubs. Fig. B.5(a-b) shows the cascade connection of resonators giving bandpass response.

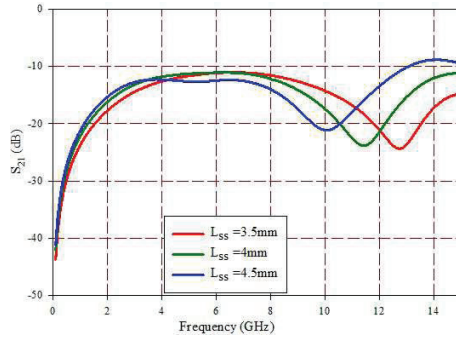
The ideal CPW structure is conveniently considered as a pair of coupled slotlines with odd and even modes referred to as the CPW mode and the slot line mode,



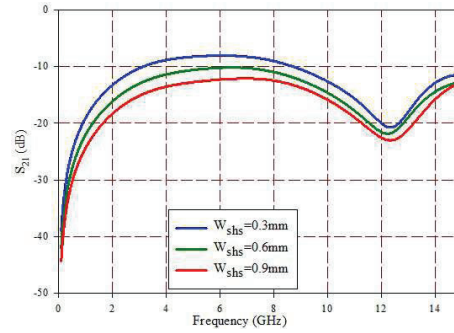
(a) A Pair of Shunt short(SHS) stub
($\lambda_g/4$ at 6.85GHz)



(b) Equivalent LC
Circuit



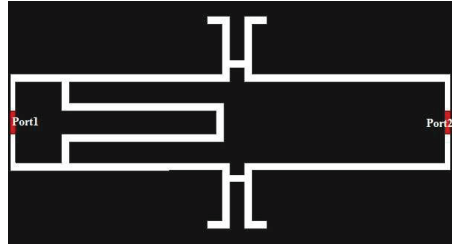
(c) Simulated S_{21} for varying
Lengths($W_{shs}=0.65\text{mm}$)



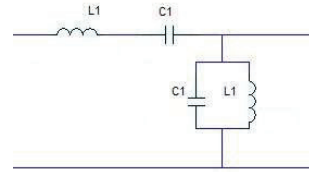
(d) Simulated S_{21} for varying
Widths($L_{shs}=4\text{mm}$)

Figure B.4: CPW Series Short Stub and Simulated Responses

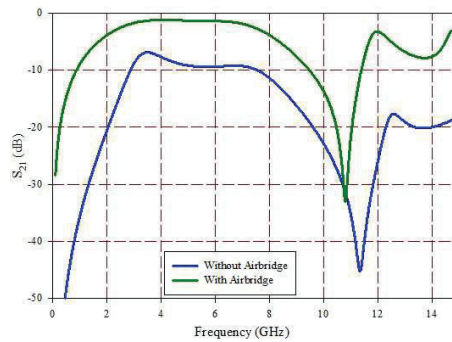
respectively. The signals on finite ground coplanar waveguide is a superposition of these two modes [6]-[7]. If there is asymmetry in the ground plane or if there exists discontinuities in the circuit, the unwanted slotline mode may get coupled to the desired CPW mode. Shunt short stubs and coupled open ends are considered as discontinuities in CPW which cause parasitic modes [8]. In order to suppress these spurious modes, crossover connections need to be made between the ground planes. Note the air bridges in Fig. B.5(a) placed across the shunt short stubs at the beginning of the discontinuity.



(a) Cascade of Series Open stub and Shunt Short stub



(b) Equivalent LC Circuit



(c) Simulated S_{21} with and without Air bridges

Figure B.5: Cascade connection of stubs showing Bandpass Response

In this type of air bridge, the unwanted slotline mode is prevented by introducing slots across the stubs. Difference in transmission characteristics with and without air bridges is shown in Fig. B.5(c).

Introduction of air bridges between the stubs suppress unwanted slotline mode giving reduced insertion loss in the passband. Performance improvement can be achieved by introducing series inductors in the form of series short stubs shorter than quarter wavelength. The three transmission line sections discussed above can be combined suitably to obtain desired bandpass characteristics. The addition of more

number of resonators can improve the characteristics as evident in Fig. B.6(a-b). The role of air bridges is clear from the surface current vectors at the centre frequency 6.85GHz shown in Fig. B.7(a-b). The required UWB bandwidth is achieved by fine tuning of the stub resonators.

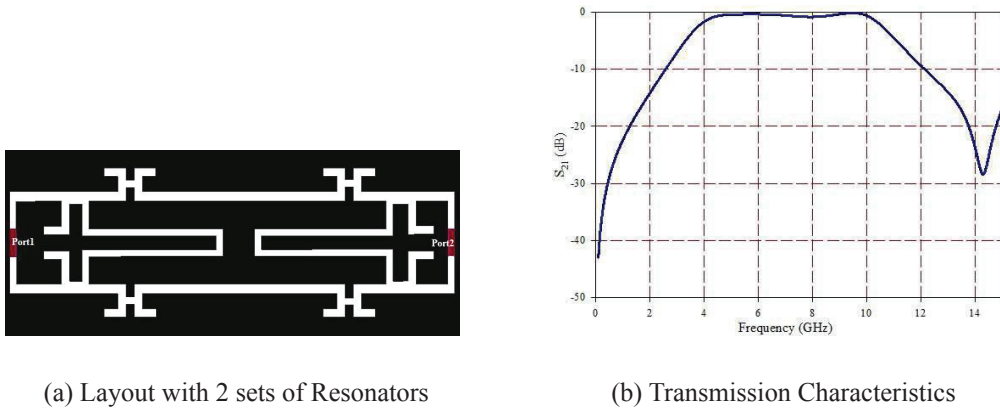


Figure B.6: Layout with a Cascade of 2 Sets of Resonators and Improved Transmission Characteristics

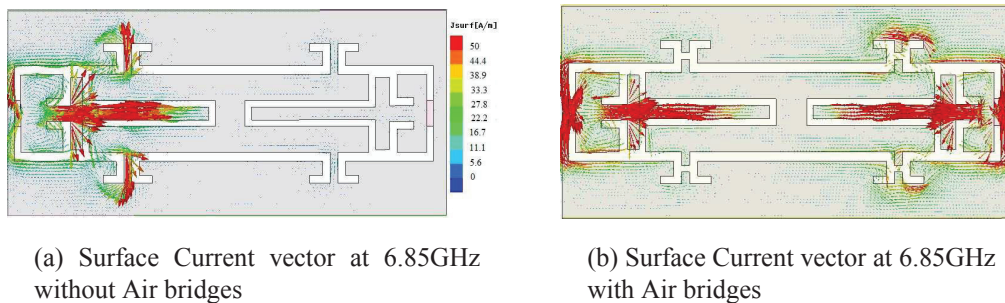


Figure B.7: Surface Current vector at 6.85GHz with and without Air bridges

B.2 Simulation Studies

Electric field and surface current at various frequencies are plotted to analyze the transmission characteristics. Capacitive nature of series open stub at lower frequencies is revealed in the plot of electric field at 1.5GHz shown in Fig. B.8.

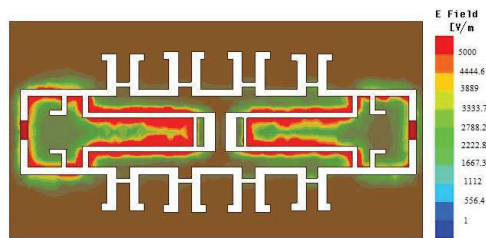
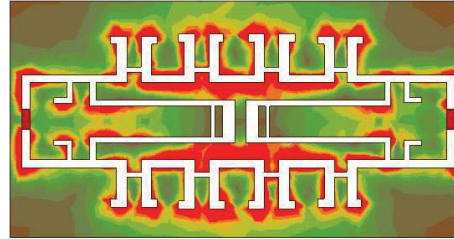


Figure B.8: Electric field at 1.5GHz

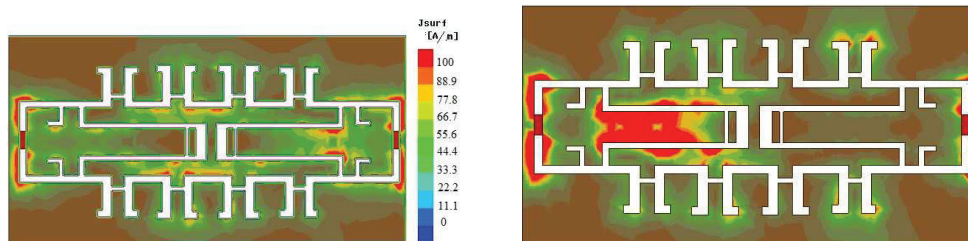
The shunt short stubs are responsible for the lower side transmission zero as indicated by the plot of surface current vector at 3.1GHz in Fig. B.9(a). At centre frequency, all the signals are coupled to the output port as shown in Fig. B.9(b). Upper band edge at 10.6GHz is determined mainly by the series open stub as evident from the current distribution in Fig. B.9(c).

B.3 Measurement Results

The filter structure is fabricated on a single sided substrate with relative permittivity of 4.4 and thickness 1.6mm. Fig. B.10 shows the photograph of the prototype filter along with the SMA connectors. The structure is compact as can be seen in figure. Standard photolithography is used for the fabrication process and the S parameter measurements



(a) Surface Current at 3.1GHz



(b) Surface Current 6.85GHz

(c) Surface Current 10.6GHz

Figure B.9: Surface Current at Various Frequencies in the Passband



Figure B.10: Photograph of the Prototype Filter

are taken using Agilent 8753ES Vector Network Analyzer. Measured results shown in Fig. B.11(a-c) agree well with the simulated results. Small discrepancies in the result can be attributed to the inaccuracies in the fabrication process and/or numerical errors in simulation. Average insertion loss is 2.2dB including those introduced by the SMA

connectors. The roll-off rate is 15dB/GHz at both band edges and the fractional bandwidth attained is 109%. The flat group delay characteristics reveal the linear phase nature of the filter, making it suitable for communication applications. Group delay is less than 0.2ns over the entire passband. Table B.1 gives a comparison of filter parameters with similar reported works. It can be seen that the proposed filter achieves the required bandwidth with comparable performance.

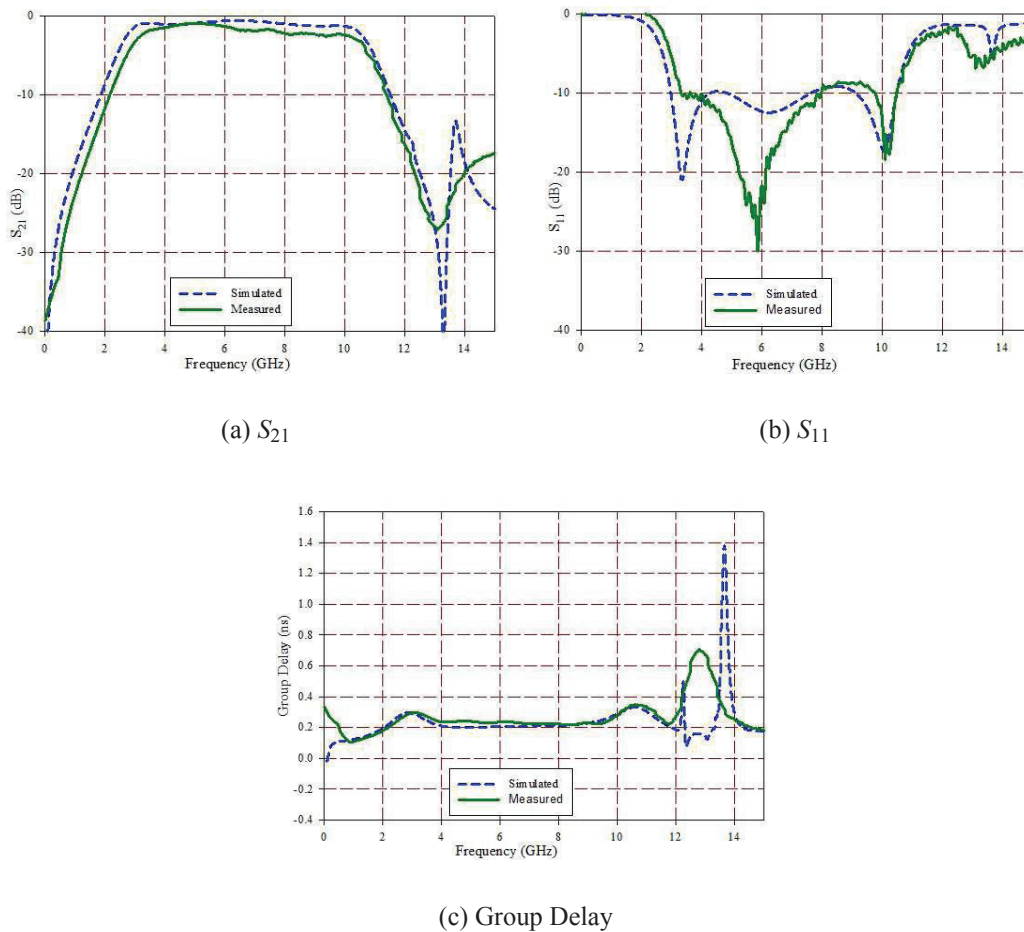


Figure B.11: Measured Results

B.4 Summary

The design is based on conventional coplanar waveguide. Hence it is easy to integrate to any PCB. Roll off achieved is 15dB/GHz on both sides and the attenuation in the stop bands is reasonable.

Table B.1: Comparison with Similar Works

Parameters/ Reference	Passband (GHz)	Insertion Loss (dB)	Roll off Rate: Lower, Upper (dB/GHz)	Attenuation : Lower,Upper (dB)	Group Delay Variations(r)	Size (mm^2)	Substrate (ϵ_r/h mm)	Remarks
[Neil Thomson, et al.,2007]	3.5-9.3	0.6	40,15	Not specified	0.2	8.8 x 2.8	3.05/0.508	Microstrip/ Coplanar
[Shau-Gang Mao, et al.,2009]	3.4-10.5	0.37	26,19	Not specified	0.28	23.5 x 5	2.2/1.57	Conductor Backed, multilayered
[SN. Wang, et al.,2009]	2.8-10.1	Not specified	30,10	28,30	0.3-0.6	36 x 36	3.48/1.524	Coplanar
[Proposed Filter]	3.06-10.6	2.2	40,17	15,15	0.2	22 x 11.5	4.4/1.6	Coplanar

Bibliography

- [1] Neil Thomson, Jia Sheng Hong, “Compact Ultra wideband Microstrip/Coplanar Waveguide Bandpass Filter”, IEEE Microwave and Wireless Components Letters, Vol. 17, 2007. pp.184-186.
- [2] Shau-Gang Mao, Yu-Zhi Chueh, Chia-Hsien Chen and Min-Chun Hsieh, “Compact Ultra-Wideband Conductor-Backed Coplanar Waveguide Bandpass Filter with a Dual Band-Notched Response”, IEEE Microwave and Wireless Components Letters, Vol.19, 2009. p.149-151.
- [3] SN. Wang and NW. Chen, “Compact Ultra-Broadband Coplanar-Waveguide Bandpass Filter with Excellent Stopband Rejection”, Progress in Electromagnetics Research, Vol.17, 2009. pp.15-28.
- [4] Zhongbao Wang, Shaojun Fang, “A CPW Dual-Band Bandpass Filter with Independently Controllable Transmission Zeros”, Radio Engineering, Vol.22, pp.739-744, Sep. 2013.
- [5] David M Pozar, “Microwave Engineering”, John Wiley and Sons Inc, USA; ISBN 0-471-17096-8.
- [6] Majid Riaziat, Reza Majidi-Ahy and I-Jaung Feng, “Propagation Modes and Dispersion Characteristics of Coplanar Waveguides”, IEEE Transactions on Microwave Theory and Techniques, Vol.38. 1990. pp.245-251.
- [7] George E Ponchak, Emmanouil M Tentzeris and Linda PB Katehi, “Characterization of the Coupling between Adjacent Finite Ground Coplanar (FGC) Waveguides”, International Journal of Microcircuits and Packaging, Vol.20. 1997. pp. 587-592.
- [8] NI. Dib, PB. Katehi and GE Ponchak, “Analysis of Shielded CPW Discontinuities with Air bridges”, IEEE MIT-S Digest, 1991. pp. 469-472.

Publications by the Author

International Journals

1. **Chettiparampil J. Bindu**, Shanta Mridula and Pezholil Mohanan, “High Selectivity Filter Employing Stepped Impedance Resonators, Series Capacitors and Defected Ground Structures for Ultra Wide Band Applications”, Progress in Electromagnetics Research C, Vol. 49, pp. 123-131, 2014.
2. **Bindu C J**, Anju Pradeep, S Mridula and P Mohanan, “Compact Planar UWB Filter Using Cascaded Resonators”, International Journal of Ultra Wideband Communications and Systems, 2015 (Accepted).
3. **Bindu C J**, S Mridula and P Mohanan, “Design, Analysis and Equivalent Circuit Modeling of a Microstrip UWB Filter”, International Journal of Simulation: Systems, Science and Technology, 2015 (Accepted).
4. Anishamol Asokan, **Bindu C J**, Anju Pradeep, Binu Paul, S Mridula, “Compact Microstrip Coupled line Bandpass Filter for C Band Applications”, International Journal of Advanced Research in Electronics and Communication Engineering (IJARECE), Vol.4, Issue 10, pp.2598-2601, Oct. 2015.

International Conferences

1. **Bindu C J**, S Mridula and P Mohanan, “Design of Compact Planar Ultra Wide Band Filter”, International Joint Colloquiums on Computer Electronics Electrical Mechanical and Civil (CEMC), Kochi, pp.114-117, Sep. 2011.
2. **Bindu.C J**, S Mridula, “Folded SIR Filter with CSRR’s for Ultra Wide Band Applications”, International Symposium on Electronic System Design organized by the IEEE Computer Society, NTU, Singapore, pp.182-185, Dec. 2013.
3. **Bindu C J**, S Mridula, P Mohanan, “Coplanar Waveguide Filter using Stub Resonators for Ultra Wideband Applications”, International Conference on Information and Communication Technologies, Kochi, India, Vol.46, pp. 1230-1237, Dec. 2014.
4. T K Ramya, **Bindu C J**, Anju Pradeep, Binu Paul, S Mridula, “Compact Tunable Filters For Broadband Applications”, International Conference on Information and Communication Technologies, Kochi, India, Vol.46, pp. 957-964, Dec. 2014.
5. **Bindu C J**, Binu Paul, S Mridula and P Mohanan, “Compact Band Notched UWB Filter for Wireless Communication Applications”, International Conference on Advances in Computing and Communications (ICACC-2015), Kochi, India. pp. 318-321, Sep. 2015.
6. **Bindu C J**, S Mridula and P Mohanan, “Equivalent Circuit Modeling of a Microstrip UWB Filter”, 9th Asia Modelling Symposium, Kuala Lumpur,

Malaysia, pp. 175- 178, Sep. 2015.

National Conferences

1. **Bindu C J**, Anju Pradeep, S Mridula, “Compact Ultra Wide Band Filter Using Chip Inductors and CSRR’s”, National Symposium on Antennas and Propagation (APSYM), pp.90-93, Dec. 2012.

Author Biodata

BINDU C J

ASSISTANT PROFESSOR, DEPARTMENT OF ELECTRICAL ENGG.
MODEL ENGINEERING COLLEGE
KOCHI, 682021, KERALA, INDIA



Educational Details

Pursuing Ph.D in the area of Planar Microwave Filters	Cochin University of Science and Technology, India
M Tech - Embedded Systems	University of Calicut, First Class 73.5%, 2008
PG Diploma in Client Server Computing	Amrita Institute of Computer Technology, 1998
PGDCA	Department of Technical Education, Govt. of Kerala, 82.1%, 1997
B Tech - Electrical Engg.	Govt. Engineering College, Thrissur, University of Calicut, 69.6%, 1988
Pre-Degree	University of Calicut, Kerala, 84.3%, 1984
S S L C	Board of public exams, Kerala, 90.6%, 1982

Biodata

IT Skills

Operating Systems	Linux, Windows, RT Linux, VxWorks
Languages	C, C++
RDBMS/GUI	Oracle/Developer 2000
Office Packages	MS Office, Lotus Notes
Hardware Simulators/Modeling Tools	Orcad, VHDL, Verilog, AutoCad
Software Simulators	MATLAB, HFSS
IDE Tools	Code Composer Studio, Tornado, VisualDSP

Career History

Since June 2001	Asst. Professor in Electrical Engineering, IHRD, Kerala, INDIA.
1998 - 2001	Manager - Projects, M/s. Corbie Infosolutions (P) Ltd, Cochin.
1991 - 1994	Design Engineer, M/s. S Madhu Associates, Cochin, Kerala, India.
1989 - 1990	M/s. O/E/N Connectors, Cochin, Kerala, India on apprenticeship.

Biodata

Publications

International Journals	4
International Conferences	6
National Conferences	1

Professional Memberships

Member, IEEE

Life Member, Indian Society of Technical Education (ISTE)

Life Member, Indian Society of Systems for Science and Engineering (ISSE)

Personal Details

Age & Date of Birth	48Years, 30th May 1967 [Female]
Permanent Address	Appachath, V. P. Thuruth, Chendamangalam, N. Parur - 683512, Kerala, India
Nationality	Indian

Index

- Air bridges, 228–230, 236
- Chip inductors, 95, 125, 142, 144, 149,
150, 152, 155, 156, 163,
170–172
 - Self-resonant frequency, 94–96,
144
- Circular patch capacitors, 97, 163
- Coplanar waveguide filter, 223
- Coupled lines, 65, 67, 68
 - Propagation, 65
- CREMA, 50
- Defected ground structures, 11, 23, 60,
210
- Dielectric constant, 50
- Dielectric loss tangent, 50
- Effective Isotropic Radiated Power, 4
- Electric field, 60, 74, 77, 84, 85, 88, 91,
108, 132, 231
- Electromagnetic simulation tools, 11,
46
 - HFSS, 47, 52
- FCC, 2, 4
- FCC Spectral Mask, 4, 6, 18
- FEM, 52
- Filter Parameters, 13
 - Frequency Domain Parameters, 13
 - S Parameters, 14
- Filters, 5
 - BAW, 8
 - Coaxial, 9
 - Dielectric resonator filters, 8
 - Hardware Digital filters, 7
 - Helical, 8
 - Lumped element filters, 7
 - Microwave filters, 7
 - RC filters, 7

- SAW, 8
- Software Digital filters, 7
- Switched Capacitive filters, 7
- Finite Element Method, 47
- Fractional bandwidth, 104, 119, 138, 156, 175, 192, 233
- Generalized design equations, 28, 110, 150, 171, 185
- Ground plane apertures, 23, 212
 - Circular apertures, 212
- Interdigital capacitor, 179, 181–183, 188, 210
- Interdigital Coupled Lines, 10, 103–105, 115, 127, 131, 147, 152, 163, 180
- Linear phase, 146
- Lumped element model, 28, 48, 113, 135, 152, 172, 188
- Lumped elements, 93
 - Capacitors, 96
 - Inductors, 93
- Magnetic field, 63, 74, 77, 84, 86, 91, 108
- Maxwell's equations, 46, 47
- Microwave integrated circuits, 8, 9
- Monolithic microwave integrated circuits, 8, 9
- Multivariable regression, 30, 45, 48, 110, 134, 150, 171, 185
- Parametric analysis, 108, 132, 134, 149, 168, 184
- Performance characteristics, 14
 - Dispersion, 10, 116, 137, 154, 173, 190
 - Group delay, 5, 10, 14, 15, 119, 139
 - Insertion loss, 6, 10, 14, 18, 105, 212
 - Linear phase, 14, 116, 120, 137, 154, 156, 173, 176, 190, 216, 233
 - Roll off rate, 14, 18, 138, 212
 - Stopband attenuation, 14, 18, 107, 119, 138, 165, 176
- Phase velocity, 66
- Photolithography, 11

- negative photolithography, 50
- Planar Components, 56
- Planar Transmission Lines, 56
 - Coplanar lines, 9
 - Coplanar Waveguide, 56, 62
 - Propagation mode, 63
 - Coplanar waveguide, 26
 - Finline, 56
 - Microstrip, 9, 56–58, 65
 - Striplines, 9, 56
 - Suspended Striplines, 56
 - Suspended striplines, 9
- Prototype filter, 51, 119, 138, 155, 175, 191, 216, 231
- Rectangular patch capacitors, 97, 144, 149, 165
- Resonators, 71
 - Acoustic wave resonators, 71
 - Cavity resonators, 71
 - Complementary split ring resonators, 24, 88, 128
 - Defected ground structures, 90, 188
 - Dumb bell DGS, 91
 - Dielectric resonators, 71
 - Half-wavelength resonators, 21
 - Lumped/semi-lumped resonators, 71
 - Open ring resonators, 82, 213
 - Open-stub, 25
 - Short-stub, 25
 - Stepped impedance resonators, 22, 79, 126, 189
 - Stub resonators, 224
 - Transmission line resonators, 71
- Shannon's formula, 3
- Stepped impedance resonators, 127
- Substrate
 - Effective dielectric constant, 59
- Surface current, 68, 69, 77, 81, 108
- Time domain parameters, 19
 - Impulse response, 19
 - Step response, 19, 20, 118, 137, 155, 174, 191
- Time Domain Performance Parameters
 - Overshoot, 19, 20, 118, 137, 154, 191

Index

Response time, 19

Ringing, 19

Rise time, 20, 118, 137, 154, 191

Settling time, 20, 119, 154, 191

Stability, 19

Ultra Wide Band, 1, 2, 5, 11

 Impulse Radio UWB, 3

 Multi band UWB, 3

Vector network analyzer, 13, 50

WiMAX, 82, 210

Wireless communication, 2

Wireless USB, 27

WLAN, 82, 210

WLAN notch, 207, 209